Engineering aromatic precursor supply and regulation in glycopeptide antibiotic producers

Dissertation

der Mathematisch-Naturwissenschaftlichen Fakultät

der Eberhard Karls Universität Tübingen

zur Erlangung des Grades eines

Doktors der Naturwissenschaften

(Dr. rer. nat.)

vorgelegt von

Jens-Peter Rodler

aus Heidelberg

Tübingen

2026

Gedruckt mit Genehmigung der Mathematisch-Naturwissenschaftlichen Fakultät der Eberhard Karls Universität Tübingen.

Tag der mündlichen Qualifikation:	01.04.2026
Dekan:	Prof. Dr. Thilo Stehle
1. Berichterstatter/-in:	apl. Prof. Dr. Evi Stegmann
2. Berichterstatter/-in:	Prof. Dr. Karl Forchhammer

Inhalt

A. Abbreviations

°C	degree Celsius
4-HPP	4-hydroxyphenylpyruvate
µM	Micromolar
mM	Millimolar
A. balhimycina	*Amycolatopsis balhimycina*
A. coloradensis	*Amycolatopsis coloradensis*
Act. teichomyceticus	*Actinoplanes teichomyceticus*
BGC	Biosynthetic gene cluster
Bht	β-hydroxytyrosine
DAD	Diode Array Detector
Dahp	3-Deoxy-D-arabinoheptulosonate 7-phosphate synthase
DAHP	3-Deoxy-D-arabinoheptulosonate 7-phosphate
Dpg	Dihydroxyphenylglycine
E4P	Erythrose-4-phosphate
E. coli	*Escherichia coli*
GPA	Glycopeptide antibiotic
HmaS	4-hydroxymandelate synthase
HmO	4-hydroxymandelate oxidase
Hpg	Hydroxyphenylglycine
HPLC	High performance liquid chromatography
kb	Kilobase
NRPS	Non-ribosomal peptide synthetase
Pdh	Prephenate dehydrogenase
Pdt	Prephenate dehydratase
PEP	Phosphoenolpyruvate
Phe	Phenylalanine
rpm	Revolutions per minute
S. aquilus	*Streptomyces aquilus*
S. fumanus	*Streptomyces fumanus*
S. varsoviensis	*Streptomyces varsoviensis*
Trp	Tryptophane
Tyr	Tyrosine
Val	Valine

B. Zusammenfassung

Glykopeptid-Antibiotika (GPAs) sind klinisch unverzichtbare Naturstoffe, die von Aktinobakterien produziert werden. Zu den bekanntesten Vertretern zählen Vancomycin und Teicoplanin, die als Reserveantibiotika zur Behandlung schwerer Infektionen durch multiresistente grampositive Pathogene eingesetzt werden. GPAs werden anhand von Unterschieden in der Peptidstruktur, den Quervernetzungen sowie den Modifikationen in die Typen I-V eingeteilt. Ihre Biosynthese ist außerordentlich anspruchsvoll und erfordert eine präzise Koordination der komplexen biosynthetischen Gencluster (BGC), spezifischer Regulationsnetzwerke, komplexe Biosynthesewege sowie eine kontinuierliche Versorgung mit aromatischen nicht-proteinogenen Aminosäuren wie Hydroxyphenylglycin (Hpg), β-Hydroxytyrosin (Bht) und Dihydroxyphenylglycin (Dpg), deren Vorstufen 4-Hydroxyphenylpyruvat (4-HPP) und Tyrosin (Tyr) aus dem Shikimatweg hervorgehen. Trotz intensiver industrieller Optimierung ist die GPA-Produktion weiterhin durch Feedback-Regulierungsmechanismen des Primärstoffwechsels, regulatorische Engpässe sowie die häufige transkriptionelle Inaktivität von BGCs limitiert.

In dieser Arbeit wurden Stoffwechselwegoptimierungen und regulatorische Aktivierungsstrategien kombiniert, um diese Limitationen systematisch zu adressieren. Hierzu wurde zunächst der Shikimatweg in Produzenten kanonischer GPAs metabolisch optimiert. In GPA-Produzenten ist bekannt, dass zentrale Enzyme dieses Weges – die 3-Desoxy-D-arabino-heptulosonat-7-phosphat-Synthase (Dahp) und die Prephenat-Dehydrogenase (Pdh) – nicht nur im Primärstoffwechsel, sondern zusätzlich als duplizierte Isoenzyme innerhalb der jeweiligen Biosynthesegencluster (BGCs) kodiert. Diese BGC-kodierten Isoenzyme spielen eine zentrale Rolle bei der Aufrechterhaltung des Vorstufenflusses. Biochemische Analysen und genetische Modifikationen in den Produzenten zeigten, dass nicht allein die katalytische Effizienz, sondern insbesondere Feedback-Regulation dieser Enzyme ihren Einfluss auf die GPA-Biosynthese bestimmt. Die gezielte Überproduktion von Enzymen, deren Feedback-Regulation untersucht wurde, führte zu einer signifikanten Steigerung der Balhimycin-, Ristomycin- und Teicoplanin-Produktion in *Amycolatopsis balhimycina*, *Amycolatopsis japonica* und *Actinoplanes teichomyceticus*.

Das Ziel des zweiten Teils der Arbeit war die Aktivierung sogenannter stiller Typ V GPA BGCs, die mittels Genome Mining in Genomen von drei Aktinomyceten identifiziert

wurden. Zur Aktivierung dieser BGCs wurden die im ersten Teil der Arbeit gewonnenen Erkenntnisse genutzt, um eine ausreichende Versorgung mit den für die GPA-Biosynthese erforderlichen Vorstufen 4-HPP und Tyr sicherzustellen. Da unter Standardlaborbedingungen keine GPA Produktion identifiziert werden konnte, wurden zur Aktivierung dieser BGCs Strategien kombiniert, die die heterologe und endogene Überexpression von StrR- und LuxR-ähnlichen stoffwechselweg-spezifischen Regulatoren mit der modularen Bereitstellung von Hpg- und Dpg-Vorstufen verknüpft. Trotz dieser gezielten regulatorischen und metabolischen Interventionen konnte keine Typ V GPA-Produktion nachgewiesen werden.

Zusammenfassend liefert diese Arbeit einen systematischen Rahmen zur Optimierung der GPA-Biosynthese. Sie zeigt, dass die Produktion eine sorgfältige Abstimmung zwischen Feedback-regulierter Vorstufenversorgung und gezielter Aktivierung der BGC erfordert. Die Ergebnisse verdeutlichen die zentralen Faktoren für die Steuerung der Biosynthese und liefern wertvolle Leitlinien für zukünftige Ansätze zur Verbesserung von GPA-Ausbeuten in Aktinobakterien.

C. Summary

Glycopeptide antibiotics (GPAs) are clinically indispensable natural products produced by actinomycetes. Exemplary are vancomycin and teicoplanin, which are used as last-resort antibiotics against multidrug-resistant Gram-positive pathogens. GPAs are classified into type I-V based on differences in peptide scaffold, crosslinking patterns and tailoring reactions. Their biosynthesis is exceptionally demanding, requiring tight coordination between biosynthetic gene cluster (BGC), specific regulatory networks, complex biosynthetic pathways and a sustained supply of aromatic amino acids, such as hydroxyphenylglycine (Hpg), β-hydroxytyrosine (Bht) and dihydroxyphenylglycine (Dpg), whose precursor 4-hydroxyphenylpyruvate (4-HPP) and tyrosine (Tyr) are derived from the shikimate pathway. Despite extensive industrial optimization, GPA production remains limited by feedback-regulated primary metabolism, regulatory constraints and the frequent transcriptional silence of BGCs.

In this work, we combined metabolic pathway engineering and regulatory activation strategies to systematically address these limitations. We employed metabolic engineering in producers of canonical GPAs, whose respective BGCs encode duplicated isoenzymes of key enzymes of the shikimate pathway – 3-deoxy-D-arabinoheptulosonate-7-phosphate synthase (Dahp) and prephenate dehydrogenase (Pdh). These isoenzymes play a central role in sustaining precursor flux. Biochemical analyses and genetic manipulation of the producers revealed that feedback regulation, rather than catalytic efficiency alone, limits or promotes GPA biosynthesis. Consistently, feedback-aware overexpression of key enzymes substantially enhanced balhimycin, ristomycin and teicoplanin production in *Amycolatopsis balhimycina*, *Amycolatopsis japonica* and *Actinoplanes teichomyceticus*.

The aim of the second part of this work was the activation of silent type V GPA BGCs that had been identified by genome mining in the genomes of three actinomycetes. To activate these BGCs, insights gained in the first part of the study were applied to ensure sufficient supply of the GPA biosynthetic precursors 4-HPP and Tyr. As no GPA production could be detected under standard laboratory conditions, activation strategies were pursued that combined heterologous and endogenous overexpression of StrR- and LuxR-like pathway-specific regulators with modular precursor supply systems for Hpg and Dpg. Despite these targeted regulatory and metabolic interventions, no production of type V GPAs could be detected.

Together, this work provides a systematic framework for the optimization of GPA biosynthesis. It demonstrates that efficient production requires careful alignment between feedback-regulated precursor supply and targeted activation of BGCs. These results highlight key factors governing biosynthetic control and provide valuable guiding principles for future approaches aimed at improving GPA yields in actinobacteria.

D. List of publications and manuscripts

Primary research article:

1. “Metabolic engineering of the shikimate pathway in *Amycolatopsis* strains for optimized glycopeptide antibiotic production”. *Metabolic Engineering*, 2023

Valentina Goldfinger, Marius Spohn, **Jens-Peter Rodler**, Melanie Sigle, Andreas Kulik, Max J. Cryle, Johanna Rapp, Hannes Link, Wolfgang Wohlleben, Evi Stegmann

2. “Exploring shikimate pathway enzyme diversity for engineering of glycopeptide antibiotic biosynthesis”

Jens-Peter Rodler*, Oleksandr Yushchuk*, Athina Gavriilidou, Anna-Katharina Siegert, Andreas Kulik, Wolfgang Wohlleben, Nadine Ziemert, Evi Stegmann

*Shared first authors and equal contribution

The following review article discusses the biosynthesis of glycopeptide antibiotics and constitutes an integral part of the introduction section of this thesis:

1. “Animating insights into the biosynthesis of glycopeptide antibiotics”. *Current Opinion in Microbiology*, 2024

Athina Gavriilidou, Martina Adamek, **Jens-Peter Rodler**, Noel Kubach, Anna Voigtländer, Leon Kokkoliadis, Chambers C Hughes, Max J. Cryle, Evi Stegmann, Nadine Ziemert

Preprint I contributed to but not included in this thesis:

1. “Phylogenetic distance and structural diversity directing a reclassification of glycopeptide antibiotics”. *bioRxiv,* 2023

Athina Gavriilidou, Martina Adamek, **Jens-Peter Rodler**, Noel Kubach, Susanna Kramer, Daniel H. Huson, Max J. Cryle, Evi Stegmann, Nadine Ziemert

1. Introduction

1.1 Natural products as antibiotics

Natural products, referred to as secondary or specialized metabolites, have long been central to the fight against infectious diseases. Although they are not essential for life, they likely confer evolutionary advantages to the producer organism (O'Connor, 2015). Produced predominantly by microorganisms such as *Actinomycetes*, these metabolites play crucial ecological roles in interspecies competition and communication. Among them, *Streptomyces* species have been the most extensively studied and are responsible for the biosynthesis of numerous clinically important antibiotics. The golden age of antibiotics, started by the discovery of penicillin and streptomycin, demonstrated how natural products could revolutionize medicine (Brown and Wright, 2016). Most existing antibiotic classes, including β-lactams, aminoglycosides, tetracyclines, macrolides and glycopeptide antibiotics (GPAs), are of natural origin (Gavriilidou et al., 2023).

These natural products are produced by various biosynthetic pathways encoded in so-called biosynthetic gene clusters (BGCs). These BGCs encode biosynthetic pathways for different classes of natural products, including polyketides (PKs), ribosomally synthesized and post-translationally modified peptides (RiPPs), and non-ribosomal peptides (NRPs). PKs include macrolides such as erythromycin, used against respiratory pathogens, and tetracyclines, which remain broad-spectrum antibiotics despite decades of clinical use. To the class of RiPPs belongs the prominent lantibiotic nisin, which exemplifies the potency and structural ingenuity of this class and is used as a food preservative (Ziemert et al., 2016). The class of NRPs encompasses GPAs, including the clinically relevant vancomycin and teicoplanin, which are used against multidrug-resistant Gram-positive pathogens, especially methicillin-resistant bacteria (Nicolaou et al., 1999). Their clinical value stems from a highly conserved mode of action, the sequestration of the peptidoglycan precursor lipid II by non-covalent binding to the D-alanyl-D-alanine (D-Ala-D-Ala) terminus of the precursor, thereby inhibiting both transglycosylation and transpeptidation (Yim et al., 2014). Because their target is both extracellular and essential, GPAs remain indispensable for the treatment of severe infections caused by multidrug-resistant Gram-positive pathogens.

Nevertheless, the extensive and often indiscriminate use of antibiotics has accelerated the emergence and global spread of resistance, giving rise to what is now described

as the post-antibiotic era (Brown and Wright, 2016). Even GPAs, long considered resilient to resistance development, are increasingly compromised, most notably by the emergence of vancomycin-resistant enterococci (VRE). This development underscores the urgent need for novel antibiotics that can evade or overcome existing resistance mechanisms. At the same time, discovery pipelines have slowed down, partially due to the repeated isolation of known compounds (Lewis, 2020). Nevertheless, genomic and bioinformatic analyses revealed that only 3 % of the natural products potentially encoded in bacterial genomes have been experimentally characterized (Gavriilidou et al., 2022).

1.2 Glycopeptide antibiotics – types and structural differences

GPAs are a structurally diverse class of antibiotics mainly produced by filamentous Actinobacteria, including *Amycolatopsis*, *Streptomyces* and *Actinoplanes* and related genera (Waglechner et al., 2019; Yim et al., 2014). Vancomycin, isolated from *Amycolatopsis orientalis* in 1953 (Levine, 2006), teicoplanin, derived from *Actinoplanes teichomyceticus* and in clinical use since the mid-1980s (Borghi et al., 1984), balhimycin, a vancomycin type GPA produced by *Amycolatopsis balhimycina* (Pelzer et al., 1999), ristocetin, produced by *Amycolatopsis japonica* (Spohn et al., 2014), and avoparcin, produced by *Amycolatopsis coloradensis* (Labeda, 1995), exemplify the diversity found across different actinomycete producers.

Structurally, type I-IV GPAs consist of a rigid heptapeptide backbone assembled by non-ribosomal peptide synthesis. The constituent amino acids include besides proteinogenic amino acids also the non-proteinogenic aromatic amino acids β-hydroxytyrosine (Bht), 4-hydroxyphenylglycine (Hpg) and 3,5-dihydroxyphenylglycine (Dpg) derived from the shikimate pathway (Goldfinger et al., 2023). A defining feature of GPAs is the presence of oxidative crosslinks between the aromatic side chains, catalyzed by cytochrome P450 enzymes (Brieke et al., 2015; Haslinger et al., 2015), which create a rigid, cup-shaped scaffold that enables high-affinity binding to the peptidoglycan precursor lipid II (Gavriilidou et al., 2024; Loll et al., 1998; Perkins, 1969; Reynolds, 1989; Yim et al., 2014).

The various GPA types (types I-IV) are defined primarily by their peptide backbone composition and crosslinking patterns (Figure 1). The heptapeptide backbone of type I GPAs such as vancomycin or balhimycin consists of two proteinogenic, leucine (Leu) and asparagine (Asn), and five non-proteinogenic amino acids, including Bht at amino

acid position 2/6, Hpg at position 4/5 and Dpg at position 7. The aromatic amino acids are crosslinked through three phenolic/biaryl crosslinks (Hadatsch et al., 2007; Puk et al., 2004; Stegmann et al., 2010, 2006a). The heptapeptide backbone of type II GPAs with avoparcin as example differs from type I by the aromatic amino acids Hpg and/or phenylalanine (Phe) at position 1 and 3, replacing the aliphatic residues. Type III GPAs, such as ristocetin, are characterized by complete crosslinking of all aromatic amino acids residues, which gives rise to an additional crosslink compared to type I/II GPAs. Type IV GPAs exemplified by teicoplanin share the fully aromatic, crosslinked backbone of type III GPAs but are further distinguished by additional lipid acyl side chains attached to the sugar residues. They also lack the hydroxyl group on tyrosine (Tyr) at position 2. Beyond their peptide core, GPAs are further diversified through tailoring modifications. These include glycosylation, halogenation, methylation, sulfation and lipid acylation during biosynthesis (Stegmann et al., 2010).

Compared to types I-IV, type V GPAs form a distinct group of compounds, considered an outlier class regarding their structure and mode of action. For these reasons, there has been a proposal to reclassify them as glycopeptide-related peptides (GRPs) (Gavriilidou et al., 2023).

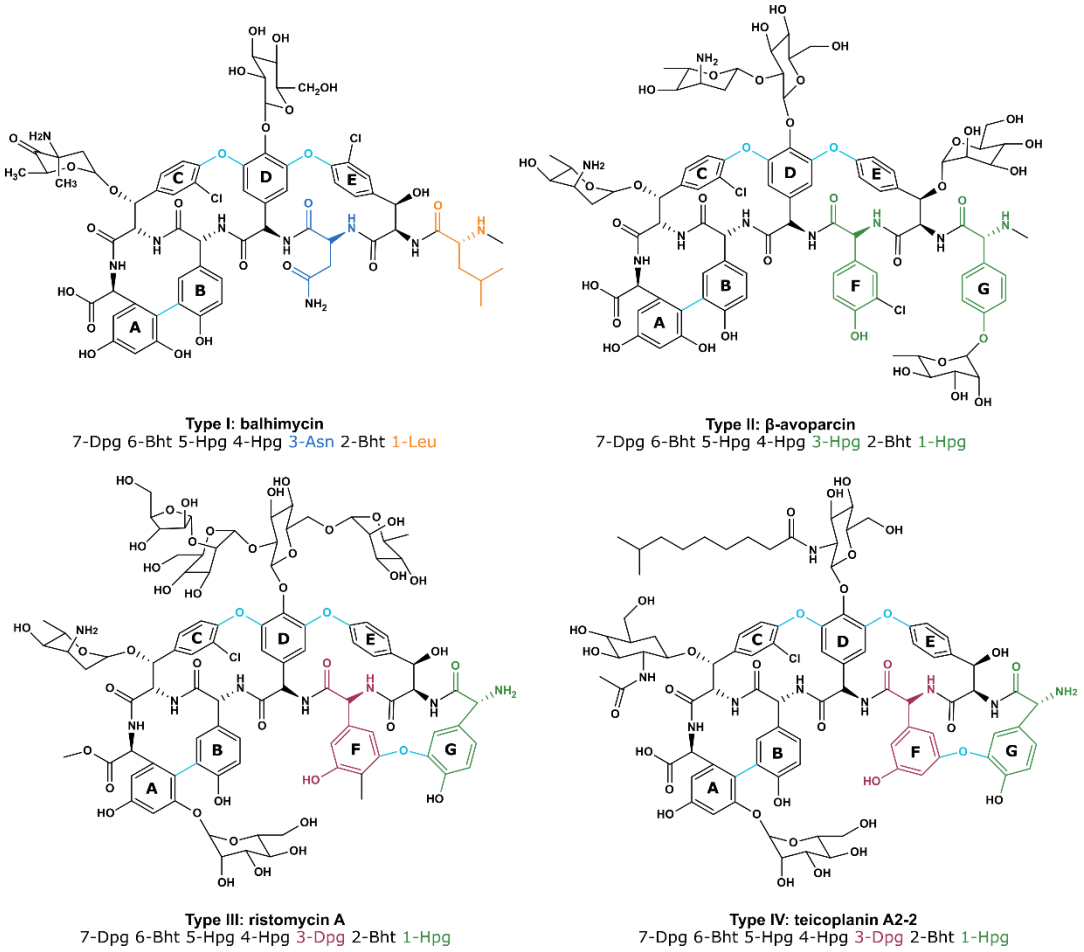

Figure 1: Structure of GPAs type I-IV. For each type of GPA, one representative is shown. Type 1: balhimycin, type II: β-avoparcin, type III: ristomycin A, type IV: teicoplanin A2-2. Abbreviations: Leu, leucine; Bht, β-hydroxytyrosine; Asn, asparagine; Hpg, 4-hydroxyphenylglycine; Dpg, 3,5-dihydroxyphenylglycine.

1.3 Reclassification of GPAs

The fundamental differences between type I-V and type V GPAs have raised the question of whether type V GPAs should still be considered GPAs in the strict sense. Recent phylogenetic and structural analyses suggest that they represent an evolutionarily and functionally distinct lineage, prompting the proposal to reclassify them as glycopeptide-related peptides (GRPs) (Gavriilidou et al., 2023).

The reclassification of type V GPAs into GRPs has been proposed to better reflect their unique evolutionary history, structural composition, and bioactivity. GRPs encompass compounds such as complestatin, kistamicin, corbomycin, and GP6738 (Figure 2), which often feature longer or non-canonical peptide backbones, lack glycosyl modifications, and contain atypical crosslinking patterns such as Trp-Hpg biaryl linkages (M. Xu et al., 2022). The absence of sugar moieties and the presence of unprecedented ring systems emphasize their chemical distinctness (Gavriilidou et al., 2023).

The most striking divergence lies in their mode of action. Unlike classical GPAs, these molecules do not bind lipid II but rather inhibit bacterial autolysins, thereby preventing peptidoglycan remodeling and cell division (Culp et al., 2020; M. Xu et al., 2022). Importantly, this mechanism circumvents classical resistance strategies such as D-Ala-D-lactate (Lac) substitution, which undermine lipid II-binding GPAs. Consequently, GRPs retain potent activity against vancomycin-resistant enterococci (VRE) (Culp et al., 2020).

Combined, the phylogenetic separation of their biosynthetic loci, their non-canonical chemical architectures, and their unique mode of action demonstrate that type V GPA represent a fundamentally divergent group within GPAs (Gavriilidou et al., 2023). Distinguishing GRPs from classical GPAs provides a clearer framework for exploring their evolutionary origins and exploiting their therapeutic potential. However, it is important to lay out that the term GRP has not yet been formally adopted by the broader scientific community. Therefore, in this work they will be referred to as type V GPAs.

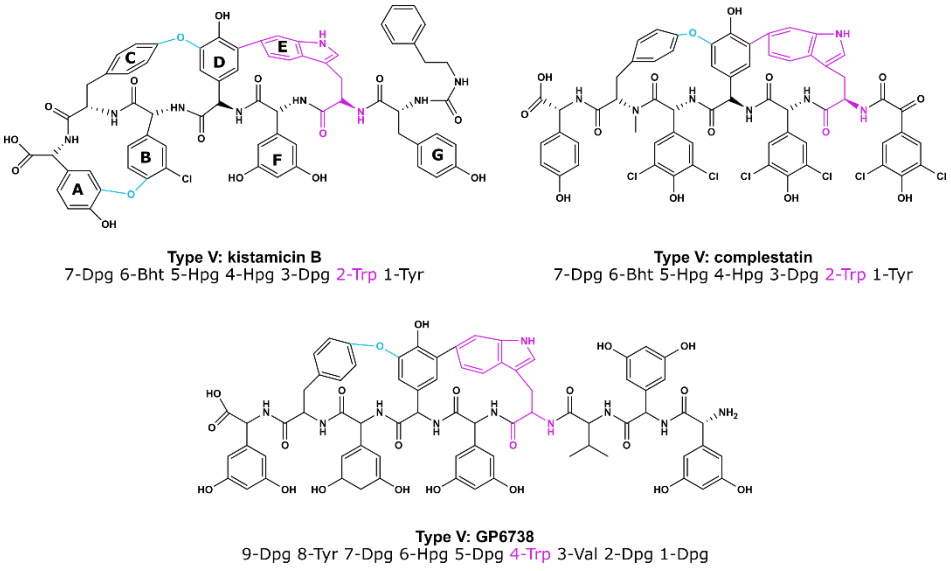

Figure 2: Structures of GPA type V. Chemical structure of kistamicin B, complestatin and GP6738. All type V GPAs contain the Tyr-Hpg-Trp dual crosslinks. GP6738 bears a nonapeptide with a Val at position 3. Abbreviations: Tyr; tyrosine; Hpg, 4-hydroxyphenylglycine; Dpg, 3,5-dihydroxyphenylglycine; Val, valine.

1.4 Biosynthesis of GPAs

The biosynthesis of GPAs is directed by large BGCs, typically ranging from 60-90 kb, which encode all functions required for GPA assembly. These BGCs comprise genes encoding non-ribosomal peptide synthetases (NRPS), tailoring enzymes, precursor biosynthesis, resistance determinants and regulatory genes (Stegmann et al., 2010; Yim et al., 2014). Owing to the clinical relevance of GPAs, the biosynthetic pathways of type I-IV GPAs have been extensively studied. The biosynthesis can be divided into

three main steps: the synthesis of non-proteinogenic amino acids, the formation of the peptide backbone by the NRPSs and the subsequent modification of the peptide backbone (Gavriilidou et al., 2024).

The synthesis of the aromatic non-proteinogenic amino acids Bht, Hpg and Dpg is encoded withing the GPA BGCs. The precursors for the biosynthesis of Bht and Hpg are tyrosine (Tyr) and 4-hydroxyphenylpyruvate (4-HPP), which are derived from the shikimate pathway (see 1.5). Additionally, Tyr acts as the amino donor for Dpg synthesis, which requires malonyl-CoA as a precursor (Chen and Walsh, 2001; Gavriilidou et al., 2024; Toma et al., 2015).

Depending on the type of GPA, the synthesis of Bht can follow two different ways. In the first mechanism, Tyr is incorporated into the peptide backbone during NRPS assembly and subsequently hydroxylated, a reaction that is catalyzed by a non heme ion oxygenase (Hansen et al., 2023; Kaniusaite et al., 2019; Stinchi et al., 2006). In the second mechanism, Bht is synthesized before its incorporation into the peptide backbone. A minimal NRPS activates Tyr, which is then hydroxylated by a cytochrome P450 monooxygenase. After cleavage from the minimal NRPS module by a specific thioesterase, the free Bht is incorporated into the main assembly line (Haslinger et al., 2015; Miller and Gulick, 2016; Mulyani et al., 2010; Puk et al., 2004).

The biosynthesis of Hpg requires two enzymes that are encoded in the GPA BGCs, a 4-hydroxymandelate oxidase (HmO) and a 4-hydroxymandelate synthase (HmaS). The enzymes use the shikimate pathway intermediate 4-HPP to synthesize 4-hydroxybenzoylformate. This is further converted to Hpg by the addition of the amino group derived from Tyr through an aminotransferase (Pgat) (Choroba et al., 2000).

A subcluster within GPA BGCs encodes the four enzymes, DpgA-D, that are required for the synthesis of Dpg from malonyl-CoA. The enzyme set comprises a type III polyketide synthase and modifying enzymes that catalyze the condensation of malonyl-CoA moieties to form 3,5-dihydroxyphenylglyoxylate. Subsequent transamination by the aminotransferase (Pgat), that is also involved in Hpg biosynthesis, results in Dpg (Chen et al., 2001; Pfeifer et al., 2001).

At the core of the GPA biosynthesis lies the NRPS machinery, a multimodular enzymatic system that functions as an assembly line for the characteristic heptapeptide scaffold. Each NRPS module incorporates a specific amino acid through

specific catalytic domains (Yim et al., 2014). The adenylation (A) domain recognizes and activates the amino acids and incorporates them into the growing peptide chain. The activated amino acid is covalently linked as a thioester to the thiol group of the phosphopantetheine arm within an adjacent peptidyl carrier protein (PCP) domain (Miller and Gulick, 2016; Recktenwald et al., 2002). The bound amino acid is then transferred to the acceptor pocket of the condensation (C) domain where the PCP-bound substrates are merged. Conversion of the L-configured amino acid into its D-form can occur via epimerization domains (E) within certain modules. The modules are organized collinearly, so that their order defines the sequence of the product (Yim et al., 2014), which forms the conserved foundation upon which all GPA structures are built.

Following NRPS assembly, the linear heptapeptide undergoes oxidative cyclization by crosslinking enzymes, which are recruited to the last module of the NRPS (Gavriilidou et al., 2024). GPA-specific cytochrome P450 enzymes catalyze the formation of biaryl and phenolic crosslinks between aromatic side chains, yielding a rigid three-dimensional structure (Bischoff et al., 2005; Greule et al., 2018; Stegmann et al., 2010, 2006b). The enzymes are recruited by a domain that is unique to GPA biosynthesis, known as the X-domain (Haslinger et al., 2015). After crosslinking, the terminal thioesterase domain catalyzes the release of the peptide from the NRPS complex (Peschke et al., 2018).

Beyond oxidative crosslinking, GPAs are extensively diversified through post-assembly tailoring reactions. Glycosyltransferases attach one or more sugar moieties to the aglycone. Additionally, GPAs exhibit modifications like methylation, sulfation of hydroxyl groups or the acylation of sugar moieties (Nicolaou et al., 1999).

A comprehensive illustration of the complex biosynthesis of vancomycin can be found in an animated video (https://youtu.be/TGAgC4c8hvo) which we published in our review (Gavriilidou et al., 2024).

1.5 The shikimate pathway

The shikimate pathway is a central metabolic route that connects primary carbohydrate metabolism with the formation of aromatic compounds. In GPA-producing actinomycetes, the shikimate pathway provides the precursors for the synthesis of unusual amino acids building blocks that are indispensable for the peptide scaffolds of

these antibiotics. Thus, the pathway forms a crucial interface between primary and secondary metabolism.

The shikimate pathway converts phosphoenolpyruvate (PEP) and erythrose-4-phosphate (E4P) into chorismate through seven consecutive enzymatic steps (Bentley, 1990; Mir et al., 2015). Chorismate is the branching point in the shikimate pathway, diverging into multiple routes, leading to the biosynthesis of aromatic acids (Phe, Tyr, tryptophane (Trp)), folate cofactors, ubiquionone and siderophores (Dosselaere and Vanderleyden, 2001). The pathway begins with the condensation of PEP and E4P to yield 3-deoxy-D-arabino-heptulosonate 7-phosphate (DAHP), a reaction catalyzed by DAHP synthase (Dahp) and driven by the energy of a phosphate bond. DAHP is then cyclized by 3-dehydroquinate synthase, generating 3-dehydroquinate (DHQ), followed by dehydration of DHQ by 3-deydroquinate dehydratase to form 3-dehydroshikimate, which is then reduced by the shikimate dehydrogenase to produce shikimate. A shikimate kinase phosphorylates the shikimate ring and the 5-enolpyruvylshikimate-3-phosphate (EPSP) synthase catalyzes the reaction to obtain EPSP. In the final step, the chorismate synthase eliminates the phosphate group from EPSP and introduces a double bond, yielding chorismate (Bentley, 1990; Gibson and Pittard, 1968; Mir et al., 2015). Chorismate is processed into prephenate by the chorismate mutase. Prephenate is a common precursor in the biosynthesis of Tyr and Phe. It can be used by the prephenate dehydrogenase (Pdh) in the biosynthesis of Tyr or by the prephenate dehydratase (Pdt) in the biosynthesis of Phe (Bentley, 1990).

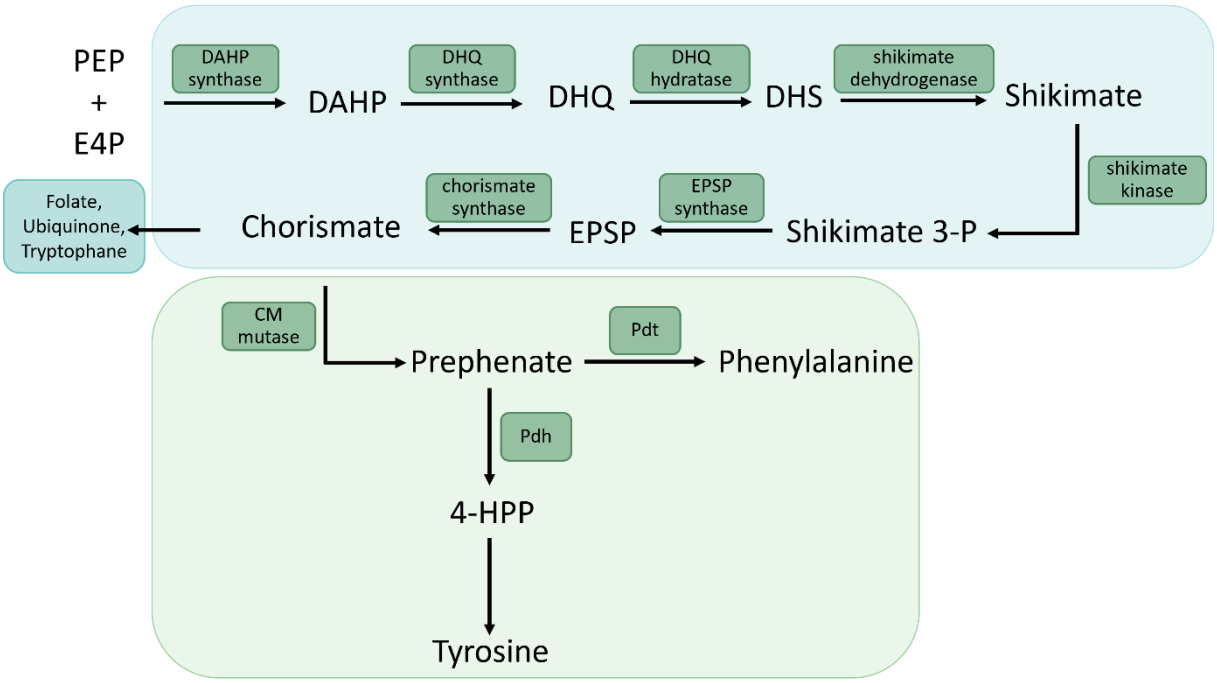

Figure 3: Shikimate pathway. Abbreviations: DAHP, 3-deoxy-D-arabino-heptulosonate 7-phosphate; DHQ, 3-dehydroquinate; DHS, 3-dehydroshikimate; EPSP, 5-enolpyruvyshikimate3-phosphate; 4-HPP, 4-hydroxyphenylpyruvate; CM, chorismate; Pdt prephenate dehydratase; Pdh, prephenate dehydrogenase; PEP, phosphoenolpyruvate; E4P, erythrose 4-phosphate

1.5.1 Regulation of the shikimate pathway

The regulation of metabolic pathways is fundamental to cellular homeostasis, ensuring that metabolic flux is balanced between primary biosynthetic needs and the flexible demands imposed by environmental change. Typically, control is exerted at rate-limiting steps, which correspond to the first irreversible reaction of a pathway or to a key branch point where metabolites are directed into alternative routes. Rate-limiting enzymes are subject to multiple levels of regulation, including transcriptional control, covalent modification and allosteric feedback inhibition by end products (Heinrich et al., 1977; Kloosterman et al., 2003).

The shikimate pathway exemplifies a highly regulated and complex system because it generates not only the aromatic amino acids Tyr, Phe and Trp, but also a broad range of primary and secondary metabolites. The first reaction, catalyzed by Dahp, is a central point and is subject to extensive allosteric inhibition by the end products of the pathway (Light et al., 2012; Light and Anderson, 2013). Dahps occur in two major forms: type I enzymes, subdivided into Iα and Iβ, which are generally inhibited by Tyr, Phe and Trp, and type II enzymes, which are only inhibited by Tyr and additionally repressed by Phe (Light and Anderson, 2013). Dahp encoded within GPA BGCs belong to type I, whereas those encoded elsewhere in the genome of the producers can belong to either type.

This regulatory differentiation is well documented in *Amycolatopsis balhimycina*, where $Dahp_{pim}$ is inhibited by both Phe and Tyr, while $Dahp_{sec}$ is inhibited only by Tyr. Notably, equimolar concentrations of Phe and Tyr amplify the inhibition of $Dahp_{prim}$, whereas Phe antagonized the Tyr-dependent inhibition of $Dahp_{sec}$ (Goldfinger et al., 2023). Comparable regulatory patterns have been observed in *Amycolatopsis methanolica* and *Amycolatopsis mediterranei*. In *A. methanolica*, two isoenzymes of Dahps display distinct feedback profiles: type I is inhibited by Trp, Phe and Tyr, whereas type II is inhibited only by Tyr and Phe. In contrast, *A. mediterranei* possesses a single Dahp that is feedback inhibited only by Trp. (De Boer et al., 1989; Euverink et al., 1995).

Chorismate mutase (CM), which directs the flux into the Phe/Tyr branch, represents another critical control point and is allosterically inhibited by Tyr or Phe (Dosselaere and Vanderleyden, 2001). Further branch-specific regulation occurs at Pdt, which is typically sensitive to feedback inhibition by Phe and/or Tyr (Bentley, 1990). At the terminal branch point of the shikimate pathway, Pdh channels flux into the Tyr biosynthesis (Abou-Zeid et al., 1995; Euverink et al., 1995). Pdh belongs to the TyrA family, whose members are classified based on their substrate preferences: Pdh utilizes prephenate, arogenate dehydrogenase utilizes arogenate, and cyclohexadienyl dehydrogenase can utilize either prephenate or arogenate. All Pdhs share a conserved catalytic core domain, and a subset additionally contains a C-terminal ACT regulatory domain (Song et al., 2005). In Actinobacteria, two major TyrA clusters have been described: the first comprises NAD^+/$NADP^+$ dependent enzymes from *Corynebacterium*, *Mycobacterium*, and *Bifidobacterium* species, whereas the second includes NAD^+ specific enzymes from other actinobacterial lineages. (Song et al., 2005).

Actinomycetes such as *Amycolatopsis, Streptomyces* and *Actinoplanes* have evolved dedicated solutions to ensure the supply of precursors for secondary metabolism. Across GPA producers, it has been show that they carry additional copies of *dahp* and *pdh*, which are found within GPA BGCs. (Thykaer et al., 2010; Waglechner et al., 2019).

1.6 Metabolic engineering of GPA producers

Metabolic engineering is broadly defined as the targeted modification of cellular metabolic pathways to enhance the production of a desired compound through recombinant DNA techniques (Baltz, 2016; Pickens et al., 2011). In actinobacteria, where complex secondary metabolite pathways are tightly regulated and metabolically

demanding, metabolic engineering is a powerful and systematic approach to improve microbial production of antibiotics (Bilyk and Luzhetskyy, 2016).

Early metabolic engineering efforts in antibiotic-producing actinomycetes primarily focused on regulatory genes controlling biosynthetic pathways. Manipulation of pathway-specific or global regulators proved highly effective in enhancing production of diverse antibiotics, including actinorhodin and undecylprodigiosin in *Streptomyces coelicolor* (Fernández-Moreno et al., 1991; Narva and Feitelson, 1990), FK506 in *Streptomyces tsukubaensis* (Huang et al., 2013b), and moenomycin in *Streptomyces ghanaensis* (Makitrynskyy et al., 2013). In parallel, direct overexpression of biosynthetic genes within antibiotic pathways was shown to increase yields, as demonstrated for clavulanic acid in *Streptomces clavuligerus* (Hung et al., 2007) and simocyclinone in S*treptomyces antibioticus* Tü6040 (Horbal et al., 2012).

Metabolic engineering strategies expanded toward precursor supply pathways, recognizing that biosynthesis of secondary metabolites is often limited by the availability of key building blocks. Enhancing precursor flux proved successful in multiple systems: overexpression of the phosphoglucomutase gene *pgm* or the acetyl-CoA carboxylase *ovmGIH* improved intracellular pool of glucose-1-phosphate and malonyl-CoA in *Streptomyces argillaceus* and therefore increased mithramycin production (Zabala et al., 2013). Likewise, overexpression of acetyl-CoA carboxylase increased malonyl-CoA availability and resulted in a six-fold increase in actinorhodin production in *S. coelicolor* (Ryu et al., 2006).

GPA BGCs are tightly controlled by cluster-encoded transcriptional regulators (StrR- and LuxR-like regulators), which have been extensively studied in *A. balhimycina* (Shawky et al., 2007), *Nonomuraea gerenzanensis* (Alduina et al., 2018; Grasso et al., 2015) and *Act. teichomyceticus* (Horbal et al., 2014; Yushchuk et al., 2019). Bbr, a StrR-like regulator, from *A. balhimycina* binds directly to the promoter region of the balhimycin biosynthesis genes (Shawky et al., 2007) and heterologous expression of *bbr* in *A. japonica* activated ristomycin production (Spohn et al., 2014). In *Act. teichomycticus* the overexpression of the StrR-like regulator *tei15** and LuxR-like regulator *tei16** led to increased teicoplanin production (Horbal et al., 2014). Nonetheless, many BGCs with the potential to produce GPAs remain transcriptionally silent under standard laboratory conditions. This means that, although these BGCs encode the full enzymatic machinery required for GPA biosynthesis, their products are

often undetectable, limiting both functional characterization and compound discovery. Even when transcriptional activation is achieved, GPA production can remain limited by metabolic burden and precursor scarcity. Indeed, as mentioned above, GPA synthesis requires large amounts of non-proteinogenic aromatic amino acids (Bht, Hpg and Dpg), which are derived from the shikimate pathway and impose strong demands on central carbon metabolism (Gavriilidou et al., 2024).

Consequently, metabolic engineering of GPA producers has focused on identifying flux-controlling steps and coordinating regulatory activation with precursor supply. A prominent example is the balhimycin producer *A. balhimycina*, where the high demand for tyrosine-derived precursors was identified as a key metabolic bottleneck. Engineering of the shikimate pathway through overexpression of $dahp_{sec}$ and *pdt* increased balhimycin production (Goldfinger et al., 2023; Thykaer et al., 2010).

Regulator-based strategies are a powerful complementary tool to increase GPA production. Overexpression of pathway-specific regulators has improved production in several GPA producers, either via overexpression of endogenous or heterologous expression of StrR-like regulators (Andreo-Vidal et al., 2023; Spohn et al., 2014). In parallel, heterologous expression and chassis development are common strategies in order to decouple complex GPA regulation from native hosts and to standardize production backgrounds (Li et al., 2025; Xu et al., 2020).

1.7 Aim of this work

GPAs are clinically indispensable natural products whose biosynthesis places exceptionally high demands on cellular metabolism, in particular on the shikimate pathway supplying key GPA building blocks. As a consequence, GPA production remains constrained by complex regulatory networks, feedback-controlled primary metabolism, and cryptic or inefficient expression of BGCs.

To overcome these limitations, this work focused on identifying key metabolic and regulatory bottlenecks in GPA production and to develop transferable metabolic engineering strategies to enhance yields and enable the activation of poorly expressed or silent GPA BGCs in actinobacteria.

The first aim was to elucidate the role of shikimate-pathway precursor supply in producers of canonical GPAs. Using *Amycolatopsis* and *Actinoplanes* species as model systems, this work investigated the functional and regulatory diversity of key shikimate-pathway enzymes (Dahp and Pdh), including their cluster-situated isoenzymes. By combining biochemical characterization with targeted overexpression and deletion studies, this study assessed how feedback regulation and enzyme specialization influence aromatic precursor flux and, ultimately GPA production, and how this knowledge can be exploited for yield improvement in industrially relevant strains.

The second aim was to extend metabolic engineering concepts beyond established GPA producers to less characterized strains. Genome mining and *in silico* analysis were used to identify type V GPA BGCs in *Streptomyces* species that differ markedly from canonical GPA BGCs with respect to gene content, regulatory architecture and precursor biosynthetic capacity. Targeted activation strategies, including genetic manipulation of regulatory elements, heterologous expression and metabolic engineering of precursor supply were developed and evaluated. By combining regulatory activation with enhancement of shikimate-pathway derived precursor flux, this work aimed to test integrated activation strategies that align transcriptional control with metabolic capacity for the activation of silent GPA BGCs, with a focus on their applicability to actinomycetes.

Together, this work aimed to establish an experimentally grounded framework for metabolic engineering of GPA biosynthesis, bridging detailed enzymatic insights with applied strategies for activating and improving GPA production in both canonical and non-canonical GPA-producing actinobacteria.

2. Materials and methods

2.1 Bacterial strains and plasmids

The bacterial strains used and generated in this work are listed in Table 1, the plasmids used in this study are listed in Table 2. *Escherichia coli* NovaBlue was used for cloning purposes and *E. coli* ET12567 pUZ8002 was used for conjugation purposes (Kieser et al., 2000).

Table 1: Strains used in this study.

Strain	Relevant feature(s)	Source or reference
Escherichia coli		
NovaBlue	Host for cloning	Novagen
ET12567 pUZ8002	Used for conjugative transfer of plasmid DNA (dam-13::Tn9 dcm-6), pUZ8002 (ΔoriT)	(Kieser et al., 2000)
***Streptomyces varsoviensis* DSM40677**		
***Streptomyces fumanus* JCM 4477**		
***Streptomyces aquilus* JCM 33584**		

Table 2: Plasmids used in this study.

Plasmids	Relevant feature(s)	Source or reference
pSET152	ΦC31-based integrative vector, *apra*^{r}	(Kieser et al., 2000)
pRM4	pSET152 derivative, ΦC31 *attP,* constitutive promoter *ermE**p, *apra*^{r}	(Menges et al., 2007)
pSET152_sp44	pSET152 derivative, ΦC31 *attP,* constitutive promoter *SP44**, *apra*^{r}	(Edenhart et al., 2020)
pIJ10257_sp44	ribosome binding site and multicloning site from pIJ8723 cloned into pMS81, constitutive promoter *SP44**, *hyg*^{r}	This work
pRM4 derivatives		
pRM4_StrR	*staQ*, *tei15**, *kis_strR*, *CNQ525_strR* and *bbr* under the control of *ermE**p	This work
pRM4_Hpg	*hmaS*, *hmO* and *pgat* under the control of *ermE**p	This work
pRM4_Hpg_StrR	*hmaS*, *hmO*, *pgat*, *staQ* and *tei15** under the control of *ermE**p	This work
pRM4_Hpg_Bbr_Dahp	*hmaS*, *hmO*, *pgat*, bbr and $dahp_{sec}$ under the control of *ermE**p	This work
pRM4_Tei16_Dbv3	*tei16** an *dbv3* under the control of *ermE**p	This work
pRM4_Sfu_StrR	$strR_{Sfu}$ under the control of *ermE**p	This work
pRM4_Sfu_LuxR	$luxR_{Sfu}$ under the control of *ermE**p	This work
pRM4_Sfu_StrRLuxR	$strR_{Sfu}$ and $luxR_{Sfu}$ under the control of *ermE**p	This work

pRM4_StAq_StrR	*strR*$_{StAq}$ under the control of *ermE**p	This work
pRM4_StAq_LuxR	*luxR*$_{StAq}$ under the control of *ermE**p	This work
pRM4_StAq_StrRLuxR	*strR*$_{StAq}$ and *luxR*$_{StAq}$ under the control of *ermE**p	This work
pSET152_s44 derivatives		
pSET152_sp44_StrR	*staQ*, *tei15** and *bbr* under the control of *SP44**	This work
pSET152_sp44_Bbr_Dahp_Hpg	*bbr*, *dahp*$_{sec}$, *hmaS*, *hmO* and *pgat* under the control of *SP44**	This work
pIJ10257_sp44 derivatives		
pIJ_sp44_dpg	*dpgA*, *dpgB*, *dpgC and dpgD* under the control of *SP44**	This work

2.2 Plasmid generation

All the plasmids used in this study (Table 2) were cloned following the same principle, unless otherwise mentioned. DNA fragments were amplified using oligonucleotide primers listed in Table 4. The corresponding fragments were cloned into pRM4, pSET152_sp44 or pIJ10257_sp44 via NEBuilder HiFi DNA Assembly (NEB) following the manufacturer´s protocol.

The plasmids pRM4_hpg_strR and pRM4_hpg_bbr_strR were constructed by cloning the DNA fragments containing the erythromycin promoter *ermE**p, *staQ* and *tei15** (2306 bp) or *bbr* (1003 bp) and *dahp*$_{sec}$ (1127 bp) into *Hind*III linearized pRM4_hpg, respectively.

All generated recombinant vectors were verified through restriction digestion and sequencing at Eurofins Genomics.

2.3 Media and culture conditions

Streptomyces varsoviensis, *Streptomyces fumanus* and *Streptomyces aquilus* were grown in 20 ml tryptic soy broth (TSB) on an orbital shaker (120 rpm) as a preculture or for DNA extraction. Spores were harvested from strains grown on mannitol soya flour (MS) agar plates.

For GPA production, the strains were cultivated in R5, Amycolatopsis-medium (AMY) and Streptomyces antibiotic activity medium (SAM) (Table 3) on an orbital shaker (120 rpm) for 5-7 days..

Table 3: Media used in this study.

Medium	Preparation (1L)
R5 medium	103 g Saccharose 0.25 g K_2SO_4 10.12 g $MgCl_2$ (x6H_2O) 10 g Glucose 0.1 g Casaminoacids (Difco) 5 g Yeast extract 5.73 g TES Buffer 2 ml trace element solution pH 7.2 After autoclaving supplement with: 80 mL $CaCl_2$ (3.86%) 10 mL KH_2PO_4 (0.54%) 15 mL L-proline (20%)
Amycolatopsis medium (AMY)	20 g Glucose 20 g Galactose 10 g Bacto Soytone 2 g $(NH_4)_2SO_4$ 2 g $CaCO_3$ pH 7.4
Streptomyces antibiotic activity medium (SAM)	15 g Glucose 15 g Soytone 5 g NaCl 1 g Yeast extract 1 g $CaCO_3$ 2.5 mL Glycerol pH 6.8

2.4 Conjugal transfer of plasmids

Plasmids were transferred into *S. varsoviensis* DSM 40677, *S. fumanus* or *S. aquilus* via intergeneric conjugation (Kieser et al., 2000) using spores. Successful integration of the plasmid into the genome was verified via PCR.

Table 4: Oligonucleotide primers used in this study.

Primer	Nucleotide sequence (5'-3')	Purpose
257_bbr_fw	gcccgctgtgagtggatccgacgagagttgacatattcgct	Cloning of pRM4_StrR
258_bbr_rv	ATATCAAGCTTAGATCTCATAtcatcccgcggccagct	Cloning of pRM4_StrR
259_CNQ525_StrR_fw	tcgcgacctgaatgcgggtcatcgatgggcttca	Cloning of pRM4_StrR
260_CNQ525_StrR_rv	tcggatccactcacagcgggcgggcg	Cloning of pRM4_StrR
261_Kis_StrR_fw	261_Kis_StrR_fw	Cloning of pRM4_StrR
263_Teico_StrR_fw	aaaccgcatagatggagatggagatcagttcactcagcct	Cloning of pRM4_StrR
264_Teico_StrR_rv	tgacccacattcagctcgccatccgctcct	Cloning of pRM4_StrR
265_StaQ_fw	ccatctccatctatgcggtttcggtgaccctgcc	Cloning of pRM4_StrR
266_StaQ_rv	CTAGCCAGGGGAGGACCCATAatgagggagatggcgttgcagc	Cloning of pRM4_StrR

273_pJR10_fw	GCAGGAATTCGATATCAAGCTtcagctcgccatccgctcct	Cloning of pRM4_Hpg_StrR
274_JR10_rv	ggatagTATGAGATCTAAGCTAGGTCCAGCCCGACCCGAG	Cloning of pRM4_Hpg_StrR
275_pJR11_Kis_StrR_rv	275_pJR11_Kis_StrR_rv	Cloning of pRM4_StrR
290_Sfu_luxR_fw	GATAAGCTAGCCAGGGGAGGACCCAgtgaatctcagtgaacgagacggagaactgc	Cloning of pRM4_Sfu_LuxR
291_Sfu_luxR_rv	AATTCGATATCAAGCTTAGATCTCAtcaccgcccgttcggtgagc	Cloning of pRM4_Sfu_LuxR
297_Sfu_StrR_fw	TAAGCTAGCCAGGGGAGGACCCAgtggaacccgaagaggaggaaatcaatcagcaacc	Cloning of pRM4_Sfu_StrR
298_Sfu_StrR_rv	AATTCGATATCAAGCTTAGATCTCAtcagctaatctgtgcgacctcctcctcga	Cloning of pRM4_Sfu_StrR
299_bbr_fw	cgcggctgggatagTATGAGATCTAgtggatccgacgagagttgacatattcgct	Cloning of pRM4_Hpg_Bbr_Dahp
300_bbr_rv	ggtgtgggtcattcatcccgcggccagctcggtcgccc	Cloning of pRM4_Hpg_Bbr_Dahp
301_dahp_fw	ggccgcgggatgaatgacccacaccgtcgc	Cloning of pRM4_Hpg_Bbr_Dahp
302_dahp_rv	CCCGGGCTGCAGGAATTCGATATCAtcagcttgcttgcttgccgagct	Cloning of pRM4_Hpg_Bbr_Dahp
323_SfuStrR_fw	GATAAGCTAGCCAGGGGAGGACCCAgtggaacccgaagaggaggaaatcaatcagcaac	Cloning of pRM4_Sfu_StrRLuxR
324_SfuStrR_rv	CCCGGGCTGCAGGAATTCGATATCAtcaccgcccgttcggtgagcaggggc	Cloning of pRM4_Sfu_StrRLuxR
342_dbv3_fw	acgcagtgtcacctacagccgcactgcctcacg	Cloning of pRM4_dbv3_tei16
343_dbv3_rv	GATAAGCTAGCCAGGGGAGGACCCAgagtgctgttcgggcgagatcgtgaactgaag	Cloning of pRM4_dbv3_tei16
360_StAq_StrR_fw	GATAAGCTAGCCAGGGGAGGACCCAattcaggtactcgcggcggcgcagaat	Cloning of pRM4_StAq_StrR
361_StAq_StrR_rv	CCCGGGCTGCAGGAATTCGATATCAAGCTTtcagccgatctgggcgacgt	Cloning of pRM4_StAq_StrR
362_StAq_LuxR_fw	GATAAGCTAGCCAGGGGAGGACCCAtgtgaagctccatgaaagggacggagaactcggt	Cloning of pRM4_StAq_LuxR
363_StAq_LuxR_rv	CCCGGGCTGCAGGAATTCGATATCAAGCTTtcatctgacattcggcgagcaggaggcct	Cloning of pRM4_StAq_LuxR
376_StAq_StrRLuxR_fw	GTATCGATAAGCTAGCCAGGGGAGGACCCAattcaggtactcgcggcggcgcagaatc	Cloning of pRM4_StAq_StrLuxR
377_StAq_StrRLuxR_rv	GATCCCCCGGGCTGCAGGAATTCGATATCAtcatctgacattcggcgagcaggagg	Cloning of pRM4_StAq_StrLuxR
421_pRM4sp44_hpg_fw	AATTCGATATCAAGCTTAGATCTCActatcccagccgcgcg	Cloning of pSET152_sp44_hpg
422_pRM4sp44_hpg_rv	TCTAAGTAAGGAGTAGGCTGACAttgacttccgattcgactgtccagaatttcgag	Cloning of pSET152_sp44_hpg
423_pRM4sp44_dpg_fw	ATCTAAGTAAGGAGTAGGCTGACAatgacgaccagcatcgaacccgc	Cloning of pSET152_sp44_dpg

424_prM4sp44_dpg_rv	TCGATATCAAGCTTAGATCTCAtcaacccggccggtattcccc	Cloning of pSET152_sp44_dpg
425_pRM4sp44_StrR_fw1	tcggatccactcagctcgccatccgctcctccg	Cloning of pSET152_sp44_StrR
426_pRM4sp44_StrR_rv1	TAAGTAAGGAGTAGGCTGACAatgagggagatggcgttgcagc	Cloning of pSET152_sp44_StrR
427_pRM4sp44_StrR_fw2	ggcgagctgagtggatccgacgagagttgacatattcgct	Cloning of pSET152_sp44_StrR
428_pRM4sp44_StrR_rv2	CGATATCAAGCTTAGATCTCAtcatcccgcggccagc	Cloning of pSET152_sp44_StrR
429_pRM4sp44_hpgbbrdahp_fw1	cggaagtcaatcagcttgcttgcttgccgagcttt	Cloning of pSET152_sp44_hpg_bbr_dahp
430_pRM4sp44_hpgbbrdahp_rv1	TAAGTAAGGAGTAGGCTGACAgtggatccgacgagagttgacatattcgc	Cloning of pSET152_sp44_hpg_bbr_dahp
431_pRM4sp44_hpgbbrdahp_fw2	CGATATCAAGCTTAGATCTCActatcccagccgcgcggtgatgagc	Cloning of pSET152_sp44_hpg_bbr_dahp
432_pRM4sp44_hpgbbrdahp_rv2	agcaagctgattgacttccgattcgactgtccagaatttcgag	Cloning of pSET152_sp44_hpg_bbr_dahp

2.5 Identification of StrR-binding sites

To identify putative StrR-binding sites within GPA BGCs the web-based tool MEME-FIMO (https://meme-suite.org/meme/doc/fimo.html) was used (Bailey et al., 2015). As a input motif the published StrR-binding motif (GTTCGActG NNNNNNNNNNN CagTcGAAC**)** (Shawky et al., 2007) was used to scan the GPA BGCs from *S. fumanus*, *S. varsoviensis* DSM 40677 and *S. aquilus*.

3. Results

3.1 Identification of silent type V GPA BGCs in *Streptomyces* strains

GPA BGCs contain a recruitment domain unique to GPA biosynthesis, called the X-domain. This domain was used to perform an *in silic*o screening of public databases (Gavriilidou et al., 2023) to identify strains harboring a GPA BGC. Three *Streptomyces* strains were identified that harbor BGCs encoding putative type V GPAs (Figure 4). These include *Streptomyces fumanus*, *Streptomyces aquilus* and *Streptomyces varsoviensis*.

Both genomes of *S. fumanus* and *S. aquilus* contain a BGC predicted to encode a decapeptide GPA. Although the overall BGC architectures are similar, the predicted amino acid compositions of the resulting peptides differ. The predicted decapeptide from *S. fumanus* is mainly composed of Dpg, with eight Dpg residues and a central valine (Val)-Tyr motif. In contrast, the predicted decapeptide from *S. aquilus* contains eight Dpg residues and two Hpg residues (Figure 4). Both BGCs contain putative resistance genes, genes encoding StrR-like and LuxR-like transcriptional regulators, and genes involved in Dpg biosynthesis. The putative resistance genes encode a two-component system and a peptidoglycan binding protein. Their involvement in the resistance mechanism has to be experimentally validated. A notable difference between the two BGCs is the number of cytochrome P450 monooxygenases: the *S. fumanus* BGC contains two P450 monooxygenase genes, whereas only a single P450 monooxygenase gene is present in the *S. aquilus* BGC. Despite the predicted presence of Hpg residues in the *S. fumanus* decapeptide, no genes associated with Hpg biosynthesis were identified within the BGC.

For *S. varsociensis*, two distinct BGCs predicted to encode type V GPAs were identified within the same genome. To our knowledge, this represents the first report of a bacterial strain harboring two independent GPA BGCs. BGC 1 encodes a heptapeptide consisting of four Hpg residues, one Trp, one Tyr, and two Dpg residues. In contrast, BGC 2 is predicted to encode a heptapeptide composed exclusively of Dpg residues (Figure 4).

Both BGCs identified in *S. varsoviensis* DSM 40677 encode two P450 monooxygenases but differ substantially in their remaining gene content. BGC 2 contains genes for Dpg biosynthesis, which are absent in BGC 1. In contrast, BGC 1 harbors several regulatory genes and include a gene encoding Dahp, a key enzyme

involved in shikimate-pathway precursor supply. Neither of the *S. varsoviensis* DSM 40677 BGCs encode StrR- or LuxR-like regulators, which are commonly found in canonical GPA BGCs. Additionally, BGC 1 contains two genes encoding putative transporters presumably involved in GPA export.

Overall, the identified BGCs display characteristic features of type V GPA BGCs, including reduced gene content compared to canonical GPA BGCs. Notably, these BGCs lack genes encoding glycosyltransferases, halogenases, methyltransferases, and in some cases, enzymes involved in precursor biosynthesis.

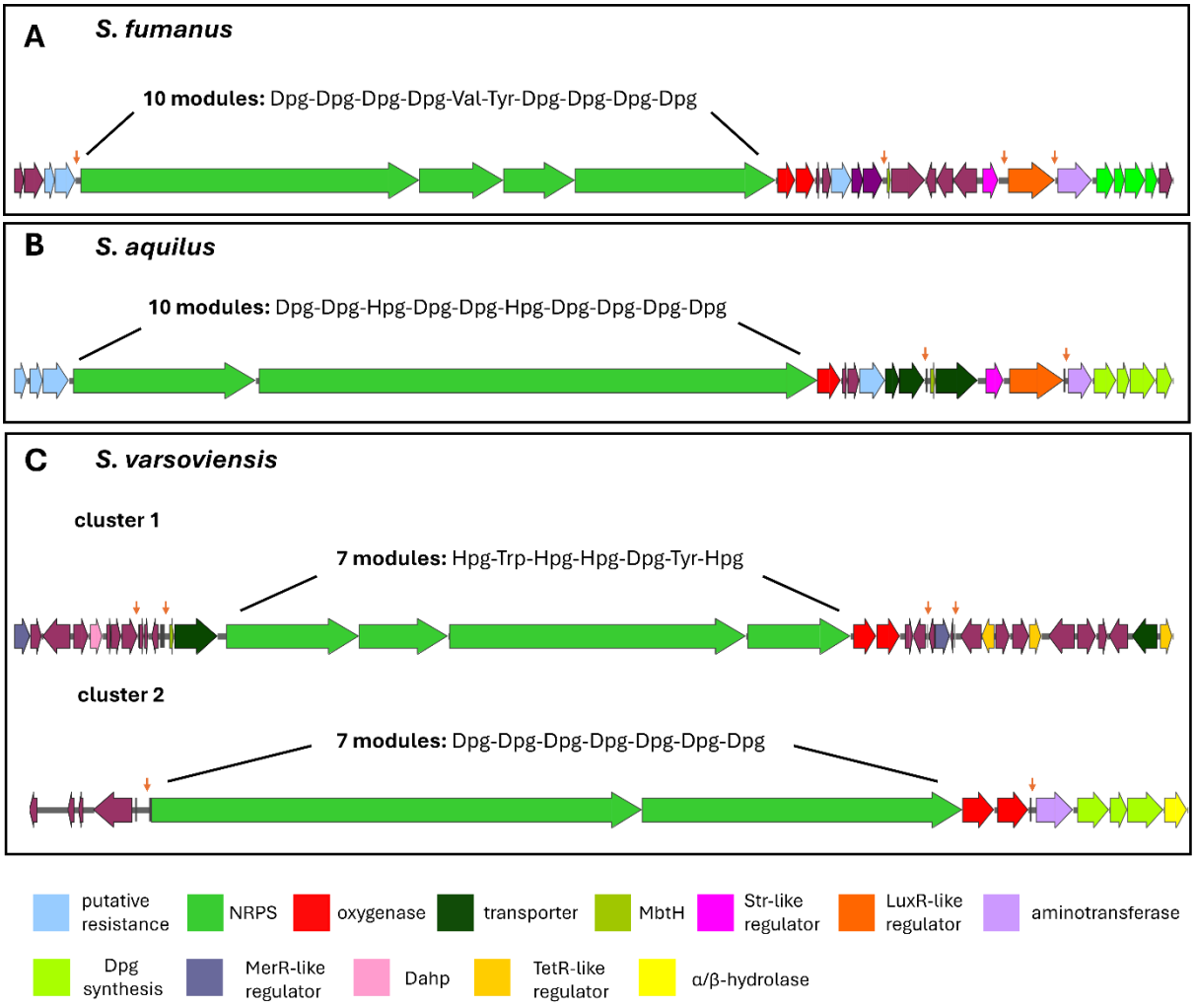

Figure 4: Type V GPA BGCs identified in Streptomyces. [A] *S. fumanus* contains a BGC encoding for type V decapeptide. [B] *S. aquilus* harbors a BGC encoding for type V decapeptde. [C] *S. varsoviensis* DSM 40677 contains two BGCs encoding for type V heptapeptide. Orange arrows indicate identified StrR-binding sites.

Dpg, dihydroxyphenylglycine; Hpg, hydroxyphenylglycine; Tyr, tyrosine; Val, valine.

To evaluate GPA production across all strains, cultures were grown in up to three different GPA production media (R5, SAM and AMY medium). Several peaks were observed in the HPLC-UV/DAD chromatogram (Appendix, Figure A1). The predicted

peptide scaffold of each BGC helps us to estimate the putative mass of each GPA. We calculated this putative mass based on the linear peptide (*S. fumanus*: 1601.51 g/mol; *S. aquilus* 1637.50 g/mol; *S. varsoviensis* DSM 40677 BGC 1: 1129.39g/mol and BGC 2: 1173.31 g/mol) and screened all the MS-chromatograms for a mass in the range of the predicted mass. No GPA-related compounds were detected, indicating that the corresponding GPA BGCs were presumably not expressed under the standard laboratory conditions tested.

3.2 Influence of StrR-like and LuxR-like regulators on GPA production

StrR-like and LuxR-like transcriptional regulators are widely conserved components of GPA BGCs and play a central role in the positive regulation of GPA production. StrR-like regulators typically function as pathway-specific activators by directly binding to conserved promoter elements within the BGC, thereby coordinating the transcription of biosynthetic, tailoring, and resistance genes. LuxR-like regulators are frequently encoded adjacent to StrR-like regulators and further enhance pathway expression, either by activating complementary subsets of biosynthetic genes or by integrating additional regulatory inputs.

Functional studies in multiple GPA-producing actinomycetes, including *Amycolatopsis balhimycina*, *Actinoplanes teichomyceticus* and *Streptomyces toyocaensis* have demonstrated that deletion or inactivation of StrR-like or LuxR-like regulators leads to severe reduction or complete loss of antibiotic production, whereas their overexpression often results in increased GPA titers. Prerequisite for effective regulator-based activation strategies is the presence of conserved StrR binding sites within the target BGC. Accordingly, the BGCs of *S. fumanus*, *S. aquilus* and *S. varsoviensis* DSM 40677 were screened *in silico* for StrR binding motifs using the previously published consensus sequence as a reference (Shawky et al., 2007). This analysis revealed the presence of a binding site upstream of the genes encoding the NRPS in the BGC of *S. fumanus* and *S. varsoviensis* DSM 40677 (Figure 4), and the presence of an StrR binding site upstream of the genes encoding the MbtH-like protein and the aminotransferase Pgat in all clusters. Interestingly, in the BGC of *S. fumanus* an StrR binding site was also predicted upstream of the gene encoding a LuxR-like regulator.

Building on this knowledge, we combined the well characterized StrR-like regulators (*tei15**, *staQ* and *bbr*) with two regulators from a type V GPA BGCs (*kis_strR* and

CNQ525_strR) to construct a plasmid that contains StrR-like regulators from different GPA types. Therefore, the genes *tei15**, *staQ*, *kis_strR* and *bbr* encoding StrR-like regulators from the teicoplanin, A47934, kistamicin and balhimycin BGCs respectively, as well as *CNQ525_strR* from the marine *Streptomyces sp.* CNQ525, were cloned into the integrative vector pRM4 under the control of the constitutive promoter *ermE**p, resulting in the plasmid pRM4_StrR. In addition, a second variant of this regulatory tool was constructed by cloning *staQ, tei15** and *bbr* under control of the synthetic promoter *SP44** into pSET152_sp44, yielding pSET152_sp44_StrR.

Given the previously observed positive effects of LuxR-like regulators on natural product production (Andreo-Vidal et al., 2023; Li et al., 2022), the *luxR* homologs *tei16** and *dbv3* were cloned into pRM4, resulting in the plasmid pRM4_Tei16_Dbv3.

S. fumanus and *S. aquilus* GPA BGCs encode endogenous StrR-like and LuxR-like regulators. These genes were overexpressed either individually or in combination using pRM4-based constructs, resulting in pRM4_Sfu_StrR, pRM4_Sfu_LuxR. pRM4_Sfu_StrRLuxR, pRM4_StAq_StrR, pRM4_StAq_LuxR, and pRM4_StAq_StrRLuxR.

All the generated plasmids were individually introduced in the three *Streptomyces* strains via intergeneric conjugation (see 2.4) and the obtained recombinant strains were verified for integration of the plasmids. At least three clones of each recombinant strain were cultivated in up to three different production media (R5, SAM and AMY). Culture supernatants were extracted using butanol or ethyl acetate. Pellets were extracted using acetone/methanol (50:50). Culture supernatants and all extracts were analyzed by HPLC-MS (data not shown). Representative chromatograms are shown for *S. fumanus* pRM4_StrR and *S. aquilus* pRM4_StrR (Appendix, Figure A2), and for *S. fumanus* pRM4_Tei16_Dbv3 (Appendix Figure A3). Under the experimental conditions tested, no GPA-related compounds were detected in any of the recombinant strains.

3.3 Improving precursor biosynthesis for GPA production

GPA biosynthesis is highly dependent on the availability of aromatic amino acid, in particular Hpg, Bht and Dpg. Canonical GPA BGCs typically encode dedicated gene sets for the biosynthesis of these non-proteinogenic amino acids. Hpg biosynthesis requires L-4-hydroxymandelate synthase (HmaS) and L-4-hydroxymandelate oxidase

(Hmo), while Dpg biosynthesis is mediated by the *dpg* operon, consisting of the type III polyketide synthase *dpgA* and the modifying enzymes *dpgB-D*, which iteratively condense malonyl-CoA units into 3,5-dihydroxyphenylglyoxylate. In both pathways, a dedicated aminotransferase (Pgat) is required to generate the final amino acid product. The primary precursors for Hpg and Bht biosynthesis are derived from the shikimate pathway, whose key enzymes Dahp and Pdh are frequently encoded within GPA BGCs.

The prediction of the amino acid sequence of type V GPAs shows that they consist mainly of Hpg and Dpg moieties (Figure 4). In many cases the corresponding BGCs lack the dedicated genes for the biosynthesis of these building blocks, as it is the case for *S. aquilus*, which lacks Hpg biosynthesis genes or *S. varsoviensis* DSM 40677 where both BGC 1 and BGC 2 lack Hpg biosynthesis genes and BGC 1 lacks the *dpg* operon. Additionally, *dahp* and *pdh* are missing in the BGCs of *S. fumanus*, *S. aquilus* and *S. varsoviensis* DSM 40677 BGC 2 (Figure 4). This motivated us to design plasmids that provide the complete biosynthetic machinery for either Hpg or Dpg biosynthesis or improve precursor supply via heterologous expression of the well-characterized $dahp_{sec}$ gene from *A. balhimycina*, which has previously been shown to positively influence on balhimycin production.

To construct pRM4_Hpg, the corresponding genes for Hpg biosynthesis (*hmO*, *hmaS* and *pgat*) were amplified from the well-characterized balhimycin BGC of *A. balhimycina* and cloned into pRM4 under control of the constitutive promoter *ermE**p. The *dpg*-operon *(dpgA-dpgD*) was amplified from the balhimycin BGC and cloned into a pIJ10257-derivate under the control of the constitutive *SP44** promoter, resulting in pIJ_sp44_dpg. The pRM4-based construct carries an apramycin resistance marker and a ΦC31 attachment site, whereas the pIJ10257-based plasmid confers hygromycin resistance and contains a ΦBT1 attachment site. The two different resistance markers and attachment sites allow us to introduce both plasmids into one strain. With this logic, the *dpg* operon was specifically cloned into a pIJ10257 derivative to enable its use in strains lacking both Hpg- and Dpg-biosynthetic genes.

To improve precursor supply for GPA biosynthesis, we decided to construct a plasmid that is able to simultaneously enhance transcriptional activation of the GPA BGC and increase precursor flux from the shikimate pathway and provide the aromatic amino acid Hpg. To construct this multifunctional precursor-enhancement plasmid, we cloned

dahp$_{sec}$ together with the GPA BGC encoded regulator *bbr* and the Hpg biosynthesis genes *hmaS*, *hmO* and *pgat* into pRM4 under the control of the constitutive promoter *ermE**p, resulting in pRM4_Hpg_Bbr_Dahp.

This plasmid is particularly suited for strains such as *S. aquilus* and *S. varsoviensis* DSM 40677 in which Hpg residues are required for GPA biosynthesis but the corresponding precursor pathway are incomplete or absent.

The plasmids pRM4_Hpg and pRM4_Hpg_Bbr_Dahp were introduced individually into *S. aquilus* and *S. varsoviensis* DSM 40677 via intergeneric conjugation (see 2.4). The plasmid pIJ_Dpg was introduced into *S. fumanus*, into *S. aquilus* WT and *S. varsoviensis* DSM 40677 WT and recombinant strains, carrying prM4_Hpg or pRM4_Hpg_Bbr_Dahp. Integration of the plasmids into the recombinant strains was verified via PCR. At least three clones of each recombinant strain were cultivated in up to three different production media (R5, SAM and AMY). Culture supernatants were extracted using butanol or ethyl acetate. Pellets were extracted using acetone/methanol (50:50). Culture supernatant and all extracts were analyzed via HPLC-MS (data not shown). A representative chromatogram is shown for *S. varsoviensis* pRM4_Hpg_Bbr_Dahp (Appendix, Figure A4).

Despite the effort, all attempts to identify a putative mass corresponding to the predicted GPA structures, even under different production conditions and extraction methods, failed.

4 Discussion

4.1 Type V GPA BGCs in the context of recent phylogeny-driven reclassification

The putative type V GPA BGCs identified in *S. fumanus*, *S. aquilus* and *S. varsoviensis* are consistent with recent phylogenetic and structural analyses that redefine this group as fundamentally distinct from canonical GPAs. A defining feature of all three BGCs is their reduced gene content compared to canonical GPA BGCs, most notably the absence of genes encoding glycosylation, halogenation and other post-aglycone modification enzymes. These characteristics closely match the defining criteria of type V GPAs as described by Gavriilidou et al. (2023). The predicted variability in peptide length and amino acid composition further supports classifying these BGCs as type V GPAs. In particular, the presence of a Trp cross-linked to the central Hpg highlights

their clear divergence from canonical GPA biosynthetic pathways (Gavriilidou et al., 2023). Well described type V GPAs include rimomycin, misaugamycin, corbomycin and GP6738 (M. Xu et al., 2022). Both corbomycin and GP6738 possess nonapeptide scaffolds, however, decapeptide type V GPAs, such as those predicted from *S. fumanus* and *S. aquilus* have not yet been chemically characterized.

In line with these observations, a recent study reported the discovery of new GPAs termed varsomycins, in *Streptomyces varsoviensis* (CGMCC 4.1431) (Li et al., 2025). Varsomycins lack the extensive post-aglycone tailoring modifications characteristic of canonical GPAs and were therefore assigned to the recently defined type V GPA family. Their classification as novel compounds is supported by both their unusually compact and minimal biosynthetic gene cluster architecture, which lacks dedicated genes for regulation, resistance, and precursor biosynthesis, and by their distinct chemical structures, including a 3,5-dihydroxyphenylalanine (Dpa) residue at position 5 and an unprecedented biphenyl cross-link that has not been observed in previously characterized GPAs from other producers (Li et al., 2025).

The 38 kb GPA BGC identified in *S. varsoviensis* (CGMCC 4.1431) is markedly smaller than both BGC 1 (60 kb) and BGC 2 (44 kb) previously identified in *S. varsoviensis* DSM 40677, and encodes only the NRPS, a MbtH-like protein, a transporter, and the P450 monooxygenases. In contrast, BGC 1 and BGC 2 from *S. varsoviensis* DSM 40677 harbor additional genes for Dpg biosynthesis, *dahp*, genes encoding TetR regulators and several genes encoding proteins with unknown function. Notably, the experimentally determined heptapeptide scaffold of the varsomycincs closely resembles the compound structure predicted for BGC 1 from *S. varsoviensis* DSM 40677. In our original analysis, uncertainty regarding the identity of the residue at position 5 led us to assign the closest known match, a Dpg. However, the varsomycincs were shown to incorporate a Dpa at this position (Li et al., 2025). In light of this new structural information, the A-domain specificity and amino acid prediction for BGC 1 should be revisited.

A particularly notable finding in our study is the presence of two independent GPA BGCs within a single genome of *S. varsoviensis* DSM 40677. To date, no other GPA-producing actinomycete has been reported to harbor multiple GPA BGCs. This observation expands the current understanding of genomic organization of GPA

biosynthesis and raises important questions regarding regulatory hierarchy, resource distributions and evolutionary origin.

Structural predictions for both BGC 1 and BGC 2 indicate incorporation of Dpg residues into the heptapeptide scaffold. However, genes required for Dpg biosynthesis are present only in BGC 2 and are absent in BGC 1. In addition, neither BGC encodes canonical pathway-specific regulatory proteins (StrR-like and LuxR-like regulators). Together, these observations suggest that the two BGCs may be subject to distinct regulatory controls or could function in an interdependent manner, with BGC 2 potentially supplying Dpg precursors for the heptapeptide encoded by BGC 1.

As no GPA-related compounds could be detected in *S. fumanus*, *S. aquilus* and *S. varsoviensis* under the conditions tested, the corresponding BGCs are presumed to be transcriptionally silent. Numerous strategies have been developed to activate such silent BGCs, one of the most widely used being the introduction of pathway-specific or heterologous positive regulatory genes placed under the control of a strong constitutive promoter.

The use of pathway-specific transcriptional regulators as primary activation tools is strongly supported by experimental studies across multiple producers of canonical GPAs (Horbal et al., 2014; Spohn et al., 2014; M. Xu et al., 2022; Xu et al., 2020). In these systems, StrR-like and LuxR-like regulators function as master switches that coordinately control the expression of entire BGCs.

One of the best characterized examples is the pathway specific regulator of the balhimycin BGC in *A. balhimycina*. The StrR-like regulator Bbr was shown to be essential for balhimycin biosynthesis by binding upstream of the biosynthetic genes *bbr, tba, oxyA, orf7* and *dvaA* thereby activating their transcription (Shawky et al., 2007). Bbr has also been successfully applied to activate cryptic GPA BGCs in heterologous hosts. In *A. japonica*, heterologous expression of *bbr* under the control of the constitutive promoter *ermE**p enabled detectable production of ristomycin A (Spohn et al., 2014). A similar approach was also used for enhancing ristomycin production in *Amycolatopsis sp.* TNS16 (Liu et al., 2021). In both strains, constitutive overexpression of the native StrR-like regulator also resulted in increased ristomycin production (Liu et al., 2021; Spohn et al., 2014).

Another well studied StrR-like regulator is StaQ from the A47934 GPA BGC from *S. toyocaensis* (Pootoolal et al., 2002). StaQ has been successfully used for activating or increasing production of type V GPA via heterologous expression, as demonstrated for rimomycin, misaugamycin and varsomycin production (Li et al., 2025; M. Xu et al., 2022).

Teicoplanin biosynthesis in *Act. teichomyceticus* is controlled by a dual-regulatory system encoded within the BGC, consisting of the StrR-like regulator Tei15* and the LuxR-like regulator Tei16* (Li et al., 2004; Sosio et al., 2004). These two regulators act cooperatively to activate the teicoplanin production. Deletion of either regulator gene resulted in a loss of teicoplanin production, whereas overexpression led to increased product titers (Horbal et al., 2014). Tei15* directly controls transcription of the majority of genes within the BGC, while Tei16* primarily regulates *tei15** expression, highlighting a hierarchical regulatory network. Given that both *S. fumanus* and *S. aquilus* encode StrR-like and LuxR-like regulators homologous to Tei15* and Tei16*, respectively, overexpression of these regulators, either individually or in combination, appeared a rational strategy for BGC activation. In the recombinant strains, where these regulators were overexpressed, no GPA-related compounds were detected.

The repeated demonstration of StrR-like regulators as master activators of GPA across diverse producer strains, provided the rationale for designing two “superplasmids” (pRM4_StrR and pSET152_sp44_StrR), which combine StrR-like regulator genes from different GPA types.

In addition, cross-regulatory interactions between LuxR-like regulators have been reported. Notably, Tei16* (teicoplanin) and Dbv3 (A40926) were shown to cross-complement the *dbv3** knockout in *N. gerenzanensis* ATCC 39727 and the *tei16** knockout in *Act. teichomyceticus*, respectively (Andreo-Vidal et al., 2023). While heterologous expression of *dbv3* in *Act. teichomyceticus* increased teicoplanin production, *tei16** overexpression in *N. gerenzanensis* did not enhance A40926 production. Based on these findings, the plasmid pRM4_Tei16_Dbv3 was designed to introduce heterologous LuxR-like regulator genes even in strains that encode both StrR-like and LuxR-like regulators within their GPA BGCS.

However, in the recombinant strains no mass signals corresponding to the predicted GPA structures were detected. Although we identified several StrR-binding sites in the BGCs and therefore expected the introduction of regulator genes to promote transcription of biosynthetic genes, it cannot be excluded that additional requirements for productive GPA biosynthesis were not met under the tested conditions. In particular, limited precursor availability, potentially resulting from missing biosynthetic genes or insufficient metabolic flux through the shikimate pathway, may have restricted product formation to levels below the detection limit of HPLC–MS.

To exclude the possibility that the lack of detectable compounds was due to absent or insufficient gene expression under the conditions tested, additional analyses were performed. Transcriptional analyses of the biosynthetic genes were carried out for *S. aquilus* WT and a recombinant strain carrying pRM4_StAq_StrR based on experiments performed by a former master's student (Anna-Katharina Siegert). Detectable transcripts for both *nrps* genes, the regulator *staq_srtR*, and the *dpg*-operon were observed (Appendix, Figure A5), indicating that the core biosynthetic genes were transcriptionally active despite the absence of detectable GPA-related compounds.

Taken together, despite the negative outcomes, the extensive experimental evidence from canonical GPA systems nevertheless strongly validates a regulator-based activation strategy for silent GPA BGCs. In the context of type V GPA BGCs, many of which lack complete endogenous regulatory modules, heterologous expression of well-characterized StrR- and LuxR-like regulators therefore represents a rational and experimentally grounded approach to activate biosynthetic gene expression.

4.2 Metabolic engineering of precursor supply as a complementary activation tool

Beyond transcriptional activation, insufficient precursor availability represents a major bottleneck in the activation of silent BGCs in actinobacteria (Li et al., 2021; Wohlleben et al., 2012). Even when biosynthetic genes are expressed, product formation may remain undetectable if the host cannot sustain sufficient metabolic flux toward the required building blocks. This limitation is particularly striking for type V GPAs, whose biosynthesis relies heavily on non-proteinogenic aromatic amino acids such as Hpg and Dpg, both derived from the shikimate pathway (Gavriilidou et al., 2024).

The incomplete precursor biosynthetic capacity observed in the identified type V BGCs (Gavriilidou et al., 2023) strongly supports the integration of metabolic engineering approaches into activation strategies. A classic example demonstrating that precursor feeding alone can reveal otherwise silent or weakly expressed natural products in actinobacteria is the discovery of calcium-dependent antibiotics (CDAs) in *Streptomyces coelicolor* (Lakey et al., 1983). Subsequent feeding experiments with specific amino acids and precursors analogous altered peptide composition and increased detectable production levels, thereby enabling structural elucidation of CDA derivatives (Hojati et al., 2002).

In the context of type V GPA BGCs, precursor limitation is likely to be even more severe (Gavriilidou et al., 2023; Waglechner et al., 2019). The BGCs identified in *S. fumanus*, *S. aquilus* and *S. varsoviensis* DSM 40677 lack complete biosynthetic pathways for Hpg and/or Dpg, indicating a reliance on host metabolism or exogenous supply. In such systems, feeding with Hpg and/or Dpg represents a powerful strategy to assess whether transcriptionally activated BGCs are capable of product formation.

The plasmid-based precursor supply systems developed in our study extend the rationale of classical feeding experiments into a stable, genetically encoded format. The use of modular plasmids supplying complete Hpg or Dpg biosynthetic pathways therefore enables a logical and scalable activation strategy. By sourcing these genes from the well-characterized balhimycin BGC, the designed constructs leverage enzymes with proven functionality and regulatory compatibility. The use of different antibiotic resistance markers and vectors further enhances flexibility, enabling the simultaneous introduction of multiple activation tools into a single host.

Despite this rational design, HPLC-MS analysis of recombinant strains harboring pRM4_Hpg and/or pIJ_sp44_dpg did not reveal detectable GPA-related compounds under the conditions tested. Combinatorial strategies integrating heterologous expression of StrR-like regulator genes together with the Hpg biosynthetic genes (pRM4_Hpg_StrR), in conjunction with expression of the *dpg* operon (pIJ_sp44_dpg), failed to yield detectable mass signals corresponding to the predicted GPA structures.

In contrast, a similar approach proved successful in the recent discovery of varsomycins. In that study, the corresponding BGC was heterologously expressed in *S. coelicolor* M1154, combined with the expression of the conserved StrR-like regulator

gene *staQ*, and the strain supplemented with Hpg and Dpg. Alternatively, *staQ* expression was combined with heterologous expression of Hpg and Dpg biosynthesis genes. Both strategies resulted in successful production of varsomycins in an optimized heterologous host (Li et al., 2025).

Of particular interest in our present study is the multifunctional plasmid combining $dahp_{sec}$, *bbr* and Hpg biosynthesis genes. This design directly addresses two major limitations of silent BGC activation; insufficient precursor flux from the shikimate pathway and inadequate transcriptional activation of the BGC. By coupling a pathway-specific regulator with a key precursor supplying enzymes, this construct exemplifies an integrated activation strategy that aligns with current trends in metabolic engineering. However, the introduction of this plasmid (pRM4_Hpg_Bbr_Dahp) into the tested strains did not result in the detection of GPA-related metabolites under the experimental conditions tested, indication that additional regulatory or host-specific constraints likely limit detectable production or activation of the BGC.

Activation of silent GPA BGCs in *S. fumanus*, *S. aquilus* and *S. varsoviensis* proved to be challenging, as none of the applied rational activation strategies resulted in detectable mass signals corresponding to the predicted GPA structures. To further exclude insufficient gene expression as limiting factor, comprehensive transcriptional analyses of all recombinant strains could be performed. Notable, recent studies reporting the discovery of new type V GPAs have predominantly relied on heterologous expression of the corresponding BGC in optimized host strains rather than native producers (Li et al., 2025; M. Xu et al., 2022; Xu et al., 2020). Accordingly, a logical next step is the heterologous expression of these BGCs in suitable chassis strains such as *Streptomyces coelicolor* M1154 (Gomez-Escribano and Bibb, 2011) or *A. japonica* DI (Hansen et al., 2023), the latter lacking the native ristomycin NRPS genes (*rpsA-rpsD*) and having been successfully employed for the production of the ancient GPA paleomycin.

Such combined activation strategies are particularly relevant for type V GPA BGCs, which frequently lack genes for precursor biosynthesis and therefore depend strongly on host metabolic capacity (Gavriilidou et al., 2023). In producer strains such as *S. aquilus* and *S. varsoviensis* DSM 40677, where Hpg biosynthesis are absent despite an apparent requirement for this precursor, targeted precursor supplementation is likely prerequisite for detectable GPA production. Importantly, the

regulatory and activation strategies explored in this present study can be readily transferred to heterologous expression systems carrying type V GPA BGCs, providing a robust framework for activating silent BGCs and improving GPA production in engineered hosts.

5. Publications

5.1 Publication 1: Metabolic engineering of the shikimate pathway in *Amycolatopsis* strains for optimized glycopeptide antibiotic production

Valentina Goldfinger, Marius Spohn, **Jens-Peter Rodler**, Melanie Sigle, Andreas Kulik, Max J. Cryle, Johanna Rapp, Hannes Link, Wolfgang Wohlleben, Evi Stegmann

Metabolic Engineering, Volume 78, July 2023, Pages 84-92

https://doi.org/10.1016/j.ymben.2023.05.005

5.1.1 Summary of results

GPAs such as type I vancomycin and type IV teicoplanin represent an important class of natural products used to treat infections caused by multidrug-resistant Gram-positive pathogens, including methicillin-resistant *Staphylococcus aureus* (MRSA). Despite their medical relevance, GPA production is often limited by the tight regulation and provision of precursor supply in actinomycetes, creating a major bottleneck for efficient biosynthesis.

GPAs possess a highly crosslinked and glycosylated heptapeptide core composed largely of aromatic non-proteinogenic amino acids, including Hpg, Bht and Dpg. Hpg and Bht are derived from 4-hydroxyphenylpyruvate (4-HPP) and Tyr , respectively, which are produced via the shikimate pathway. In addition, Tyr serves as the amino group donor for Hpg and Dpg biosynthesis. The shikimate pathway is tightly regulated through feedback inhibition mediated by its end products (Tyr, Phe and Trp), creating a major bottleneck in the supply of aromatic precursors required for GPA biosynthesis. GPA producers harbor duplicated copies of the key shikimate pathway genes, *dahp* and *pdh*. While the primary copies ($dahp_{prim}$ and pdh_{prim}) support essential metabolism, secondary copies ($dahp_{sec}$ and pdh_{sec}) are encoded within the GPA BGC, suggesting an evolutionary strategy to uncouple antibiotic biosynthesis from feedback control.

These gene duplications have been proposed to represent a specialized regulatory adaptation that allows GPA producers to partially circumvent feedback inhibition and sustain precursor flux during antibiotic biosynthesis.

The goal of the study was to i) characterize the biochemical properties and regulatory behavior of primary-metabolism enzymes ($Dahp_{prim}$ and Pdh_{prim}) versus BGC encoded enzymes ($Dahp_{sec}$ and Pdh_{sec}), and ii) determine how target manipulation of these nodes, along with the Phe branch pathway, affects GPA production in *A. balhimycina*. The optimized metabolic engineering strategy was applied to *A. japonica* to enhance the production of ristomycin A, a diagnostically relevant type III GPA.

Comparative BlastP sequence analysis revealed substantial divergence between isoenzymes, indicating functional specialization. In *A. balhimycina* the $Dahp_{prim}$ and $Dahp_{sec}$ share 58% identity and the two Pdh enzymes share 38% identity.

Both sets of genes were cloned, heterologously expressed in *E. coli*, the corresponding enzymes were purified via Ni-NTA affinity chromatography and were subjected to

kinetic and inhibition assays to compare their catalytic properties and allosteric regulation.

Dahp catalyzes the first committed step of the shikimate pathway, condensing E4P and PEP to form DAHP. $Dahp_{prim}$ and $Dahp_{sec}$ exhibited similar kinetic behavior toward PEP, with K_M values of ca. 8-10 µM and comparable V_{max} values (Publication 1: Table 4, Figure S2). However, $Dahp_{sec}$ showed a 3-fold higher affinity for E4P (K_M = 46 µM vs. K_M = 134 µM for $Dahp_{prim}$) but a lower maximal V_{max}, suggesting that $Dahp_{sec}$ is finetuned for efficiency under substrate-limited conditions (Publication 1: Table 4, Figure S2). The regulatory behavior was studied in enzyme assays in the presence of aromatic amino acids Tyr, Phe and Trp, which are known feedback inhibitors of the shikimate pathway. Striking differences were revealed in the allosteric regulation of $Dahp_{prim}$ and $Dahp_{sec}$. Tyr and Phe strongly inhibited $Dahp_{prim}$, reducing activity to 56% and 67%, respectively, and to 39% when supplied together (Publication 1: Table 5, Table S1, Table S2). In contrast, $Dahp_{sec}$ was inhibited only by Tyr (to ~33%), while Phe caused minimal inhibition (~90% residual activity). When Phe and Tyr were added together, Phe partially antagonized the Tyr-dependent inhibition, restoring the activity to ~ 60%. The reaction rates of both enzymes were not affected by addition of Trp (Publication 1: Table 5, Table S1, Table S2). These results demonstrate that $Dahp_{sec}$ is less tightly regulated by end-product inhibition, retaining activity under high intracellular Phe concentrations, indicating an evolutionary adaptation to support continuous precursor supply during intense antibiotic production.

Pdh catalyzes the oxidative decarboxylation of prephenate to 4-HPP with reduction of NAD^+ to NADH, representing the final branching point toward Tyr biosynthesis. The kinetic properties of the two Pdh isoenzymes were studied by measurements based on NADH formation at 340 nm. Pdh_{prim} displayed a 100-fold higher affinity for prephenate compared to Pdh_{sec} (Pdh_{prim} K_M = ~920 µM, Pdh_{sec} K_M = ~10 µM). Both enzymes exhibited a comparable catalytic rate (Pdh_{prim} V_{max} = 57.6 µM min^{-1}, Pdh_{sec} V_{max} = 44. µM min^{-1}) (Publication 1: Table 6, Figure S5). Regarding their allosteric regulation, that neither enzyme was inhibited by Tyr or Phe (Publication 1: Table 7, Figure S7). These findings imply that the major regulatory checkpoint within the shikimate pathway operates at $Dahp_{sec}$.

To assess how these biochemical differences translate into cellular metabolism, we manipulated the expression of *$dahp_{prim}$, $dahp_{sec}$*, *pdh_{prim}* and *pdh_{sec}* in *A. balhimycina*,

and quantified balhimycin titers via HPLC. Each gene was either overexpressed using the constitutive promotor *ermE**p or deleted via homologous recombination. Attempts to delete pdh_{prim} were unsuccessful, even after screening more than ~100 clones, suggesting that the gene is essential for primary metabolism.

In *A. balhimycina* WT balhimycin production accounted for 0.04 ± 0.006 mg/ml per mg/ml protein in culture. The overexpression of $dahp_{sec}$ yielded a 4.4-fold increase in production, whereas $dahp_{prim}$ overexpression reduced yield. Deletion of $dahp_{prim}$ or $dahp_{sec}$ decreased production by 37% and 17%, respectively (Publication 1: Figure 2). These results indicate that both Dahp enzymes contribute to overall shikimate flux, but only $Dahp_{sec}$ specifically enhances precursor supply for secondary metabolism.

Overexpression of either pdh_{prim} or pdh_{sec} reduced balhimycin production to 46% and 39% of wild type levels, likely due to excessive Tyr accumulation, which inhibits $Dahp_{sec}$ and decreases shikimate-pathway flux (Publication 1: Figure 2).

Given the Tyr-mediated inhibition of $Dahp_{sec}$ and the antagonistic role of Phe, we supplemented *A. balhimycina* cultures with 5 mM Phe and quantified balhimycin titers. Phe feeding doubled production relative to the wild type (Publication 1: Figure 2), confirming the hypothesis that high concentrations of Phe may partially reverse the inhibitory effect of Tyr. Consistently, overexpression of prephenate dehydratase (Pdt), which converts prephenate to phenylpyruvate, the direct Phe precursor (Publication 1: Figure 1), increased balhimycin titers 4-fold, reaching levels similar to those obtained by $dahp_{sec}$ overexpression (Publication 1: Figure 2).

To determine whether these findings are generalizable across GPA producers, we applied the same metabolic engineering strategy to *A. japonica*, the natural producer of ristomycin A. The ristomycin heptapeptide backbone contains seven aromatic non-proteinogenic amino acids, creating a particularly high demand for shikimate-derived precursors. We overexpressed the pathway-specific transcriptional activator *ajrR* under *ermE**p to generate a stable chassis strain, *A. japonica* $ajrR^+$. The recombinant strain produced 25-fold more ristomycin A than the wildtype strain. Introducing additional copies of *pdt* and $dahp_{sec}$ from *A. balhimycina* into the chassis strain further increased production. Ristomycin levels increased 28-fold in in *A. japonica* $ajrR^+/pdt^+$ and 35-fold in *A. japonica* $ajrR^+/pdt^+/dahp_{sec}{}^+$ (Publication 1: Figure 3). The optimized

strain produced 1.68 ± 0.18 g/l ristomycin A after 120 h of fermentation, equivalent to 130 mg ristomycin A per cell dry weight and a production rate of 1.1 mg/h/g DCW.

Collectively, these results demonstrate that metabolic control within the shikimate pathway is a key determinant of GPA production. Targeted manipulation of *dahp*$_{sec}$ and *pdt* provided a powerful and broadly applicable strategy for yield optimization in industrial antibiotic producers.

5.1.2 Publication 1

Metabolic engineering of the shikimate pathway in Amycolatopsis strains for optimized glycopeptide antibiotic production

Author list:
*Valentina Goldfinger[a,1,4], Marius Spohn[a,2,4], **Jens-Peter Rodler[b]**, Melanie Sigle[a,3], Andreas Kulik[a,b], Max J. Cryle[c,d,e], Johanna Rapp[f], Hannes Link[f,g], Wolfgang Wohlleben[a,h], Evi Stegmann[a,b,h,*]*

Author affiliations and footnotes:
[a]Interfaculty Institute of Microbiology and Infection Medicine Tübingen, Microbiology/Biotechnology, University of Tübingen, Auf der Morgenstelle 28, 72076, Tübingen, Germany
[b]Interfaculty Institute of Microbiology and Infection Medicine Tübingen, Microbial Bioactive Compounds, University of Tübingen, Auf der Morgenstelle 28, 72076, Tübingen, Germany
[c]Department of Biochemistry and Molecular Biology, The Monash Biomedicine Discovery Institute, Monash University, Clayton, VIC, 3800, Australia
[d]EMBL Australia, Monash University, Clayton, VIC, 3800, Australia
[e]ARC Centre of Excellence for Innovations in Peptide and Protein Science, Monash University, Clayton, VIC, 3800, Australia
[f]Interfaculty Institute of Microbiology and Infection Medicine Tübingen, Bacterial Metabolomics, University of Tübingen, Auf der Morgenstelle 25, 72076, Tübingen, Germany
[g]Interfaculty Institute of Microbiology and Infection Medicine Tübingen, Cluster of Excellence CMFI, Bacterial Metabolomics University of Tübingen, Auf der Morgenstelle 25, 72076, Tübingen, Germany
[h]German Centre for Infection Research (DZIF), Partner Site Tübingen, Tübingen, Germany
[*]Corresponding author. Interfaculty Institute of Microbiology and Infection Medicine Tübingen, Microbial Bioactive compounds, University of Tübingen, Auf der Morgenstelle 28, 72076, Tübingen, Germany.

[1]Present Address: Immatics Biotechnologies GmbH, Paul-Ehrlich-Str. 15, 72076 Tübingen, Germany.
[2]Present Address: Fraunhofer Institute for Molecular Biology and Applied Ecology (IME), Branch for Bioresources, Ohlebergsweg 12, Gießen, 35392, Germany.
[3]Present Address: Interfaculty Institute for Cell Biology, Department of Immunology, University of Tübingen, Auf der Morgenstelle 15, 72076 Tübingen, Germany.
[4]Authors contributed equally.

Abstract

Glycopeptide antibiotics (GPA) consist of a glycosylated heptapeptide backbone enriched in aromatic residues originating from the shikimate pathway. Since the enzymatic reactions within the shikimate pathway are highly feedback-regulated, this raises the question as to how GPA producers control the delivery of precursors for GPA assembly. We chose *Amycolatopsis balhimycina*, the producer of balhimycin, as a model strain for analyzing the key enzymes of the shikimate pathway. *A. balhimycina* contains two copies each of the key enzymes of the shikimate pathway, deoxy-D-arabino-heptulosonate-7-phosphate synthase (Dahp) and prephenate dehydrogenase (Pdh), with one pair ($Dahp_{sec}$ and Pdh_{sec}) encoded within the balhimycin biosynthetic gene cluster and one pair ($Dahp_{prim}$ and Pdh_{prim}) in the core genome. While overexpression of the *dahp*$_{sec}$ gene resulted in a significant (>4-fold) increase in balhimycin yield, no positive effects were observed after overexpression of the *pdh*$_{prim}$ or *pdh*$_{sec}$ genes. Investigation of allosteric enzyme inhibition revealed that cross-regulation between the tyrosine and phenylalanine pathways plays an important role. Tyrosine, a key precursor of GPAs, was found to be a putative activator of prephenate dehydratase (Pdt), which catalyzes the first step reaction from prephenate to phenylalanine in the shikimate pathway. Surprisingly, overexpression of *pdt* in *A. balhimycina* led to an increase in antibiotic production in this modified strain.
In order to demonstrate that this metabolic engineering approach is generally applicable to GPA producers, we subsequently applied this strategy to *Amycolatopsis japonicum* and improved the production of ristomycin A, which is used in diagnosis of genetic disorders.

Graphical Abstract

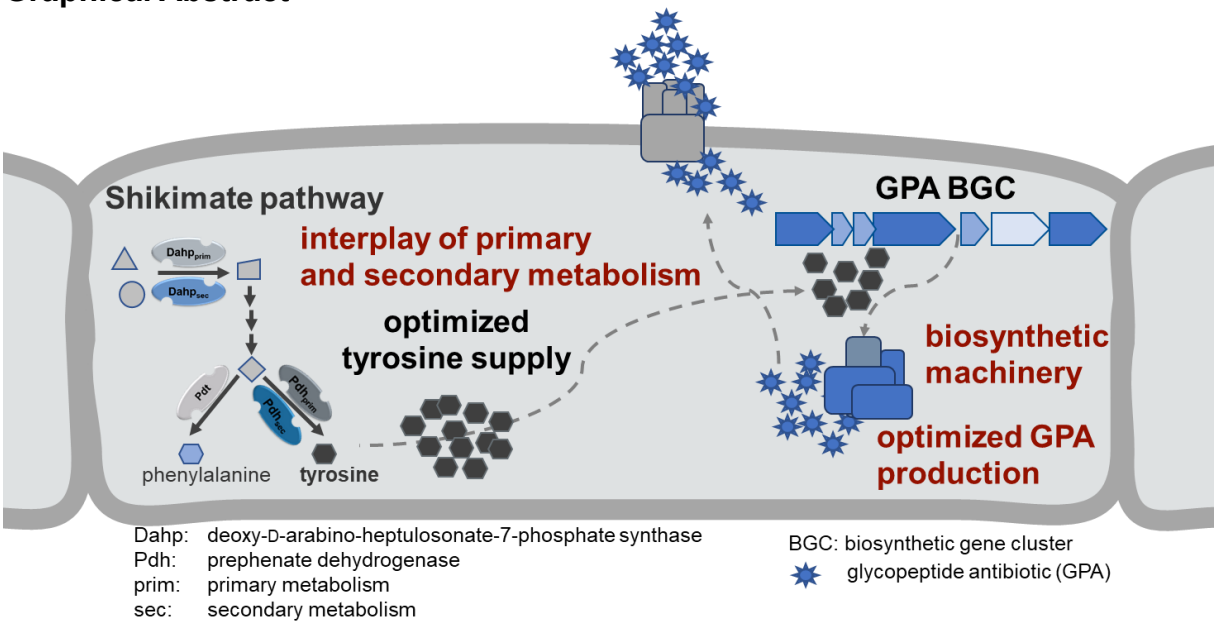

Keywords
balhimycin, ristomycin, precursor optimization, aromatic amino acids, GPA, shikimate pathway, pathway engineering

Abbreviations
Asn, asparagine; BGC, biosynthetic gene cluster; DAHP, deoxy-D-arabinoheptulosonate 7-phosphate; Dahp, deoxy-D-arabino-heptulosonate 7-phosphate synthase; Dpg, 3,5-dihydroxyphenylglycine; GPA, glycopeptide antibiotic; Hpg, 3hydroxyphenylglycine; 4-HPP, 4-hydroxyphenylpyruvate; *β*-Ht, *β*-hydroxytyrosine; Leu, leucine; Pdh, prephenate dehydrogenase; Phe, phenylalanine; Pdt, pheprephenate dehydratase; Trp, tryptophan; Tyr, tyrosine.

Introduction

The glycopeptide antibiotics (GPAs), including vancomycin (type I) and teicoplanin (type IV) are important antibiotics in clinical use against multidrug-resistant Gram-positive pathogens, especially methicillin-resistant bacteria (Nicolaou et al., 1999). Increasing bacterial resistance to antibiotics has led to the development of second-generation GPAs to overcome resistance to these antibiotics (Blaskovich et al., 2018). However, their dependence on *in vivo* biosynthesis of the GPA heptapeptide core limits their production. Beyond antibiotic activity, the GPA ristomycin A (also called ristocetin A; type III) (Grundy et al., 1956) is applied to detect widespread hereditary genetic disorders such as von Willebrand disease and Bernard-Soulier syndrome (Sarji et al., 1974). Given the importance of GPAs and our reliance on their biosynthesis, it is necessary to understand and optimize their biosynthesis in producer strains.

Type I-IV GPAs are composed of seven amino acids and are assembled by non-ribosomal peptide synthesis. The heptapeptide backbone of type I GPAs consists of two proteinogenic (leucine (Leu) and asparagine (Asn)) and five non-proteinogenic amino acids, with the latter including *β*-hydroxytyrosine (*β*-Ht) at positions 2/6, 3hydroxyphenylglycine (Hpg) at positions 4/5 and 3,5-dihydroxyphenylglycine (Dpg) at position 7. The aromatic side chains of these non-proteinogenic amino acids are crosslinked by cytochrome P450 enzymes to form a rigid, cup-shaped structure that binds to its target, the D-alanyl-D-alanine (D-Ala-D-Ala) terminus of bacterial cell wall precursors. The various type I GPAs can be distinguished by differences in glycosylation, methylation and chlorination patterns, while retaining the same amino acid sequence. The heptapeptide backbone of ristomycin (type III) and teicoplanin-like (type IV) GPAs differs from type I backbones by the exchange of Leu and Asn by Hpg and Dpg, respectively. Type IV GPAs also lack the β-hydroxyl group on tyrosine (Tyr) at position 2. The aromatic side chains of Hpg-1 and Dpg-3 are additionally crosslinked in type III and IV GPAs.

The biosynthesis, regulation of GPAs and self-resistance mechanism of their producers have been elucidated in detail (reviewed e.g. in Stegmann et al., 2010; Wohlleben et al. 2012; Hansen et al, 2022; Zhao et al., 2021, Stegmann et al., 2014; Unsleber et al., 2019; and Kilian et al., 2016; Menges et al., 2007; Shawky et al., 2007). The limited genetic accessibility of the vancomycin producer *Amycolatopsis orientalis* was the reason for investigating numerous aspects on the model of vancomycin-like antibiotic balhimycin (differing only in glycosylation pattern from vancomycin), produced by *Amycolatopsis balhimycina*. Furthermore, essential biosynthetic steps in GPA biosynthesis have been biochemically characterized, include oxygenase, halogenase reactions as well as the synthesis of the heptapeptide backbone by the non-ribosomal peptide synthetases (Geib et. al., 2010; Puk et al., 2004, Mulyani et al., 2010; Greule et al., 2019; Hansen et al., 2022; Haslinger et al., 2015; Peschke et al., 2017; Schoppet et al., 2019).

GPA biosynthesis requires the supply of nonproteinogenic amino acids, provided by the conversion of primary metabolites predominantly from the shikimate pathway (hydroxyphenylpyruvate (4-HPP) and Tyr). For high-yield GPA production, the availability of nonproteinogenic aromatic amino acids Hpg, Dpg, *β*-Ht may be a limiting factor. Redirecting and manipulating primary metabolism to increase this precursor pool is therefore a viable approach to increase the yield of GPA biosynthesis (Thykaer

et al., 2010). The biosynthesis of *β*-Ht and Hpg requires the aromatic amino acid Tyr and 4-HPP, respectively, as precursors (Hubbard et al., 2000; Puk et al., 2004). In addition, Tyr is also the amino group donor in the biosynthesis of Hpg and Dpg (Pfeifer et al., 2001) (Fig. 1). The extensive requirement for Tyr and 4-HPP highlights the importance of the shikimate pathway for the synthesis of GPAs. 3-Deoxy-D-arabinoheptulosonate 7-phosphate (DAHP) synthase (Dahp) is the first enzyme of the shikimate pathway, condensing the pentose phosphate pathway intermediate Derythrose-4-phosphate and the glycolytic pathway intermediate phosphoenol pyruvate to form DAHP. Prephenate dehydrogenases (Pdh) facilitate the generation of 4-HPP that is further processed into Tyr via transamination (Fig. 1). Since the shikimate metabolism is tightly regulated by feedback mechanisms (Kloosterman et al., 2003; Lutke-Eversloh and Stephanopoulos, 2007), bacteria have developed alternative mechanisms to circumvent this regulation to ensure the supply of precursors for secondary metabolism. Producers of GPAs, for example, have acquired a second copy of the key shikimate pathway genes *dahp* and *pdh*, which are found within GPA biosynthetic gene clusters (BGCs).

To understand the effects of these additional shikimate pathway genes, the role of $dahp_{sec}$ and pdh_{sec} in the balhimycin BGC has been studied by overexpression and deletion in *A. balhimycina*. Overexpression of $dahp_{sec}$ alone and in combination with pdh_{sec} significantly enhanced balhimycin production, whereas overexpression of pdh_{sec} decreased balhimycin yield (Thykaer et al., 2010). The deletion of $dahp_{sec}$ resulted in lower balhimycin production, while deletion of pdh_{sec} showed no significant effect compared to the wild type.

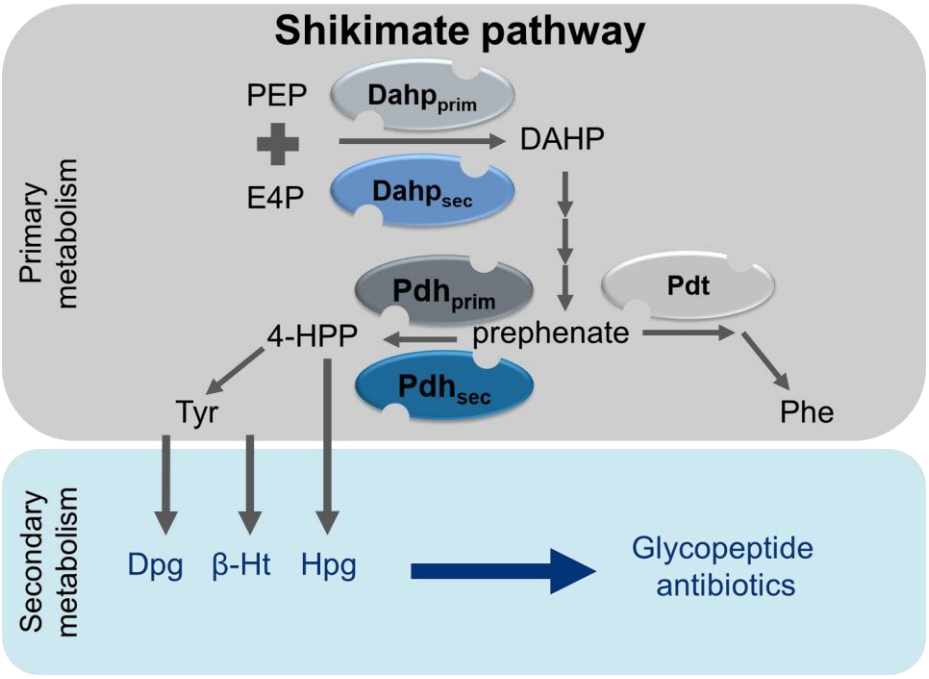

Figure 1: Interplay of primary and secondary metabolism within glycopeptide antibiotic producer strains

$dahp_{prim}$ and pdh_{prim}: genes encoding the key enzymes of the shikimate pathway (Dahp, 3-deoxy-D-arabinoheptulosonate-7-phosphate synthase and Pdh, prephenate dehydrogenase) $dahp_{sec}$ and pdh_{sec}: genes located in the balhimycin biosynthetic gene cluster encoding Dahp and Pdh isoenzymes,
Pdt, prephenate dehydratase; PEP, phosphoenolpyruvate; E4P, erythrose-4phosphate; DAHP, 3-deoxy-D-arabino-heptulosonate 7-phosphate; 4-HPP, 4hydroxyphenylpyruvate; Tyr, tyrosine; Phe, phenylalanine; Dpg, 3,5dihydroxyphenylglycine; *β*-Ht, *β*-hydroxytyrosine; Hpg, 4-hydroxyphenylglycine.

Given these results, further studies are warranted to unlock the mechanistic details that underpin these complex *in vivo* results. In this study we investigated the enzymatic properties of the BGC encoded $Dahp_{sec}$ and Pdh_{sec} from the *A. balhimycina* in comparison to their isoenzymes from the primary metabolism. We particularly emphasized their allosteric feedback inhibition by the three proteinogenic aromatic amino acids. The understanding gained enabled us to streamline the production of the commercially relevant ristomycin A in *Amycolatopsis japonicum,* to yields of up to 1.68 ± 0.18 g/l, demonstrating the general importance of metabolic engineering approaches to increase the production of GPAs in commercial producer strains, thereby improving our access to these important secondary metabolites for future clinical application.

Material and Methods

Bacterial strains and plasmids

The strains used in this study are listed in Table 1 and the plasmids used for this study are listed in Table 2. *Escherichia coli* XL1-blue and NovaBlue were used for cloning purposes, *Escherichia coli* Rosetta 2(DE3) pLyssS was used for protein expression and the methylation-deficient strain *E. coli* ET12567 was used to obtain unmethylated DNA for the transformation of *Amycolatopsis balhimycina* and *Amycolatopsis japonicum.*

Table 4: Strains used in this study.

Strain	Relevant feature(s)	Source or reference
Escherichia coli		
XL1-Blue	host for cloning	Bullock et al., 1987
ET12567	methylation-deficient strain	MacNeil et al., 1992
NovaBlue	host for cloning	Novagen
Rosetta 2(DE3) pLyssS	host for protein expression	Novagen
Amycolatopsis balhimycina		
DSM 5908	Wild type, balhimycin producer	Nadkarni et al., 1994b
$dahp_{prim}^{+}$	*dahp*$_{prim}$ (GenBank ID: FN594522.1) overexpression strain	this work
$dahp_{sec}^{+}$	*dahp*$_{sec}$ overexpression strain	Thykaer et al., 2010
pdh_{prim}^{+}	*pdh*$_{prim}$ (GenBank ID: FN594521.1) overexpression strain	this work
pdh_{sec}^{+}	*pdh*$_{sec}$ overexpression strain	Thykaer et al., 2010
pdt^{+}	*pdt* (GenBank ID: OQ352441) overexpression strain	this work
$dahp_{sec}^{+}/pdt^{+}$	*dahp*$_{sec}$ and *pdt* overexpression strain	this work
$\Delta dahp_{prim}$	*dahp*$_{prim}$ deletion mutant	this work
$\Delta dahp_{sec}$	*dahp*$_{sec}$ deletion mutant	Thykaer et al., 2010
Δpdh_{sec}	*pdh*$_{sec}$ deletion mutant	Thykaer et al., 2010
Amycolatopsis japonicum		
MG417-CF17	Wild type, ristomycin producer	Nishikiori et al., 1984
$ajrR^{+}$	*ajrR* overexpression strain	Spohn et al., 2014
$ajrR^{+}/pdt^{+}$	*ajrR* and *pdt* overexpression strain	this work
$ajrR^{+}/pdt^{+}/dahp^{+}$	*ajrR, pdt* and *dahp* overexpression strain	this work

Table 5: Plasmids used in this study.

Plasmids	Relevant feature(s)	Source or reference
pJET derivatives		
pJET1.2/blunt	Blunt end cloning vector, *apra*^{r}	Fermentas
pJET*pdt*	pJET with *pdt*	this work
pJET*dahp*$_{sec}$	pJET with *dahp*$_{sec}$	this work
pJET*dahp*$_{prim}$	pJET with *dahp*$_{prim}$	this work
pJETdahpF1	pJET with flanking region 1 for deletion of *dahp*$_{prim}$	this work
pJETdahpF2	pJET with flanking region 2 for deletion of *dahp*$_{sec}$	this work
pRM4 derivatives		
pRM4	pSET152 derivative, ΦC31 *attP,* constitutive promoter *ermE**p, *apra*^{r}	Menges et al., 2007
pRM4*pdt*	*pdt* under the control of *ermE**p	this work
pRM4*dahp*$_{sec}$*pdt*	*pdt* and *dahp*$_{sec}$ under the control of *ermE**p	this work
pRM4*dahp*$_{prim}$	*dahp*$_{prim}$ under the control of *ermE*p*	this work
pRM4*pdh*$_{prim}$	*pdh*$_{prim}$ under the control of *ermE*p*	this work
pIJ10257 derivatives		
pIJ10257	ΦBT1 *attP*, *ermE**p, *hyg*^{r}	Bibb et al, 1985
pIJ-*ajrR*	*ajrR* under the control of *ermE**p	this work
Plasmids for Expression of Recombinant Proteins		
pET-30 Ek/LIC	expression vector, T7lac promoter, *kanr*, N-terminal fusion tags, optional C-terminal His-Tag	Novagen
pET-30*dahp*$_{prim}$	construct for heterologous production of 6xHis Dahp$_{prim}$ from *A. balhimycina*	this work
pET-30*dahp*$_{sec}$	construct for heterologous production of 6xHis Dahp$_{sec}$ from *A. balhimycina*	this work
pET-30*pdh*$_{prim}$	construct for heterologous production of 6xHis Pdh$_{prim}$ from *A. balhimycina*	this work
pET-30*pdh*$_{sec}$	construct for heterologous production of 6xHis Pdh$_{sec}$ from *A. balhimycina*	this work
pSP1 derivatives		
pSP1	non-replicative plasmid, *amp*^{r}, *ery*^{r}	Pelzer et al., 1977
pSPΔ*dahp*$_{prim}$	contains flanking region for deletion of *dahp*$_{prim}$	this work

Media and culture conditions

Amycolatopsis balhimycina was precultured from R5-agar plates in 20 ml of R5 medium for 2 days at 27 °C on an orbital shaker (180 rpm). For the main culture 100 ml of R5 medium was inoculated with 2 ml of preculture and cultivated for 48 h for DNA extraction or up to 5 days for balhimycin production assays.

Liquid cultures of *Amycolatopsis japonicum* were grown for 48 h in tryptic soy broth (TSB) as a preculture or for DNA extraction. For glycopeptide antibiotic (GPA) production 100 ml production medium (2 % galactose, 1 % soytone, 0.2 % $(NH_4)_2SO_4$, 0.2 % $CaCO_3$, pH 7.4) was inoculated with 2 ml of preculture and incubated for 5 days at 27 °C.

Escherichia coli strains were grown in LB (Bertani, 1951) at 37 °C. Liquid cultures were shaken at 180 rpm. Media were supplemented with antibiotics when necessary to maintain plasmids.

Plasmid construction and transformation

Genomic DNA from *A. balhimycina* was extracted using the peqGOLD Bacterial DNA Kit from liquid cultures that had been cultivated for 48 h. All steps were performed as instructed by the manufacturer. Plasmid DNA from *E. coli* for preliminary analysis in cloning experiments was prepared using alkaline lysis (Birnboim and Doly, 1979) and for large scale preparation the PureYield™ Plasmid Midiprep (Promega) was used. Plasmid DNA for sequencing was isolated using the QIAprep Spin Miniprep Kit. PCR was performed to generate DNA fragments for downstream applications such as cloning and expression of recombinant proteins by using the KAPAHiFi™ DNA Polymerase. For other applications such as detection of specific DNA sequences in the genome the Taq DNA polymerase was used. DNA fragments of expected sizes were gel extracted using the illustra GFX™ Gel Band Purification Kit. Initial cloning of genes into pJET1.2 (Thermo Scientific) was performed using blunt end ligation following the supplier's instructions. The cloning of genes into the integrative pRM4 vector as well as the non-replicative pSP1 vector, linearized using the corresponding restriction enzymes, was achieved using the T4 DNA Ligase (Fermentas). The ligation mixtures were transferred into *E. coli* XL1-Blue. Plasmids for production of recombinant proteins were cloned using ligation-independent cloning into the ready to-use linearized pET-30 EK/LIC vector (Novagen) by the manufacturer's instructions. The corresponding fragments were amplified using primer pairs ovdahpprimF2/ovdahpprimR2 for *dahp*$_{\text{prim}}$, dahpsecF/dahpsecR for *dahp*$_{\text{sec}}$, pdh-primF/pdh-prim-R for *pdh*$_{\text{prim}}$ as well as pdh-sec-F/pdh-sec-R for *pdh*$_{\text{sec}}$ (Table 3). The ligation mixture was transferred into *E. coli* NovaBlue. Clones were checked for correct insertion by restriction digestion and plasmids with expected restriction patterns were sequenced.

For the overexpression of *dahp*$_{\text{prim}}$ and *pdh*$_{prim}$ the plasmids pRM4*dahp*$_{prim}$ and pRM4*pdh*$_{prim}$ were constructed using the corresponding primer pairs dahpprim1/dahpprim2, and pdhprim1/pdhprim2 to amplify the fragments containing restriction sites NdeI/BamHI, respectively. The fragments were cloned into pRM4 vector to create pRM4*dahp*$_{prim}$ and pRM4*pdh*$_{prim}$ (Table 2). For the overexpression of *pdt* the plasmid pRM4*pdt* and for overexpression of *dahp*$_{sec}$ and *pdt* together the plasmid pRM4*dahp*$_{sec}$*pdt* was constructed. The corresponding fragments were amplified using primer pairs pdehydratase pRM4-1/ pdehydratase pRM4-2 as well as dahp-coexpress-pdt_1/dahp-coexpress-pdt_2. The primers contained restriction sites at the 5' and 3' ends (NdeI/BamHI and BamHI/XbaI, respectively). The fragments were cloned into pRM4 vector to create pRM4*pdt* and pRM4*dahp*$_{sec}$*pdt* (Table 3).

For the deletion of *dahp*$_{prim}$ the plasmid pSP1Δ*dahp*$_{prim}$ was constructed. Flanking regions were amplified using primer pairs dahpprdelFr1FP/dahpktfrag1-2 and dahpktfrag2-1/dahpktfrag2-2 containing restriction sites at the 3' and 5' ends (PstI/XbaI and XbaI/EcoRI, respectively). The fragment was cloned into pSP1 vector to generate pSP1Δ*dahp*$_{prim}$.

The plasmids for overexpression (pRM4*dahp*$_{prim}$, pRM4*pdh*$_{prim}$, pRM4*pdt* and pRM4*dahp*$_{sec}$*pdt*) and deletion (pSP1Δ*dahp*$_{prim}$) were transferred into the

methylationdeficient *E. coli* ET12567 (MacNeil et al., 1992) and isolated for direct transformation (Pelzer et al., 1997)of *A. balhimycina*. The integration of the vector into the chromosome via ΦC31 *attP* site was confirmed by PCR screening using primer pairs ErmEXgene RP/ErmEXgene FP or apra1/apraproof (Table 3). Deletion of $dahp_{prim}$ was confirmed by PCR screening using primer pair intdahpprFP/intdahpprRP.

To generate an overexpression strain of *A. japonicum* that enables the downstream engineering by application of pRM4-based plasmids, the *ajrR* overexpression system was switched to the compatible plasmid pIJ10257. The *ajrR* coding region was taken from pRM4-*ajrR* (Spohn et al., 2014) and inserted into pIJ10257 downstream of *ermE**p using the restriction enzymes NdeI and HindIII. For the transfer of pIJ-*ajrR* into *A. japonicum* via intergeneric conjugation, the plasmid was transferred into the methylation-deficient *E. coli* ET12567/pUZ8002 strain carrying the genes required for plasmid transfer (*tra* genes) on the plasmid pUZ8002 (Paget et al., 1999). Conjugation procedure was performed as previously described (Stegmann et al., 2001).

Table 3: Primers

Primer	Sequence (5' to 3')	Relevant feature(s)
pdehydratase pRM4-1	AATCATATGCGGCCCCGTAGCCTGGGT	cloning of pRM4*pdt*
pdehydratase pRM4-2	AATGGATCCTCACGCCACGTCCCCCTTGCGG	
dahp-coexpress-pdt_1	ATATGGATCCCAGGGGAGGACCTCGTGGCCGCGATGACCCACACCGTCGCCACG	cloning of pRM4*dahp$_{sec}$pdt*
dahp-coexpress-pdt_2	ATATTCTAGATTCAGCTTGCTTGCTTGCCGAGC	
pSETermE-rev	ATGCTAGTCGCGGTTGA	Verification of the integration of pRM4 constructs into *A. balhimycina* genome
pRM4 RP	GGCGATTAAGTTGGGTAACG	Verification of the integration of pRM4 constructs into *A. balhimycina* genome
ErmEXgene RP	CTGCAAGGCGATTAAGTTGG	Verification of the integration of pRM4 constructs into *A. balhimycina* genome
ErmEXgene FP	TTATGCTTCCGGCTCGTATG	Verification of the integration of pRM4 constructs into *A. balhimycina* genome
ovdahpprimF2	GACGACGACAAGATTACACTCTCCGTCGGACC	cloning of pET-30*dahp$_{prim}$*
ovdahpprimR2	GAGGAGAAGCCCGGTTCAGCGGCG	
dahpsecF	GACGACGACAAGATTGCCGCGATGACCCAC	cloning of pET-30*dahp$_{sec}$*
dahpsecR	GAGGAGAAGCCCGGTTCAGCTTGCTTGCTTGCC	
pdh prim F	GACGACGACAAGATTCGAGATGTATGCGTG	cloning of pET-30*pdh$_{prim}$*
pdh prim R	GAGGAGAAGCCCGGTCTACTGGACTTCGCC	
pdh sec F	GACGACGACAAGATTACCATCGAGAAAGCG	cloning of pET-30*pdh$_{sec}$*
pdh sec R	GAGGAGAAGCCCGGTCTAACGCCCCGGGGA	
dahpprim1	AATCATATGACACTCTCCGTCGGACC	cloning of pRM4*dahp$_{prim}$*
dahpprim2	TTAGGATCCTCAGCGGCGCGCCCGCACGGC	
pdhprim1	AATCATATGCGAGATGTATGCGTGATCGGGCTCGGGCTG	cloning of pRM4*pdh$_{prim}$*
pdhprim2	TTAGGATCCCTACTGGACTTCGCCGGTCGC	
dahpprdelFr1FP	TTACTCCAGCTTGGCTCAGCCGAAGAAGAC	flanking region 1 for pSP1Δ*dahp*$_{prim}$
dahpktfrag1-2	ATTTCTAGACGCGGGGTGGTCCTTCCTGGTGGACAC	
dahpktfrag2-1	TTATCTAGAGAGGTCCCCGGCCTGGGGGTCCCCCGGTT	flanking region 2 for pSP1Δ*dahp*$_{prim}$
dahpktfrag2-2	AATGAATTCCGATCCTGGCCGGCAACCACCTGGCGG	
apra1	GGCATCGCATTCTTCG	Verification of the integration of pRM4 constructs into *A. balhimycina* genome
apraproof	CATGTGCAGCTCCATCAG	Verification of the integration of pRM4 constructs into *A. balhimycina* genome

Heterologous production of recombinant proteins in *E. coli*

E. coli Rosetta 2(DE3) pLysS was used for the heterologous production of recombinant N-terminal 6xHis tagged fusion protein from *A. balhimycina* including Dahp synthases ($Dahp_{prim}$ and $Dahp_{sec}$) and Pdhs (Pdh_{prim} and Pdh_{sec}). Genes were amplified using primer pairs for $dahp_{prim}$ (ovdahpprimF2 and ovdahpprimR2), $dahp_{sec}$ (dahpsecF and dahpsecR), pdh_{prim} (pdh prim F and pdh prim R), pdh_{sec} (pdh sec F and pdh sec R) (Table 3). Fragments with the expected size were cloned into the expression vector pET-30 EK/LIC using T4 DNA polymerase (Novagen) and transferred into *E. coli* NovaBlue. Constructs were verified by restriction digestion (NcoI/XbaI, BglII/ApaI and SphI/HpaI, respectively). Sequence-verified constructs were transferred into *E. coli* Rosetta 2(DE3) pLysS. For protein production the cells were grown in 500 ml LB medium with 35 µg/ml kanamycin and 30 µg/ml chloramphenicol using 2 L Erlenmeyer flasks to an optical density of 0.6 at 600 nm. Protein production under the T7 promotor was induced by the addition of IPTG to a final concentration of 1 mM (0.75 mM for Pdh_{prim}) and cultures incubated at 18 °C (13 °C for Pdh_{prim}) on a horizontal rotation shaker at 180 rpm overnight. Cells were collected by centrifugation at 7.500 rpm and stored at -80 °C prior to protein purification. Cell pellets were resuspended in lysis buffer containing 20 mM Tris/HCL (for Pdhs) or 20 mM BIS-TRIS propane/HCl (for Dahp synthases), 500 mM NaCl, 20 mM imidazole, 1 mg/ml lysozyme, 20 m $MgCl_2$, 1-fold protease inhibitors and 1 mM DNase I at pH 7.5 and the cells disrupted by sonication 3 to 6 times for 30 sec. The soluble proteins were purified and eluted using 300 mM imidazole containing buffer (BIS-TRIS propane/HCl pH 7.5 20 mM, 0.5 M NaCl, 300 mM imidazole pH 7.5, 1 mM TCEP, MnSO4 0.1 mM) from a Nickel-NTA column and fractions containing pure protein were pooled and stored in 50 mM Tris/HCl (for Pdhs) or 50 mM BIS-TRIS propane/HCl (for Dahp synthases), 150 mM NaCl, 1 mM TCEP, 0.2 mM PEP, pH 7.5.

Enzymatic characterization of Dahp synthase

As the initial reaction of the shikimate pathway, Dahp condenses PEP and E4P to DAHP. To determine kinetics of this enzyme, the consumption rate of PEP at 232 nm was measured on UV suitable microtiter plates and calculated according to the Beer-Lambert Law with ε_{232} = 28.000 L/mol∗cm. In this assay the initial reaction rates were measured as a triplicate at varied concentration of E4P and fixed concentration of PEP as well as *vice versa*. The reaction buffer contained 50 mM BIS-TRIS propane/HCl at pH 7.5, 1 mM TCEP, 0.1 mM $MnSO_4$, 0.3 mM PEP or E4P (fixed or varied, respectively), 10 µg/ml DAHP. For inhibition studies, 100 µM of PEP and 103.5 µM E4P was used with the addition of 200 µM Tyr, phenylalanine (Phe) and tryptophan (Trp) individually or combined with each other. Measurement was performed for 30 sec in 3 sec intervals. The initial reaction rates are estimated using GraFIt Data Analysis (Erithacus Software) and obtained from the slope of the tangent placed to the beginning of the observed curve. Michaelis-Menten kinetics were determined using GraphPad Prism.

Enzymatic characterization of Pdh

In the shikimate pathway Pdh catalyzes the oxidative decarboxylation of prephenate to 4-HPP under formation of NADH. To determine the kinetic characterization of Pdh the formation of NADH was measured at 340 nm and calculated according to the BeerLambert Law with ε_{340} = 6,200 L/mol∗cm. The reaction buffer contained 100 mM

Tris/HCl at pH 7.3, 0.5 mM NAD^+, 5 µg/ml Pdh_{prim} or 2.5 µg/ml Pdh_{sec}, varied concentrations of prephenate. For inhibition studies, 1 mM Tyr or Phe was used. Measurement was performed for 1 min in 6 sec intervals. Analysis of Pdh_{prim} was therefore performed at 5 µg/µl of enzyme concentration and Pdh_{sec} at 2.5 µg/µl. The measured extinction values were used to calculate the NADH formation rate, with the initial reaction rates obtained from the slope of the tangents plotted to the observed reaction curves. The values of initial reaction rates were plotted against the corresponding substrate concentrations resulting in the Michaelis-Menten saturation and used to determine the kinetic properties (K_M and V_{max}) of Pdh_{prim} and Pdh_{sec}. Michaelis-Menten kinetics were determined as described above.

Determination of protein concentration using BCA assay

This assay was performed to assess the growth rate of *A. balhimycina* strains since they do not grow in a dispersed state. The bicinchoninic acid (BCA) assay is a colorimetric protein assay where the measurement of protein concentration is based on two reactions: firstly, the reduction of Cu^{2+} to Cu^+ by a protein in the alkaline solution (Biuret reaction) and secondly, complex formation of BCA with Cu^+ at 562 nm (Smith et al., 1985). The protein concentration in the sample is determined by comparison to a protein standard with BSA and lies in the range from 2 to 2,000 µg/ml. 1 ml of cells were collected by centrifugation for 5 min at 13,000 rpm and washed twice with 1 ml PBS. Cells were disrupted by Precellys® (6,500 rpm for 20 sec, twice) and cell debris was removed by centrifugation for 20 min at 16,000 rpm at 4 °C. Supernatant was diluted (1:10) and ready to use. The Pierce® BCA Protein Assay was performed as instructed by the manufacturer.

Analysis of glycopeptide antibiotic production

The concentration of the GPA balhimycin and ristomycin in the culture supernatant was determined by high performance liquid chromatography (HPLC). HPLC was performed using an Agilent 1260 infinity LC system equipped with Agilent 1260 infinity Auto Sampler with a Nucleosil 100 C18 column (5 µm 125 x 3 mm ID). Gradient ranged from 95.5 % eluent A (0.1 % phosphoric acid) and eluent B (acetonitrile) 4.5 % to 100 % eluent B in 15 min plus additional 3 min at 100 % eluent B. The injection volume was 5 µL. Agilent 1260 infinity Dioden Array Detector (DAD) was used at wavelengths 210, 230, 260, 280, 310, 360, 435 and 500 nm.

The GPA yields were quantified with reference to standard curve of defined balhimycin and ristomycin stock solutions. The relative balhimycin and ristomycin production by all inspected strains was adjusted to their specific growth rate by either determining their total protein yield (*A. balhimycina*) or their cell dry weight (*A. japonicum*), respectively. For the determination of the protein yield 1 ml cell culture was disrupted by Precellys® and by analyzing the supernatants using a bicinchoninic acid (BCA) assay.

Results and discussion

Key enzymes of the shikimate pathway display differences in kinetic properties and allosteric regulation

In addition to genes encoding the key enzymes of the shikimate pathway (3-deoxy-D-arabinoheptulosonate-7-phosphate synthase *dahp$_{prim}$* (GenBank ID: FN594522.1) and prephenate dehydrogenase *pdh$_{prim}$* (GenBank ID: FN594521.1) from primary metabolism), most glycopeptide antibiotic (GPA) biosynthetic gene clusters (BGCs) contain the orthologous genes *dahp$_{sec}$* and *pdh$_{sec}$*. The presence of these extra copies of GPA pathway specific genes raised the question of the particular properties of the enzymes Dahp$_{sec}$ (362 amino acids (AA)) and Pdh$_{sec}$ (291 AA) in comparison to their isoenzymes from primary metabolism (Dahp$_{prim}$ (360 AA) and Pdh$_{prim}$ (322 AA)). The identity between Dahp$_{prim}$, Dahp$_{sec}$ is 58%, between Pdh$_{prim}$ and Pdh$_{sec}$ is 38%. To investigate the catalytic properties and possible allosteric regulation we heterologously produced the enzymes Dahp$_{prim}$, Dahps$_{ec}$, Pdh$_{prim}$ and Pdh$_{sec}$ of *A. balhimycina* in *E. coli* and purified them using Ni-NTA affinity chromatography.

Dahp$_{prim}$ and Dahp$_{sec}$ differ in their allosteric regulation

The kinetic properties of Dahp$_{prim}$ and Dahp$_{sec}$ were analyzed in a continuous optical assay by measuring the phosphoenol pyruvate (PEP) consumption rate at 232 nm with varied concentrations of erythrose-4-phosphate (E4P) and a fixed concentration of PEP, as well as *vice versa* (Fig. S1).

Our analysis showed that the substrate concentrations in range of 20–300 µM covered the broad area of the Michaelis-Menten saturation curve, with the reaction rate directly proportional to the enzyme amount in the range of 0.01–0.015 µg/µl for Dahp$_{prim}$ and 0.005–0.01 µg/µl for Dahp$_{sec}$. Based on this, their activity was analyzed at 0.01 µg/µl enzyme concentration, with changes in absorption at 232 nm used to calculate the PEP consumption rate. Initial reaction rates were obtained by plotting a tangent to the observed progress curve of each enzymatic reaction and determining the slope. Subsequently, the values of the initial reaction rates were used to plot the Michaelis-Menten saturation curve and determine the kinetic properties, K_M and V_{max}. This analysis revealed that both enzymes possessed comparable enzymatic properties for the substrate PEP (PEP: Dahp$_{prim}$: K_M 8.02 ± 2.7 µM, V_{max} 0.0084 ± 0.0004 µM/min; Dahp$_{sec}$: K_M 10.33 ± 2.4 µM, V_{max} 0.0094 ± 0.0003 µM/min) (Table 4, Fig. S2). Both enzymes utilized PEP with a 10-fold higher catalytic efficiency (k_{cat}/K_M) than E4P. The major difference observed between Dahp$_{sec}$ and Dahp$_{prim}$ is the higher affinity of Dahp$_{sec}$ to E4P while reaching a lower V_{max} value (Table 4, Fig. S2). Both enzymes utilized PEP with a 10-fold higher catalytic efficiency (k_{cat}/K_M) than E4P. The major difference observed between Dahp$_{sec}$ and Dahp$_{prim}$ is the higher affinity of Dahp$_{sec}$ to E4P while reaching a lower V_{max} value (Table 4, Figure S2).

Table 4: Kinetic properties of $Dahp_{prim}$ and $Dahp_{sec}$ in regard to E4P and PEP.

	$Dahp_{prim}$		$Dahp_{sec}$	
	E4P	**PEP**	**E4P**	**PEP**
K_M [µM]	**134.03** ± 20.1	**8.02** ± 2.7	**46.51** ± 11.7	**10.33** ± 2.4
V_{max} [µM/min]	**0.0122** ± 0.0008	**0.0084** ± 0.0004	**0.0057** ± 0.0004	**0.0094** ± 0.0003
k_{cat} [1/s]	**$0.8689 * 10^{-3}$**	**$0.5983 * 10^{-3}$**	**$0.4095 * 10^{-3}$**	**$0.6753 * 10^{-3}$**
k_{cat}/K_M [$s^{-1} * M^{-1}$]	**6.483**	**74.60**	**8.804**	**63.371**

Given these comparable catalytic properties, we investigated the allosteric regulation mechanisms of $Dahp_{prim}$ and $Dahp_{sec}$. To this end, enzyme activity was measured in the presence of potential inhibitors –the aromatic amino acids phenylalanine (Phe), Tyr, and tryptophan (Trp) – using fixed concentrations of the substrates E4P and PEP. Our results demonstrate inhibitory effects caused by Tyr and Phe, while the reaction rates of both enzymes were not affected by addition of Trp (Table 5, Table S1, Table S2). Both, Phe and Tyr inhibited $Dahp_{prim}$, while $Dahp_{sec}$ was only inhibited by Tyr. Equimolar combinations of Phe and Tyr enhanced the inhibition of $Dahp_{prim}$, while in contrast, Phe antagonized the Tyr-dependent inhibition of $Dahp_{sec}$. This is a remarkable difference in the allosteric nature of the enzyme encoded in the balhimycin BGC when compared to $Dahp_{prim}$ (Figure S3).

Table 5: Reaction rates of $Dahp_{prim}$ and $Dahp_{sec}$ in an enzymatic reaction with a potential inhibitor.

	$Dahp_{prim}$		$Dahp_{sec}$	
Potential Inhibitor	**Reaction Rate in**			
	[nM/min]	**%**	**[nM/min]**	**%**
-----	5.13 ± 0.60	**100**	4.33 ± 0.12	**100**
Phe	3.45 ± 0.48	**67**	3.89 ± 0.27	**90**
Tyr	2.87 ± 0.42	**56**	1.44 ± 0.01	**33**
Tyr + Phe	1.98 ± 0.11	**39**	2.61 ± 0.03	**60**
Trp	4.85 ± 0.09	**95**	4.28 ± 0.12	**99**

Pdh_{prim} and Pdh_{sec} lack feedback inhibition by tyrosine and phenylalanine

Pdh catalyzes the conversion of prephenate towards the biosynthesis of Tyr at the final branching point of the shikimate pathway (Fig. 1). Pdh is a decarboxylating oxidoreductase and requires NAD^+ as a co-factor. This allows the comparative determination of the enzymatic properties of Pdh_{prim} and Pdh_{sec} in a continuous optical assay by measuring the formation of NADH at 340 nm (Fig. S4).
Analysis of Pdh_{prim} showed that prephenate concentrations in the range of 35–3500 µM covered the broad area of the Michaelis-Menten saturation curve, whilst concentrations of up to 260 µM were sufficient to plot the Michaelis-Menten saturation curve of Pdh_{sec}. The reaction rate was directly proportional to the enzyme amount in the range of 1.25–5 µg/µl of Pdh_{prim} and in the range of 0.625–2.5 µg/µl of Pdh_{sec}. Analysis of Pdh_{prim} was therefore performed at 5 µg/µl (153 µM) of enzyme concentration and Pdh_{sec} at 2.5 µg/µl (85 µM).

Pdh_{prim} and Pdh_{sec} possessed comparable maximum rates (V_{max}) and turn over numbers (k_{cat}) with prephenate. However, our analysis revealed that Pdh_{prim} and Pdh_{sec} displayed significant differences in their affinity towards prephenate, with Pdh_{sec} displaying ~100-fold higher affinity to prephenate than Pdh_{prim} (Pdh_{sec} K_M = ~10 µM, Pdh_{prim} K_M = ~920 µM) (Table 6, Fig. S5). Given that dehydrogenases involved in tyrosine biosynthesis accept prephenate and arogenate, the low affinity of Pdh_{prim} for prephenate might indicate a preference of this enzyme for arogenate. Interestingly, only the conversion of prephenate leads to the intermediate pathway product 4-HPP that is in turn required as precursor to produce Hpg (Fig. S6), which might depict the adaption of Phd_{sec} towards GPA biosynthesis.

Table 6. Kinetic properties of Pdh_{prim} and Pdh_{sec}

	Pdh_{prim}	**Pdh_{sec}**
K_M [µM]	917.31 ± 36.7	9.55 ± 1.8
V_{max} [µM/min]	57.63 ± 1.0	44.73 ± 2.0
k_{cat} [1/s]	7.17	10.21
kcat/KM [s-1* M-1]	7.81 * 10^3	1.69 * 10^6

The allosteric regulations of Pdh_{prim} and Pdh_{sec} were investigated by determining their kinetic properties in the presence of Tyr or Phe. Comparison of KM and Vmax values showed that neither the addition of Tyr nor Phe influenced the activity of Pdh_{prim} nor of Pdh_{sec} (Table 7, Fig. S7). This indicates that the major control point in the GPA pathway specific precursor supply appears to be $Dahp_{sec}$.

Table 7. Kinetic properties of Pdh_{prim} and Pdh_{sec} in an enzymatic reaction with a potential inhibitor

	Pdh_{prim}		**Pdh_{sec}**	
Potential Inhibitor	**K_M** [µM]	**V_{max}** [µM/min]	**K_M** [µM]	**V_{max}** [µM/min]
-	**917.31** ± 36.7	**57.63** ± 1.0	**9.55** ± 1.8	**44.73** ± 2.0
Tyr	**958.78** ± 40.4	**55.66** ± 1.0	**11.49** ± 2.6	**46.12** ± 2.6
Phe	**927.96** ± 26.4	**55.93** ± 0.7	**10.86** ± 2.1	**43.24** ± 2.1

The shikimate pathway links primary and secondary metabolism in *A. balhimycina*

Alterations in the shikimate pathway affect balhimycina biosynthesis

To investigate whether $Dahp_{sec}$ is indeed the key enzyme in the production of GPAs, we explored the effect of altered *$dahp_{prim}$*, and *pdh_{prim}* expression on balhimycin production. A second copy of the genes *$dahp_{prim}$* and *pdh_{prim}*, respectively, were integrated into the genome of *A. balhimycina* under the control of the constitutive promoter *ermE**p generating the recombinant strains *A. balhimycina $dahp_{prim}^+$* and *A. balhimycina pdh_{prim}^+* . In addition, a deletion mutant lacking *$dahp_{prim}$* (*A. balhimycina Δ$dahp_{prim}$*) was generated. In our attempts to construct the *pdh_{prim}* deletion strain by homologous recombination, clones were obtained in which the *pdh_{prim}* deletion plasmid

was integrated into the genome of *A. balhimycina* via the first crossing-over event. To generate the *A. balhimycina* pdh_{prim} deletion mutant, we selected for the second cross over event. However, although ~100 clones were identified in which the plasmid was disintegrated, no clone could be identified in which the second crossover resulted in the deletion of pdh_{prim}. This led us to postulate that the deletion of pdh_{prim} is lethal. Given this, we included *A. balhimycina* $dahp_{prim}^{+}$, *A. balhimycina* pdh_{prim}^{+} and *A. balhimycina* $\Delta dahp_{prim}$ in our balhimycin production assays. The supernatants of these strains were analyzed using HPLC-DAD and compared with *A. balhimycina* $dahpsec^{+}$, *A. balhimycina* pdh_{sec}^{+}, and *A. balhimycina* $\Delta dahp_{sec}$ supernatants. The relative balhimycin production of all strains tested (Table 1) was adjusted to their specific cell growth (assessed by determining the protein content of the cultures) and normalized to the relative balhimycin production of the wild type strain (WT).

Balhimycin production of *A. balhimycina* WT accounts for 0.04 ± 0.006 mg/ml balhimycin per mg/ml protein in culture, whilst the strain in which $dahp_{sec}$ was overexpressed (*A. balhimycina* $dahp_{sec}^{+}$) demonstrated a 4.4-fold increase in balhimycin production. In contrast, overexpression of $dahp_{prim}$ (*A. balhimycina* $dahp_{prim}^{+}$) led to a reduced balhimycin production. Both deletion mutants, *A. balhimycina* $\Delta dahp_{prim}$ and *A. balhimycina* $\Delta dahp_{sec}$, exhibited a relative reduction in balhimycin production of 37% and 17% compared to *A. balhimycina* WT (Fig. 2). This shows that the two Dahp isoenzymes can likely compensate each other in sustaining the shikimate pathway and the general supply of required precursors for the balhimycin production. In conclusion, only the individual overexpression of $dahp_{sec}$ contributes to an increased balhimycin production. This further implies that the two Dahp iso-enzymes, with their demonstrated differences in feedback regulation, are specifically adapted for their predicted physiological function in driving the shikimate pathway either for primary metabolism or GPA production, respectively.

Corresponding experiments were carried out for pdh_{sec} and pdh_{prim}. The overexpression of both pdh_{prim} and pdh_{sec}, however, resulted in a reduction of balhimycin production compared to *A. balhimycina* WT (46% and 39%) (Figure 2). The explanation for this unexpected result could be that the overexpression of pdh_{prim} and pdh_{sec} initially leads to an increase in intracellular Tyr levels, but in a second step, due to allosteric inhibition of tyrosine, this leads to a decrease in Tyr production and thus balhimycin.

The interdependence of tyrosine and phenylalanine biosynthesis due to regulatory interplay in shikimate metabolism influences the provision of balhimycin precursors

Based on our observation that $Dahp_{sec}$ is strongly inhibited in its enzymatic activity by Tyr (Table 4), we hypothesized that an imbalanced increase of the intracellular Tyr titers eventually interferes with balhimycin production. Interestingly, the allosteric inhibition of $Dahp_{sec}$ by Tyr is antagonized by Phe (Table 5). We thus postulated that higher concentrations of Phe might partially reverses the inhibitory effect of Tyr, eventually balancing the metabolic flux towards GPA biosynthesis via $Dahp_{sec}$.

To test our hypothesis, we cultivated *A. balhimycina* WT in the presence of 5 mM Phe and quantified the balhimycin production. This additive feeding of *A. balhimycina* WT increased balhimycin production 2-fold (Figure 2), confirming the positive effect of Phe for the balhimycin biosynthesis. Having found that the external addition of Phe altered

balhimycin production, we directed the metabolic flux in the shikimate pathway towards Phe. Prephenate is the last common substrate in the biosynthesis of Tyr and Phe, and while Pdh catalyzes the conversion of prephenate towards Tyr, the competitive conversion of prephenate to Phe is catalyzed by the prephenate dehydratase (Pdt) (Figure 1). We therefore overexpressed *pdt* (GenBank ID: OQ352441) by integrating an extra copy of *pdt* into the genome of *A. balhimycina* under the control of the constitutive promoter *ermE**p. Compared to the WT strain, *A. balhimycina pdt*$^{+}$ showed a 4-fold increase in balhimycin production (Figure 2), demonstrating that the counterintuitive overproduction of Pdt and the forced flux of the shikimate pathway towards Phe ultimately promotes balhimycin production.

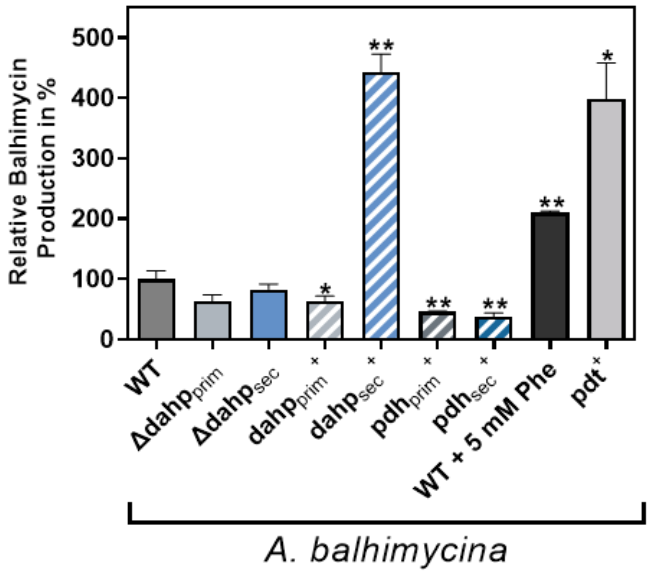

Figure 2: Balhimycin production in *A. balhimycina* mutant strains
Balhimycin yields of A. balhimycina WT, A. balhimycina dahp$_{prim}$, A. balhimycina dahp$_{sec}$, A. balhimycina dahp$_{prim}$$^{+}$, A. balhimycina dahp$_{sec}$$^{+}$, A. balhimycina pdh$_{prim}$$^{+}$, A. balhimycina pdh$_{sec}$$^{+}$, A. balhimycina WT supplemented with 5 mM Phe and *A. balhimycina pdt*$^{+}$ measured via HPLC. The values were adjusted to the culture growth and normalized to the production of *A. balhimycina* WT.

Targeted alterations of the shikimate pathway optimized ristomycin A production

Having seen the effects of altered shikimate pathway gene expression on balhimycin production, we wanted to use the same metabolic engineering strategy to increase ristomycin A (also called ristocetin A) production. Since the producer *Amycolatopsis lurida* (Grundy et al., 1956) produces only small amounts of ristomycin, the availability of ristomycin is not always guaranteed. Other strains capable of producing ristomycin have now been identified (e.g. *Amycolatopsis* sp. MJM2582 (Truman et al., 2014) and *Amycolatopsis japonicum* (Spohn et al., 2014).

In contrast to balhimycin, whose heptapeptide backbone consists of five nonproteinogenic amino acids, the ristomycin backbone contains seven non-proteinogenic amino acids. This makes the production of ristomycin A even more dependent on the supply of precursors via the shikimate pathway.

For this study, we chose the genetically accessible production strain *A. japonicum* to establish a high and stable production of ristomycin A. In previous work, we cloned the pathway-specific regulator *ajrR* under the control of the strong constitutive promoter *ermE**p in pRM4 and introduced the plasmid into *A. japonicum*. This overexpression resulted a significant increase in ristomycin A production (Spohn et al., 2014).

To be able to use the pRM4-based expression plasmids for further optimization of ristomycin A production, we first recloned the regulator *ajrR* into pIJ10257 again under the control of *ermE**p and integrated the plasmid into the chromosome of *A. japonicum* via the ΦBT*1 att* site (*A. japonicum ajrR*$^+$). *A. japonicum ajrR*$^+$ was grown in PM for 5 days and ristomycin A production titers were quantified by HPLC-DAD. The transcriptional enhancement of the ristomycin A BGC in *A. japonicum ajrR*$^+$ led to a 25-fold increased production compared to *A. japonicum* WT (Figure 3). This recombinant strain served as chassis to study ristomycin production by manipulating the expression levels of the shikimate genes. Heterologous expression of the *pdt* gene (*A. japonicum ajrR*$^+$/*pdt*$^+$) alone or in combination with the *dahp*$_{sec}$ gene (*A. japonicum ajrR*$^+$/*pdt*$^+$/*dahp*$_{sec}$$^+$) from *A. balhimycina* in *A. japonicum ajrR*$^+$ resulted in advanced ristomycin production strains. Compared to the WT, *A. japonicum ajrR*$^+$/*pdt*$^+$ and *A. japonicum ajrR*$^+$/*pdt*$^+$/*dahp*$_{sec}$$^+$ produced 28-fold and 35-fold higher ristomycin titers, respectively. These engineered strains combine overexpression of its biosynthetic genes with optimized precursor supply. *A. japonicum ajrR*$^+$/*pdt*$^+$/*dahp*$_{sec}$$^+$ yielded ristomycin A titers up to 1.68 ± 0.18 g/l in 120 h fermentation time, corresponding to 130 mg ristomycin A per g cell dry weight (DCW) and a calculated ristomycin A production rate of 1.1 mg/h/g DCW.

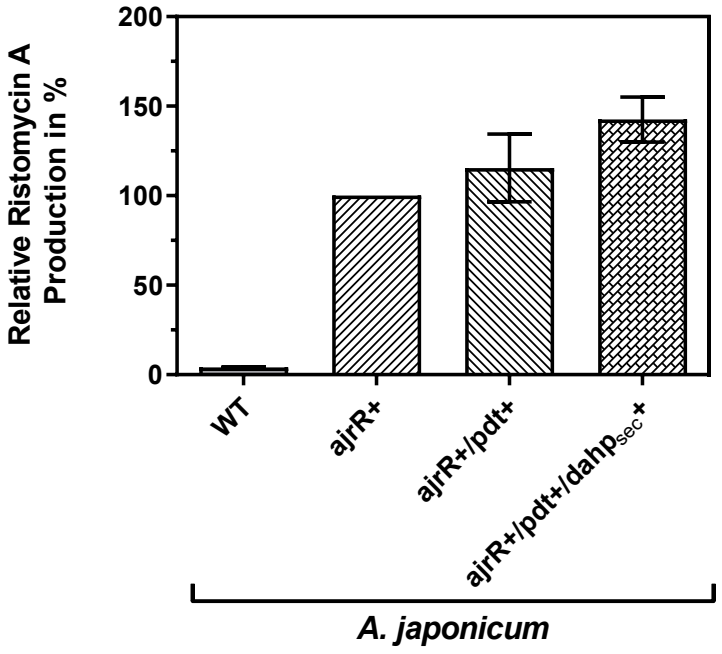

Figure 3: Ristomycin production of *A. japonicum WT* and recombinant strains.
Ristomycin yields of *A. japonicum* WT, *A. japonicum ajrR*$^+$, A. japonicum ajrR$^+$/pdt$^+$, *A. japonicum ajrR*$^+$/*pdt*$^+$/*dahp*$_{sec}$$^+$ measured via HPLC.

Conclusion

Glycopeptide antibiotics (GPAs) are highly effective antibiotics for the treatment of bacterial infections. However, their supply is critical due to the limited titer in the fermentation of actinomycetes producers. Therefore, established genetic engineering strategies (such as the overexpression of activator genes) need to be complemented by alternative approaches. We took advantage of the specificity of GPA producers, which contain, in addition to primary metabolism enzymes, second copies of the key shikimate pathway enzymes $Dahp_{sec}$ and Pdh_{sec} encoded in the GPA biosynthetic gene cluster. The enzymatic properties of the different pairs of enzymes, in particular feedback regulation, were characterized and subsequently used to increase yields by deleting and/or overexpressing the respective genes. Counterintuitive changes were also observed after manipulation of Pdt activity, which is not involved in GPA biosynthesis but in a competing reaction for the synthesis of the precursor tyrosine. These results could also be successfully implemented in another GPA producer, thus demonstrating the general applicability of this technique to GPAs of different types

Authors statement

Valentina Goldfinger, Marius Spohn and Jens-Peter Rodler conceived and designed the experiments, performed the analyses and wrote parts of the paper; Melanie Sigle, Johanna Rapp and Hannes Link contributed to the experiments.; Andreas Kulik performed the HPLC-MS analyses; Max Cryle and Wolfgang Wohlleben were involved in the development of the concept, interpretation of the results and writing of the paper; Evi Stegmann supervised the project, was involved in the conception of the experiments, interpretation of the results and writing of the manuscript.

Data availability

No data was used for the research described in the article.

Acknowledgements
We gratefully acknowledge financial support from the German Research Foundation (DFG), TRR261, project ID 398967434. MS was funded by an Innovation Grant from the University of Tübingen. We thank Dr. Libera lo Presti for invaluable comments on the manuscript.

Supplementary data

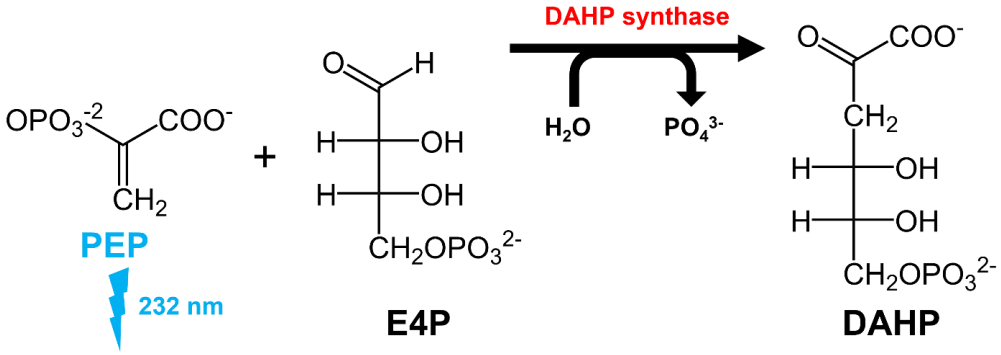

Figure S1: Enzyme assay for characterization of DAHP synthases
DAHP synthase condensates PEP and E4P to form DAHP. The reaction progress is measured at 232 nm detecting the consumption rate of PEP; PEP, phosphoenolpyruvate; E4P, D-erythrose4-phosphate; DAHP, 3-deoxy-D-arabino-heptulosonate 7-phosphate.

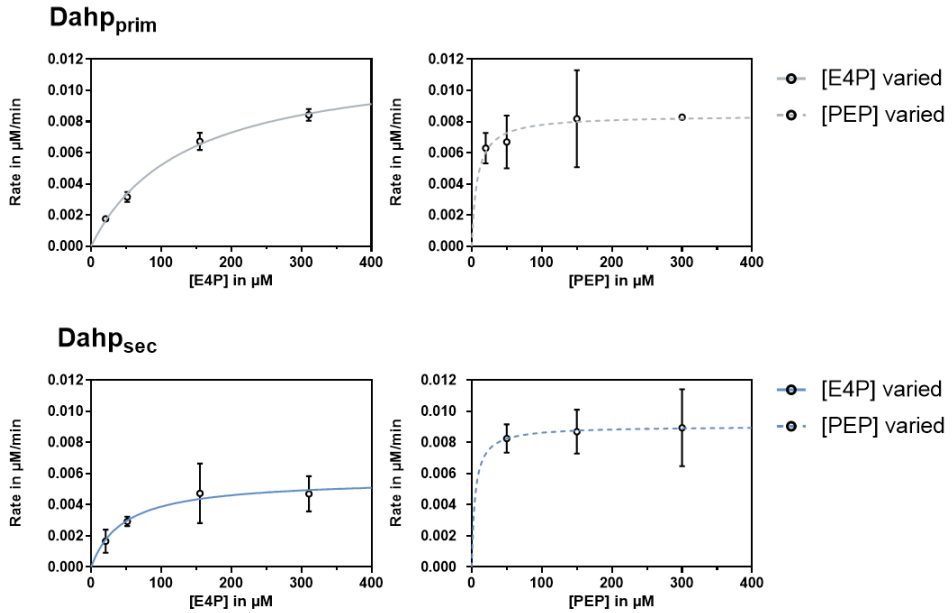

Figure S2: Kinetics of *A. balhimycina* $Dahp_{prim}$ and $Dahp_{sec}$
Michaelis-Menten saturation curve of $Dahp_{prim}$ and $Dahp_{sec}$, respectively, in regard to varied concentrations of E4P and PEP.

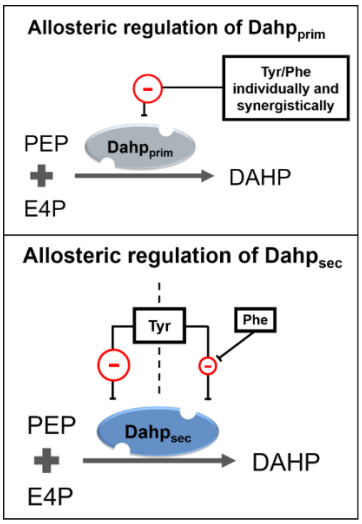

Figure S3: Allosteric regulation routes of Dahp$_{prim}$ and Dahp$_{sec}$ in *A. balhimycina*
Dahp$_{prim}$ and Dahp$_{sec}$ catalyze the condensation of PEP and E4P to form DAHP. Dahp$_{prim}$ is inhibited by Tyr and Phe. Dahp$_{sec}$ is inhibited only by Tyr. Phe weakens the inhibition of Dahp$_{sec}$ caused by Tyr. The allosteric effects are illustrated by arrows. Red circle with minus sign indicates feedback inhibition. PEP, phosphoenolpyruvate; E4P, erythrose 4-phosphate; DAHP, 3-deoxy-D-arabinoheptulosonate-7-phosphate; Tyr, tyrosine; Phe, phenylalanine.

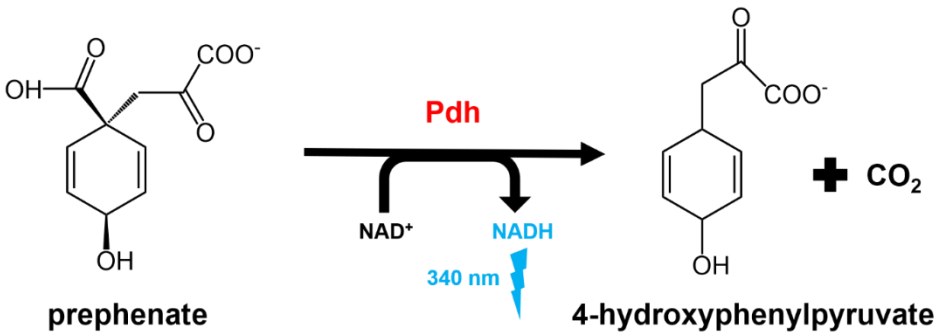

Figure S4: Enzyme assay for characterization of Pdh
Pdh catalyzes oxidative decarboxylation of prephenate to 4-hydroxyphenylpyruvate under formation of NADH, which is detectable at 340 nm. Pdh: prephenate dehydrogenase

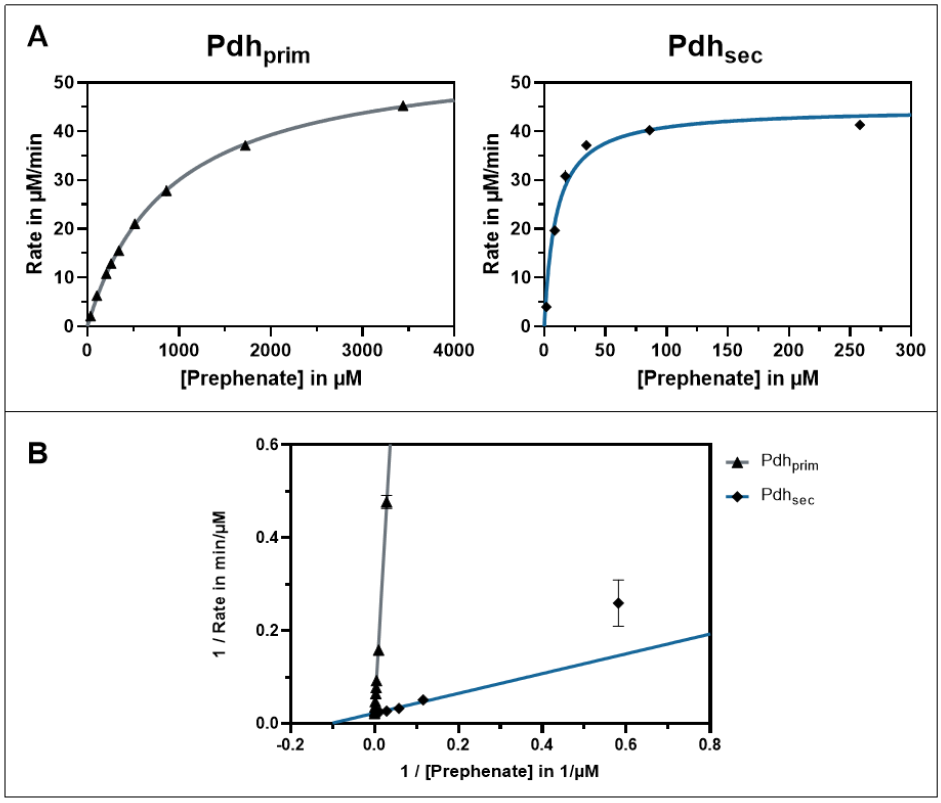

Figure S5: Kinetics of *A. balhimycina* Pdhs
Raw data used for determination of the kinetic properties in suppl. Table 3 and Table 4.
(A) Michaelis-Menten saturation curve of Pdh_{prim} and Pdh_{sec}, respectively.
(B) Lineweaver-Burk plot of received data.

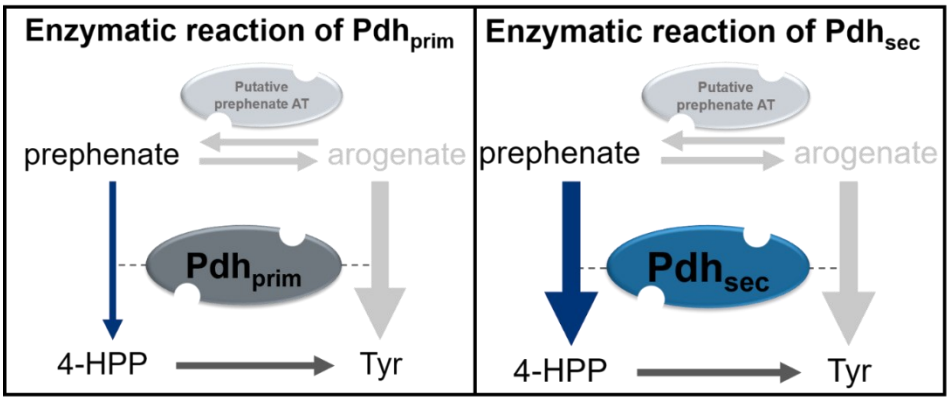

Figure S6: Substrate specificities of Pdh_{prim} and Pdh_{sec} of *A. balhimycina*
Prephenate is used by Pdh_{prim} and Pdh_{sec}. The difference in their affinity towards prephenate is reflected by the thickness of the arrows. The substrate specificity of Pdh_{prim} and Pdh_{sec} in *A. balhimycina* towards arogenate is assumed according to Song et al. (2005). Tyr is the end product of the shikimate pathway. AT , aminotransferase; 4-HPP, 4-hydroxyphenylpyruvate.

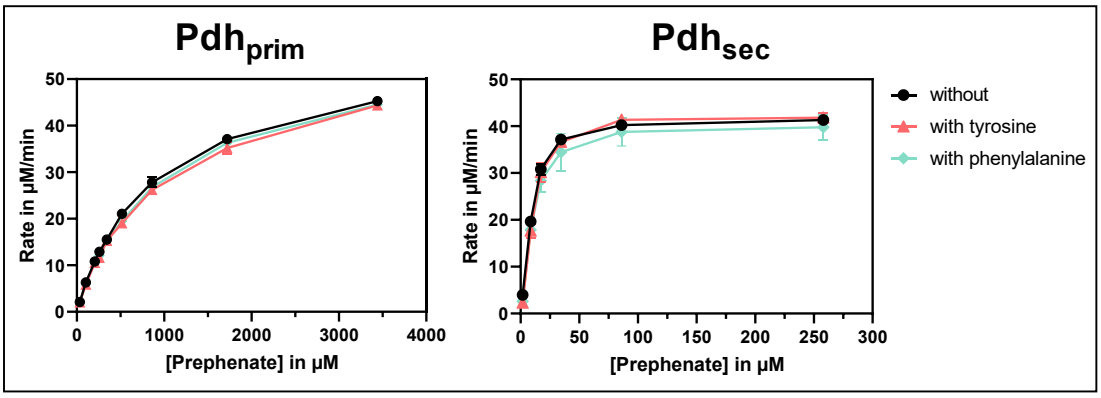

Figure S7: Kinetics of *A. balhimycina* Pdhs with addition of potential inhibitors.
Michaelis-Menten saturation curves of Pdh$_{prim}$ and Pdh$_{sec}$ with and without addition of Tyr and Phe, respectively.

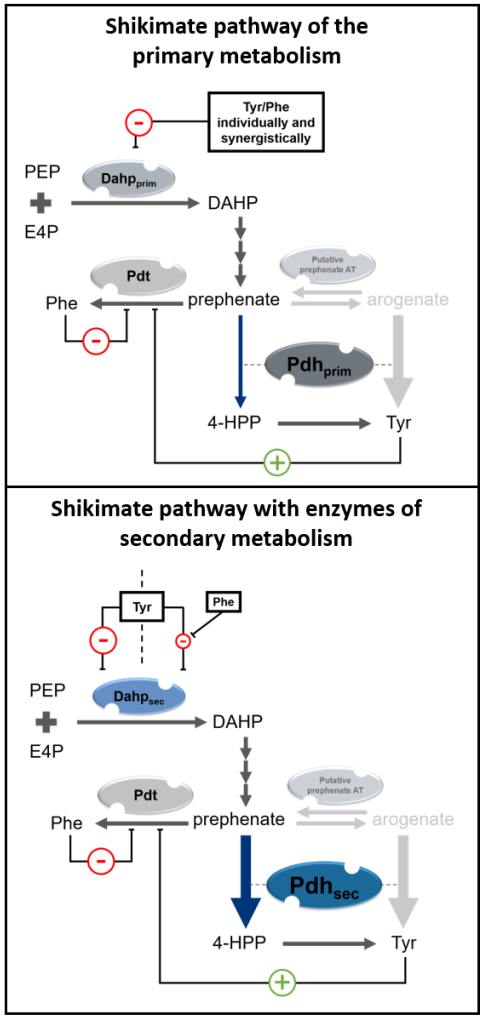

Figure S8: The shikimate pathway of primary metabolism and with enzymes of secondary metabolism in *A. balhimycina*:

Table S1: Raw data for determination of initial reaction rates of $Dahp_{prim}$ in the presence of a potential inhibitor

DAHP formation in an enzymatic reaction of $Dahp_{prim}$ in nM						
PEP [µM]		100				
E4P [µM]		103.5				
potential inhibitor		----	Trp	Phe	Tyr	Phe Tyr
time [min]			200 µM	200 µM	200 µM	200 µM each
measurement #1	0	0	0	0	0	0
	0.05	0.2569	0.1927	0.1285	0.1285	0.0642
	0.1	0.5139	0.4496	0.2569	0.3212	0.1927
	0.15	0.7066	0.6423	0.3854	0.4496	0.2569
	0.2	0.9635	0.7708	0.5139	0.5139	0.4496
	0.25	1.0920	0.9635	0.6423	0.5781	0.5139
	0.3	1.2205	1.0920	0.7708	0.7066	0.5781
	0.35	1.3489	1.1562	0.8993	0.7708	0.5781
	0.4	1.4132	1.2847	1.0277	0.8350	0.6423
	0.45	1.5416	1.3489	1.0920	0.8993	0.5781
	0.5	1.6059	1.4774	1.2205	0.9635	0.5139
measurement #2	0	0	0	0	0	0
	0.05	0.1927	0.2569	0.1927	0.0642	0.0642
	0.1	0.3854	0.4496	0.3854	0.1927	0.1927
	0.15	0.5781	0.6423	0.5781	0.3212	0.2569
	0.2	0.7066	0.8350	0.7066	0.3854	0.3854
	0.25	0.8993	1.0277	0.8993	0.4496	0.5139
	0.3	1.0277	1.2205	1.0277	0.5139	0.5781
	0.35	1.1562	1.3489	1.1562	0.6423	0.6423
	0.4	1.2847	1.4774	1.2847	0.7066	0.7066
	0.45	1.3489	1.6059	1.4132	0.8350	0.7708
	0.5	1.4774	1.7986	1.5416	0.8993	0.8350

Table S2: Raw data for determination of initial reaction rates of $Dahp_{sec}$ in the presence of a potential inhibitor

DAHP formation in an enzymatic reaction of $Dahp_{sec}$ in nM						
PEP [µM]		100				
E4P [µM]		103.5				
potential inhibitor		----	Trp	Phe	Tyr	Phe Tyr
time [min]			200 µM	200 µM	200 µM	200 µM each
measurement #1	0	0	0	0	0	0
	0.05	0.1927	0.1927	0.1927	0	0.1927
	0.1	0.4496	0.3854	0.3212	0.1285	0.2569
	0.15	0.6423	0.5139	0.4496	0.1927	0.3212
	0.2	0.7708	0.6423	0.5781	0.2569	0.3854
	0.25	0.8993	0.8350	0.7708	0.3212	0.4496
	0.3	1.0277	0.9635	0.8993	0.3854	0.5139
	0.35	1.1562	1.0920	1.0277	0.3854	0.5781
	0.4	1.2847	1.1562	1.0920	0.4496	0.5781
	0.45	1.4132	1.2205	1.2205	0.5139	0.6423
	0.5	1.5416	1.3489	1.2847	0.5139	0.7066
measurement #2	0	0	0	0	0	0
	0.05	0.1927	0.1927	0.1927	0	0.1285
	0.1	0.3854	0.3854	0.3854	0.1285	0.1927
	0.15	0.5781	0.5781	0.5781	0.1927	0.2569
	0.2	0.7066	0.7708	0.7066	0.2569	0.3212
	0.25	0.8350	0.8993	0.8993	0.3854	0.4496
	0.3	1.0277	1.0920	1.0277	0.4496	0.5139
	0.35	1.1562	1.2205	1.1562	0.5139	0.5139
	0.4	1.2847	1.3489	1.2847	0.5781	0.6423
	0.45	1.3489	1.4132	1.3489	0.6423	0.7066
	0.5	1.4774	1.4774	1.4774	0.7066	0.7708

Table S3: Raw data for determination of kinetics of Pdh_{prim} used in Figure S5

NADH+H⁺ formation in an enzymatic reaction of Pdh_{prim} in µM							
Prephenate [µM]		**34.4**	**103.2**	**206.4**	**258**	**344**	**516**
time [min]							
measurement #1	0	0	0	0	0	0	0
	0.1	0.290	0.580	0.870	1.160	1.160	2.031
	0.2	0.290	1.160	2.031	2.321	2.611	4.061
	0.3	0.580	1.741	2.901	3.771	4.061	6.092
	0.4	0.870	2.321	4.061	4.932	5.512	7.832
	0.5	0.870	2.901	4.932	6.092	6.962	9.863
	0.6	1.160	3.191	5.802	7.252	8.413	11.894
	0.7	1.450	3.771	6.962	8.413	9.863	13.634
	0.8	1.450	4.351	7.832	9.573	11.314	15.665
	0.9	1.741	4.932	8.993	10.733	12.474	17.405
	1	2.031	5.512	9.863	11.894	13.924	19.436
measurement #2	0	0	0	0	0	0	0
	0.1	0.290	0.580	1.160	1.160	1.160	2.031
	0.2	0.290	1.450	2.031	2.321	2.611	4.061
	0.3	0.580	1.741	3.191	3.771	4.061	6.092
	0.4	0.870	2.321	4.061	4.932	5.802	8.123
	0.5	1.160	3.191	5.222	6.092	7.252	9.863
	0.6	1.160	3.771	6.092	7.252	8.703	11.604
	0.7	1.450	4.061	6.962	8.413	10.153	13.634
	0.8	1.741	4.641	8.123	9.283	11.604	15.375
	0.9	1.741	5.222	8.993	10.733	13.054	17.405
	1	2.031	5.802	10.153	11.894	14.505	19.146
measurement #3	0	0	0	0	0	0	0
	0.1	0.290	0.580	0.870	1.160	1.450	1.450
	0.2	0.290	1.160	2.031	2.321	2.901	3.481
	0.3	0.580	1.741	2.901	3.481	4.351	5.802
	0.4	0.870	2.321	4.061	4.641	6.092	7.252
	0.5	0.870	2.901	4.932	5.802	7.542	9.573
	0.6	1.160	3.481	6.092	6.962	8.993	11.314
	0.7	1.160	4.061	6.962	8.123	10.443	13.924
	0.8	1.450	4.641	8.123	9.283	11.894	15.085
	0.9	1.741	5.222	8.993	10.443	13.344	17.696
	1	2.031	5.802	10.153	11.314	14.795	18.856

Table S3: Raw data for determination of kinetics of Pdh_{prim} used in Figure S5

NADH+H⁺ formation in an enzymatic reaction of Pdh_{prim} in µM						
Prephenate [µM]		**860**	**1720**	**1720**	**3440**	**3440**
time [min]						
measurement #1	0	0	0	0	0	0
	0.1	2.611	3.481	3.191	4.351	4.351
	0.2	5.222	6.962	6.382	8.413	8.703
	0.3	7.832	10.153	9.863	12.764	13.054
	0.4	10.443	13.634	13.344	16.825	17.696
	0.5	13.054	17.115	16.535	21.177	22.047
	0.6	15.665	20.306	20.016	24.948	26.398
	0.7	17.986	23.787	23.497	29.299	30.460
	0.8	20.596	26.978	26.688	33.360	34.521
	0.9	23.207	30.460	30.169	37.132	38.582
	1	25.818	33.651	33.651	41.483	42.643
measurement #2	0	0	0	0	0	0
	0.1	2.901	3.481	3.191	3.771	4.351
	0.2	5.512	6.962	6.672	8.123	8.703
	0.3	8.123	10.443	10.153	12.474	13.054
	0.4	10.733	13.924	13.634	16.535	17.405
	0.5	13.344	17.115	17.115	20.887	21.757
	0.6	15.665	20.596	20.596	24.948	26.108
	0.7	18.276	23.787	23.787	29.009	30.460
	0.8	20.596	27.269	27.269	33.360	34.521
	0.9	23.207	30.460	30.750	37.422	38.872
	1	25.528	33.941	34.231	41.483	42.933
measurement #3	0	0	0	0	0	0
	0.1	2.611	3.481	3.481	4.061	4.641
	0.2	4.932	6.962	6.672	8.413	8.703
	0.3	7.252	10.443	9.863	12.764	13.344
	0.4	9.863	13.924	13.054	16.825	17.696
	0.5	12.184	17.405	16.245	21.177	21.757
	0.6	14.795	20.887	19.436	25.528	25.818
	0.7	17.405	24.368	22.627	29.589	30.169
	0.8	19.726	27.559	25.818	33.941	34.231
	0.9	22.337	31.040	29.009	38.002	38.292
	1	24.658	34.521	32.200	42.063	42.353

Table S4: Raw data for determination of kinetics of Pdh_{sec} used in Figure S5.

NADH+H⁺ formation in an enzymatic reaction of Pdh_{sec} in µM							
Prephenate [µM]		**1.72**	**8.6**	**17.2**	**34.4**	**86**	**258**
time [min]							
measurement #1	0	0	0	0	0	0	0
	0.1	0.290	1.450	2.611	3.191	4.061	4.061
	0.2	0.290	2.611	4.641	6.382	7.832	7.832
	0.3	0.580	3.481	6.672	9.573	11.604	11.894
	0.4	0.580	3.771	8.123	12.474	15.375	15.665
	0.5	0.580	4.061	8.993	15.375	18.856	19.436
	0.6	0.580	4.351	9.863	17.405	22.627	23.207
	0.7	0.580	4.351	10.443	19.436	26.108	26.978
	0.8	0.580	4.351	10.733	21.177	29.299	30.750
	0.9	0.580	4.351	11.023	22.337	32.780	34.231
	1	0.580	4.351	11.314	23.497	35.971	38.002
measurement #2	0	0	0	0	0	0	0
	0.1	0.290	1.450	2.611	3.481	3.771	3.771
	0.2	0.290	2.611	4.641	6.382	7.542	7.542
	0.3	0.580	3.481	6.672	9.573	11.023	11.604
	0.4	0.580	3.771	8.123	12.184	14.795	15.375
	0.5	0.580	4.061	9.573	14.795	18.276	19.146
	0.6	0.580	4.351	10.443	17.115	21.757	22.917
	0.7	0.580	4.351	11.023	19.146	25.238	26.688
	0.8	0.580	4.641	11.604	20.887	28.719	30.460
	0.9	0.580	4.641	11.604	22.627	31.910	33.941
	1	0.580	4.641	11.894	23.787	35.101	37.422
measurement #3	0	0	0	0	0	0	0
	0.1	0.290	1.450	2.321	3.191	3.771	4.061
	0.2	0.580	2.611	4.351	6.382	7.542	7.542
	0.3	0.580	3.481	6.092	9.283	11.314	11.314
	0.4	0.580	4.351	7.542	12.184	14.795	15.085
	0.5	0.580	4.932	8.413	14.795	18.276	18.856
	0.6	0.580	4.641	9.283	17.115	21.757	22.337
	0.7	0.580	4.641	9.863	19.146	25.238	26.108
	0.8	0.870	5.222	10.153	20.887	28.719	29.589
	0.9	0.580	4.932	10.153	22.337	31.910	33.070
	1	0.580	5.222	10.443	23.497	35.101	36.551

References

Bertani, G., 1951. Studies on lysogenesis. I. The mode of phage liberation by lysogenic *Escherichia coli*. J Bacteriol. 62**,** 293-300.

Bibb, M.J., Janssen, G.R., Ward, J.M., 1985. Cloning and analysis of the promoter region of the erythromycin resistance gene (*ermE*) of *Streptomyces erythraeus*. Gene, 38, 215-226.

Birnboim, H. C., Doly, J., 1979. A rapid alkaline extraction procedure for screening recombinant plasmid DNA. Nucleic Acids Res. 7**,** 1513-1523.

Blaskovich, M. A. T., Hansford, K. A., Butler, M. S., Jia, Z., Mark, A. E., Cooper, M. A., 2018. Developments in glycopeptide antibiotics. ACS Infect Dis. 4**,** 715-735.

Geib, N., Weber, T., Wörtz, T., Zerbe, K., Wohlleben, W., Robinson, J.A., 2010. Genome mining in *Amycolatopsis balhimycina* for ferredoxins capable of supporting cytochrome P450 enzymes involved in glycopeptide antibiotic biosynthesis. FEMS Microbiol Lett. 306, 45-53.

Greule, A., Izore, T., Iftime, D., Tailhades, J., Schoppet, M., Zhao, Y., Peschke, M., Ahmed, I., Kulik, A., Adamek, M., Goode, R. J. A., Schittenhelm, R. B., Kaczmarski, J. A., Jackson, C. J., Ziemert, N., Krenske, E. H., De Voss, J. J., Stegmann, E., Cryle, M. J., 2019. Kistamicin biosynthesis reveals the biosynthetic requirements for production of highly crosslinked glycopeptide antibiotics. Nat Commun. 10**,** 2613.

Grundy, W. E., Sinclair, A. C., Theriault, R. J., Goldstein, A. W., Rickher, C. J., Warren, H. B., Jr., Oliver, T. J., Sylvester, J. C., 1956. Ristocetin, microbiologic properties. Antibiot Annu. 687-692.

Hansen, M. H., Stegmann, E., Cryle, M. J., 2022. Beyond vancomycin: recent advances in the modification, reengineering, production and discovery of improved glycopeptide antibiotics to tackle multidrug-resistant bacteria. Curr Opin Biotechnol. 77**,** 102767.

Haslinger, K., Peschke, M., Brieke, C., Maximowitsch, E., Cryle, M. J., 2015. X-domain of peptide synthetases recruits oxygenases crucial for glycopeptide biosynthesis. Nature. 521**,** 105-109.

Hubbard, B. K., Thomas, M. G., Walsh, C. T., 2000. Biosynthesis ofL-phydroxyphenylglycine, a non proteinogenic amino acid constituent of peptide antibiotics. Chem Biol. 7, 931-942.

Kilian, R., Frasch, H. J., Kulik, A., Wohlleben, W., Stegmann, E., 2016. The VanRS homologous two component system VnlRSAb of the glycopeptide producer *Amycolatopsis balhimycina* activates transcription of the vanHAXSc genes in Streptomyces coelicolor, but not in A. balhimycina. Microb Drug Resist. 22, 499509.

Kloosterman, H., Hessels, G. I., Vrijbloed, J. W., Euverink, G. J., Dijkhuizen, L., 2003. (De)regulation of key enzyme steps in the shikimate pathway and phenylalanine-specific pathway of the actinomycete Amycolatopsis methanolica. Microbiology (Reading). 149, 3321-3330.

Lutke-Eversloh, T., Stephanopoulos, G., 2007. L-tyrosine production by deregulated strains of Escherichia coli. Appl Microbiol Biotechnol. 75, 103-110.

MacNeil, D. J., Gewain, K. M., Ruby, C. L., Dezeny, G., Gibbons, P. H., MacNeil, T., 1992. Analysis of *Streptomyces avermitilis* genes required for avermectin biosynthesis utilizing a novel integration vector. Gene. 111**,** 61-68.

Menges, R., Muth, G., Wohlleben, W., Stegmann, E., 2007. The ABC transporter Tba of *Amycolatopsis balhimycina* is required for efficient export of the glycopeptide antibiotic balhimycin. Appl Microbiol Biotechnol. 77**,** 125-134.

Mulyani, S., Egel, E., Kittel, C., Turkanovic, S., Wohlleben, W., Süssmuth, R.D., van Pée, KH. , 2010. The thioesterase Bhp is involved in the formation of betahydroxytyrosine during balhimycin biosynthesis in *Amycolatopsis balhimycina*. Chembiochem. 11, 266-271.

Nicolaou, K. C., Boddy, C. N., Brase, S., Winssinger, N., 1999. Chemistry, Biology, and Medicine of the glycopeptide antibiotics. Angew Chem Int Ed Engl. 38**,** 2096-2152.

Paget, M. S., Chamberlin, L., Atrih, A., Foster, S. J., Buttner, M. J., 1999. Evidence that the extracytoplasmic function sigma factor sigmaE is required for normal cell wall structure in *Streptomyces coelicolor* A3(2). J Bacteriol. 181**,** 204-211.

Pelzer, S., Reichert, W., Huppert, M., Heckmann, D., Wohlleben, W., 1997. Cloning and analysis of a peptide synthetase gene of the balhimycin producer *Amycolatopsis mediterranei* DSM5908 and development of a gene disruption/replacement system. J Biotechnol. 56**,** 115-128.

Peschke, M., Brieke, C., Goode, R. J., Schittenhelm, R. B., Cryle, M. J., 2017.

Chlorinated glycopeptide antibiotic peptide precursors improve cytochrome P450-catalyzed cyclization cascade efficiency. Biochemistry. 56**,** 1239-1247.

Pfeifer, V., Nicholson, G. J., Ries, J., Recktenwald, J., Schefer, A. B., Shawky, R. M., Schroder, J., Wohlleben, W., Pelzer, S., 2001. A polyketide synthase in glycopeptide biosynthesis: the biosynthesis of the non-proteinogenic amino acid (S)-3,5-dihydroxyphenylglycine. J Biol Chem. 276**,** 38370-38377.

Puk, O., Bischoff, D., Kittel, C., Pelzer, S., Weist, S., Stegmann, E., Sussmuth, R. D., Wohlleben, W., 2004. Biosynthesis of chloro-beta-hydroxytyrosine, a nonproteinogenic amino acid of the peptidic backbone of glycopeptide antibiotics. J Bacteriol. 186**,** 6093-6100.

Sarji, K. E., Stratton, R. D., Wagner, R. H., Brinkhous, K. M., 1974. Nature of von Willebrand factor: a new assay and a specific inhibitor. Proc Natl Acad Sci U S A. 71**,** 2937-2941.

Schoppet, M., Peschke, M., Kirchberg, A., Wiebach, V., Sussmuth, R. D., Stegmann, E., Cryle, M. J., 2019. The biosynthetic implications of late-stage condensation domain selectivity during glycopeptide antibiotic biosynthesis. Chem Sci. 10**,** 118-133.

Shawky, R. M., Puk, O., Wietzorrek, A., Pelzer, S., Takano, E., Wohlleben, W., Stegmann, E., 2007. The border sequence of the balhimycin biosynthesis gene cluster from *Amycolatopsis balhimycina* contains *bbr,* encoding a StrR-like pathway-specific regulator. J Mol Microbiol Biotechnol. 13**,** 76-88.

Smith, P. K., Krohn, R. I., Hermanson, G. T., Mallia, A. K., Gartner, F. H., Provenzano, M. D., Fujimoto, E. K., Goeke, N. M., Olson, B. J., Klenk, D. C., 1985. Measurement of protein using bicinchoninic acid. Anal Biochem. 150**,** 76-85.

Song, J., Bonner, C. A., Wolinsky, M., Jensen, R. A., 2005. The TyrA family of aromatic-pathway dehydrogenases in phylogenetic context. BMC Biol. 3**,** 13.

Spohn, M., Kirchner, N., Kulik, A., Jochim, A., Wolf, F., Muenzer, P., Borst, O., Gross, H., Wohlleben, W., Stegmann, E., 2014. Overproduction of Ristomycin A by activation of a silent gene cluster in *Amycolatopsis japonicum* MG417-CF17. Antimicrob Agents Chemother. 58**,** 6185-6196.

Stegmann, E., Frasch, H. J. Wohlleben, W. 2010. Glycopeptide biosynthesis in the context of basic cellular functions. Curr Opin Microbiol, 13, 595-602.

Stegmann, E., Pelzer, S., Wilken, K., Wohlleben, W., 2001. Development of three different gene cloning systems for genetic investigation of the new species *Amycolatopsis japonicum* MG417-CF17, the ethylenediaminedisuccinic acid producer. J Biotechnol. 92**,** 195-204.

Stegmann, E., Frasch, H.J., Kilian, R., Pozzi, R., 2014. Self-resistance mechanisms of actinomycetes producing lipid II-targeting antibiotics. Int J Med Microbiol. 305, 190-195.

Thykaer, J., Nielsen, J., Wohlleben, W., Weber, T., Gutknecht, M., Lantz, A. E., Stegmann, E., 2010. Increased glycopeptide production after overexpression of shikimate pathway genes being part of the balhimycin biosynthetic gene cluster. Metab Eng. 12**,** 455-461.

Truman, A. W., Kwun, M. J., Cheng, J., Yang, S. H., Suh, J. W., Hong, H. J., 2014. Antibiotic resistance mechanisms inform discovery: identification and characterization of a novel *Amycolatopsis* strain producing ristocetin. Antimicrob Agents Chemother. 58**,** 5687-5695.

Unsleber, S., Wohlleben, W., Stegmann, E., 2019. Diversity of peptidoglycan structure Modifications and their physiological role in resistance in antibiotic producers. Int J Med Microbiol. 309, 151332.

Wohlleben, W., Mast, Y., Muth, G., Röttgen, M., Stegmann, E., Weber, T., 2012. Synthetic biology of secondary metabolite biosynthesis in actinomycetes: Engineering precursor supply as a way to optimize antibiotic production. FEBS Lett. 586, 2171-2176.

Zhao, Y., Ho, Y.T.C., Tailhades, J., Cryle, M., 2021. Understanding the glycopeptide antibiotic crosslinking cascade: *In vitro* approaches reveal the details of a complex biosynthesis pathway. Chembiochem. 22, 43-51.

5.2. Publication 2: Exploring shikimate pathway enzyme diversity for engineering of glycopeptide antibiotic biosynthesis

Jens-Peter Rodler*, Oleksandr Yushchuk*, Athina Gavriilidou, Anna Katharina Siegert, Andreas Kulik, Wolfgang Wohlleben, Nadine Ziemert, Evi Stegmann

**Shared first authors and equal contribution*

5.2.1 Summary of results

The insights gained from the detailed analysis of shikimate-pathway regulation in *A. balhimycina* provide a conceptual foundation for understanding how GPA producers secure sufficient precursor supply during secondary metabolite biosynthesis. While these findings demonstrate that BGC encoded Dahp an Pdh isoenzymes can be functionally decoupled from primary metabolic feedback control to enhance GPA production, they also raise the question of how broadly such regulatory strategies are conserved across different GPA-producing taxa.

To address this knowledge gap, the present work aimed i) to investigate the phylogenetic diversity of Dahp and Pdh isoenzymes across canonical GPA producers, ii) to characterize the biochemical and functional diversity of Dahp and Pdh from *A. coloradensis* and *Act. teichomyceticus*, and iii) to determine how this diversity influences shikimate-pathway regulation and GPA production *in vivo*. The results demonstrate that feedback regulation, rather than catalytic efficiency alone, is a critical determinant of whether shikimate-pathway enzymes can sustain precursor flux during antibiotic biosynthesis, and that exploiting this regulatory diversity provides a powerful and rational strategy for metabolic engineering of GPA production.

A comprehensive phylogenetic analysis based on maximum-likelihood inference of $Dahp_{sec}$ and Pdh_{sec} isoenzymes encoded in canonical GPA BGCs revealed evolutionary diversification (Publication 2: Figure 1, Figure 2). Enzymes from producers of the same GPA type did not consistently cluster together. $Dahp_{ACOL\_sec}$ from *A. coloradensis* clustered separately from the main *Amycolatopsis* clade and was grouped closer to $Dahp_{ATE\_sec}$ from *Act. teichomyceticus*, whereas Pdh_{ACOL_sec} aligned within a conserved *Amycolatopsis* clade that included other type II GPA producers. Pdh_{ATE_sec} formed a distinct subclade that was more closely related to Pdh homologs from *Streptomyces* species.

The divergence observed in the phylogenetic analysis of $Dahp_{sec}$ and Pdh_{sec} from *A. coloradensis* and *Act. teichomyceticus* suggests that their regulatory properties and physiological roles in shikimate-pathway control might differ substantially from the homologous enzymes studied in the type I GPA producer *A. balhimycina*.

Therefore, $dahp_{ACOL\_sec}$ and pdh_{ACOL_sec} were first investigated in an *in vivo* functional analysis, which showed that overexpression of $dahp_{ACOL\_sec}$ or pdh_{ACOL_sec} individually

reduced avoparcin production to 60-70% of wild type levels, while co-overexpression of both genes reduced production to ~5% (Publication 2: Figure 3). Deletion of *dahp*$_{ACOL\_sec}$ resulted in a 2-fold increase in avoparcin titers, whereas deletion of *pdh*$_{ACOL\_sec}$ decreased production by ~80% (Publication 2: Figure 3).

Both sets of *dahp* and *pdh* from *A. coloradensis* and *Act. teichomyceticus* were cloned, heterologously expressed in *E. coli*, the corresponding enzymes were purified via Ni-NTA affinity chromatography or using a Strep-tactin superflow column and were subjected to kinetic and inhibition assays to compare their catalytic properties and allosteric regulation.

Biochemical analysis of recombinant Dahp isoenzymes from *A. coloradensis* demonstrated substantial differences in catalytic behaviour (Publication 2: Table 4, Figure S1). Dahp$_{ACOL_prim}$ and Dahp$_{ACOL_sec}$ exhibited similar affinities for E4P, but Dahp$_{ACOL_sec}$ showed significantly higher V_{max} values and catalytic efficiencies with both substrates. Inhibition assays performed with the end products of the shikimate pathway (Tyr, Phe and Trp) revealed that Dahp$_{ACOL_prim}$ was inhibited by Phe and Trp, whereas Dahp$_{ACOL_sec}$ was strongly inhibited by all three amino acids (Publication 2: Table 5).

Kinetic studies of Dahp$_{ATE_prim}$ and Dahp$_{ATE_sec}$ from *Act. teichomyceticus* showed that Dahp$_{ATE_sec}$ possessed a higher affinity for E4P than Dahp$_{ATE_prim}$ but reached higher maximal velocities and catalytic efficiencies than Dahp$_{ATE_sec}$ with E4P and PEP (Publication 2: Table 6, Figure S2). Investigation of the regulatory mechanism of Dahp$_{ATE_prim}$ and Dahp$_{ATE_sec}$ revealed that Dahp$_{ATE_sec}$ was inhibited only by Tyr (Publication 2: Table 7). The Tyr-dependent inhibition of Dahp$_{ATE_sec}$ was partially antagonized in the presence of Phe. In contrast, Dahp$_{ATE_prim}$ was inhibited by Tyr, Phe, Trp and a combination of Tyr and Phe (Publication 2: Table 7).

Biochemical characterization of the Pdh isoenzymes from *A. coloradensis* showed that both, Pdh$_{ACOL_prim}$ and Pdh$_{ACOL_sec}$ had a low affinity for prephenate (Publication 2: Table 8). Pdh$_{ACOL_prim}$ exhibited a higher catalytic efficiency than Pdh$_{ACOL_sec}$ (Publication 2: Table 8). Inhibition assays showed that both enzymes were inhibited by Tyr. Pdh$_{ACOL_prim}$ was inhibited in the presence of Phe, whereas Pdh$_{ACOL_sec}$ showed a slight increase in its activity (Publication 2: Table 9, Figure S4). The combination of Tyr and Phe partially reversed the Tyr-dependent inhibition of Pdh$_{ACOL_sec}$ (Publication 2: Table 9).

In *Act. teichomyceticus*, Pdh_{ATE_sec} accepted prephenate as a substrate with very low affinity (Publication 2: Table 10, Figure S5), whereas Pdt_{ATE_prim} showed no measurable activity in the presence of prephenate concentrations up to 5000 µM. Pdh_{ATE_sec} was inhibited by both Tyr and Phe, but using equimolar concentrations of both amino acids did not lead to an increased inhibitory effect (Publication 2: Table 11, Figure S6).

For the *in vivo* functional analysis in *Act. teichomyceticus*, an additional endogenous copy of $dahp_{ATE\_sec}$ or a heterologous $dahp_{ABAL\_sec}$ gene was introduced into the genome of *Act. teichomyceticus*. The overexpression of $dahp_{ABAL\_sec}$ led to a more than 2-fold increase in teicoplanin production, while the strain carrying an additional copy of $dahp_{ATE\_sec}$ produced ~1.5-fold more teicoplanin than the wild type (Publication 2: Figure 4). Further investigations showed that overexpression of genes encoding Pdh isoenzymes alters teicoplanin production substantially. Overexpression of heterologous pdh_{ABAL_sec} had no detectable effect on teicoplanin production, whereas overexpression of pdh_{ATE_sec} led to a more than 3-fold increase in teicoplanin titers (Publication 2: Figure 5). In contrast, overexpression of a truncated version of pdh_{ATE_sec}, lacking the C-termin ACT-domain ($pdh_{ATE\_sec}tr$), did not increase teicoplanin titers (Publication 2: Figure 5). Overexpression of prephenate dehydratases from *A. balhimycina* (pdt_{ABAL}) or from *A. techomyceticus* (pdt_{ATE}) resulted in a 3-fold increase in teicoplanin production relative to the strain carrying the empty-vector (Publication 2: Figure 6). These effects were similar to the results obtained by feeding *Act. teichomyceticus* with 5 mM Phe (Publication 2: Figure 6).

Collectively, this study demonstrates that the shikimate pathway enzymes Dahp and Pdh display substantial phylogenetic and functional diversity across canonical GPA producers. The results show that feedback regulation, rather than catalytic efficiency alone, are key determinants of whether BGC encoded isoenzymes support sustained precursor flux for GPA biosynthesis. Importantly, this work highlights that leveraging the inherent regulatory diversity of shikimate pathway enzymes offers a rational and versatile strategy to tailor metabolic engineering approaches for GPA production across diverse producer strains.

5.2.2 Publication 2

Exploring shikimate pathway enzyme diversity for engineering of glycopeptide antibiotic biosynthesis

Author list:
Jens-Peter Rodler[a#], Oleksandr Yushchuk[b#], Athina Gavriilidou[c,d,e], Anna Katharina Siegert[a], Andreas Kulik[a], Wolfgang Wohlleben[f], Nadine Ziemert[c], Evi Stegmann[a]*

[a]Interfaculty Institute of Microbiology and Infection Medicine Tübingen, Microbial Bioactive Compounds, University of Tübingen, Auf der Morgenstelle 28, 72076, Tübingen, Germany

[b]Department of Genetics and Biotechnology, Ivan Franko National University of Lviv, Hrushevskoho St. 4, 79005 Lviv, Ukraine

[c]Translational Genome Mining for Natural Products, Interfaculty Institute of Microbiology and Infection Medicine Tübingen (IMIT), Interfaculty Institute for Biomedical Informatics (IBMI), University of Tübingen, Tübingen, Germany

[d]Department of Computational Biology, University of Lausanne, CH-1015 Lausanne, Switzerland

[e]Swiss Institute of Bioinformatics, Lausanne, Switzerland

[f]Interfaculty Institute of Microbiology and Infection Medicine Tübingen (IMIT), Department of Microbiology and Biotechnology, University of Tübingen, Auf der Morgenstelle 28, 72076 Tübingen, Germany

# equally contributes
*corresponding author

Abstract

Supply of pathway precursors is often limits the biosynthesis of specialized metabolites. Type I-IV glycopeptide antibiotics (GPAs) contain non-proteinogenic aromatic amino acids, requiring a sustained flux through the shikimate pathway. To secure precursor provision, many GPA producers encode secondary copies of 3-deoxy-D-arabino-heptulosonate-7-phosphate synthase ($Dahp_{sec}$) and prephenate dehydrogenase (Pdh_{sec}) within their biosynthetic gene clusters (BGCs). The functional diversity and regulatory logic of these isoenzymes across taxa remains insufficiently understood. Phylogenetic analysis of $Dahp_{sec}$ and Pdh_{sec} from characterized and uncharacterized GPA BGCs revealed substantial evolutionary diversification that does not correlate with GPA type or producer genus.

We biochemically characterized $Dahp_{sec}$ and Pdh_{sec} from *Amycolatopsis coloradensis* DSM 4425 (avoparcin producer) and *Actinoplanes teichomyceticus* NRRL B-16726 (teicoplanin producer), representing distinct evolutionary relatives. The analysis revealed pronounced differences in kinetic efficiency and allosteric regulation between the two enzymes. In *A. coloradensis*, $Dahp_{ACOL\_sec}$ and Pdh_{ACOL_sec} are strongly inhibited by Tyr, and $Dahp_{ACOL\_sec}$ is additionally inhibited by Phe and Trp, restricting shikimate-pathway flux and avoparcin production. In contrast, $Dahp_{ATE\_sec}$ and Pdh_{ATE_sec} from *Act. teichomyceticus* are primarily inhibited by Tyr, while Phe antagonizes this inhibition for $Dahp_{ATE\_sec}$, supporting sustained precursor flux.

Exploiting these regulatory features through targeted overexpression of $dahp_{ATE\_sec}$, as well as pdh_{ATE_sec}, significantly increased teicoplanin production. Together, our results demonstrate that feedback regulation, rather than catalytic efficiency alone, makes shikimate-pathway enzymes suitable for sustained precursor supply, and that feedback-aware enzyme selection provides a powerful strategy for rational metabolic engineering of GPA production.

Declaration of interests

☒ The authors declare that they have no known competing financial interests or personal relationships that could have appeared to influence the work reported in this paper.

☐ The authors declare the following financial interests/personal relationships which may be considered as potential competing interests:

Keywords

Glycopeptide antibiotics; Teicoplanin; Aromatic amino acids; Shikimate pathway; Pathway engineering

Abbreviations

Asn, asparagine; BGC, biosynthetic gene cluster; DAHP, deoxy-D-arabino-heptulosonate 7-phosphate; Dahp, deoxy-D-arabino-heptulosonate 7-phosphate synthase; Dpg. 3,5-dihydroxyphenylglycine; E4P, D-erythrose-4-phosphate; GPA, glycopeptide antibiotic; Hpg, 4-hydroxyphenylglycine; 4-HPP-hydroxyphenylpyruvate; Bht, β-hydroxytyrosine; NRPS, non-ribosomal peptide synthetases; Leu, leucine; Pdh, prephenate dehydrogenase; PEP, phosphoenolpyruvate; Phe, phenylalanine; Pdt, prephenate dehydratase; Trp, tryptophan; Tyr, tyrosine

Keywords
Glycopeptide antibiotics; Teicoplanin; Aromatic amino acids; Shikimate pathway; Pathway engineering

Abbreviations
Asn, asparagine; BGC, biosynthetic gene cluster; DAHP, deoxy-D-arabino-heptulosonate 7-phosphate; Dahp, deoxy-D-arabino-heptulosonate 7-phosphate synthase; Dpg. 3.5-dihydroxyphenylglycine; E4P, D-erythrose-4-phosphate; GPA, glycopeptide antibiotic; Hpg, 4-hydroxyphenylglycine; 4-HPP-hydroxyphenylpyruvate; Bht, β-hydroxytyrosine; NRPS, non-ribosomal peptide synthetases; Leu, leucine; Pdh, prephenate dehydrogenase; PEP, phosphoenolpyruvate; Phe, phenylalanine; Pdt, prephenate dehytratase; Trp, tryptophan; Tyr, tyrosine

1. Introduction

Glycopeptide antibiotics (GPAs) form a structurally diverse class of natural products predominantly synthesized by filamentous actinobacteria, including members of the genera *Amycolatopsis*, *Streptomyces*, *Actinoplanes,* and related taxa (Gavriilidou et al., 2023; Waglechner et al., 2019; Yim et al., 2014). Exemplary representatives include vancomycin (type I), isolated from *Amycolatopsis orientalis* in 1953 (Brigham and Pittenger, 1956) and used in clinics as a last resort antibiotic against Gram-positive bacteria, and teicoplanin (type IV), produced by *Actinoplanes teichomyceticus* and introduced into clinical use in the mid-1980s (Yim et al., 2014). Increasing bacterial resistance has prompted the development of second-generation GPAs, such as dalbavancin, telavancin, and oritavancin (Blaskovich et al., 2018), but reliance on *in vivo* biosynthesis of their heptapeptide core continues to constrain large-scale production.

The assembly of the GPA core is catalyzed by non-ribosomal peptide synthetases (NRPS) from a pool of proteogenic amino acids, such as leucine (Leu) and asparagine (Asn), and non-proteogenic amino acids, including *β*-hydroxytyrosine (Bht), 4-hydroxyphenylglycine (Hpg), and 3,5-dihydroxyphenylglycine (Dpg). The heptapeptide backbone is further crosslinked by cytochrome P450 monooxygenases, chlorinated, and subsequently decorated by tailoring enzymes with e.g., sulfate and methyl groups, as well as sugar residues. Type I to IV GPAs differ in the amino acid composition of the peptidic backbone, in the number and/or type of crosslinks and tailoring modifications. Since type V GPAs comprise compounds with a very different structure and mode of action (Gavriilidou et al., 2023), in this study we exclusively focused on type-I-IV (canonical) GPAs.

The requirement for the unusual aromatic amino acids Bht, Hpg, and Dpg makes GPA-producing actinomycetes extremely reliant on the shikimate pathway, a central metabolic route that connects primary carbohydrate metabolism to secondary metabolism (Goldfinger et al., 2023; Mir et al., 2015; Nicolaou et al., 1999; Thykaer et al., 2010). In its initial step, 3-deoxy-D-arabino-heptulosonate 7-phosphate (DAHP) synthase (Dahp) catalyzes the condensation of phosphoenolpyruvate (PEP) and D-erythrose-4-phosphate (E4P) to form DAHP. This intermediate is subsequently converted into chorismate through six enzymatic steps (Bentley, 1990; Mir et al., 2015). Chorismate can be converted, among other aromatic amino acids and metabolites, into tyrosine (Tyr) by the sequential action of the chorismate mutase, which converts chorismate into prephenate, and the prephenate dehydrogenase (Pdh), which oxidatively decarboxylates prephenate into 4-hydroxyphenylpyruvate (4-HPP). The latter is then transaminated to Tyr (Bentley, 1990). Tyr and 4-HPP are required as precursors for the biosynthesis of Bht and Hpg, respectively (Hubbard et al., 2000; Puk et al., 2004). Moreover, Tyr also serves as the amino group donor in the biosynthesis of both Hpg and Dpg (Pfeifer et al., 2001).

Because of the central role of the shikimate pathway in supplying key precursors for GPA biosynthesis, GPA-producing actinomycetes have evolved mechanisms to circumvent the tight feedback regulation which the shikimate pathway is subject to. For example, many producers possess additional copies of the key shikimate pathway genes, $dahp_{sec}$ and pdh_{sec}, within GPA biosynthesis gene clusters (BGCs) (Goldfinger et al., 2023). Bacterial DAHP synthases (Dahps) are generally categorized into two

types. Type I enzymes, subdivided into subtypes Iα and Iβ, are relatively short (~350 amino acids) in comparison to type II enzymes and are typically inhibited by aromatic amino acids such as Tyr and Phe or by chorismate/prephenate (Light and Anderson, 2013; Wu and Woodard, 2006). In contrast, type II enzymes are approximately 100 amino acids longer and may be inhibited by Phe, Tyr or Trp. These two types represent distinct evolutionary lineages, and genes encoding both have been identified in the genomes of GPA producers. Notably, Dahps located within GPA BGCs belong to type I, while those encoded elsewhere in the genome (*dahp*$_{prim}$) can belong to either type . Prephenate dehydrogenases belong to the TyrA family of aromatic-pathway dehydrogenases, which convert either arogenate or prephenate (or both) into Tyr. These enzymes are widespread across bacterial lineages (Bonner et al., 2008; Song et al., 2005). Within the phylum *Actinomycetota*, two major clusters of TyrA homologs have been described (Song et al., 2005). The first includes NAD^+/$NADP^+$-dependent enzymes from *Corynebacterium*, *Mycobacterium*, and *Bifidobacterium* species, while the second comprises NAD^+-specific enzymes from other actinobacteria. Many of these enzymes possess C-terminal ACT-like regulatory domains that mediate feedback control. This domain, named after the three archetypal enzymes that harbor it: aspartate kinase, chorismate mutase, and TyrA, often governs activation or inhibition by phenylalanine (Phe) (Song et al., 2005). Experimental evidence also indicates that actinobacterial TyrA enzymes display variable substrate specificities. For instance, Pdh from *Actinoplanes missouriensis* is an arogenate-specific enzyme lacking both prephenate dehydrogenase activity and Tyr feedback inhibition (Hund et al., 1989). In *A. balhimycina*, both Pdh$_{prim}$ (hereafter referred to as Pdh$_{ABAL_prim}$) and Pdh$_{sec}$ (hereafter referred to as Pdh$_{ABAL_sec}$) are resistant to feedback inhibition by Tyr and Phe. However, Pdh$_{ABAL_sec}$ shows specificity towards prephenate, whereas Pdh$_{ABAL_prim}$ appears to favor arogenate (Goldfinger et al., 2023).

We reasoned that exploring the diversity of these key enzymes in actinobacteria could provide valuable opportunities for metabolic engineering to enhance GPA production in industrially relevant actinomycete strains. Therefore, we performed a comprehensive phylogenetic analysis of Dahp and Pdh enzymes from GPA-producing actinomycetes. This revealed that Tei14* (hereafter referred to as Dahp$_{ATE_sec}$) and Tei24* (hereafter referred to as Pdh$_{ATE_sec}$) from *Act. teichomyceticus* and Dahp$_{ACOL_sec}$ and Pdh$_{ACOL_sec}$ from *A. coloradensis* form distinct phylogenetic lineages compared to Dahp$_{ABAL_sec}$ and Pdh$_{ABAL_sec}$ from *A. balhimycina* (Goldfinger et al., 2023). Building on these insights and considering the clinical importance of teicoplanin, we characterized the enzymatic properties of Dahp and Pdh from *A. coloradensis* and *Act. teichomyceticus* and performed *in vivo* functional analyses in both strains. Our findings indicate that functional diversity of Dahp and Pdh enzymes is not always reflected at the phylogenetic level, but it is worth exploring in order to develop more rational metabolic engineering strategies.

2. Material and methods

2.1 Bacterial strains and plasmids

The bacterial strains used and generated in this study are listed in Table 6, the plasmids used in this study are listed in Table 7. *Escherichia coli* NovaBlue and DH5α were used for cloning purposes, *E. coli* Rosetta 2(DE3)pLysS and *E. coli* BL21(DE3)pLysS were used for the heterologous expression of recombinant proteins, and *E. coli* ET12567 (pUZ8002) was used for conjugation purposes (Kieser et al., 2000).

Table 6: Bacterial strains used in this study.

Strain	Relevant feature(s)	Source or reference
Escherichia coli		
ET12567(pUZ8002)	Used for conjugative transfer of plasmid DNA, (dam-13::Tn9 dcm-6), pUZ8002 (Δ*oriT*).	(Kieser et al., 2000)
NovaBlue	host for cloning	Novagen
DH5α	host for cloning	MBI Fermentas
Rosetta 2(DE3)pLysS	host for protein expression	Novagen
BL21(DE3)pLysS	host for protein expression	(Davanloo et al., 1984; Studier and Moffatt, 1986)
Amycolatopsis coloradensis		
DSM 4425	wild type, avoparcin producer	(Labeda, 1995)
***dahp*$_{ACOL\_sec}^{+}$**	*dahp*$_{ACOL\_sec}$ overexpression strain	this work
***pdh*$_{ACOL\_sec}^{+}$**	*pdh*$_{ACOL\_sec}$ overexpression strain	this work
***dahp*$_{ACOL\_sec}^{+}$/*pdh*$_{ACOL\_sec}^{+}$**	*dahp*$_{ACOL\_sec}$ and *pdh*$_{ACOL\_sec}$ *overexpression strain*	this work
Δ*dahp*$_{ACOL\_sec}$	*dahp*$_{ACOL\_sec}$ deletion mutant	this work
Δ*pdh*$_{ACOL\_sec}$	*pdh*$_{ACOL\_sec}$ deletion mutant	this work
Actinoplanes teichomyceticus		
NRRL B-16726	wild type, natural producer of teicoplanin	ARS Culture Collection
(pSET152A)	derivative carrying pSET152A	this work
(pSET152)	derivative carrying pSET152	this work
***dahp*$_{ABAL\_sec}^{+}$**	derivative carrying pSAdahp$_{ABAL_sec}$	this work
***dahp*$_{ATE\_sec}^{+}$**	derivative carrying pSETdahp$_{ATE_sec}^{+}$	this work
***pdh*$_{ABAL\_sec}^{+}$**	derivative carrying pSApdh$_{ABAL_sec}^{+}$	this work
***pdh*$_{ATE\_sec}^{+}$**	derivative carrying pSApdh$_{ATE_sec}^{+}$	this work
***pdh*$_{ATE\_sec}$*tr*$^{+}$**	derivative carrying pSApdh$_{ATE_sec}$tr^{+}	this work
***pdt*$_{ABAL}^{+}$**	derivative carrying pSApdt$_{ABAL}^{+}$	this work
***pdt*$_{ATE}^{+}$**	derivative carrying pSApdt$_{ATE}^{+}$	this work

Table 7: Plasmids used in this work.

Plasmids	Relevant feature(s)	Source or reference
pSET152	ΦC31-based integrative vector, *apra*^{r}	(Kieser et al., 2000)
pSET152A	pSET152 derivative, ΦC31 *attP,* constitutive promoter *aac(3)IV*, *apra*^{r}	(Horbal et al., 2013)
pRM4	pSET152 derivative, ΦC31 *attP,* constitutive promoter *ermE*p*, *apra*^{r}	(Menges et al., 2007)
pRM4pdh$_{ACOL_sec}$	*pdh$_{ACOL_sec}$* under the control of *ermE*p*	this work
pRM4dahp$_{ACOL_sec}$	*dahp$_{ACOL_sec}$* under the control of *ermE*p*	this work
pRM4dahp$_{ACOL_sec}$/pdh$_{ACOL_sec}$	*pdh$_{ACOL_sec}$* and *dahp$_{ACOL_sec}$* under the control of *ermE*p*	this work
pSAdahp$_{ABAL_sec}$	pSET152A derivative containing *dahp$_{ABAL_sec}$* cloned via *Eco*RI/*Eco*RV sites	this work
pSApdh$_{ABAL_sec}$	pSET152A derivative containing *pdh$_{ABAL_sec}$* cloned via *Eco*RI/*Eco*RV sites	this work
pSApdh$_{ATE_sec}$	pSET152A derivative containing *pdh$_{ATE_sec}$* cloned via *Eco*RI/*Eco*RV sites	this work
pSApdh$_{ATE_sec}$tr	pSET152A derivative containing 3'-truncated variant of *pdh$_{ATE_sec}$* cloned via *Eco*RI/*Eco*RV sites	this work
pSApdt$_{ABAL}$	pSET152A derivative containing *pdt$_{ABAL}$* cloned via *Eco*RI/*Eco*RV sites	this work
pSApdt$_{ATE}$	pSET152A derivative containing *pdt$_{ATE}$* cloned via *Eco*RI/*Eco*RV sites	this work
pSETdahp$_{ATE_sec}$	pSET152 derivative carrying *dahp$_{ATE_sec}$* with its promoter region cloned via *Xba*I/*Eco*RV sites	this work
pGUSA21 derivatives		
pGUSA21	Suicide vector, *gusA*, *apra*^{r}*,* used for gene inactivation	(Pozzi et al., 2016)
pGUSA21_Δdahp$_{ACOL_sec}$	pGUSA21 deletion plasmid of *dahp*$_{ACOL\_sec}$	this work
pGUSA21_Δpdh$_{ACOL_sec}$	pGUSA21 deletion plasmid of *pdh*$_{ACOL\_sec}$	this work
Plasmids for expression of recombinant proteins		
pET30 EK/LIC	expression vector, T7lac promoter, *kan*^{r}, N-terminal fusion tags,	Novagen
pET30pdh$_{ATE_prim}$	construct for heterologous production of 6xHis Pdh$_{ATE_prim}$ from *Act. teichomyceticus*	this work
pET30pdh$_{ATE_sec}$	construct for heterologous production of 6xHis Pdh$_{ATE_sec}$ from *Act. teichomyceticus*	this work
pET30pdh$_{ACOL_prim}$	construct for heterologous production of 6xHis Pdh$_{ACOL_prim}$ from *A. coloradensis*	this work
pET11a-strep	expression vector, T7lac promoter, *amp*^{r}, C-terminal strep-tag	RG Brötz Oesterhelt (unpublished)
pET11adahp$_{ATE_prim}$-strep	construct for heterologous production of Dahp$_{ATE_prim}$-strep from *Act. teichomyceticus*	this work
pET11adahp$_{ATE_sec}$-strep	construct for heterologous production of Dahp$_{ATE_sec}$-strep from *Act. teichomyceticus*	this work

pET11adahp$_{ACOL_prim}$-strep	construct for heterologous production of Dahp$_{ACOL_prim}$-strep from *A. coloradensis*	this work
pET11adahp$_{ACOL_sec}$-strep	construct for heterologous production of Dahp$_{ACOL_sec}$-strep from *A. coloradensis*	this work
pET11pdh$_{ACOL_sec}$-strep	construct for heterologous production of Pdh$_{ACOL_sec}$-strep from *A. coloradensis*	this work

2.2 Media and culture conditions

A. coloradensis was grown in 20 mL tryptic soy broth (TSB) (Difco) on an orbital shaker (120 rpm) as a preculture or for DNA extraction. For avoparcin production assays, 100 mL of R5 medium (Kieser et al., 2000) was inoculated with 5 mL of preculture and cultivated for 7 days at 28 °C on an orbital shaker (120 rpm). Exconjugants were selected on SFM agar plates (Kieser et al., 2000).

Act. teichomyceticus strains were routinely maintained on SFM agar. Prior to conjugation, sporulating lawns of *Act. teichomyceticus* were obtained on ISP3 agar (Yushchuk et al., 2019), while transconjugants were selected on SFM agar. For chromosomal DNA isolation, *Act. teichomyceticus* strains were cultivated in E25 liquid vegetative medium (Taurino et al., 2011). The cultivation of *Act. teichomyceticus* strains was performed at 30 °C.

E. coli strains were grown in Lysogeny Broth (Bertani, 1951) at 37 °C. Liquid cultures were shaken at 180 rpm. Media were supplemented with antibiotics when necessary to maintain plasmids.

2.3 Plasmid generation for gene expression in *Act. teichomyceticus* and *A. coloradensis*

To generate the pSAdahp$_{ABAL_sec}$, pSApdh$_{ABAL_sec}$, pSApdh$_{ATE_sec}$, pSApdh$_{ATE_sec}$tr, pSApdt$_{ABAL}$, and pSApdt$_{ATE}$ plasmids, DNA fragments containing the corresponding open reading frames were amplified using the oligonucleotide primers listed in Table S1. These fragments were then subcloned into the *Eco*RV restriction endonuclease recognition site of the pJET1.2 plasmid (ThermoFisher Scientific). The DNA fragments containing *dahp$_{ABAL_sec}$* (1,080 bp), *pdh$_{ABAL_sec}$* (887 bp), *pdh$_{ATE_sec}$* (1,132 bp), *pdh$_{ATE_sec}$tr* (871 bp), *pdt$_{ABAL}$* (944 bp), *pdt$_{ATE}$* (1,017 bp) were excised from pJET-based constructs with *Eco*RV and *Eco*RI restriction endonucleases, and subsequently cloned into *Eco*RV/*Eco*RI recognition sites of the pSET152A (Horbal et al., 2013). The same strategy was employed to clone the DNA fragment containing *dahp$_{ATE_sec}$* open reading frame, along with the putative promoter region (1,503 bp) into pSET152 (Kieser et al., 2000), using *Xba*I/*Eco*RV recognition sites. This generated the pSETdahp$_{ATE_sec}$ vector.

For the overexpression of *pdh*$_{ACOL\_sec}$, *dahp*$_{ACOL\_sec}$, individually or together, the plasmids pRM4pdh$_{ACOL_sec}$, pRM4dahp$_{ACOL_sec}$, pRM4dahp$_{ACOL_sec}$/pdh$_{ACOL_sec}$ were constructed. The corresponding fragments were amplified using oligonucleotide primers listed in Table S1. The fragments *dahp*$_{ACOL\_sec}$ (1074 bp) for pRM4dahp$_{ACOL_sec}$, *pdh*$_{ACOL\_sec}$ (1106 bp) for pRM4pdh$_{ACOL_sec}$ as well as *pdh*$_{ACOL\_sec}$ (1096 bp) and

dahp$_{ACOL\_sec}$ (1066 bp) for pRM4dahp$_{ACOL_sec}$/pdh$_{ACOL_sec}$ were cloned into pRM4 via NEBuilder HiFi DNA Assembly (NEB) following manufacturers protocol.
All generated recombinant vectors were verified through restriction mapping and sequencing at Eurofins Genomics.

2.4 Deletion of *dahp*$_{ACOL\_sec}$ and *pdh*$_{ACOL\_sec}$ in *A. coloradensis* DSM 4425

For the deletion of *dahp*$_{ACOL\_sec}$ and *pdh*$_{ACOL\_sec}$ in *A. coloradensis* via homologous recombination, the plasmids pGUSA21_Δdahp$_{ACOL_sec}$ and pGUSA21_Δpdh$_{ACOL_sec}$ were constructed. DNA fragments containing 1.5 kb flanking regions up- and downstream of the corresponding gene were amplified using the oligonucleotide primers listed in Table S1. The fragments delta_*pdh*$_{ACOL_sec}$1 (1702 bp) and delta_*pdh*$_{ACOL_sec}$2 (1594 bp) for pGUSA21_Δpdh$_{ACOL_sec}$ and delta_*dahp*$_{ACOL_sec}$1 (1553 bp) delta_*dahp*$_{ACOL_sec}$2 (1541 bp) for pGUSA21_Δdahp$_{ACOL_sec}$ were cloned into pGUSA21 via NEBuilder HiFi DNA Assembly (NEB) following manufacturers protocol. Sequenced verified plasmids were transferred into *E. coli* ET12567 (pUZ8002) and delivered to *A. coloradensis* via conjugation. The obtained transconjugants were selected on SFM agar plates (Kieser et al., 2000) containing 100 µg/µL apramycin and 40 µg/µL X-Gluc (5-bromo-4-chloro-1H-indol-3-yl β-D-glucuronic acid). Single crossing-over of the plasmid into the chromosome was determined by blue-white screening and verified by PCR.

The obtained single crossover mutant strains *A. coloradensis* pGUSA21_Δdahp$_{ACOL_sec}$ and *A. coloradensis* pGUSA21_Δpdh$_{ACOL_sec}$ were used for the generation of the *in frame* deletion mutants *A. coloradensis* Δ*pdh*$_{ACOL\_sec}$ and *A. coloradensis* Δ*dahp*$_{ACOL\_sec.}$ The single crossover mutant strains were cultivated in 100 mL R5 medium at 29 °C and 120 rpm under apramycin selection for 2 days. The mycelium was washed and used for inoculation of 100 mL R5 medium without antibiotics and cultivated at 29 °C and 120 rpm for 24 h. The culture was then cultivated at 37 °C for 24 h. The mycelium was harvested by centrifugation and protoplasts were prepared as previously described (Stegmann et al., 2001). Diluted protoplasts were plated on R5 agar plates containing 40 µg/µL X-Gluc and white colonies were screened for deletion of Δ*pdh*$_{ACOL\_sec}$ or Δ*dahp*$_{ACOL\_sec}$ using oligonucleotide primers (Table S1). Additionally, obtained mutants were verified by sequencing.

2.5 Conjugal transfer of plasmids

Plasmids were transferred into *Act. teichomyceticus* (using spores as recipient-cells) via intergeneric conjugation with *E. coli* ET12567 (pUZ8002), as described earlier (Ha et al., 2008; Horbal et al., 2014). Plasmid transfer into *A. coloradensis* was carried out via intergeneric conjugation (Kieser et al., 2000), with minor adaptations to the protocol. Mycelia from a TSB plate was used instead of spores.

2.6 Heterologous production of recombinant proteins in *E. coli*

For the heterologous production of recombinant N-terminal 6x his-tagged fusion proteins (Pdh_{ACOL_prim}, Pdh_{ATE_prim} and Pdh_{ATE_sec}) or C-terminal strep tagged fusion proteins ($Dahp_{ACOL\_prim}$, $Dahp_{ACOL\_sec}$, Pdh_{ACOL_sec}, $Dahp_{ATE\_prim}$ and $Dahp_{ATE\_sec}$) *E. coli* Rosetta 2(DE3)pLysS or *E. coli* BL21(DE3)pLysS were used. The genes were amplified using oligonucleotide primers (Table S1), pdh_{ACOL_prim} and pdh_{ATE_prim} and pdh_{ATE_sec} were cloned into the expression vector pET30 EK/LIC using T4 DNA polymerase (Novagen). The amplified fragments containing $dahp_{ATE\_sec}$, $dahp_{ATE\_prim}$, pdh_{ACOL_sec}, $dahp_{ACOL\_sec}$ and $dahp_{ACOL\_prim}$ were cloned into pET11a-strep using NEBuilder HiFi DNA Assembly (NEB) following manufacturer's protocol. Constructs were verified by sequencing and transferred into *E. coli* Rosetta2(DE3)pLysS (pET30pdh_{ATE_prim}, pET30pdh_{ATE_sec}, pET11a$dahp_{ATE_sec}$-strep, pET30pdh_{ACOL_prim}, pET11apdh_{ACOL_sec}-strep and pET11a$dahp_{ACOL_sec}$-strep) or *E. coli* BL21(DE3)pLysS (pET11a$dahp_{ATE_prim}$-strep and pET11a$dahp_{ACOL_prim}$-strep). For protein production, the cells were grown in 1 L of LB medium supplemented with antibiotics using 2 L Erlenmeyer flasks to an optical density of 0.6 at 600 nm. Protein production under the T7 promoter was induced by the addition of IPTG to a final concentration of 1 mM and incubated at 18 °C (13°C for Pdh_{ATE_prim} and Pdh_{ACOL_prim}) on an orbital shaker at 180 rpm overnight. Cells were collected by centrifugation at 10.000 rpm and stored at -80 C prior to protein purification. His-tagged proteins were purified as previously described (Goldfinger et al., 2023). Cells of strep-tagged proteins were disrupted the same way as His-tagged proteins. The soluble proteins were purified using Strep-tactin superflow columns (IBA Lifescieces) and eluted using 100 mM Tris/HCl pH 7.3 (pH 7.5 for Dahp), 500 mM NaCl, 1 mM EDTA and 2.5 mM desthiobiotin. Fractions containing pure protein were pooled and stored as described (Goldfinger et al., 2023).

2.7 Enzymatic characterization of Dahp

As the first reaction in the shikimate pathway, Dahp catalyzes the condensation of PEP and E4P to form DAHP. The enzymatic kinetics were determined as previously described (Goldfinger et al., 2023). The reaction buffer contained the following enzyme concentrations: 0.01 µg/µL for $Dahp_{ATE\_prim}$, 0.01 µg/µL for $Dahp_{ATE\_sec}$, 0.01 µg/µL for $Dahp_{ACOL\_prim}$ and 0.01 µg/µL for $Dahp_{ACOL\_sec}$. For inhibition studies, 100 µM of PEP (50 µM of PEP for $Dahp_{ACOL\_prim}$) and 100 µM of E4P (50 µM of E4P for $Dahp_{ACOL\_prim}$) in combination with 200 µM tyrosine (Tyr), phenylalanine (Phe) and tryptophan (Trp) individually or Tyr and Phe combined were used. The enzyme kinetics were determined using GraphPad Prism.

2.8 Enzymatic characterization of Pdh

In the shikimate pathway, prephenate dehydrogenase (Pdh) catalyzes the oxidative decarboxylation of prephenate to 4-HPP, producing NADH. The enzymatic kinetics were assessed using the method previously described (Goldfinger et al., 2023). The following enzyme concentrations were used in the reaction buffer 0.15 µg/µL for Pdh_{ATE_sec}, 0.05 µg/µL for Pdh_{ACOL_prim} and 0.15 µg/µL for Pdh_{ACOL_sec}. The enzyme kinetics were determined using GraphPad Prism.

2.9 Teicoplanin production and analysis

A working cell bank (WCB) was prepared for each *Act. teichomyceticus* strain following the procedure described earlier (Taurino et al., 2011). For the pre-culture step, 1.5 mL of the WCB was added to 80 mL of E25 media in a 500 mL baffled Erlenmeyer flask and cultivated on a rotary shaker at 220 RPM and 30 °C for 72 h. To initiate the main culture, 5% of the preculture was transferred to 80 mL of TM1 in a 500 mL baffled Erlenmeyer flask. After 140 h of cultivation, 1 mL of the main culture was collected and mixed with 1 mL of boric buffer (100 mM H_3BO_3, 100 mM NaOH, pH 12). The mixtures were vigorously vortexed for 5 min and then centrifuged at 13,000 rpm for 10 min. Teicoplanin concentrations in the supernatant were measured using HPLC, as previously described (Taurino et al., 2011), with a commercial teicoplanin standard as a reference (Sigma-Aldrich). Throughout the work, teicoplanin yields represent the total amount of 5 major teicoplanin congeners produced ($T\text{-}A^{2\text{-}1}$, $T\text{-}A^{2\text{-}2}$, $T\text{-}A^{2\text{-}3}$, $T\text{-}A^{2\text{-}4}$, $T\text{-}A^{2\text{-}5}$ in the sample). Statistical analyses were performed using OriginPro 2021 (v. 9.8.0.200). Data are presented as mean ± SD of independent biological replicates (>3). Pairwise comparisons between the control with empty vector and individual experimental conditions were conducted using an unpaired two-tailed Student's *t*-test with Welch's correction. A p-value < 0.05 was considered statistically significant.

2.10 Avoparcin production and analysis

The supernatant of the production cultures was directly used as a sample and analyzed by HPLC-ESI-MS using a Nucleosil 100 C18 column (3 µm, 100x2 mm) with a precolumn (10x2 mm) (Dr. Maisch GmbH, Ammerbuch-Entringen, Germany) and an Ultra Trap system XCT 6330 (Agilent Technologies, Waldbronn, Germany). Detection of *m/z* values was conducted with DataAnalysis for 6300 series Ion Trap HPLC/MS 6.1 version 3.4 software (Bruker Daltonik GmbH). Analysis was carried out at a flow rate

of 400 µL/min with gradient elution. The HPLC parameters were as follows: Solvent A was 0.1% formic acid in water, and solvent B 0.06% formic acid in acetonitrile. Gradient elution was performed from 0-100% solvent B over 15 min. UV spectroscopic data were collected by a DAD detector in the range of 230-600 nm. The MS parameters were as follows: ESI ionization alternating between positive and negative mode, the capillary voltage was 3.5 kV, and the temperature was 350 °C.

Statistical analyses were performed using GraphPad Prism. Data are presented as mean ± SD of independent biological replicates. Pairwise comparisons between WT and individual experimental conditions were conducted using an unpaired two-tailed Student's *t*-test with Welch's correction. A p-value < 0.05 was considered statistically significant.

2.11 Phylogenetic analysis of Pdh and Dahp

The dataset of GPA and GRP encoding BGCs was gathered following the methodology presented in a prior paper studying the evolution of the BGC (Gavriilidou et al., 2023). A filtering step was applied to keep only the BGCs encoding the biosynthesis of true GPAs, and to dereplicate them. Details on the BGC can be found in the table *Cluster_Summary.xlsx*.

The detection of Pdh and Dahp homologs was conducted with the help of the zol tool v1.6.15 (Salamzade et al., 2025). The relevant orthologous groups (OGs) were identified based on proteins with known function. Our dataset included one OG of Pdh and two different OGs of Dahp, which were merged to recreate their evolutionary history. Details on the orthology inference and relevant groups can be found in the table *Orthogroups.xlsx*. More details on the relevant genes can be found in the table *Cluster_Gene_Summary.xlsx*.

Multiple Sequence Alignments (MSAs) of the protein sequences were performed with the mafft tool v7.525 (2024/Mar/13) (Katoh and Standley, 2013). The relevant files are provided in the supplementary information (*Dahp_MSA.faa*, *Pdh_MSA.faa*).

Phylogenetic trees were built with iqtree multicore version 2.0.7 for Linux 64-bit built Apr 1 2024 (Katoh and Standley, 2013; Minh et al., 2020). iqtree was first run only in model testing mode, checking for all bacteria-suitable evolutionary models and then in tree-building mode based on the best fitting maximum likelihood model (JTT+F+I+G4 for Pdh and JTTDCMut+F+R3 for Dahp). The relevant files are provided in the supplementary information (*Dahp_iqtree.treefile*, *Pdh_iqtree.treefile*). The figures of the Pdh and Dahp trees were generates using iTOL (Letunic and Bork, 2024) visualizations of these files (based on table *Cluster_Summary.xlsx*).

3. Results and discussion

3.1 Phylogenetic analysis of $Dahp_{sec}$ and Pdh_{sec} across GPA-producing actinobacteria

To explore the diversity of the key enzymes from the shikimate pathway Dahp and Pdh across different actinobacteria that harbor a BGC encoding the biosynthesis of a type I-IV GPA, we performed a phylogenetic analysis based on multi-sequence alignment. The presence of *$dahp_{sec}$* was not always correlated with that of *pdh_{sec}* genes: in several GPA BGCs, *$dahp_{sec}$* was absent. The analysis revealed that enzymes from producers of the same GPA type do not necessarily cluster together (Figure 4 and Figure 5). $Dahp_{ACOL\_sec}$ from *A. coloradensis* stood out because it is one of the few *Amycolatopsis* proteins that branch separately from other *Amycolatopsis* $Dahp_{\_sec}$ enzymes, forming a distinct subclade more closely related to $Dahp_{ATE\_sec}$ from *Act. teichomyceticus* (Figure 1). $Dahp_{ATE\_sec}$ forms a subclade associated with type III and type IV GPA producers and is clearly separated as a distant relative of the *Amycolatopsis* group (Figure 4). This is also reflected in the phylogenetic placement of Pdh_{ATE_sec} forming its own subclade (Figure 5). In contrast, Pdh_{ACOL_sec} clusters with the majority of the *Amycolatopsis* Pdh_{sec} enzymes (Figure 5).
In previous work, we biochemically and functionally characterized $Dahp_{ABAL\_sec}$ and Pdh_{ABAL_sec} from *A. balhimycina*, the producer of balhimycin, and leveraged these insights to increase ristomycin (a type III GPA) production in *Amycolatopsis japonica* through metabolic engineering (Goldfinger et al., 2023). Here, to explore the function of $Dahp_{sec}$ and Pdh_{sec} across evolutionary boundaries and to determine whether differences in sequence and phylogenetic placement translate into altered enzymatic properties, we selected $Dahp_{ACOL\_sec}$ and Pdh_{ACOL_sec} and $Dahp_{ATE\_sec}$ and Pdh_{ATE_sec} for further analyses. This choice was motivated by i) the observation that they cluster in different clades and are also evolutionarily distinct from $Dahp_{ABAL\_sec}$ and Pdh_{ABAL_sec}, and ii) the notion that *A. coloradensis* and *Act. teichomyceticus* produce the type II and type IV GPAs avoparcin and teicoplanin, respectively, which differ in heptapeptide composition from the previously studied type I GPA balhimycin and the type III GPA ristomycin (Goldfinger et al., 2023).

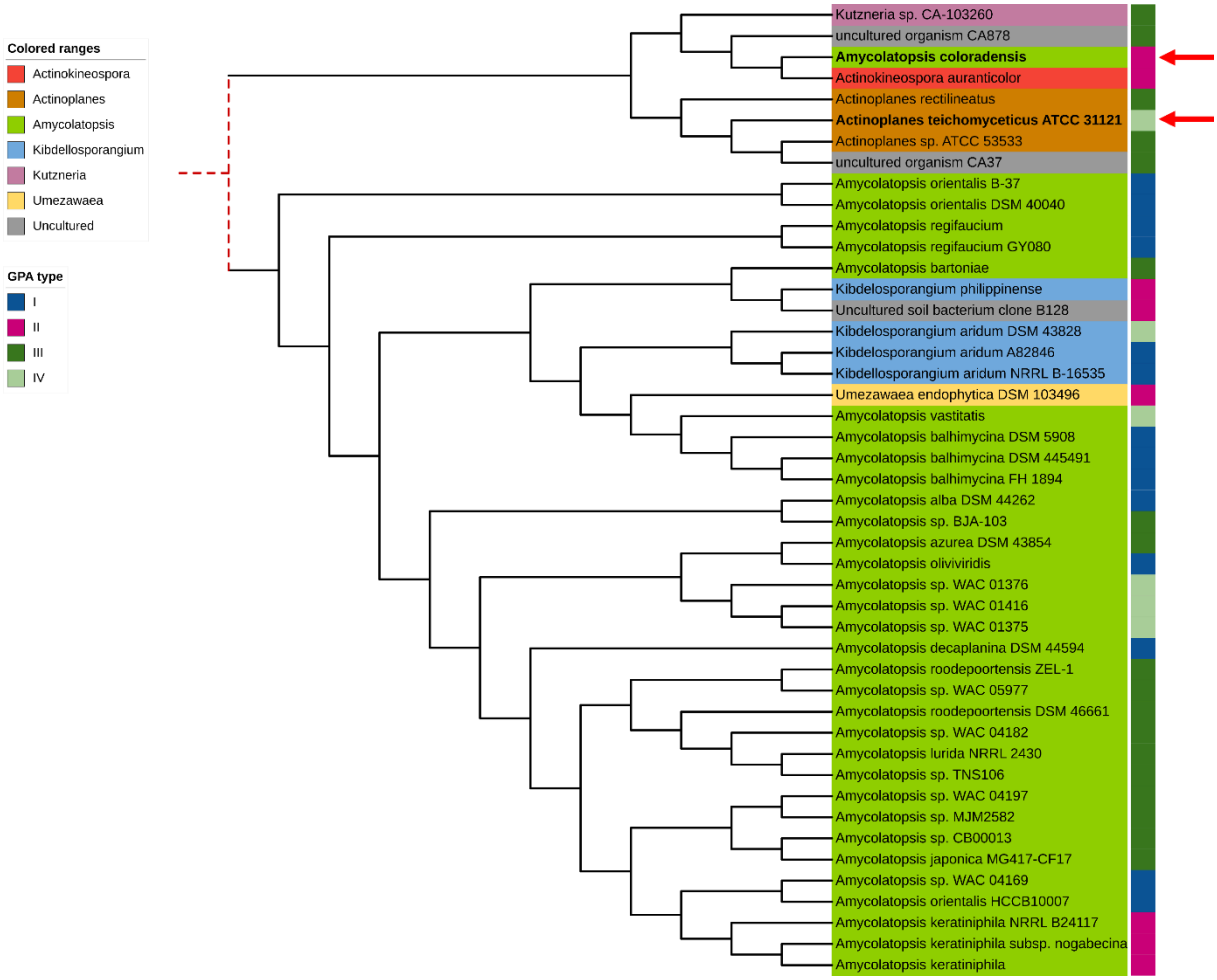

Figure 4: Phylogenetic analysis of Dahp$_{sec}$ found within GPA biosynthetic gene clusters (BGCs). Phylogenetic tree (maximum likelihood model JTTDCMut+F+R3, branch lengths were ignored) of Dahp$_{sec}$ enzymes encoded in canonical GPA BGCs from actinobacteria. The dotted red line represents a very long branch in the tree, consistent with the two types of Dahp being evolutionarily distinct (see Supplementary for more details). Genera as well as strains, and corresponding (predicted) GPA types are color-coded as indicated.

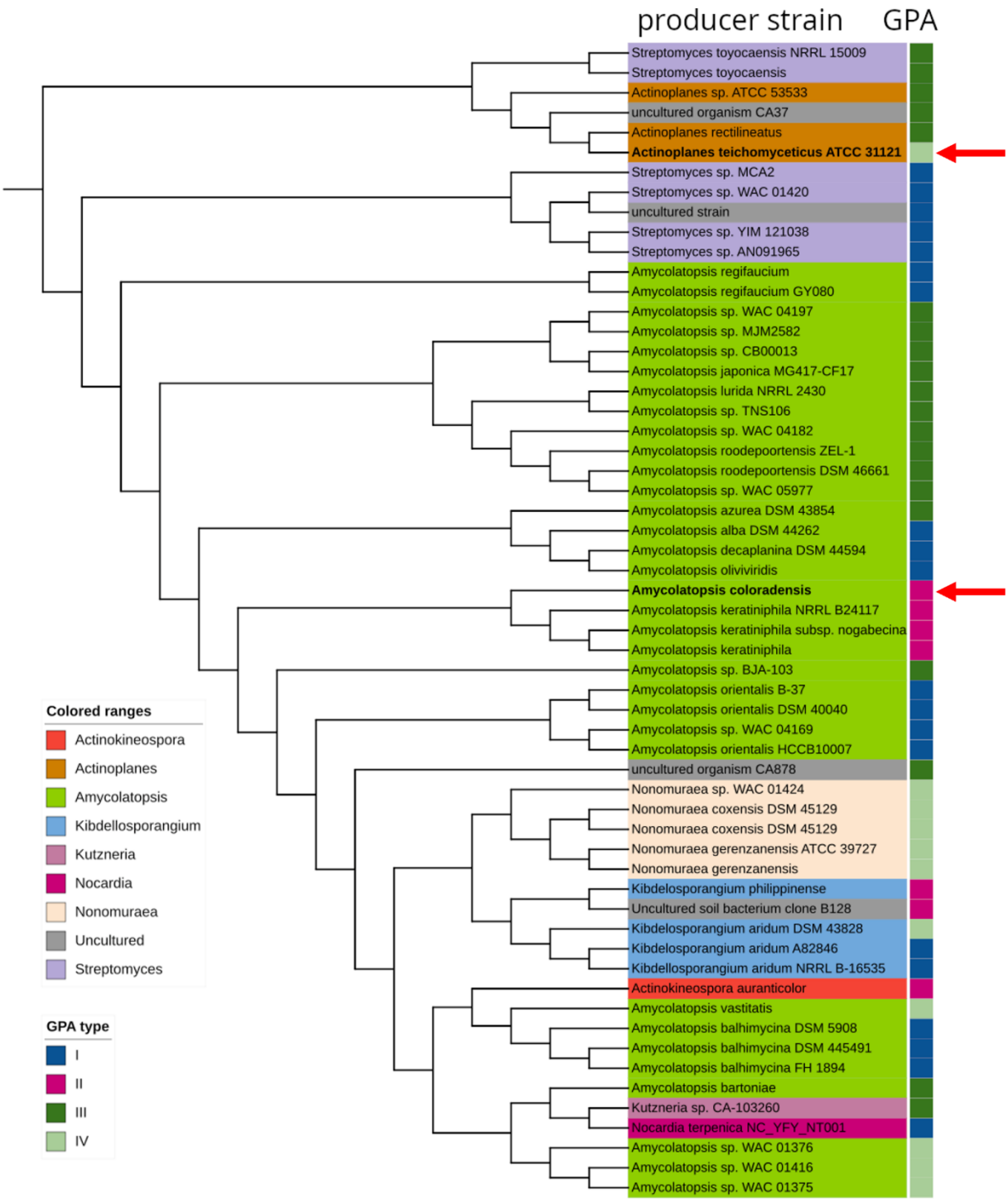

Figure 5: Phylogenetic analysis of Pdh_{sec} found within GPA biosynthetic clusters (BGCs). Phylogenetic tree (maximum likelihood model JTT+F+I+G4, branch lengths were ignored) of Pdh_{sec} enzymes encoded in canonical GPA BGCs from actinobacteria. Genera as well as strains, and corresponding (predicted) GPA types are color-coded as indicated.

3.2 Overexpression of Dahp$_{ACOL_sec}$ and Pdh$_{ACOL_sec}$ in *A. coloradensis* DSM 4425 results in a significant decrease in avoparcin production

The low sequence identity (Supplementary discussion) and phylogenetic divergence between Dahp$_{ACOL_sec}$ and Dahp$_{ABAL_sec}$ (Figure 4) prompted us to analyse functional differences between the two enzymes. We included in the analysis Pdh isoenzymes as well. Therefore, we integrated *dahp$_{ACOL_sec}$* and *pdh$_{ACOL_sec}$* individually or together in the chromosome of *A. coloradensis* under the control of the strong constitutive promoter *ermE*p.* In parallel, we generated deletion mutants lacking *pdh$_{ACOL_sec}$* (*A. coloradensis* Δ*pdh$_{ACOL_sec}$*) and *dahp$_{ACOL_sec}$* (*A. coloradensis* Δ*dahp$_{ACOL_sec}$*) via homologous recombination. In previous work, we showed that overexpression of *dahp$_{ABAL_sec}$* increases balhimycin yields 4.4-fold in *A. balhimycina*, while its deletion only slightly decreases it (14%) (Goldfinger et al., 2023). Surprisingly, in *A. coloradensis* we observed the opposite*:* overexpression of *dahp$_{ACOL_sec}$* led to a reduction in avoparcin titers (60-70% of the wild type levels*),* while its deletion led to a 2-fold increase in avoparcin production (Figure 6). Similar to the results in *A. balhimycina*, overexpression of *pdh$_{ACOL_sec}$* led to a reduction in avoparcin up to 60-70% of the wild type levels, while simultaneous overexpression of both *dahp$_{ACOL_sec}$* and *pdh$_{ACOL_sec}$* caused a significant decrease in production, with only 5% of the wild type levels remaining. Single deletion of *pdh$_{ACOL_sec}$* also strongly impaired production with an 80% reduction, which is reminiscent of the phenotype of *A. balhimycina* Δ*pdh$_{ABAL_sec}$* (Goldfinger et al., 2023)*.*

This functional analysis suggested that Dahp$_{ACOL_sec}$ may be subject to alternative feedback regulation compared to the *A. balhimycina* enzyme, prompting us to examine its biochemical properties in detail.

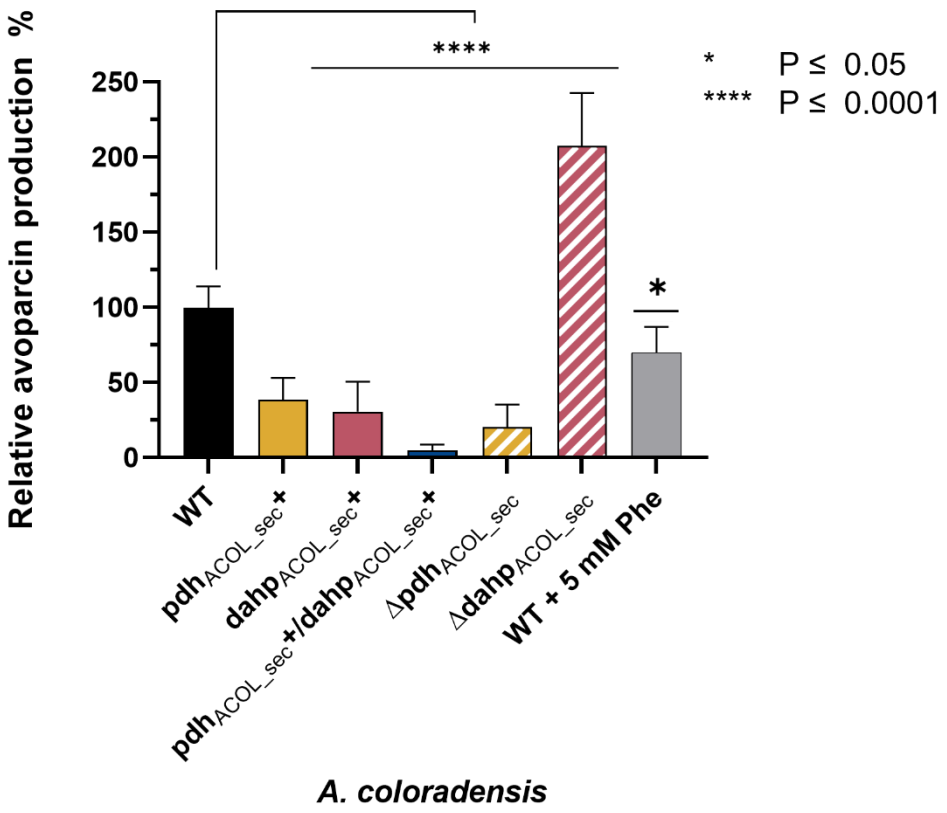

Figure 6: Avoparcin production of the *A. coloradensis* mutant strains. Avoparcin yields of *A. coloradensis* WT, *A. coloradensis* $pdh_{ACOL\_sec}^{+}$, *A. coloradensis* $dahp_{ACOL\_sec}^{+}$, *A. coloradensis* $pdh_{ACOL\_sec}^{+}/dahp_{ACOL\_sec}^{+}$, *A. coloradensis* Δpdh_{ACOL_sec}, *A. coloradensis* $\Delta dahp_{ACOL\_sec}$ and *A. coloradensis* WT + 5 mM Phe was measured via HPLC. The values were normalized to the culture growth and are expressed in percent relative to the WT levels, which were set to 100%. Overexpression of the gene is indicated by a "+". Data represent the mean ± SD of independent biological replicates (WT, n = 10; $pdh_{ACOL\_sec}^{+}$, n = 6; $dahp_{ACOL\_sec}^{+}$, n = 6; $pdh_{ACOL\_sec}^{+}/dahp_{ACOL\_sec}^{+}$, n = 7, Δpdh_{ACOL_sec}, n = 9; $\Delta dahp_{ACOL\_sec}$, n = 9; WT + 5 mM Phe, n = 4). Statistical significance was assessed by pairwise comparison of each condition against WT using an unpaired two-tailed Student's *t*-test wit Welch's correction (GraphPad Prism). A *p*-value < 0.05 was considered statistically significant. * indicates p ≤ 0.05; **** indicated p ≤ 0.0001.

3.3 $Dahp_{ACOL\_sec}$ is strongly feedback regulated

We recombinantly produced the primary metabolic isoenzyme $Dahp_{ACOL\_prim}$ and the secondary isoenzyme $Dahp_{ACOL\_sec}$ and characterized their kinetic and regulatory properties. As both enzymes use phosphoenolpyruvate (PEP) and erythrose-4-phosphate (E4P) as substrates, we measured the consumption rate of PEP at 232 nm, maintaining one substrate at a fixed concentration while varying the other and vice versa, as previously described (Goldfinger et al., 2023).

Using substrate concentrations in the range of 25-300 µM covered the broad area of the Michaelis-Menten saturation curve (Figure S1). The reaction rates were directly proportional to the enzyme amount for both enzymes and in the range of 0.01-0.02 µg/µL. To determine the initial reaction rates, the assay was carried out with an enzyme concentration of 0.01 µg/µL, a tangent was plotted to the observed progress curve of each enzyme concentration, and the slope was determined. The values of the initial reaction rates were then used to plot the Michaelis-Menten saturation curve. This analysis revealed that both enzymes possess a similar affinity for the substrate E4P (PEP fixed: $Dahp_{ACOL\_prim}$ K_M = 28.69 ± 1.9 µM; $Dahp_{ACOL\_sec}$ K_M = 26.44 ± 5.41 µM),

but $Dahp_{ACOL\_sec}$ exhibits a 10-fold higher V_{max} (0.0255 ± 0.00065 µM/min) compared to $Dahp_{ACOL\_prim}$ (0.00224 ± 0.00003 µM/min) (Table 8, Figure S1). $Dahp_{ACOL\_sec}$ showed a higher affinity for PEP (K_M = 16.74 ± 2.51 µM) while reaching a 3.5-fold higher V_{max} (V_{max} = 0.01747 ± 0.0006 µM/min) compared to $Dahp_{ACOL\_prim}$ (E4P fixed: K_M = 37.28 ± 3.86 µM, V_{max} = 0.00481± 0.00013 µM/min). $Dahp_{ACOL\_sec}$ used both substrates with a 7-fold higher catalytic efficiency (k_{cat}/K_M) than $Dahp_{ACOL\_prim}$ (Table 8). Overall, the kinetic analysis indicated that $Dahp_{ACOL\_sec}$ is a more efficient catalyst than $Dahp_{ACOL\_prim}$ and has a particularly high specificity for PEP.

To assess whether the distinct kinetic properties of $Dahp_{ACOL\_sec}$ are accompanied by altered allosteric regulation, we measured initial reaction rates at fixed PEP and E4P concentrations in the presence of the aromatic amino acids Phe, Tyr, and Trp. Both isoenzymes were inhibited by Phe and Trp, whereas Tyr selectively inhibited $Dahp_{ACOL\_sec}$, reducing its activity to approximately 35 % of the uninhibited control (Table 9). An equimolar combination of Phe and Tyr antagonized Phe-mediated inhibition of $Dahp_{ACOL\_prim}$ but had no such effect on $Dahp_{ACOL\_sec}$, indicating fundamentally different regulatory mechanisms between the two isoenzymes.

Functionally, this dual feedback inhibition provides a plausible explanation for the strong reduction in avoparcin production observed upon overexpression of *$dahp_{ACOL\_sec}$*. Elevated levels of $Dahp_{ACOL\_sec}$ are likely to increase intracellular Tyr and Phe concentrations, thereby reinforcing allosteric inhibition and restricting precursor flux through the shikimate pathway. Consistent with this model, external supplementation of Phe to *A. coloradensis* WT reduced avoparcin production (Figure 3), whereas deletion of *$dahp_{ACOL\_sec}$* resulted in a 2-fold increase in yield, indicating that precursor supply is more efficiently maintained by $Dahp_{ACOL\_prim}$ in the absence of the tightly regulated secondary isoenzyme.
In contrast, previous work showed that in *A. balhimycina* both $Dahp_{ABAL\_prim}$ and $Dahp_{ABAL\_sec}$ are predominantly inhibited by Tyr, with Phe partially antagonizing this inhibition in $Dahp_{ABAL\_sec}$ (Goldfinger et al., 2023). Thus, whereas $Dahp_{ABAL\_sec}$ supports sustained shikimate-pathway flux under production conditions, $Dahp_{ACOL\_sec}$ is constrained by dual feedback inhibition mediated by Tyr and Phe. This divergence correlates with the low sequence similarity between the two enzymes and suggests that feedback control strategies have evolved independently among GPA producers. Together, these findings demonstrate that higher catalytic efficiency does not necessarily translate into improved precursor supply; instead, the nature of allosteric regulation determines whether a Dahp isoenzyme promotes or restricts GPA biosynthesis.

Table 8: Kinetic properties of $Dahp_{ACOL\_prim}$ and $Dahp_{ACOL\_sec}$ in regard to E4P and PEP. Kinetic parameters were determined from three independent replicates. Values are reported as median ± SD.

	$Dahp_{ACOL\_prim}$		$Dahp_{ACOL\_sec}$	
	PEP fixed	**E4P fixed**	**PEP fixed**	**E4P fixed**
V_{max} [µM/min]	0.00224 ± 0.00003	0.00481± 0.00013	0.0255 ± 0.00065	0.01747 ± 0.0006
K_M [µM]	28.69 ± 1.9	37.28 ± 3.86	26.44 ± 5.41	16.74 ± 2.51
k_{cat} [1/s]	0.1425	0.305	0.872	1.053
k_{cat}/K_M [M^{-1} s^{-1}]	4.91 * 10^3	8.59 * 10^3	33 *10^3	62.9 * 10^3

Table 9: Reaction rates of $Dahp_{ACOL\_prim}$ and $Dahp_{ACOL\_sec}$ in an enzymatic reaction with a potential inhibitor. Kinetic parameters were determined from three independent replicates. Values are reported as median ± SD.

Potential Inhibitor (200 µM each)	$Dahp_{ACOL\_prim}$		$Dahp_{ACOL\_sec}$	
	Reaction Rate in			
	[nM/min]	%	[nM/min]	%
---	5.77 ± 0.86	100	27.32 ± 2.05	100
Phe	2.93 ± 0.06	50.73	10.38 ± 1.69	38.00
Tyr	6.12 ± 3.77	106. 08	9.62 ± 1.91	35.21
Trp	1.71 ± 0.46	29.65	12.43 ± 0.36	45.49
Tyr+Phe	5.51 ± 0.15	95.59	10.56 ± 1.69	38.67

3.4 Tyr-dependent inhibition of $Dahp_{ATE\_sec}$ is antagonized by Phe

Building on the insights gained from the characterization of $Dahp_{ACOL}$ isoenzymes and motivated by the phylogenetic distinctiveness of $Dahp_{ATE\_sec}$ (Figure 4) and its low sequence identity to other $Dahp_{sec}$ proteins, we investigated the biochemical properties of the Dahp isoenzymes from *Act. teichomyceticus*. To this end, $Dahp_{ATE\_prim}$ and $Dahp_{ATE\_sec}$ were recombinantly produced, and their kinetic and regulatory parameters were analyzed using the same experimental framework as for the *A. coloradensis* enzymes.

The kinetic analysis of the Dahp isoenzymes from *Act. teichomyceticus* showed that the substrate concentration in range of 25 to 300 µM covered the broad area of the Michaelis-Menten saturation curve (Figure S2). The reaction rate was directly proportional to the enzyme concentration in the range of 0.005 µg/µL to 0.01 µg/µL for $Dahp_{ATE\_prim}$ and 0.01 µg/µL to 0.015 µg/µL for $Dahp_{ATE\_sec}$. Therefore, the enzymatic characterization of both enzymes was carried out at 0.01 µg/µL enzyme concentrations. While $Dahp_{ATE\_sec}$ showed a higher affinity for E4P (K_M = 7.56 ± 0.536 µM) than $Dahp_{ATE\_prim}$ (K_M = 15.81 ± 1.01 µM), $Dahp_{ATE\_prim}$ reached substantially higher maximal velocities with both substrates (Table 10, Figure S2). For PEP in particular, $Dahp_{ATE\_prim}$ displayed an enhanced catalytic efficiency (k_{cat}/K_M = 946 $*10^3$ $M^{-1}s^{-1}$) compared to $Dahp_{ATE\_sec}$ (k_{cat}/K_M = 28 $*10^3$ $M^{-1}s^{-1}$). These results indicate that $Dahp_{ATE\_prim}$ is the dominant catalyst in *Act. teichomyceticus.*

With respect to allosteric regulation by fixed concentrations of Phe, Tyr, or Trp, we found that, while $Dahp_{ATE\_prim}$ was inhibited by all three aromatic amino acids to various degrees, as well as the combination Tyr + Phe, $Dahp_{ATE\_sec}$ was only inhibited by Tyr (Table 11) while Trp slightly activated the enzyme. Interestingly, Tyr-dependent inhibition of $Dahp_{ATE\_sec}$ was antagonized by Phe, suggesting a fine-tuned regulatory mechanism balancing Tyr and Phe pools during shikimate pathway flux in *Act. teichomyceticus*.
In summary, the biochemical characterization of Dahp isoenzymes revealed that $Dahp_{ACOL\_sec}$ from *A. coloradensis* is strongly inhibited by all three amino acids,

whereas $Dahp_{ATE\_sec}$ from *Act. teichomyceticus* and $Dahp_{ABAL\_sec}$ from *A. balhimycina* are primarily inhibited by Tyr, with Phe acting antagonistically. These findings indicate that evolutionary divergence of Dahp isoenzymes within GPA BGCs is not necessarily reflected in the biochemical properties of the enzymes. In fact, in terms of *in vitro* activity and allosteric regulation, $Dahp_{ATE\_sec}$ and $Dahp_{ABAL\_sec}$ are closer than expected based on their phylogenetic distance, while $Dahp_{ACOL\_sec}$ and $Dahp_{ABAL\_sec}$ show dissimilarities at all levels.

Table 10: Kinetic properties of $Dahp_{ATE\_prim}$ and $Dahp_{ATE\_sec}$ in regard to E4P and PEP. Kinetic parameters were determined from three independent replicates. Values are reported as median ± SD.

	$Dahp_{ATE\_prim}$		$Dahp_{ATE\_sec}$	
	PEP fixed	**E4P fixed**	**PEP fixed**	**E4P fixed**
V_{max} [µM/min]	0.03168 ± 0.00038	0.03754 ± 0.00043	0.01149 ± 0.00009	0.01426 ± 0.00028
K_M [µM]	15.81 ± 1.01	25.06 ± 1.19	7.56 ± 0.536	31.35 ± 2.39
k_{cat} [1/s]	2.0	2.37	0.707	0.877
k_{cat}/K_M [M^{-1} s^{-1}]	126 *10^3	946 *10^3	96.6 *10^3	28 *10^3

Table 11: Reaction rates of $Dahp_{ATE\_prim}$ and $Dahp_{ATE\_sec}$ in an enzymatic reaction with a potential inhibitor. Kinetic parameters were determined from three independent replicates. Values are reported as median ± SD.

Potential Inhibitor (200 µM each)	$Dahp_{ATE\_prim}$		$Dahp_{ATE\_sec}$	
	Reaction Rate in			
	[nM/min]	**%**	**[nM/min]**	**%**
---	31.44 ± 1.30	100	8.21 ± 0.1206	100
Phe	22.39 ± 4.65	71.24	7.77 ± 0.5812	94.54
Tyr	19.35 ± 1.73	61.54	3.69 ± 0.4992	44.88
Trp	12.06 ± 2.66	38.37	9.01 ± 0.8665	109.72
Tyr+Phe	21.58 ± 3.20	68.63	6.65 ± 0.3667	80.931

3.5 Pdh_{ACOL_prim} and Pdh_{ACOL_sec} are feedback inhibited by tyrosine and phenylalanine in *A. coloradensis*

The observed phylogenetic difference between Pdh_{ATE_sec}, Pdh_{ACOL_sec} and Pdh_{ABAL_sec} prompted us to characterize also the biochemical properties of the primary and secondary Pdh enzymes from *A. coloradensis* and *Act. teichomyceticus.*

Pdh catalyzes the oxidative decarboxylation of prephenate to 4-HPP, reducing NAD^+ to NADH in the process. Since this reaction requires NAD^+ as a cofactor, we determined the enzymatic properties of Pdh_{ACOL_prim} and Pdh_{ACOL_sec} by monitoring the formation of NADH at 340 nm in an optical assay. The observed reaction rates were directly proportional to the enzyme amount in the range of 0.0125 µg/µL to 0.05 µg/µL for Pdh_{ACOL_prim} and 0.05 µg/µL to 0.15 µg/µL for Pdh_{ACOL_sec} (Figure S3). Therefore, the analysis of Pdh_{ACOL_prim} was performed at 0.05 µg/µL and for Pdh_{ACOL_sec} at 0.15 µg/µL. The broad area of the Michaelis-Menten saturation curve (Figure S3) was covered by substrate concentrations in the range of 150 µM to 2000 µM (Table 12). Both enzymes displayed a low affinity towards prephenate, with Pdh_{ACOL_sec} possessing a 1.6-fold higher K_M value than Pdh_{ACOL_prim} (Pdh_{ACOL_prim} K_M = 614.6 ± 62.162 µM; Pdh_{ACOL_sec} K_M = 1011 ± 122.7 µM). The high K_M values are consistent with previous reports that dehydrogenases involved in Tyr biosynthesis in actinomycetes may preferentially use arogenate as their physiological substrate rather than prephenate (Goldfinger et al., 2023; Song et al., 2005). In terms of catalytic performance, Pdh_{ACOL_prim} exhibited a substantially higher V_{max} and 9-fold greater catalytic efficiency (kcat/KM) compared to Pdh_{ACOL_sec} (Table 12), indicating that it is a more effective catalyst.

Building on these kinetic characterizations, we investigated allosteric regulation by aromatic amino acids. Both isoenzymes were subject to feedback inhibition, but with notable differences. Pdh_{ACOL_prim} activity was reduced in the presence of Tyr and Phe (Table 13, Figure S4). By contrast, Pdh_{ACOL_sec} was strongly inhibited by Tyr, whereas Phe slightly stimulated its activity. Interestingly, when Phe and Tyr were supplied together, Phe partially antagonized the Tyr-dependent inhibition of Pdh_{ACOL_sec}.
These regulatory profiles differ from Pdh_{ABAL_sec}, which is largely insensitive to Tyr and Phe (Goldfinger et al., 2023). The Tyr- and Phe-dependent regulation of Pdh_{ACOL_sec} suggests that this enzyme may have evolved to carefully balance precursor supply in *A. coloradensis,* preventing imbalances in aromatic amino acid pools and restricting excessive flux into avoparcin biosynthesis. These findings are consistent with our observation that overexpression of *pdh_{ACOL_sec}* reduced avoparcin production (Figure 6), likely due to allosteric inhibition by Tyr, as elevated intracellular Tyr levels resulting from overexpression could reinforce feedback inhibition of Pdh_{ACOL_sec}.

Table 12: Kinetic properties of Pdh_{ACOL_prim} and Pdh_{ACOL_sec}. Kinetic parameters were determined from three independent replicates. Values are reported as median ± SD.

	Pdh_{ACOL_prim}	Pdh_{ACOL_sec}
V_{max} [µM/min]	110.5 ± 4.53	53.19 ± 3.03
K_M [µM]	614.6 ± 62.162	1011 ± 122.7
k_{cat} [1/s]	1.18	0.217
k_{cat}/K_M [M^{-1} s^{-1}]	1.92* 10^3	0.215 *10^3

Table 13: Kinetic properties of Pdh_{ACOL_prim} and Pdh_{ACOL_sec} in an enzymatic reaction with a potential inhibitor. Kinetic parameters were determined from three independent replicates. Values are reported as median ± SD.

Potential Inhibitor (200 µM each)	Pdh_{ACOL_prim}			Pdh_{ACOL_sec}		
	K_M [µM]	V_{max} [µM/min]	V_{max} [%]	K_M [µM]	V_{max} [µM/min]	V_{max} [%]
-	614.6 ± 62.16	110.5 ± 4.53	100	1011 ± 122.77	53.19 ± 3.03	100
Tyr	570.8 ± 71.39	7.732 ±0.38	6.99	703.3 ± 124.34	12.55 ± 0.89	23.59
Phe	325.1 ± 55.46	73.33 ± 3.99	66.36	1373 ± 70.38	57.95 ± 1.57	108.94
Tyr+Phe	629.6 ± 56.14	21.06 ± 0.76	19.05	1798 ± 480.63	35.46 ± 5.55	66.66

3.6 Pdh_{ATE_sec} is feedback inhibited by tyrosine

Following our kinetic and regulatory analyses of Pdh isoenzymes from *A. coloradensis*, we investigated the corresponding enzymes from *Act. teichomyceticus*, anticipating that Pdh_{ATE_sec} would display distinct biochemical features based on the phylogenetic and sequence comparison (Figure 5 and supplementary discussion).

Prephenate concentrations in the range of 500 to 4000 µM covered the broad area of the Michaelis-Menten saturation curve (Figure S5). The enzyme displayed reaction rates that were directly proportional to the enzyme concentration in the range of 0.075 µg/µl to 0.15 µg/µl. The assays were performed at 0.15 µg/µl. In contrast to Pdh_{ATE_sec}, Pdh_{ATE_prim} showed no measurable activity with prephenate, even up to 5000 µM. Consistently, Pdh_{ATE_prim} was shown to belong to the $TyrA_a$ family of dehydrogenases, which are arogenate (Agn)-specific (Song et al., 2005). Agn may as well be the preferred substrate for Pdh_{ATE_sec}. This enzyme accepts prephenate as a substrate but with very low affinity (K_M = 3230 µM) (Table 14, Figure S5), even higher than the already high K_M values of the *A. coloradensis* Pdh isoenzymes (Table 12). This is consistent with a $TyrA_c$ enzyme, which can use both Agn and prephenate but generally favors Agn (Bonner et al., 2008).

Pdh_{ATE_sec} harbors a C-terminal ACT-like regulatory domain, suggesting potential allosteric regulation by aromatic amino acids. Consistent with this, Pdh_{ATE_sec} was inhibited by both Tyr and Phe, but equimolar concentrations of both aromatic amino acids did not lead to an enhanced inhibitory effect (Table 15, Figure S6). The regulatory pattern resembles that of *A. coloradensis* Pdh_{ACOL_sec}, which also harbors an ACT-like regulatory domain.

Overall, these results highlight distinct strategies of feedback regulation among GPA producers. In *A. coloradensis*, both Pdh isoenzymes are feedback-sensitive and display high apparent K_M values, consistent with TyrAa/TyrAc-type dehydrogenases.

This dual regulation likely balances Tyr and Phe homeostasis but limits precursor flux toward avoparcin biosynthesis. In *Act. teichomyceticus*, the properties of Pdh_{ATE_prim} and the poorly efficient Pdh_{ATE_sec} similarly indicate a focus on maintaining metabolic balance rather than maximizing precursor supply. By contrast, in *A. balhimycina*, the shikimate pathway appears optimized for production: $Dahp_{ABAL\_sec}$ drives balhimycin yield, while both Pdh_{ABAL} isoenzymes lack feedback inhibition, ensuring a stable flux toward Tyr even under conditions of elevated aromatic amino acid pools (Goldfinger et al., 2023). These comparisons suggest that GPA producers have evolved feedback regulation strategies that either prioritize robust antibiotic production or preserve metabolic homeostasis, reflecting evolutionary divergence in pathway control.

Table 14: Kinetic properties of Pdh_{ATE_sec}. Kinetic parameters were determined from three independent replicates. Values are ported as median ± SD.

	Pdh_{ATE_sec}
V_{max} [µM/min]	26.15 ± 3.36
K_M [µM]	3230 ± 746.89
k_{cat} [1/s]	0.109
k_{cat}/K_M [M^{-1} s^{-1}]	33.83

Table 15: Kinetic properties of Pdh_{ATE_sec} in an enzymatic reaction with a potential inhibitor.

Potential Inhibitor (200 µM each)	Pdh_{ATE_sec}		
	K_M [µM]	V_{max} [µM/min]	V_{max} [%]
-	3230 ± 746	26.15 ± 3.36	100
Tyr	2305 ± 375	17.86 ± 1.44	68.29
Phe	2782 ± 266	22.82 ± 1.15	87.265
Tyr+Phe	3055 ± 712	18.76 ± 2.39	71.73

3.7 Overexpression of genes encoding Dahp enzymes from different GPA producers increases teicoplanin production in *Act. teichomyceticus* NRRL B-16726

Our biochemical analyses (here and previously, (Goldfinger et al., 2023) revealed that, despite their evolutionary divergence, $Dahp_{ATE\_sec}$ and $Dahp_{ABAL\_sec}$ exhibit a similar feedback regulation by Tyr, which is antagonized by Phe. Since overexpression of $dahp_{ABAL\_sec}$ leads to increased balhimycin production in *A. balhimycina*, we tested whether overexpression of either enzyme in *Act. teichomyceticus* may have a similar positive effect on teicoplanin production.

To this aim, we integrated $dahp_{ABAL\_sec}$ or an additional copy of $dahp_{ATE\_sec}$ in the chromosome of *Act. teichomyceticus* NRRL B-16726 under the control of the strong apramycin promoter (*aac(3)IVp*) (yielding recombinant *Act. teichomyceticus*

dahp$_{ABAL\_sec}^{+}$) and the native promoter (yielding *Act. teichomyceticus dahp*$_{ATE\_sec}^{+}$), respectively. The latter decision was mainly based on two observations: firstly, *dahp*$_{ATE\_sec}$ exists as an independent transcriptional unit within the teicoplanin (*tei*) BGC; secondly, *dahp*$_{ATE\_sec}$ shows robust expression in *Act. teichomyceticus* NRRL B-16726 under teicoplanin production conditions (Yushchuk et al., 2019). The pSET152 vector and its derivatives integrate into the *Act. teichomyceticus* chromosome at the ΦC31 *attB* attachment site, which is located far from the *tei* BGC (Figure S9). This integration has no impact on teicoplanin production (Horbal et al., 2013). When we quantified teicoplanin production in recombinant *Act. teichomyceticus* strains, overexpression of the heterologous ***dahp***$_{ABAL\_sec}$ increased teicoplanin titers by more than 2-fold (Figure 4). The strain carrying an additional copy of the endogenous ***dahp***$_{ATE\_sec}$ produced 1.5-fold more teicoplanin than the control (Figure 4). No significant changes in the biomass accumulation were observed.

Collectively, introducing genes encoding Dahp isoenzymes with a similar feedback regulation pattern, appears to enhance teicoplanin production in *Act. teichomyceticus*.

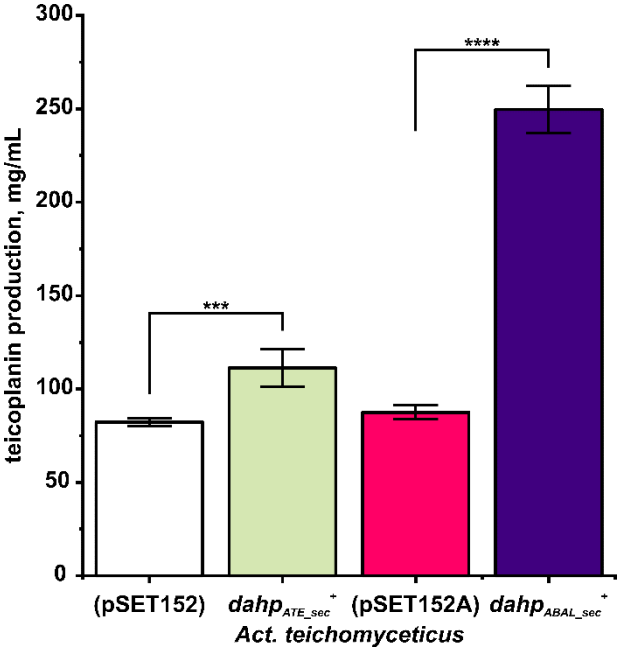

Figure 7: Teicoplanin production levels (mg/L) in recombinant *Act. teichomyceticus* strains overexpressing native and heterologous *dahp* genes (*dahp*$_{ATE\_sec}^{+}$ and *dahp*$_{ABAL\_sec}^{+}$, respectively) compared with the corresponding empty-vector controls (pSET152 and pSET152A). Data are presented as mean value ± SD of independent biological replicates (pSET152, n = 3; pSET152A, n = 3; *dahp*$_{ATE\_sec}^{+}$, n = 6; *dahp*$_{ABAL\_sec}^{+}$, n = 9). Statistical significance was assessed by pairwise comparison of the production level in each overexpression strain with its respective control (*dahp*$_{ATE\_sec}^{+}$ vs pSET152 and dahp$_{ABAL_sec}$ vs pSET152A) using an unpaired two-tailed Student's *t*-test with Welch's correction (please see Methods section). A *p*-value < 0.05 was considered statistically significant. *** indicates $p \leq 0.001$; **** indicates $p \leq 0.0001$.

3.8 The regulatory ACT-like domain influences the activity of Pdh and teicoplanin production in *Act. teichomyceticus* NRRL B-16726

Unlike Pdh$_{ATE_sec}$ and Pdh$_{ACOL_sec}$, which harbor a C-terminal extension resembling an ACT-like regulatory domain and are susceptible to allosteric regulation by Tyr and Phe, Pdh$_{ABAL_sec}$ is rather small (291 a.a.) and lacks this regulatory module. Despite these structural differences, both Pdh$_{ATE_sec}$ and Pdh$_{ABAL_sec}$ belong to the same family of actinobacterial TyrA proteins (Song et al., 2005). Notably, overexpression of the corresponding gene in *A. balhimycina* was previously shown to negatively affect balhimycin production (Thykaer et al., 2010). Based on these observations, we

speculated that the absence of the ACT-domain in Pdh_{ABAL_sec} may underlie its distinct regulatory behavior and its impact on antibiotic production.

To investigate the impact of different Pdhs on teicoplanin production, we overexpressed both *pdh*$_{ATE\_sec}$ and *pdh*$_{ABAL\_sec}$ in *Act. teichomyceticus,* yielding *Act. teichomyceticus pdh*$_{ATE\_sec}^{+}$ and *Act. teichomyceticus pdh*$_{ABAL\_sec}^{+}$ recombinant strains. Additionally, a truncated version of *pdh*$_{ATE\_sec}$ (comprising only the first 861 nucleotides, *pdh*$_{ATE\_sec}$*tr*) was overexpressed to examine the influence of the putative ACT-domain in Pdh_{ATE_sec} (*Act. teichomyceticus pdh*$_{ATE\_sec}$*tr*$^{+}$). In all cases, genes of interest were placed under the control of *aac(3)IVp.* All constructs were integrated in the chromosome (see previous section), and the levels of teicoplanin production were assessed in all recombinant strains. Overexpression of *pdh*$_{ABAL\_sec}^{+}$ had no visible impact on teicoplanin production (Figure 8). In contrast, strains overexpressing *pdh*$_{ATE\_sec}^{+}$ exhibited teicoplanin production rates more than three times higher than the strain carrying the empty vector (Figure 8). Interestingly, in strains overexpressing *pdh*$_{ATE\_sec}$*tr*$^{+}$, we observed amounts of teicoplanin similar to the empty control and *pdh*$_{ABAL\_sec}$ overexpressing strains. However, we cannot rule out the possibility that truncated Pdh_{ATE_sec} might be misfolded due to the deletion of the ACT domain, although this is unlikely, as the latter is connected to the catalytic domain with a 9 aa flexible linker implying the independent folding of both. In that case, the observed teicoplanin production would likely reflect the activity of the endogenous wild-type enzyme alone.

Overall, these results indicate that the C-terminal region of Pdh_{ATE_sec} is required for the stimulatory effect of *pdh*$_{ATE\_sec}$ overexpression on teicoplanin biosynthesis. full-length Pdh_{ATE_sec} led to a moderate increase in teicoplanin titers, consistent with a regulated contribution of this enzyme to precursor supply. By contrast, deletion of the C-terminal region eliminated this positive effect, indicating that the regulatory domain is required for productive redirection of metabolic flux toward GPA biosynthesis.

Among actinobacterial Pdh enzymes (Song et al., 2005), only a limited number have been enzymatically characterized. One example is the Pdh from *Microtetraspora glauca*, which is subject to synergistic feedback inhibition by Phe, Tyr, and tryptophan (Speth et al., 1989). In contrast, Pdh_{ABAL_sec} and the truncated variant of Pdh_{ATE_sec} lack an ACT-like regulatory domain and are therefore not subject to feedback inhibition by aromatic amino acids. The absence of feedback control in these enzymes may cause an unregulated increase in intracellular Tyr levels, which can be diverted into Phe biosynthesis (Calhoun et al., 1973; Speedie and Park, 1980). Such metabolic rerouting would explain why overproduction of unregulated Pdh variants confers no benefit (and may even be detrimental) to GPA production, as observed for teicoplanin and balhimycin (Thykaer et al., 2010). By contrast, feedback-regulated full-length Pdh_{ATE_sec} would be expected to permit only a moderate expansion of the Tyr pool – sufficient to stimulate teicoplanin biosynthesis without promoting competing Phe synthesis.

Notably, although Pdh_{ACOL_sec} and Pdh_{ATE_sec} both contain ACT domains, overexpression of Pdh_{ACOL_sec} in *A. coloradensis* decreases avoparcin production (Figure 6). This difference likely reflects distinct allosteric regulation of $Dahp_{ATE\_sec}$ and $Dahp_{ACOL\_sec}$: elevated intracellular Tyr inhibits not only Pdh_{ACOL_sec} but also $Dahp_{ACOL\_sec}$, thereby restricting flux through the shikimate pathway. Accumulating Phe may further exacerbate this effect by suppressing $Dahp_{ACOL\_sec}$ activity . In

Act. teichomyceticus, by contrast, Phe positively influences $Dahp_{ATE\_sec}$, preventing pathway shutdown and thereby enabling enhanced teicoplanin production.

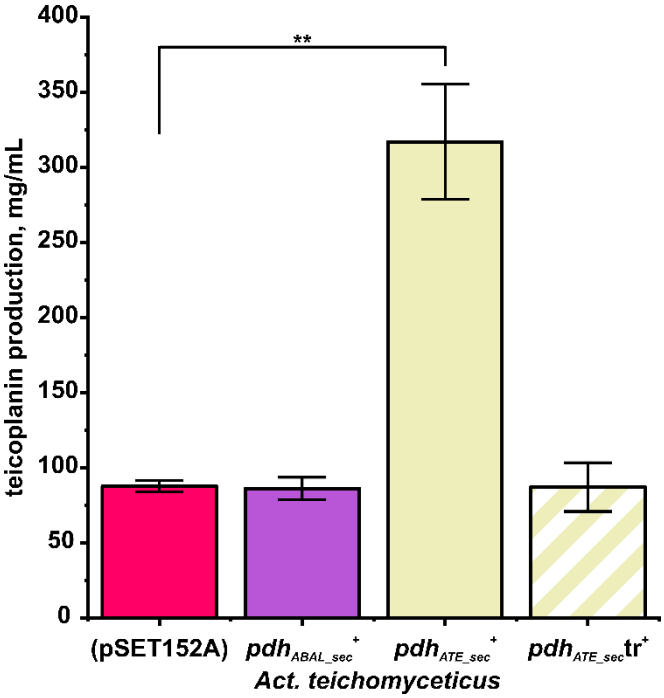

Figure 8: Teicoplanin production levels (mg/L) in recombinant *Act. teichomyceticus* strains overexpressing native and heterologous *pdh* genes ($pdh_{ATE\_sec}^{+}$, $pdh_{ATE\_sec}tr^{+}$, and $pdh_{ABAL\_sec}^{+}$, respectively) compared with the empty-vector control (pSET152A). Data are presented as mean value ± SD of independent biological replicates (pSET152, n = 3; $pdh_{ABAL\_sec}^{+}$, n = 9; $pdh_{ATE\_sec}^{+}$, n = 3; $pdh_{ATE\_sec}tr^{+}$, n = 3). Statistical significance was assessed by pairwise comparison of the production level in each overexpression strain with the empty-vector control using an unpaired two-tailed Student's *t*-test with Welch's correction (please see Methods section). A *p*-value < 0.05 was considered statistically significant. ** indicates $p \leq 0.01$.

3.9 Rebalancing phenylalanine and tyrosine biosynthesis increases glcopeptide antibiotic production

In bacteria, prephenate produced via the shikimate pathway can be further converted into either Tyr or Phe. The conversion to Phe is catalyzed by prephenate-dehydratases (Pdts). Many actinobacterial Pdts are activated by Tyr and inhibited by Phe (Abou-Zeid et al., 1995; De Boer et al., 1989), including an experimentally characterized Pdt from *Amycolatopsis mediterranei* (Tianhui and Chiao, 1989). This experimentally characterized Pdt shares over 90% sequence identity with the Pdt from *A. balhimycina* (Pdt_{ABAL}) and 61% sequence similarity with the Pdt from *Act. teichomyceticus* (Pdt_{ATE}), suggesting partial functional conservation. Overproduction of Pdt_{ABAL} increased balhimycin titers by approximately 4-fold relative to the wild-type *A. balhimycina* strain (Goldfinger et al., 2023).

Therefore, we reasoned that overexpressing the *pdt* genes from *A. balhimycina* and *Act. teichomyceticus* would initially result in an excess of Phe, leading to feedback inhibition of the Pdt activity and consequently elevating intracellular Tyr levels. An expanded Tyr pool could, in turn, stimulate GPA biosynthesis.

To test this hypothesis, we supplemented *Act. teichomyceticus* cultures with 5 mM Phe, which increased teicoplanin production by up to 2-fold (Figure 9). Prompted by this result, we generated *Act. teichomyceticus* strains overexpressing pdt_{ABAL} and

pdt$_{ATE}$ via chromosomal integration of the corresponding genes under the control of the *aac(3)IVp* promoter. Analysis of the antibiotic production revealed that both recombinant *Act. teichomyceticus* strains produced up to 3-fold more teicoplanin than the strain carrying the empty vector (Figure 9).

Comparable channeling of prephenate toward Tyr biosynthesis under conditions of Phe excess has been reported in *Pseudomonas aeruginosa* and *Streptomyces refuineus* (Calhoun et al., 1973; Speedie and Park, 1980). In those studies, Tyr pools increased upon supplementation with high concentrations of Phe, consistent with feedback inhibition of Pdt activity by Phe.

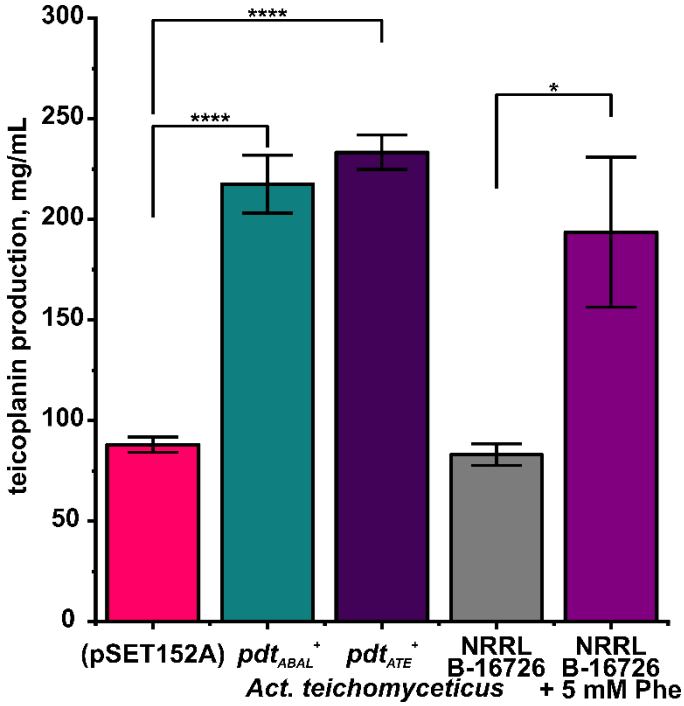

Figure 9: Teicoplanin production levels (mg/L) in recombinant *Act. teichomyceticus* strains overexpressing heterologous and native *pdt* genes (*pdt*$_{ATE}^{+}$ and *pdt*$_{ABAL}^{+}$, respectively) compared with the empty-vector control (pSET152A) as well as in the NRRL B-16726 (the wild type) and NRRL B-16726 supplemented with 5 mM Phe. Data are presented as mean value ± SD of independent biological replicates (pSET152, n = 3; *pdt*$_{ATE}^{+}$, n = 6; *pdt*$_{ABAL}^{+}$, n = 9; NRRL B-16726, n = 3; NRRL B-16726 + 5 mM Phe, n = 3). Statistical significance was assessed by pairwise comparison of the production level in each overexpression strain with the empty-vector control using an unpaired two-tailed Student's *t*-test with Welch's correction (please see Methods section). A *p*-value < 0.05 was considered statistically significant. * indicates $p \leq 0.05$; **** indicates $p \leq 0.0001$.

4. Conclusion

A major bottleneck in large-scale GPA bioproduction - is the limited supply of precursors, which are derived primarily from the shikimate pathway. This study provides a proof of concept that exploring the functional diversity of key shikimate-pathway enzymes – specifically Dahp and Pdh – across representative GPA producers can guide more effective metabolic engineering strategies to increase the production of clinically-relevant GPAs, as demonstrated by increased teicoplanin production in this study.

Comparative analysis of phylogenetically distinct Dahp and Pdh enzymes from *A. coloradensis* and *Act. teichomyceticus* revealed major biochemical and functional differences, most notably between Dahp$_{ACOL_sec}$ and Dahp$_{ABAL_sec}$, and between Pdh$_{ATE_sec}$ and Pdh$_{ABAL_sec}$. These findings pinpointed unique metabolic strategies used by different actinomycetes when it comes to balancing the carbon and nitrogen flux between primary and secondary metabolism, and exposed distinct key players for

increasing GPA yields (Figure 10). Specifically, $Dahp_{ABAL\_sec}$ appears to be a key determinant of balhimycin productivity in *A. balhimycina*, whereas Pdh_{ATE_sec} and Pdh_{ACOL_sec} emerge as key players in *A. coloradensis* and *Act. teichomyceticus*.

Our findings also indicate that phylogenetic distance is not always reflected in distinct biochemical and regulatory properties, as exemplified here by the distantly related but biochemically similar $Dahp_{ATE\_sec}$ and $Dahp_{ABAL\_sec}$. This suggests that, while functional predictions can be made based on phylogenetic distance, these have to be validated experimentally before embarking on any metabolic engineering strategy. Continuing to explore the diversity of key enzymes in the biosynthesis of GPAs in the future has the potential to broaden the enzymatic space for *in vivo* and biocatalyst-based engineering approaches.

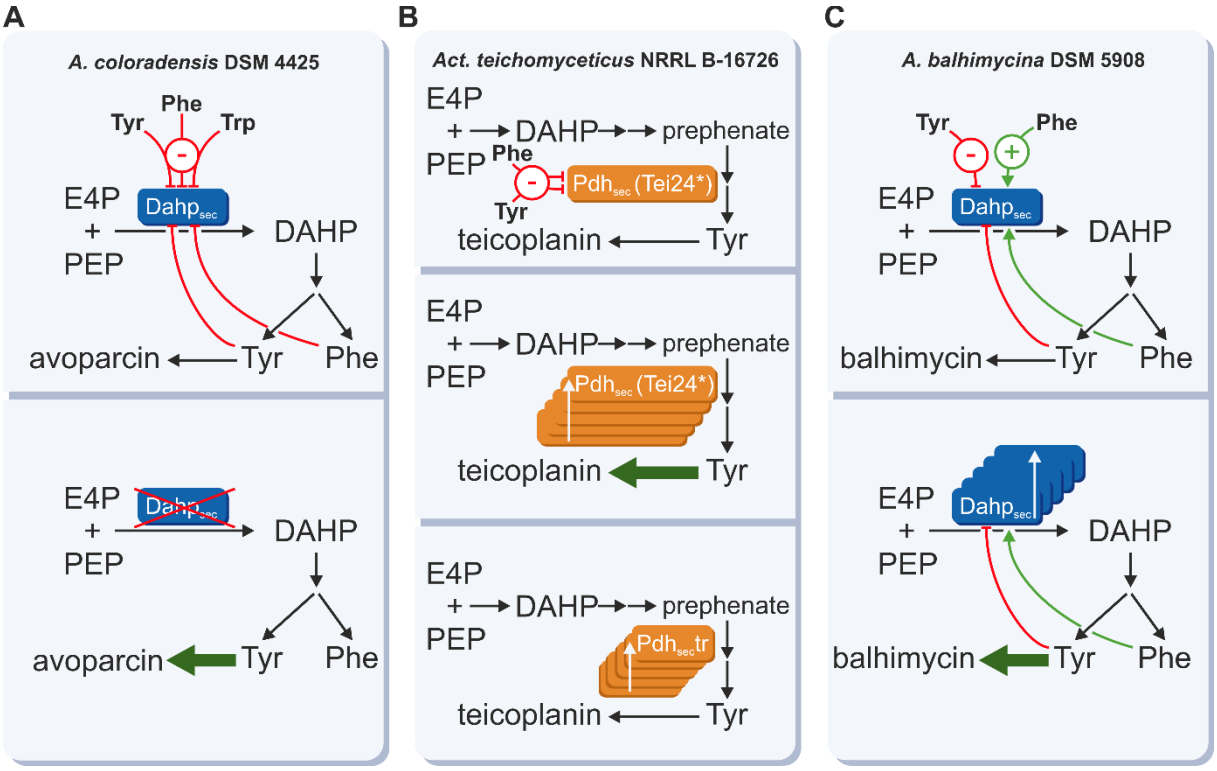

Figure 10: Overview of key players of the shikimate pathway for GPA production in different GPA producers. [A] *A. coloradensis* $Dahp_{sec}$ is inhibited by Tyr, Phe and Trp. When $dahp_{ACOL\_sec}$ is deleted, GPA production in *A. coloradensis* is increased. **[B]** *Act. teichomyceticus* Pdh_{sec} is inhibited by Tyr and Phe. When additional copies of pdh_{ATE_sec} are introduced in the genome, GPA production is increased. Introducing copies of $pdh_{ATE\_sec}tr$ doesn't increase GPA production. **[C]** *A. balhimycina* $Dahp_{sec}$ is inhibited by Tyr but Phe can antagonize the inhibition. When additional copies of $dahp_{ABAL\_sec}$ are introduced, GPA production is increased.

Supplementary Information

BlastP analysis of $Dahp_{sec}$ and Pdh_{sec}

Consistent with the phylogenetic results, BlastP analysis revealed a high degree of similarity (79.83%) between $Dahp_{ACOL\_prim}$ (WP_076154649.1) and $Dahp_{ABAL\_prim}$ (GenBank ID: FN594522.1) as well as a 78.03% similarity between Pdh_{ACOL_prim} (WP_076164136.1) and Pdh_{ABAL_prim} (GenBank ID: FN594521.1). While Pdh_{ACOL_sec} (WP_076160587.1) showed a high similarity (82.61%) to Pdh_{ABAL_sec} (WP_020646204.1), $Dahp_{ACOL\_sec}$ (WP_076160568.1) and $Dahp_{ABAL\_sec}$ (GenBank: CAG25757.1) exhibited only 26.77% sequence identity. Amino acid sequence comparison between the corresponding enzymes from *Act. teichomyceticus* and *A. balhimycina* revealed that $Dahp_{ABAL\_sec}$ and $Dahp_{ATE\_sec}$ (GenBank ID: GIF17153.1) shared a low degree of similarity (30.95%), while $Dahp_{ABAL\_prim}$ and $Dahp_{ATE\_prim}$ (WP_122976155.1) shared 58.72% identity. Pdh_{ATE_sec} (GenBank ID: GIF17143.1) and Pdh_{ATE_prim} (GenBank ID: GIF11287.1) shared a similar degree of similarity of 51.01% and 45.62%, respectively, with the corresponding enzymes in *A. balhimycina*. Sequence comparison of Dahps and Pdhs from *A. coloradensis* and *Act. teichomyceticus* showed that $Dahp_{ACOL\_sec}$ and $Dahp_{ATE\_sec}$ share a high similarity of 71.13%, while $Dahp_{ACOL\_prim}$ and $Dahp_{ATE\_prim}$ share 59.13% similarity. This is also reflected in the phylogenetic analysis. A lower identity was observed when comparing Pdh_{ACOL_sec} and Pdh_{ATE_sec} (49.68%), as well as $Pdh_{ACOL_prim}$and Pdh_{ATE_prim} (46.08%).

Table S1: Oligonucleotide primers used in this study.

Primer	Nucleotide sequence (5'-3')*	Purpose
tei14_F	AAAGATATCGATCCGGACCGACGCGGTTG	*dahp$_{ATE_sec}$* (*tei14**) cloning
tei14_R	TTTTTCTAGATGAGCAGGGCATACAGGCCG	
tei24_F	TTTGATATCGGAGGGTCGACGTGCGCACTCTTCT	*pdh$_{ATE_sec}$* (*tei24**) cloning
tei24_R	TTTGAATTCGCTCAGCGGTGCGGCCCTCG	
tei24_tr_R	TTTGAATTCTCACGCCCCGGCGGGCGGCCGGGT	*pdh$_{ATE_sec}$tr (tei24*tr)* cloning
pdtate_F	TTTTGATATCGGAGGGGCGCAATGCCCGGAACGCC	*pdt$_{ATE}$* cloning
pdtate_R	TTTTGAATTCGCACGGAAAGCCTCGGTG	
pdtbal_F	TTTTGATATCGGAGGACCCATATGCGGCCCCGTAG	*pdt$_{ABAL}$* cloning into pSET152A
pdtbal_R	TTTTGAATTCTCACGCCACGTCCCCCTTGC	
dahpbal_F	TTTTGATATCGGAGGCCGCGATGACCCACACCGT	*dahp$_{ABAL_sec}$* cloning into pSET152A
dahpbal_R	TTTTGAATTCATCAGCTTGCTTGCTTGCCG	
pdhbal_F	TTTTGATATCGGAGGGCGCCGGTGACCATCGAGAAAGCGCT	*pdh$_{ABAL_sec}$* cloning into pSET152A
pdhbal_R	TTTTGAATTCCTAACGCCCCGGGGAACCC	
amR_F	CGGGGTCTGACGCTCAGTGGA	*aac(3)IV* Amplification
amR_R	AGCGTCTGCTCCGCCATTCG	
204_delta_Acoldahp_fw	CGCGTCGACGTCATATGGATCctcctcgatgggcaccgt	Flanking region 1 for pGUSA21_Δdahp$_{ACOL_sec}$
205_delta_Acoldahp_rv	cgagggagacacaatcgcctgcccggcg	Flanking region 1 for pGUSA21_Δdahp$_{ACOL_sec}$
206_delta2_Acoldahp_fw	gggcaggcgattgtgtctccctcggaaaaggcg	Flanking region 2 for pGUSA21_Δdahp$_{ACOL_sec}$
207_delta2_Acoldahp_rv	CGCCACGGCGATATCGGATCccgctggccgaactggtgttccggacggc	Flanking region 2 for pGUSA21_Δdahp$_{ACOL_sec}$
212_pMR4_Acol_dahp_fw	TCAAGCTTAGATCTCATAtcacgccacgaggctc	Cloning of pRM4dahp$_{ACOL_sec}$
213_pRM4_Acol_dahp_rv	GCCAGGGGAGGACCCATAatggtgatcgtgatggcgcc	Cloning of pRM4dahp$_{ACOL_sec}$
214_pRM4_Acol_pdh_fw	TCAAGCTTAGATCTCATAaactaacgcggcacggg	Cloning of pRM4pdh$_{ACOL_sec}$
215_pRM4_Acol_pdh_rv	GCCAGGGGAGGACCCATAgtgcccatcgagaaggcgcttgtggt	Cloning of pRM4pdh$_{ACOL_sec}$
216_delta_Acolpdh_fw	CGCGTCGACGTCATATGGATCcgtagagcaggttttcccgga	Flanking region 1 for pGUSA21_Δpdh$_{ACOL_sec}$

217_delta_Acolpdh_rv	aaggagtagcgttgctgctcccgatgtcg	Flanking region 1 for pGUSA21_Δpdh$_{ACOL_sec}$
218_delta2_Acolpdh_fw	ggagcagcaacgctactccttatgccgt	Flanking region 2 for pGUSA21_Δpdh$_{ACOL_sec}$
219_delta2_Acolpdh_rv	CCGCCACGGCGATATCGGATCgcctaatcaggacggcgaacagcctag	Flanking region 2 for pGUSA21_Δpdh$_{ACOL_sec}$
220_pRM4_Acolpdh_fw	TCAAGCTTAGATCTCATAactaacgcggcacggg	Cloning of pRM4dahp$_{ACOL_sec}$/pdh$_{ACOL_sec}$
221_pRm4_Acolpdh_rv	gtggcgtgagtgcccatcgagaaggcgctt	Cloning of pRM4dahp$_{ACOL_sec}$/pdh$_{ACOL_sec}$
222_pRM4_Acoldahp_fw	gatgggcactcacgccacgaggctcgct	Cloning of pRM4dahp$_{ACOL_sec}$/pdh$_{ACOL_sec}$
223_pRM4_acoldahp_rv	GCCAGGGGAGGACCCATAaatggtgatcgtgatggcgcccg	Cloning of pRM4dahp$_{ACOL_sec}$/pdh$_{ACOL_sec}$
244_Acol_deltapdh_fw	gatcccagatctgggcgcc	Verification of the deletion of *pdh* in *A. colordaensis* Δ*pdh*$_{ACOL\_sec}$
416_delta_Acolpdh_rv	ctgggccaaaaacgccccg	Verification of the deletion of *pdh* in *A. colordaensis* Δ*pdh*$_{ACOL\_sec}$
248_deltadahp_fw	gcgttgcggtgcttgatctcc	Verification of the deletion of *pdh* in *A. colordaensis* Δ*dahp*$_{ACOL\_sec}$
249_deltadahp_rv	cgacatcaccagggcgagg	Verification of the deletion of *pdh* in *A. colordaensis* Δ*dahp*$_{ACOL\_sec}$
282_pGUS_Fw	GTGCAATACGAATGGCGAAAAGCC	Verification of the integration of pRM4 or pGUSA21 constructs into *A. coloradensis* genome
283_pGUS_rv	CCGGGCAGGATAGGTGAAGT	Verification of the integration of pRM4 or pGUSA21 constructs into *A. coloradensis* genome
403_pET30_Act_Pdhprim_fw	GAGGAGAAGCCCGGTTCAggcgggatagcggtcagtttc	Cloning of pET30pdh$_{ATE_prim}$
404_pET30_Act_pdhprim_rv	GACGACGACAAGcggatcgcggtcatcg	Cloning of pET30pdh$_{ATE_prim}$
162_Act_pdhsec_rv	GAGGAGAAGCCCGGTtcagcggtgcggccctcg	Cloning of pET30pdh$_{ATE_sec}$
176_Act_pdhsec_fw	GACGACGACAAGCGCACTCTTCTCGTGATCGGAACC	Cloning of pET30pdh$_{ATE_sec}$
407_pET30_Acol_Pdhprim_fw	GAGGAGAAGCCCGGTtcaagagacctcgccgatcg	Cloning of pET30pdh$_{ACOL_prim}$
408_pET30_Acol_Pdhprim_rv	GACGACGACAAGatcgggctcgggttgatcg	Cloning of pET30pdh$_{ACOL_prim}$
378_Act_dahpprim_fw	ctttaagaaggagatggccgatgaccgccctgaggtacagc	Cloning of pET11adahp$_{ATE_prim}$-strep
379_Act_dahpprim_rv	cgggtggctccaagcgctgagcgtgcggcgcttgg	Cloning of pET11adahp$_{ATE_prim}$-strep
232_Actdahp_Cstrep_fw	ctttaagaaggagatggccgATGGTCGTTGTGATGGCGCCG	Cloning of pET11adahp$_{ATE_sec}$-strep
233_Actdahp_Cstrep_rv	cgggtggctccaagcgctCACCGCGGCGGGAACG	Cloning of pET11adahp$_{ATE_sec}$-strep
236_Acoldahp_Cstrep_fw	ctttaagaaggagatggccgATGGTGATCGTGATGGCGCC	Cloning of pET11adahp$_{ACOL_sec}$-strep

237_Acoldahp_Cstrep_rv	cgggtggctccaagcgctCGCCACGAGGCTCGCTCC	Cloning of pET11adahp$_{ACOL_sec}$-strep
382_Acol_dahpprim_fw	ctttaagaaggagatggccgatgtctccctccgctgacactc	Cloning of pET11adahp$_{ACOL_prim}$-strep
383_Acol_dahpprim_rv	cgggtggctccaagcgctccgccgcgagtcgatgg	Cloning of pET11adahp$_{ACOL_prim}$-strep
238_Acolpdh_Cstrep_fw	ctttaagaaggagatggccgGTGCCCATCGAGAAGGCGCTTGTG	Cloning of pET11apdh$_{ACOL_sec}$-strep
239_Acolpdh_Cstrep_rv	cgggtggctccaagcgctACGCGGCACGGGCGGAACG	Cloning of pET11apdh$_{ACOL_sec}$-strep

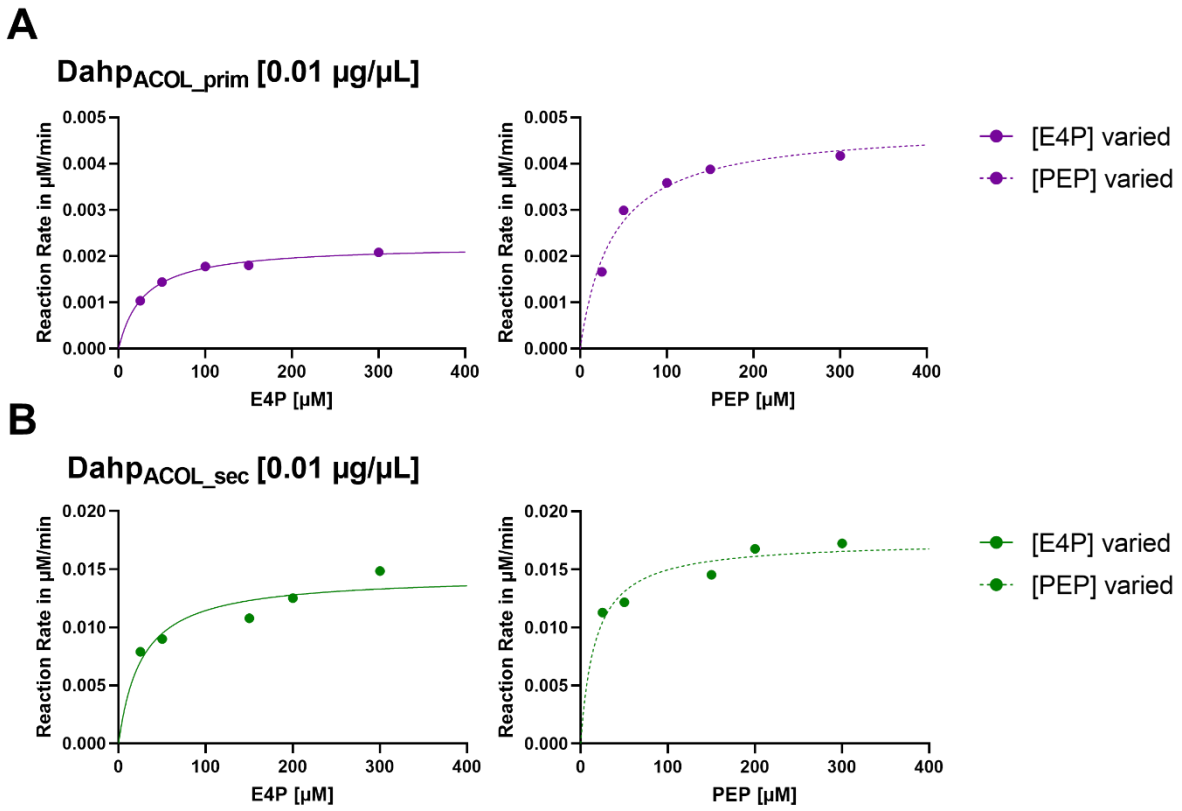

Figure S1: Kinetics of *A. coloradensis* Dahp$_{ACOL_prim}$ and Dahp$_{ACOL_sec}$.

Michaelis-Menten saturation curve of Dahp$_{ACOL_prim}$ [A] and Dahp$_{ACOL_sec}$ [B] determined using varying concentrations of E4P and PEP. Data are derived from three independent replicates and are presented as median values with standard deviation.

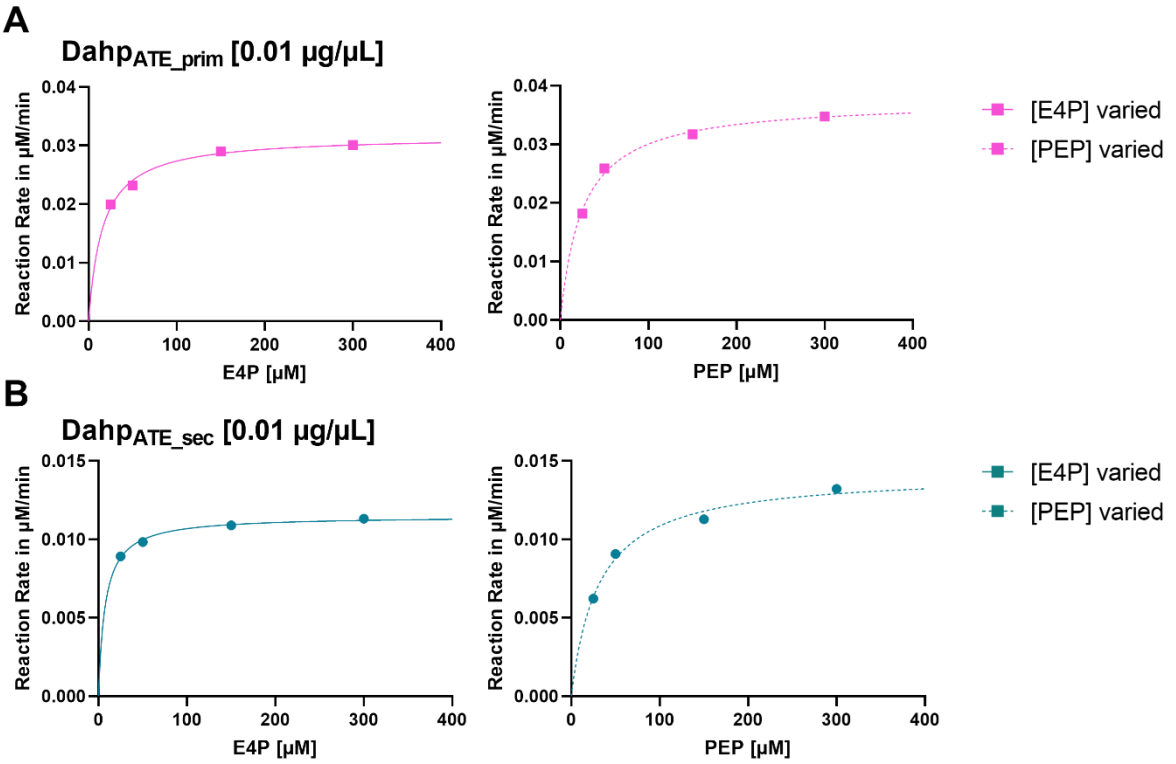

Figure S2: Kinetics of *Act. teichomyceticus* $Dahp_{ATE\_prim}$ and $Dahp_{ATE\_sec}$.

Michaelis-Menten saturation curve of $Dahp_{ATE\_prim}$ [A] and $Dahp_{ATE\_sec}$ [B] determined using varying concentrations of E4P and PEP. Data are derived from three independent replicates and are presented as median values with standard deviation.

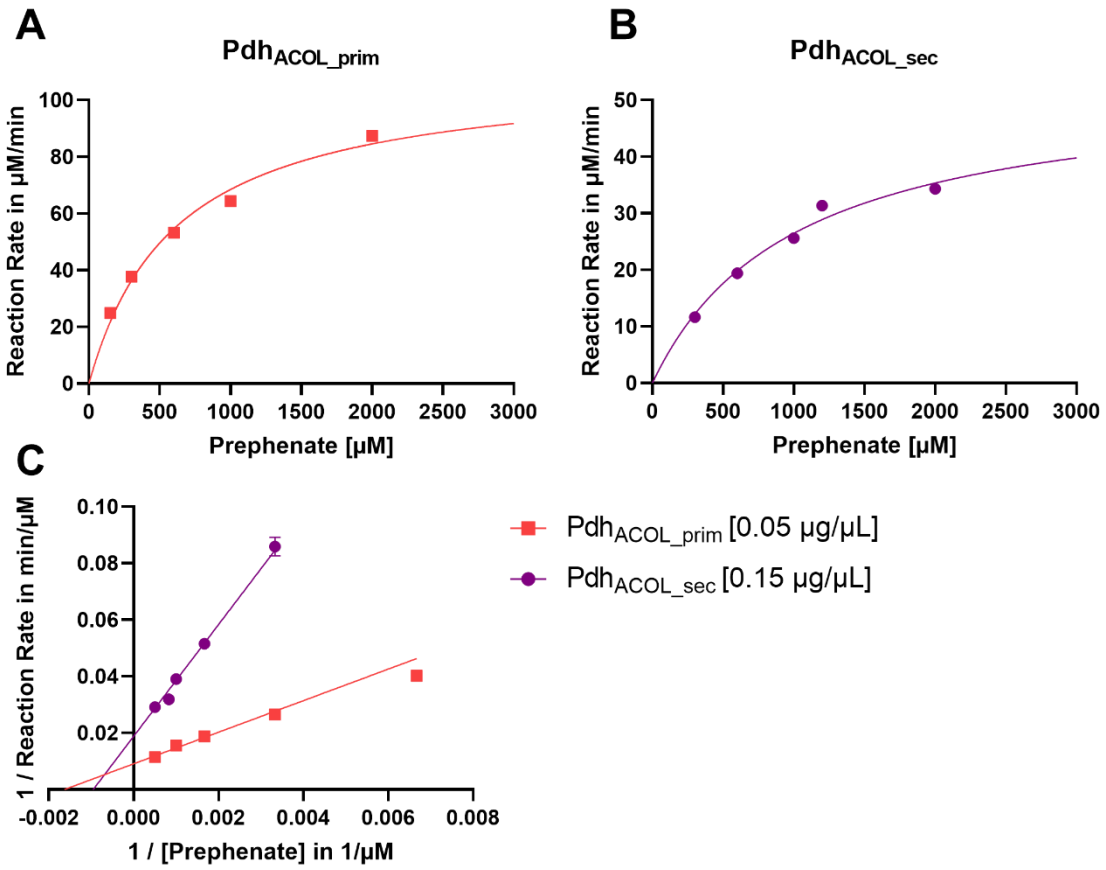

Figure S3: Kinetics of *A. coloradensis* Pdhs

Michaelis-Menten saturation curve of Pdh_{ACOL_prim} [A] and Pdh_{ACOL_sec} [B].
[C] Lineweaver-Burk plot of received data.
Data are derived from three independent replicates and are presented as median values with standard deviation.

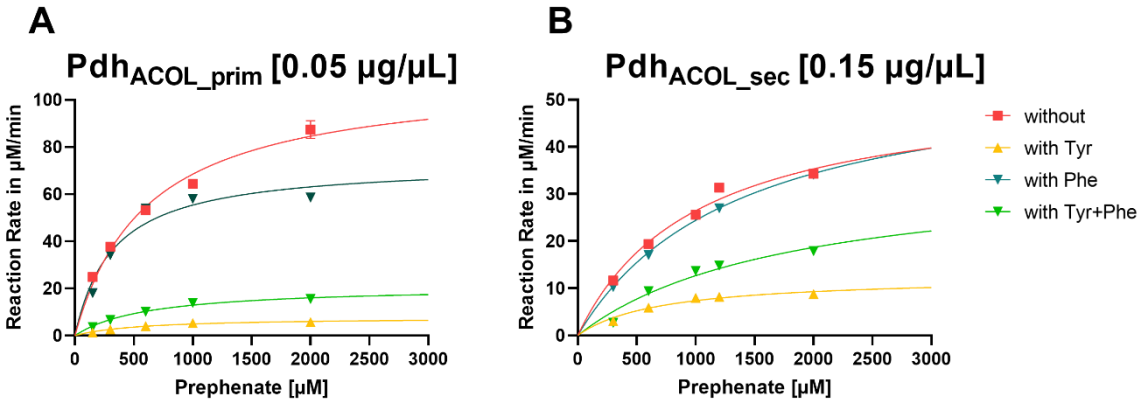

Figure S4: Kinetics of *A. coloradensis* Pdhs in the presence of potential inhibitors.

Michaelis-Menten saturation curves of Pdh_{ACOL_prim} [A] and Pdh_{ACOL_sec} [B] with and without addition of 200 µM Tyr and 200 µM Phe. **Data are derived from three independent replicates and are presented as median values with standard deviation.**

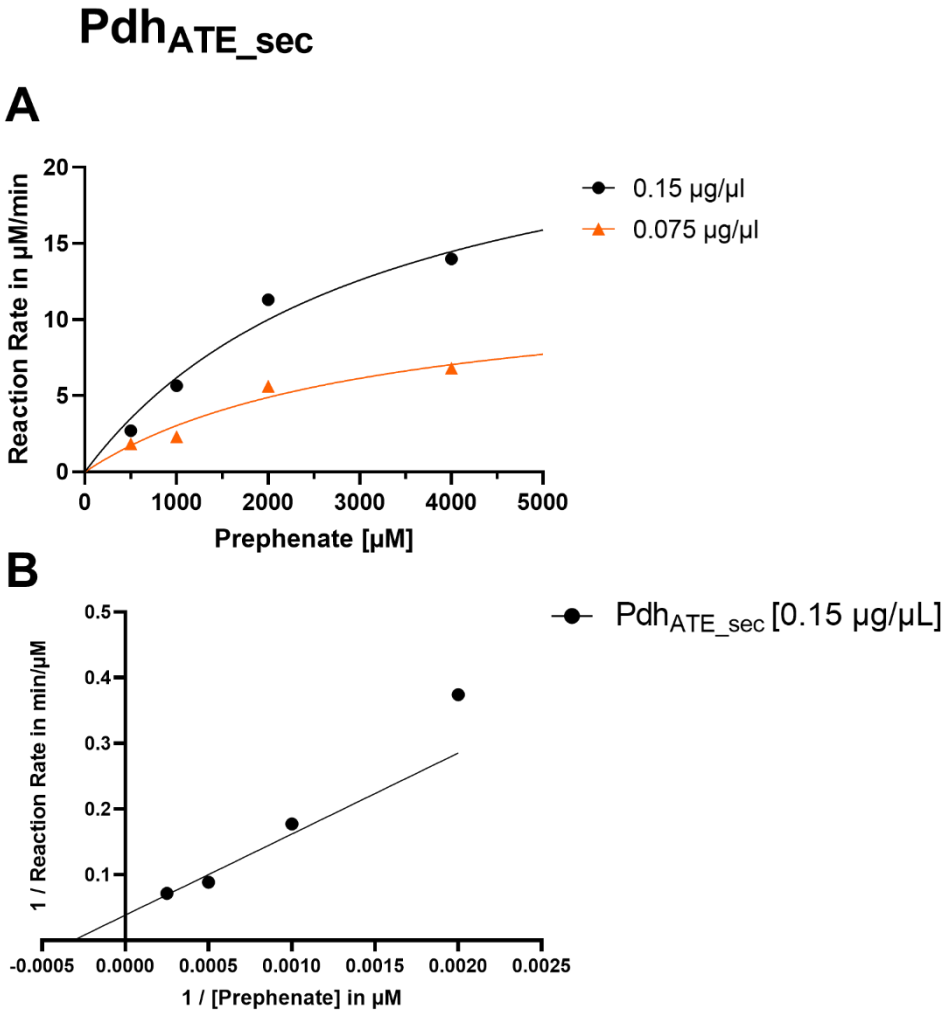

Figure S5: Kinetics of *Act. teichomyceticus* Pdh_{ATE_sec}.

[A] Michaelis-Menten saturation curve of Pdh_{ATE_sec}.
[B] Lineweaver-Burk plot of received data.
Data are derived from three independent replicates and are presented as median values with standard deviation.

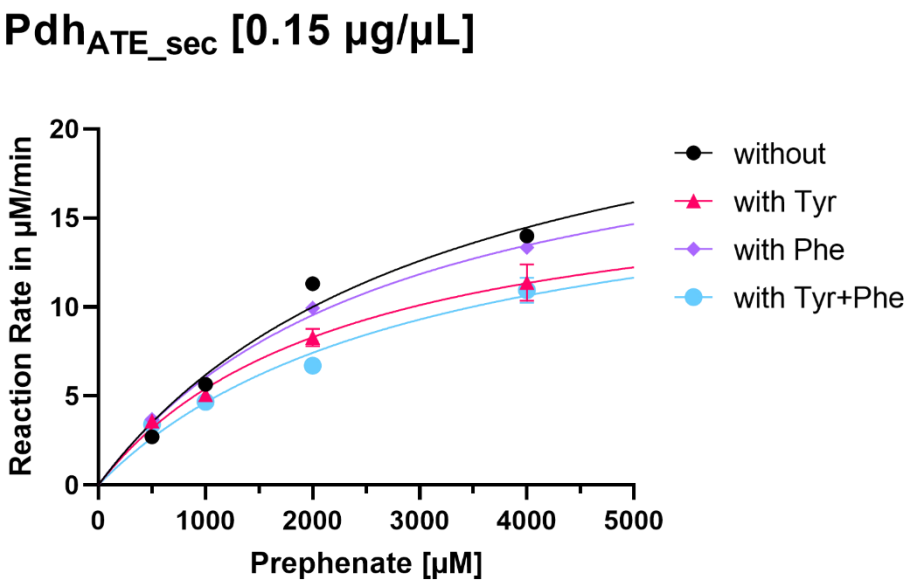

Figure S6: Kinetics of *Act. teichomyceticus* Pdh$_{ATE_sec}$ in the presence of potential inhibitors.

Michaelis-Menten saturation curves of Pdh$_{ATE_sec}$ with and without addition of 200 µM Tyr and 200 µM Phe. **Data are derived from three independent replicates and are presented as median values with standard deviation.**

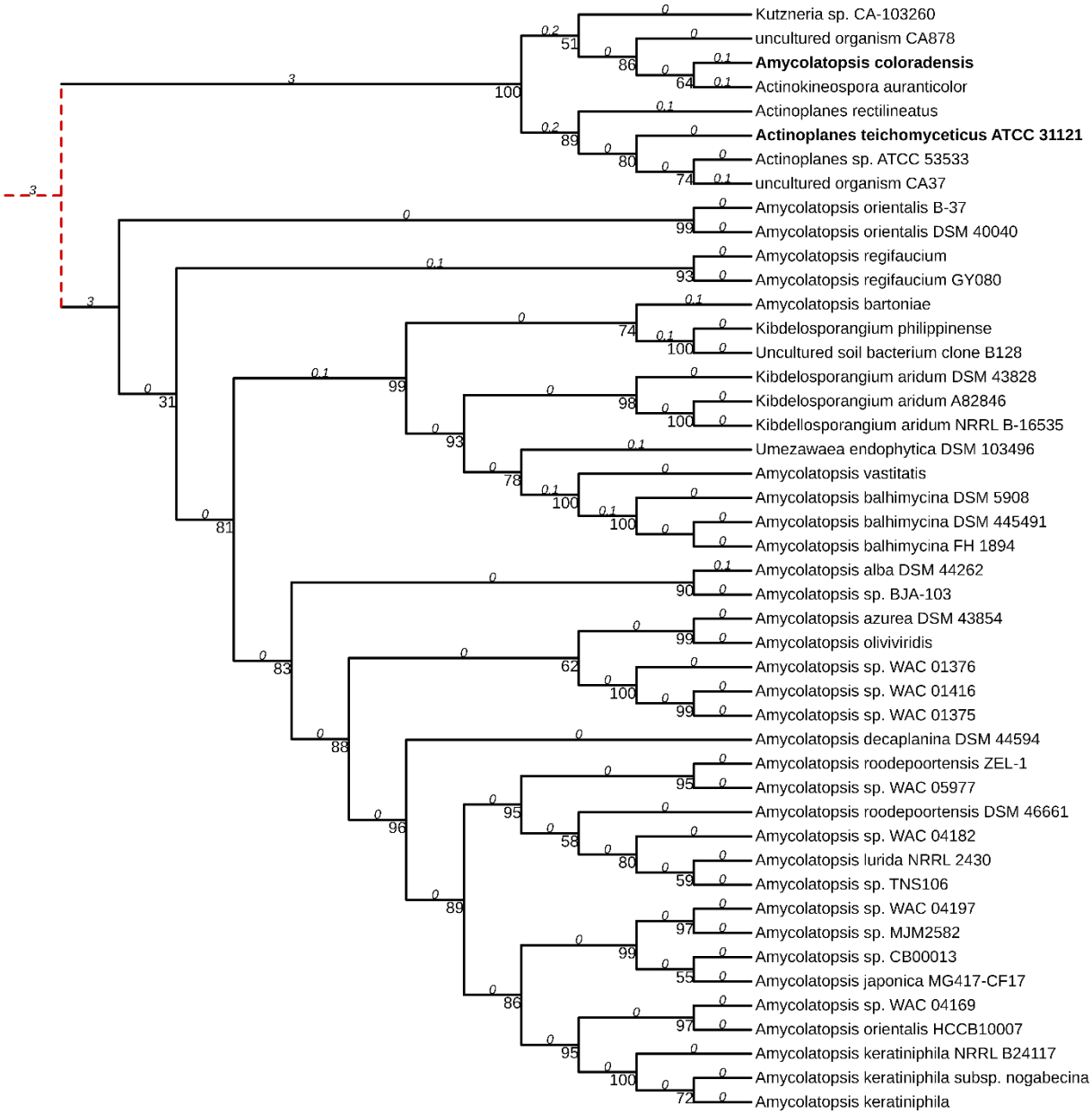

Figure S7: Phylogenetic analysis of Dahp. Branch lengths are ignored for visualization purposes, but are labelled in the middle of each branch. The bootstrap values are shown by each node. The red dotted branch is especially long, which is consistent with the placement of the two types of Dahps in different OGs by the orthology inference tool.

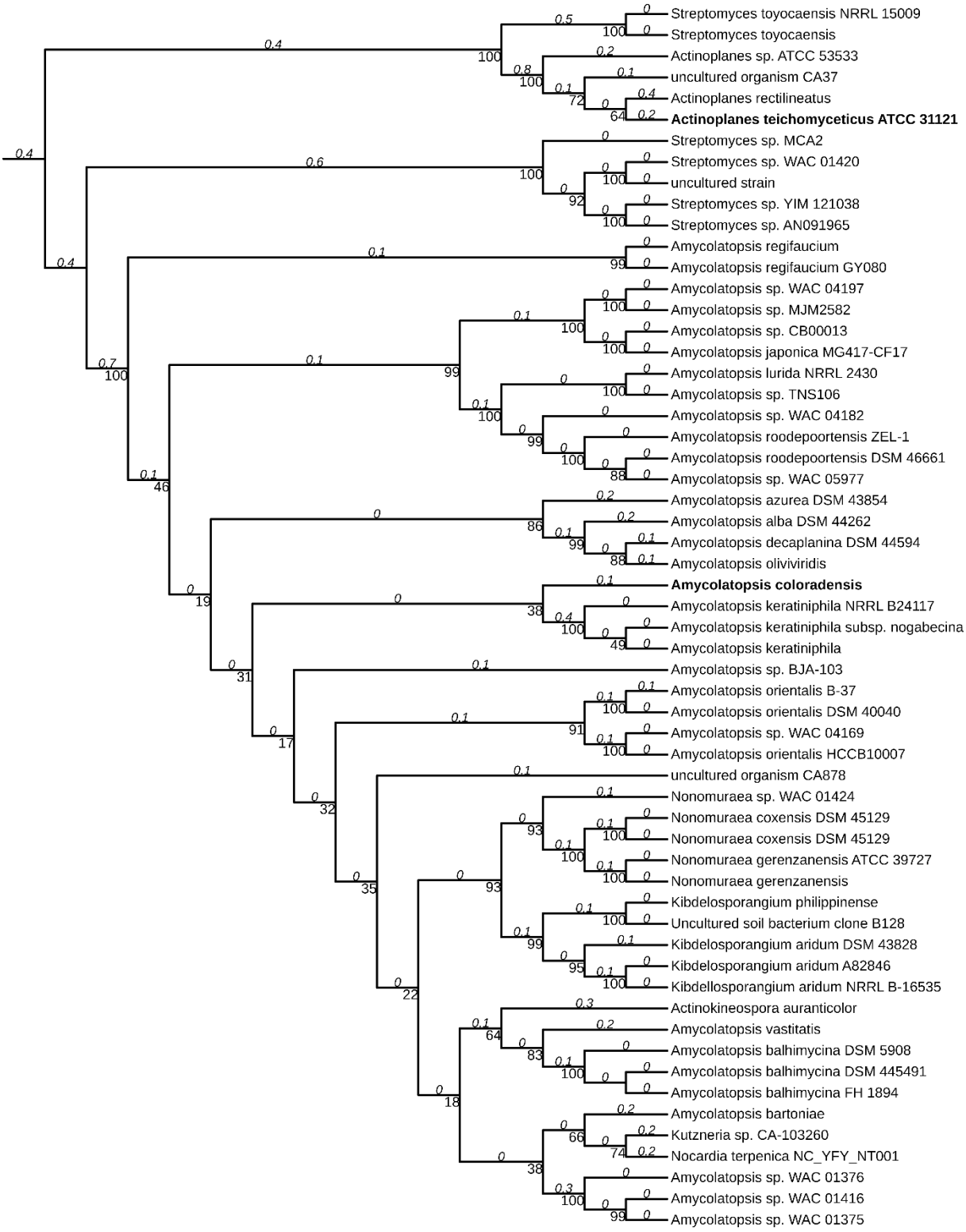

Figure S8: Phylogenetic analysis of Pdh. Branch lengths are ignored for visualization purposes, but are labelled in the middle of each branch. The bootstrap values are shown by each node.

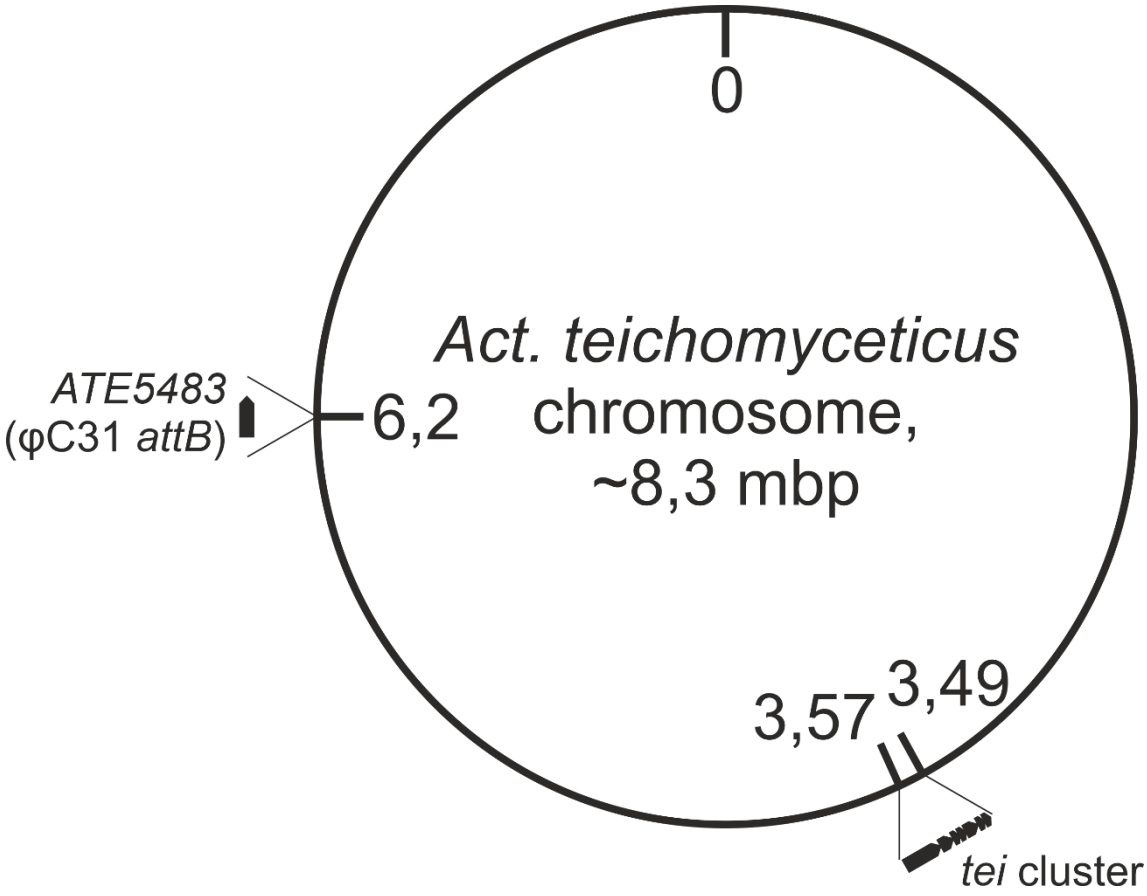

Figure S9: Relative positions of teicoplanin BGC and φC31 *attB* site on the chromosome of *Act. teichomyceticus.*

References

Abou-Zeid, A., Euverink, G., Hessels, G.I., Jensen, R.A., Dijkhuizen, L., 1995. Biosynthesis of L-phenylalanine and L-tyrosine in the actinomycete *Amycolatopsis methanolica* . Appl. Environ. Microbiol. 61, 1298–1302. https://doi.org/10.1128/aem.61.4.1298-1302.1995

Bentley, R., 1990. The shikimate pathway - a metabolic tree with many branches. Crit. Rev. Biochem. Mol. Biol. 25, 307–384. https://doi.org/10.3109/10409239009090615

Bertani, G., 1951. Studies on lysogenesis I: the mode of phage liberation by lysogenic *Escherichia coli*. J. Bacteriol. 62, 293–300. https://doi.org/10.1128/jb.62.3.293-300.1951

Blaskovich, M.A.T., Hansford, K.A., Butler, M.S., Jia, Z., Mark, A.E., Cooper, M.A., 2018. Developments in glycopeptide antibiotics. ACS Infect. Dis. 4, 715–735. https://doi.org/10.1021/acsinfecdis.7b00258

Bonner, C.A., Disz, T., Hwang, K., Song, J., Vonstein, V., Overbeek, R., Jensen, R.A., 2008. Cohesion group approach for evolutionary analysis of TyrA, a protein family with wide-ranging substrate specificities. Microbiol. Mol. Biol. Rev. MMBR 72, 13–53, table of contents. https://doi.org/10.1128/MMBR.00026-07

Brigham, R.B., Pittenger, R.C., 1956. *Streptomyces orientalis*, n. sp., the source of vancomycin. Antibiot. Chemother. Northfield Ill 6, 642–647.

Calhoun, D.H., Pierson, D.L., Jensen, R.A., 1973. Channel-shuttle mechanism for the regulation of phenylalanine and tyrosine synthesis at a metabolic branch point in Pseudomonas aeruginosa. J. Bacteriol. 113, 241–251. https://doi.org/10.1128/jb.113.1.241-251.1973

Davanloo, P., Rosenberg, A.H., Dunn, J.J., Studier, F.W., 1984. Cloning and expression of the gene for bacteriophage T7 RNA polymerase. Proc. Natl. Acad. Sci. U. S. A. 81, 2035–2039. https://doi.org/10.1073/pnas.81.7.2035

De Boer, L., Vrijbloed, J.W., Grobben, G., Dijkhuizen, L., 1989. Regulation of aromatic amino acid biosynthesis in the ribulose monophosphate cycle methylotroph *Nocardia sp.* 239. Arch. Microbiol. 151, 319–325. https://doi.org/10.1007/BF00406558

Gavriilidou, A., Adamek, M., Rodler, J.-P., Kubach, N., Kramer, S., Huson, D.H., Cryle, M.J., Stegmann, E., Ziemert, N., 2023. Phylogenetic distance and structural diversity directing a reclassification of glycopeptide antibiotics. https://doi.org/10.1101/2023.02.10.526856

Goldfinger, V., Spohn, M., Rodler, J.-P., Sigle, M., Kulik, A., Cryle, M.J., Rapp, J., Link, H., Wohlleben, W., Stegmann, E., 2023. Metabolic engineering of the shikimate pathway in *Amycolatopsis* strains for optimized glycopeptide antibiotic production. Metab. Eng. 78, 84–92. https://doi.org/10.1016/j.ymben.2023.05.005

Ha, H.-S., Hwang, Y.-I., Choi, S.-U., 2008. Application of conjugation using ϕC31 att/int system for *Actinoplanes teichomyceticus*, a producer of teicoplanin. Biotechnol. Lett. 30, 1233–1238. https://doi.org/10.1007/s10529-008-9671-z

Horbal, L., Kobylyanskyy, A., Truman, A.W., Zaburranyi, N., Ostash, B., Luzhetskyy, A., Marinelli, F., Fedorenko, V., 2014. The pathway-specific regulatory genes, *tei15** and *tei16**, are the master switches of teicoplanin production in *Actinoplanes teichomyceticus*. Appl. Microbiol. Biotechnol. 98, 9295–9309. https://doi.org/10.1007/s00253-014-5969-z

Horbal, L., Kobylyanskyy, A., Yushchuk, O., Zaburannyi, N., Luzhetskyy, A., Ostash, B., Marinelli, F., Fedorenko, V., 2013. Evaluation of heterologous promoters for genetic analysis of *Actinoplanes teichomyceticus*—Producer of teicoplanin, drug of last defense. J. Biotechnol. 168, 367–372. https://doi.org/10.1016/j.jbiotec.2013.10.018

Hubbard, B.K., Thomas, M.G., Walsh, C.T., 2000. Biosynthesis of L-*p*-hydroxyphenylglycine, a non-proteinogenic amino acid constituent of peptide antibiotics. Chem. Biol. 7, 931–942. https://doi.org/10.1016/S1074-5521(00)00043-0

Hund, H.K., Bär, G., Lingens, F., 1989. Purification and properties of arogenate dehydrogenase from *Actinoplanes missouriensis*. Z. Naturforschung C J. Biosci. 44, 797–801. https://doi.org/10.1515/znc-1989-9-1017

Katoh, K., Standley, D.M., 2013. MAFFT Multiple Sequence Alignment Software Version 7: Improvements in Performance and Usability. Mol. Biol. Evol. 30, 772–780. https://doi.org/10.1093/molbev/mst010
Kieser, T., Bibb, M.J., Buttner, M.J., Chater, K.F., Hopwood, D.A., 2000. Practical Streptomyces genetics. The John Innes Foundation, Norwich.
Labeda, D.P., 1995. *Amycolatopsis coloradensis sp. nov.*, the avoparcin (LL-AV290)-producing strain. Int. J. Syst. Evol. Microbiol. 45, 124–127. https://doi.org/10.1099/00207713-45-1-124
Letunic, I., Bork, P., 2024. Interactive Tree of Life (iTOL) v6: recent updates to the phylogenetic tree display and annotation tool. Nucleic Acids Res. 52, W78–W82. https://doi.org/10.1093/nar/gkae268
Light, S.H., Anderson, W.F., 2013. The diversity of allosteric controls at the gateway to aromatic amino acid biosynthesis. Protein Sci. Publ. Protein Soc. 22, 395–404. https://doi.org/10.1002/pro.2233
Menges, R., Muth, G., Wohlleben, W., Stegmann, E., 2007. The ABC transporter Tba of *Amycolatopsis balhimycina* is required for efficient export of the glycopeptide antibiotic balhimycin. Appl. Microbiol. Biotechnol. 77, 125–134. https://doi.org/10.1007/s00253-007-1139-x
Minh, B.Q., Schmidt, H.A., Chernomor, O., Schrempf, D., Woodhams, M.D., von Haeseler, A., Lanfear, R., 2020. IQ-TREE 2: new models and efficient methods for phylogenetic inference in the genomic era. Mol. Biol. Evol. 37, 1530–1534. https://doi.org/10.1093/molbev/msaa015
Mir, R., Jallu, S., Singh, T.P., 2015. The shikimate pathway: Review of amino acid sequence, function and three-dimensional structures of the enzymes. Crit. Rev. Microbiol. 41, 172–189. https://doi.org/10.3109/1040841X.2013.813901
Nicolaou, K.C., Boddy, C.N., Bräse, S., Winssinger, N., 1999. Chemistry, biology, and medicine of the glycopeptide antibiotics. Angew. Chem. Int. Ed Engl. 38, 2096–2152. https://doi.org/10.1002/(sici)1521-3773(19990802)38:15%3C2096::aid-anie2096%3E3.0.co;2-f
Pfeifer, V., Nicholson, G.J., Ries, J., Recktenwald, J., Schefer, A.B., Shawky, R.M., Schröder, J., Wohlleben, W., Pelzer, S., 2001. A polyketide synthase in glycopeptide biosynthesis: the biosynthesis of the non-proteinogenic amino acid (S)-3,5-dihydroxyphenylglycine. J. Biol. Chem. 276, 38370–38377. https://doi.org/10.1074/jbc.M106580200
Pozzi, R., Coles, M., Linke, D., Kulik, A., Nega, M., Wohlleben, W., Stegmann, E., 2016. Distinct mechanisms contribute to immunity in the lantibiotic NAI-107 producer strain *Microbispora* ATCC PTA-5024. Environ. Microbiol. 18, 118–132. https://doi.org/10.1111/1462-2920.12892
Puk, O., Bischoff, D., Kittel, C., Pelzer, S., Weist, S., Stegmann, E., Süssmuth, R.D., Wohlleben, W., 2004. Biosynthesis of chloro-β-hydroxytyrosine, a nonproteinogenic amino acid of the peptidic backbone of glycopeptide antibiotics. J. Bacteriol. 186, 6093–6100. https://doi.org/10.1128/jb.186.18.6093-6100.2004
Salamzade, R., Tran, P.Q., Martin, C., Manson, A.L., Gilmore, M.S., Earl, A.M., Anantharaman, K., Kalan, L.R., 2025. zol and fai: large-scale targeted detection and evolutionary investigation of gene clusters. Nucleic Acids Res. 53, gkaf045. https://doi.org/10.1093/nar/gkaf045
Song, J., Bonner, C.A., Wolinsky, M., Jensen, R.A., 2005. The TyrA family of aromatic-pathway dehydrogenases in phylogenetic context. BMC Biol. 3, 13. https://doi.org/10.1186/1741-7007-3-13
Speedie, M.K., Park, M.O., 1980. Regulation of tyrosine biosynthesis by phenylalanine in anthramycin-producing *Streptomyces refuineus*. J. Antibiot. (Tokyo) 33, 579–584. https://doi.org/10.7164/antibiotics.33.579
Speth, A.R., Hund, H.-K., Lingens, F., 1989. Terminal phenylalanine and tyrosine biosynthesis of *Microtetraspora glauca* 370, 591–600. https://doi.org/10.1515/bchm3.1989.370.1.591
Stegmann, E., Pelzer, S., Wilken, K., Wohlleben, W., 2001. Development of three different gene cloning systems for genetic investigation of the new species *Amycolatopsis japonicum* MG417-CF17, the ethylenediaminedisuccinic acid producer. J. Biotechnol., Biochemical Engineering: Trends and Potentials 92, 195–204. https://doi.org/10.1016/S0168-1656(01)00360-1

Studier, F.W., Moffatt, B.A., 1986. Use of bacteriophage T7 RNA polymerase to direct selective high-level expression of cloned genes. J. Mol. Biol. 189, 113–130. https://doi.org/10.1016/0022-2836(86)90385-2
Taurino, C., Frattini, L., Marcone, G.L., Gastaldo, L., Marinelli, F., 2011. *Actinoplanes teichomyceticus* ATCC 31121 as a cell factory for producing teicoplanin. Microb. Cell Factories 10, 82. https://doi.org/10.1186/1475-2859-10-82
Thykaer, J., Nielsen, J., Wohlleben, W., Weber, T., Gutknecht, M., Lantz, A.E., Stegmann, E., 2010. Increased glycopeptide production after overexpression of shikimate pathway genes being part of the balhimycin biosynthetic gene cluster. Metab. Eng. 12, 455–461. https://doi.org/10.1016/j.ymben.2010.05.001
Tianhui, X., Chiao, J.S., 1989. Regulation of the biosynthetic pathway of aromatic amino acids in *Nocardia mediterranei*. Biochim. Biophys. Acta BBA - Gen. Subj. 991, 6–11. https://doi.org/10.1016/0304-4165(89)90020-2
Waglechner, N., McArthur, A.G., Wright, G.D., 2019. Phylogenetic reconciliation reveals the natural history of glycopeptide antibiotic biosynthesis and resistance. Nat. Microbiol. 4, 1862–1871. https://doi.org/10.1038/s41564-019-0531-5
Wu, J., Woodard, R.W., 2006. New insights into the evolutionary links relating to the 3-deoxy-D-arabino-heptulosonate 7-phosphate synthase subfamilies. J. Biol. Chem. 281, 4042–4048. https://doi.org/10.1074/jbc.M512223200
Yim, G., Thaker, M.N., Koteva, K., Wright, G., 2014. Glycopeptide antibiotic biosynthesis. J. Antibiot. (Tokyo) 67, 31–41. https://doi.org/10.1038/ja.2013.117
Yushchuk, O., Horbal, L., Ostash, B., Marinelli, F., Wohlleben, W., Stegmann, E., Fedorenko, V., 2019. Regulation of teicoplanin biosynthesis: refining the roles of *tei* cluster-situated regulatory genes. Appl. Microbiol. Biotechnol. 103, 4089–4102. https://doi.org/10.1007/s00253-019-09789-w

5.3. Discussion

5.3.1 Shikimate-pathway isoenzymes can be leveraged for metabolic engineering of GPA production

GPA production depends heavily on the availability of precursors from the shikimate pathway. The biosynthesis of Bht, Hpg, and Dpg requires precursor molecules derived from Tyr and 4-HPP (Chen et al., 2001; Pfeifer et al., 2001; Puk et al., 2004). However, the shikimate pathway is tightly regulated by aromatic amino acids through allosteric regulation (Kloosterman et al., 2003; Lütke-Eversloh and Stephanopoulos, 2007), making these precursors limiting under native physiological conditions. GPA producers contain copies of the key enzymes of the shikimate pathway that are encoded within their BGCs. Duplication of Dahp and Pdh is found within BGCs in several different strains. *Streptomyces spectabilis* contains a gene encoding SpnJ (Dahp) within the spectinabilin BGCs (Seong Choi et al., 2010). In the myxobacterium *Stigmatella aurantiaca Sg a15* there are three Dahp isoenzymes, $AroA_{001}$ (type I Dahp), $AroA_2$ and $AroA_{A5}$ (type II Dahp), which are involved in aurachin biosynthesis (Silakowski et al., 2000). This raised the question whether these isoenzymes have particular properties to ensure sufficient precursor supply for GPA biosynthesis.

The *in vivo* functional analysis in *A. balhimycina* revealed that overexpression of *pdh* variants and $dahp_{prim}$ had minimal or even negative impacts. In contrast, the overexpression of the cluster-encoded $Dahp_{sec}$ plays a dominant role in sustaining balhimycin production. These results confirm earlier observations that the first committed step of the shikimate pathway represents a major metabolic bottleneck (Bentley, 1990; Thykaer et al., 2010) and highlight the importance of understanding the regulatory context to design engineering strategies.

Beyond intrinsic pathway bottlenecks, competition for shared metabolic precursors represents an additional factor shaping secondary metabolite production. Redirecting precursor flux by eliminating competing biosynthetic routes has proven to be an effective strategy to enhance antibiotic yields. A well characterized example is wuningmycin production in *Streptomyces ahygroscopicus,* where the polyene macrolides tetramycin A, tetramycin B, and nystatin are synthesized from the common precursors malonyl-CoA or methylmalonyl-CoA. Deletion of the tetramycin biosynthetic gene *ttmS1* abolished tetramycin biosynthesis ad resulted in a 10-fold increase in

nystatin production (Ren et al., 2014), demonstrating that relieving precursor competition can substantially enhance target antibiotic yields.

The robust increase in balhimycin titers following the overexpression of *pdt* expanded the regulatory picture of the shikimate pathway in *A. balhimycina* (Goldfinger et al., 2023). Pdt converts prephenate into Phe and shifts the flux away from Tyr, which is required for GPA precursors (Hubbard et al., 2000; Pfeifer et al., 2001). Since Tyr acts as an inhibitor of $Dahp_{sec}$ while Phe can antagonize the Tyr-dependent inhibition, the observation aligned with classical studies in *Pseudomonas aeruginosa* and *Streptomyces refuineus*, that showed the regulatory interplay between Phe and Tyr biosynthesis (Calhoun et al., 1973; Speedie and Park, 1980). By elevating intracellular Phe levels, *pdt* overexpression likely disrupts feedback inhibition, resulting in a larger pool of precursors for GPA biosynthesis. This was also in line with the results obtained from external supplementation of Phe in *A. balhimycina* (Goldfinger et al., 2023).

To test whether this metabolic engineering approach could be generalized on other GPA producer strains, the same approach was tested on the ristomycin A producer*, A. japonica* (Spohn et al., 2014). Ristomycin A biosynthesis demands for aromatic precursors are even higher due to the heptapeptide backbone structure that contains only aromatic amino acids.

Previous results showed significant increase in ristomycin A production by overexpression of the pathway-specific regulator *ajrR* (Spohn et al., 2014). In *Streptomyces tsukubaensis,* it has been shown that overexpression of *dahp,* combined with the overexpression of the acetyl-CoA carboxylase (*accA2*) and the glucose-6-phosphate dehydrogenase (*zwf2*)*,* enhanced the production of the macrolide FK506 (Huang et al., 2013a). Combining the overexpression of *ajrR* with our metabolic engineering approach increased ristomycin A production ~35-fold (1.7 g/L^{-1}) compared to the wild type. These results demonstrate that targeted manipulation of precursor metabolism can be remarkably effective when combined with regulatory enhancement or other metabolic pathway related genes. The transferability of the engineering strategy from *A. balhimycina* to *A. japonica* shows this approach is potentially generalizable for improving yields across *Amycolatopsis* species.

5.3.2 Dahp isoenzymes as key flux-controlling nodes in GPA biosynthesis

To expand the knowledge about the key enzymes Dahp and Pdh of the shikimate pathway in GPA producers and to determine whether homologous BGC encoded isoenzymes share equivalent functions, we performed phylogenetic analysis based on a multi-sequence alignment approach. *A. coloradensis* and *Act. teichomyceticus* form distinct phylogenetic and biosynthetic lineages and differ from *A. balhimycina*.

This observation is reflected in the kinetic properties of the enzymes. *A. coloradensis* $Dahp_{ACOL\_sec}$ displays the highest catalytic efficiency, yet it is the most susceptible to inhibition by Tyr and Phe. These properties help explain why overexpression of $dahp_{ACOL\_sec}$ suppresses avoparcin production, while deletion of $dahp_{ACOL\_sec}$ enhances it. Dahp catalyzes the first step in the shikimate pathway, and overexpression of $dahp_{ACOL\_sec}$ initially increases the overall flux through the shikimate pathway, resulting presumably in higher intracellular concentrations of the aromatic amino acids (Tyr, Phe, Trp), which ultimately shut down the pathway by inhibiting $Dahp_{ACOL\_sec}$.

In contrast, $Dahp_{ABAL\_sec}$ and $Dahp_{ATE\_sec}$ are inhibited only by Tyr and therefore have a positive effect on GPA production when overexpressed. This is in line with the more than 2-fold increase in teicoplanin production when heterologous $dahp_{ABAL\_sec}$ was introduced into the genome of *Act. teichomyceticus*.

Similar diversity in allosteric regulation has been described in other bacterial systems. For example, *Corynebcaterium glutamicum* contains two Dahps isoenzymes, AroF and AroG: AroF is inhibited by Tyr and Phe, whereas AroG is only inhibited by Trp (Liu et al., 2008). Related subspecies also exhibit distinct patterns: *C. glutamicum subsp. lactofermentum* harbors a Dahp that is sensitive exclusively to Tyr (Liao et al., 2001), while Dahp from *C. glutamicum subsp. flavum* is inhibited by both Tyr and Phe, with synergistic inhibition when both are present (Shiio et al., 1974). Likewise, the well characterized *E. coli* isoenzymes, AroG, AroF and AroH, each display different inhibition profiles by Phe, Tyr and Trp. (Cui et al., 2019).

Together, these examples show that Dahp isoenzymes from closely related organisms differ in their allosteric regulation. Even $Dahp_{ACOL\_sec}$ and $Dahp_{ATE\_sec}$, which are closely related based on phylogenetic analysis, show distinct functions in the *in vivo* analysis, which disproves our hypothesis that these isoenzymes share equivalent functions.

5.3.3 Pdh isoenzymes differ in their substrate-specificity and regulatory role

The biochemical analysis of Pdh isoenzymes showed variable substrate specificities that are consistent with the broader diversity reported within the TyrA family (Bonner et al., 2008; Song et al., 2005). Pdh_{ATE_prim} was shown to be part of the $TyrA_a$-family of dehydrogenases, which are arogenate specific (Song et al., 2005). This was consistent with the results of our biochemical analysis of Pdh_{ATE_prim}, which was unable to perform the reaction even in the presence of concentrations up to 5000 µM prephenate. Interestingly, Pdh_{ABAL_prim} was also described as a $TyrA_a$-dehydrogenase (Song et al., 2005). The biochemical properties showed that it is able to use prephenate as a substrate, although the high K_M values indicate that this is not the preferred substrate.

In *A. coloradensis*, both Pdh isoenzymes are feedback-sensitive and likely belong to the $TyrA_a$ or $TyrA_c$ family of dehydrogenases (Bonner et al., 2008), consistent with their high K_M values for prephenate. Based on their regulatory properties, we hypothesize that they help to maintain Tyr/Phe homeostasis, but also restrict metabolic flux toward avoparcin biosynthesis. Based on the biochemical behavior of Pdh_{ACOL_sec}, we conclude that *A. coloradensis* prioritizes metabolic balance over generating a high flux of shikimate-derived precursors for GPA production. A similar situation likely applies in *Act. teichomyceticus*: the primary prephenate dehydrogenase Pdh_{ATE_prim} belongs to the $TyrA_a$-family (Bonner et al., 2008) and therefore exclusively utilizes arogenate rather than prephenate as a substrate, while the low catalytic efficiency of Pdh_{ATE_sec} suggests a regulatory role focused on maintain metabolic balance rather than maximizing precursor supply.

5.3.4 Role of ACT regulatory domain in controlling precursor flux

Pdh_{ATE_sec} and Pdh_{ACOL_sec} both harbor a C-terminal ACT-regulatory domain, which is missing in Pdh_{ABAL_sec}. We hypothesized that the absence of the ACT-domain in Pdh_{ABAL_sec} might be the reason for its negative effect on balhimycin production when the gene is overexpressed (Thykaer et al., 2010). This regulatory domain is involved in allosteric regulation by Tyr as shown for *Bacillus anthracis* (Shabalin et al., 2020). This is in line with the observed results for Pdh isoenzymes from *A. coloradensis* and *Act. teichomyceticus*, which are both inhibited by Tyr. Pdh_{ABAL_sec} lacks the ACT-terminal domain and shows no change in activity in the presence of a potential inhibitor. Interestingly, overexpression of pdh_{ATE_sec} increased teicoplanin production more than 3-fold. To investigate the function of the ACT-domain on GPA production, a truncated

version of *pdh*$_{ATE\_sec}$ was overexpressed, which had no visible impact on teicoplanin production and showed similar levels as the overexpression of *pdh*$_{ABAL\_sec}$ in *Act. teichomyceticus*. It can't be excluded that deletion of the ACT domain compromised protein stability. Therefore, the measured teicoplanin levels are likely a result of the activity of the endogenous wild type *pdh*$_{ATE\_sec}$ copy rather than the truncated enzyme.

Our results demonstrate that the C-terminal region of Pdh$_{ATE_sec}$ is required for the positive effect on teicoplanin production observed upon its overexpression. Overexpression of *pdh*$_{ATE\_sec}$ presumably increases the intracellular Tyr pool, which in turn stimulates teicoplanin biosynthesis. However, Tyr accumulation is insufficient to enhance Phe biosynthesis and remains limited because Tyr allosterically regulates Pdh$_{ATE_sec}$. In contrast, overexpression of the unregulated variants Pdh$_{ABAL_sec}$ or Pdh$_{ATE_sec}$tr presumably causes a rapid and uncontrolled rise in Tyr levels, which either fails to improve or even suppresses GPA production, as observed in our study and previously reported for balhimycin biosynthesis (Thykaer et al., 2010).

In *A. coloradensis*, where Pdh$_{ACOL_sec}$ also contains an ACT-domain, the overexpression of *pdh*$_{ACOL\_sec}$ results in decreased avoparcin titers, which is in contrast to our observation in *Act. teichomyceticus*. This difference becomes clear when considering the broader regulatory context: Dahp$_{ATE_sec}$ and Dahp$_{ACOL_sec}$ differ in their allosteric regulation. In *A. coloradensis*, an increase in intracellular Tyr inhibits not only Pdh$_{ACOL_sec}$ but also Dahp$_{ACOL_sec}$, thereby reducing the overall flux through the shikimate pathway. Residual Phe enhances this effect by further inhibiting Dahp$_{ACOL_sec}$. In contrast, Dahp$_{ATE_sec}$ is positively influenced by Phe, allowing precursor flux to be maintained and enabling enhanced teicoplanin production.

5.3.5 Implications for metabolic engineering of GPA production

Aromatic amino acids (Tyr, Phe, and Trp) are crucial building blocks for pharmaceuticals, such as antidepressants and antitumor drugs. Tyr is used as an essential dietary component for patients with L-phenylketonuria (Li et al., 2020). The wide range of aromatic acid usage has prompted shikimate pathway engineering approaches in several different producer strains (Rodriguez et al., 2014). Overexpression of *aroA* (Dahp) and *tyrA* (Pdh) in *Bacillus amyloliquefaciens* led to an increase in L-tyrosine levels (Ji et al., 2025). A similar approach was used in *Bacillus licheniformis* where the co-overexpression of *aroA* and *tyrA* increased production of L-

DOPA, a promising drug for treating Parkinson's disease (Y. Xu et al., 2022). In *Pseudomonas fluorescens,* the Dahp isoenzyme PhcZ, located within the phenazine BGCs, belongs to the type II Dahps, similar to the Dahps from *S. coelicolor* and *S. rimosus.* This enzyme lacks feedback inhibition, and deletion of the corresponding gene *phzC* led to a 90% decrease in phenazine titers (Wang et al., 2022). A similar phenomenon has been shown for *Pseudomonas aeruginosa* and *Pseudomonas chloroaphis* Dahp isoenzymes, which also lack feedback inhibition (Sterritt et al., 2018) and were described as suitable overexpression candidates (Jin et al., 2015; Liu et al., 2016).

Given our previous findings showing a positive effect of Phe on balhimycina production, we sought to determine whether a similar mechanism operates in teicoplanin biosynthesis. In actinobacteria, prephenate dehydratases (Pdt) catalyze the conversion of prephenate to Phe and are activated by Tyr and inhibited by Phe through classical feedback regulation (Abou-Zeid et al., 1995; De Boer et al., 1989). This regulatory pattern has been experimentally demonstrated for Pdt from *Amycolatopsis mediterranei* (Tianhui and Chiao, 1989), which shares a high sequence identity with Pdt_{ATE} (61%) from *Act. teichomyceticus* and Pdt_{ABAL} (90%) from *A. balhimycina*, suggesting functional conservation across these enzymes.

We hypothesized that increasing intracellular Phe would inhibit Pdt activity, thereby elevating Tyr levels and stimulating GPA biosynthesis. Our experimental results confirmed this model: overexpression of pdt_{ABAL} or pdt_{ATE} in *Act. teichomyceticus* resulted in a 3-fold increase in teicoplanin production compared to the empty vector control. Moreover, external addition of Phe also enhanced teicoplanin titers, supporting the proposed mechanism. These findings align with our previous observations in *A. balhimycina* and are consistent with earlier reports in *Pseudomonas aeruginosa* and *Streptomyces refuineus* (Calhoun et al., 1973; Speedie and Park, 1980).

Collectively, our findings demonstrate that exploring the functional diversity of the key enzymes of the shikimate pathway, Dahp and Pdh, enables more effective metabolic engineering strategies to enhance GPA production, as shown for the clinically relevant teicoplanin and ristomycin A, which is used in the diagnosis of genetic disorders. By integrating phylogenetic analyses with biochemical characterization and *in vivo* functional studies of Dahp and Pdh, we identified major differences among orthologs, in particular, between $Dahp_{ACOL\_sec}$ and $Dahp_{ABAL\_sec}$ as well as Pdt_{ATE_sec} and

Pdh_{ABAL_sec}. In *A. balhimycina,* $Dahp_{ABAL\_sec}$ plays a central role in enhancing balhimycin production and can also be leveraged to enhance ristomycin A and teicoplanin yields in their respective producers. In contrast, in *A. coloradensis* and *Act. teichomyceticus*, the key enzymes appear to be Pdh_{ACOL_sec} and Pdh_{ATE_sec}. Notably, phylogenetic relation does not necessarily correlate with biochemical behavior, as shown by the divergent properties of $Dahp_{ATE\_sec}$ and $Dahp_{ABAL\_sec}$. Thus, continuing to explore the enzymatic diversity within GPA biosynthetic pathways will deepen the understanding of regulatory mechanisms and further improve strategies for metabolic engineering.

6. Literature

Abou-Zeid, A., Euverink, G., Hessels, G.I., Jensen, R.A., Dijkhuizen, L., 1995. Biosynthesis of L-phenylalanine and L-tyrosine in the actinomycete *Amycolatopsis methanolica* . Appl. Environ. Microbiol. 61, 1298–1302. https://doi.org/10.1128/aem.61.4.1298-1302.1995

Alduina, R., Sosio, M., Donadio, S., 2018. Complex regulatory networks governing production of the glycopeptide A40926. Antibiotics 7, 30. https://doi.org/10.3390/antibiotics7020030

Andreo-Vidal, A., Yushchuk, O., Marinelli, F., Binda, E., 2023. Cross-talking of pathway-specific regulators in glycopeptide antibiotics (teicoplanin and A40926) production. Antibiotics 12, 641. https://doi.org/10.3390/antibiotics12040641

Bailey, T.L., Johnson, J., Grant, C.E., Noble, W.S., 2015. The MEME Suite. Nucleic Acids Res. 43, W39–W49. https://doi.org/10.1093/nar/gkv416

Baltz, R.H., 2016. Genetic manipulation of secondary metabolite biosynthesis for improved production in *Streptomyces* and other actinomycetes. J. Ind. Microbiol. Biotechnol. 43, 343–370. https://doi.org/10.1007/s10295-015-1682-x

Bentley, R., 1990. The shikimate pathway - a metabolic tree with many branches. Crit. Rev. Biochem. Mol. Biol. 25, 307–384. https://doi.org/10.3109/10409239009090615

Bilyk, O., Luzhetskyy, A., 2016. Metabolic engineering of natural product biosynthesis in actinobacteria. Curr. Opin. Biotechnol., Chemical biotechnology • Pharmaceutical biotechnology 42, 98–107. https://doi.org/10.1016/j.copbio.2016.03.008

Bischoff, D., Bister, B., Bertazzo, M., Pfeifer, V., Stegmann, E., Nicholson, G.J., Keller, S., Pelzer, S., Wohlleben, W., Süssmuth, R.D., 2005. The biosynthesis of vancomycin-type glycopeptide antibiotics—a model for oxidative side-chain cross-linking by oxygenases coupled to the action of peptide synthetases. ChemBioChem 6, 267–272. https://doi.org/10.1002/cbic.200400328

Bonner, C.A., Disz, T., Hwang, K., Song, J., Vonstein, V., Overbeek, R., Jensen, R.A., 2008. Cohesion group approach for evolutionary analysis of TyrA, a protein family with wide-ranging substrate specificities. Microbiol. Mol. Biol. Rev. MMBR 72, 13–53, table of contents. https://doi.org/10.1128/MMBR.00026-07

Borghi, A., Coronelli, C., Faniuolo, L., Allievi, G., Pallanza, R., Gallo, G.G., 1984. Teichomycins, new antibiotics from *Actinoplanes teichomyceticus* nov. sp. IV. Separation and characterization of the components of teichomycin (teicoplanin). J. Antibiot. (Tokyo) 37, 615–620. https://doi.org/10.7164/antibiotics.37.615

Brieke, C., Peschke, M., Haslinger, K., Cryle, M.J., 2015. Sequential in vitro cyclization by cytochrome P450 enzymes of glycopeptide antibiotic precursors bearing the X-domain from nonribosomal peptide biosynthesis. Angew. Chem. Int. Ed. 54, 15715–15719. https://doi.org/10.1002/anie.201507533

Brown, E.D., Wright, G.D., 2016. Antibacterial drug discovery in the resistance era. Nature 529, 336–343. https://doi.org/10.1038/nature17042

Calhoun, D.H., Pierson, D.L., Jensen, R.A., 1973. Channel-shuttle mechanism for the regulation of phenylalanine and tyrosine synthesis at a metabolic branch point in *Pseudomonas aeruginosa*. J. Bacteriol. 113, 241–251. https://doi.org/10.1128/jb.113.1.241-251.1973

Chen, H., Tseng, C.C., Hubbard, B.K., Walsh, C.T., 2001. Glycopeptide antibiotic biosynthesis: enzymatic assembly of the dedicated amino acid monomer (S)-3,5-dihydroxyphenylglycine. Proc. Natl. Acad. Sci. U. S. A. 98, 14901–14906. https://doi.org/10.1073/pnas.221582098

Chen, H., Walsh, C.T., 2001. Coumarin formation in novobiocin biosynthesis: beta-hydroxylation of the aminoacyl enzyme tyrosyl-S-NovH by a cytochrome P450 NovI. Chem. Biol. 8, 301–312. https://doi.org/10.1016/s1074-5521(01)00009-6

Choroba, O.W., Williams, D.H., Spencer, J.B., 2000. Biosynthesis of the vancomycin group of antibiotics: involvement of an unusual dioxygenase in the pathway to (S)-4-hydroxyphenylglycine. J. Am. Chem. Soc. 122, 5389–5390. https://doi.org/10.1021/ja000076v

Cui, D., Deng, A., Bai, H., Yang, Z., Liang, Y., Liu, Z., Qiu, Q., Wang, L., Liu, S., Zhang, Y., Shi, Y., Qi, J., Wen, T., 2019. Molecular basis for feedback inhibition of tyrosine-regulated 3-deoxy-d-arabino-heptulosonate-7-phosphate synthase from *Escherichia coli*. J. Struct. Biol. 206, 322–334. https://doi.org/10.1016/j.jsb.2019.04.001

Culp, E.J., Waglechner, N., Wang, W., Fiebig-Comyn, A.A., Hsu, Y.-P., Koteva, K., Sychantha, D., Coombes, B.K., Van Nieuwenhze, M.S., Brun, Y.V., Wright, G.D., 2020. Evolution-guided discovery of antibiotics that inhibit peptidoglycan remodelling. Nature 578, 582–587. https://doi.org/10.1038/s41586-020-1990-9

De Boer, L., Vrijbloed, J.W., Grobben, G., Dijkhuizen, L., 1989. Regulation of aromatic amino acid biosynthesis in the ribulose monophosphate cycle methylotroph *Nocardia sp.* 239. Arch. Microbiol. 151, 319–325. https://doi.org/10.1007/BF00406558

Dosselaere, F., Vanderleyden, J., 2001. A metabolic node in action: chorismate-utilizing enzymes in microorganisms. Crit. Rev. Microbiol. 27, 75–131. https://doi.org/10.1080/20014091096710

Edenhart, S., Denneler, M., Spohn, M., Doskocil, E., Kavšček, M., Amon, T., Kosec, G., Smole, J., Bardl, B., Biermann, M., Roth, M., Wohlleben, W., Stegmann, E., 2020. Metabolic engineering of *Amycolatopsis japonicum* for optimized production of [*S,S*]-EDDS, a biodegradable chelator. Metab. Eng. 60, 148–156. https://doi.org/10.1016/j.ymben.2020.04.003

Euverink, G.J., Hessels, G.I., Franke, C., Dijkhuizen, L., 1995. Chorismate mutase and 3-deoxy-D-arabino-heptulosonate 7-phosphate synthase of the methylotrophic actinomycete *Amycolatopsis methanolica*. Appl. Environ. Microbiol. 61, 3796–3803. https://doi.org/10.1128/aem.61.11.3796-3803.1995

Fernández-Moreno, M.A., Caballero, J.L., Hopwood, D.A., Malpartida, F., 1991. The act cluster contains regulatory and antibiotic export genes, direct targets for translational control by the *bldA* tRNA gene of *Streptomyces*. Cell 66, 769–780. https://doi.org/10.1016/0092-8674(91)90120-n

Gavriilidou, A., Adamek, M., Rodler, J.-P., Kubach, N., Kramer, S., Huson, D.H., Cryle, M.J., Stegmann, E., Ziemert, N., 2023. Phylogenetic distance and structural diversity directing a reclassification of glycopeptide antibiotics. https://doi.org/10.1101/2023.02.10.526856

Gavriilidou, A., Adamek, M., Rodler, J.-P., Kubach, N., Voigtländer, A., Kokkoliadis, L., Hughes, C.C., Cryle, M.J., Stegmann, E., Ziemert, N., 2024. Animating insights into the biosynthesis of glycopeptide antibiotics. Curr. Opin. Microbiol. 82, 102561. https://doi.org/10.1016/j.mib.2024.102561

Gavriilidou, A., Kautsar, S.A., Zaburannyi, N., Krug, D., Müller, R., Medema, M.H., Ziemert, N., 2022. Compendium of specialized metabolite biosynthetic diversity encoded in bacterial genomes. Nat. Microbiol. 7, 726–735. https://doi.org/10.1038/s41564-022-01110-2

Gibson, F., Pittard, J., 1968. Pathways of biosynthesis of aromatic amino acids and vitamins and their control in microorganisms. Bacteriol. Rev. 32, 465–492.

Goldfinger, V., Spohn, M., Rodler, J.-P., Sigle, M., Kulik, A., Cryle, M.J., Rapp, J., Link, H., Wohlleben, W., Stegmann, E., 2023. Metabolic engineering of the shikimate pathway in *Amycolatopsis* strains for optimized glycopeptide antibiotic production. Metab. Eng. 78, 84–92. https://doi.org/10.1016/j.ymben.2023.05.005

Gomez-Escribano, J.P., Bibb, M.J., 2011. Engineering *Streptomyces coelicolor* for heterologous expression of secondary metabolite gene clusters. Microb. Biotechnol. 4, 207–215. https://doi.org/10.1111/j.1751-7915.2010.00219.x

Grasso, L.L., Maffioli, S., Sosio, M., Bibb, M., Puglia, A.M., Alduina, R., 2015. Two master switch regulators trigger A40926 biosynthesis in *Nonomuraea sp.* strain ATCC 39727. J. Bacteriol. https://doi.org/10.1128/jb.00262-15

Greule, A., Stok, J.E., De Voss, J.J., Cryle, M.J., 2018. Unrivalled diversity: the many roles and reactions of bacterial cytochromes P450 in secondary metabolism. Nat. Prod. Rep. 35, 757–791. https://doi.org/10.1039/c7np00063d

Hadatsch, B., Butz, D., Schmiederer, T., Steudle, J., Wohlleben, W., Süssmuth, R., Stegmann, E., 2007. The biosynthesis of teicoplanin-type glycopeptide antibiotics: assignment of p450 mono-oxygenases to side chain cyclizations of glycopeptide a47934. Chem. Biol. 14, 1078–1089. https://doi.org/10.1016/j.chembiol.2007.08.014

Hansen, M.H., Adamek, M., Iftime, D., Petras, D., Schuseil, F., Grond, S., Stegmann, E., Cryle, M.J., Ziemert, N., 2023. Resurrecting ancestral antibiotics: unveiling the origins of modern lipid II targeting glycopeptides. Nat. Commun. 14, 7842. https://doi.org/10.1038/s41467-023-43451-4

Haslinger, K., Peschke, M., Brieke, C., Maximowitsch, E., Cryle, M.J., 2015. X-domain of peptide synthetases recruits oxygenases crucial for glycopeptide biosynthesis. Nature 521, 105–109. https://doi.org/10.1038/nature14141

Heinrich, R., Rapoport, S.M., Rapoport, T.A., 1977. Metabolic regulation and mathematical models. Prog. Biophys. Mol. Biol. 32, 1–82.

Hojati, Z., Milne, C., Harvey, B., Gordon, L., Borg, M., Flett, F., Wilkinson, B., Sidebottom, P.J., Rudd, B.A.M., Hayes, M.A., Smith, C.P., Micklefield, J., 2002. Structure, biosynthetic origin, and engineered biosynthesis of calcium-dependent antibiotics from *Streptomyces coelicolor*. Chem. Biol. 9, 1175–1187. https://doi.org/10.1016/S1074-5521(02)00252-1

Horbal, L., Kobylyanskyy, A., Truman, A.W., Zaburranyi, N., Ostash, B., Luzhetskyy, A., Marinelli, F., Fedorenko, V., 2014. The pathway-specific regulatory genes, *tei15** and *tei16**, are the master switches of teicoplanin production in *Actinoplanes teichomyceticus* . Appl. Microbiol. Biotechnol. 98, 9295–9309. https://doi.org/10.1007/s00253-014-5969-z

Horbal, L., Rebets, Y., Rabyk, M., Makitrynskyy, R., Luzhetskyy, A., Fedorenko, V., Bechthold, A., 2012. SimReg1 is a master switch for biosynthesis and export of simocyclinone D8 and its precursors. AMB Express 2, 1. https://doi.org/10.1186/2191-0855-2-1

Huang, D., Li, S., Xia, M., Wen, J., Jia, X., 2013a. Genome-scale metabolic network guided engineering of *Streptomyces tsukubaensis* for FK506 production improvement. Microb. Cell Factories 12, 52. https://doi.org/10.1186/1475-2859-12-52

Huang, D., Xia, M., Li, S., Wen, J., Jia, X., 2013b. Enhancement of FK506 production by engineering secondary pathways of *Streptomyces tsukubaensis* and exogenous feeding strategies. J. Ind. Microbiol. Biotechnol. 40, 1023–1037. https://doi.org/10.1007/s10295-013-1301-7

Hubbard, B.K., Thomas, M.G., Walsh, C.T., 2000. Biosynthesis of L-*p*-hydroxyphenylglycine, a non-proteinogenic amino acid constituent of peptide antibiotics. Chem. Biol. 7, 931–942. https://doi.org/10.1016/S1074-5521(00)00043-0

Hung, T.V., Malla, S., Park, B.C., Liou, K., Lee, H.C., Sohng, J.K., 2007. Enhancement of clavulanic acid by replicative and integrative expression of *ccaR* and *cas2* in *Streptomyces clavuligerus* NRRL3585. J. Microbiol. Biotechnol. 17, 1538–1545.

Ji, A., Zou, D., Ma, A., Wei, X., 2025. Rational design of DAHP synthase and prephenate dehydrogenase for metabolic engineering of *Bacillus amyloliquefaciens* to produce L-tyrosine. Int. J. Biol. Macromol. 307, 142076. https://doi.org/10.1016/j.ijbiomac.2025.142076

Jin, K., Zhou, L., Jiang, H., Sun, S., Fang, Y., Liu, J., Zhang, X., He, Y.-W., 2015. Engineering the central biosynthetic and secondary metabolic pathways of *Pseudomonas aeruginosa* strain PA1201 to improve phenazine-1-carboxylic acid production. Metab. Eng. 32, 30–38. https://doi.org/10.1016/j.ymben.2015.09.003

Kaniusaite, M., Tailhades, J., Marschall, E.A., Goode, R.J.A., Schittenhelm, R.B., Cryle, M.J., 2019. A proof-reading mechanism for non-proteinogenic amino acid incorporation into glycopeptide antibiotics. Chem. Sci. 10, 9466–9482. https://doi.org/10.1039/C9SC03678D

Kieser, T., Bibb, M.J., Buttner, M.J., Chater, K.F., Hopwood, D.A., 2000. Practical Streptomyces genetics. The John Innes Foundation, Norwich.

Kloosterman, H., Hessels, G.I., Vrijbloed, J.W., Euverink, G.J., Dijkhuizen, L., 2003. (De)regulation of key enzyme steps in the shikimate pathway and phenylalanine-specific pathway of the actinomycete *Amycolatopsis methanolica*. Microbiology 149, 3321.

Labeda, D.P., 1995. *Amycolatopsis coloradensis sp. nov.*, the avoparcin (LL-AV290)-producing strain. Int. J. Syst. Evol. Microbiol. 45, 124–127. https://doi.org/10.1099/00207713-45-1-124

Lakey, J.H., Lea, E.J.A., Rudd, B.A.M., Wright, H.M., Hopwood, D.A., 1983. A new channel-forming antibiotic from *Streptomyces coelicolor* A3(2) which requires calcium for its activity. Microbiology 129, 3565–3573. https://doi.org/10.1099/00221287-129-12-3565

Levine, D.P., 2006. Vancomycin: a history. Clin. Infect. Dis. Off. Publ. Infect. Dis. Soc. Am. 42 Suppl 1, S5-12. https://doi.org/10.1086/491709

Lewis, K., 2020. The science of antibiotic discovery. Cell 181, 29–45. https://doi.org/10.1016/j.cell.2020.02.056

Li, S., Li, Z., Pang, S., Xiang, W., Wang, W., 2021. Coordinating precursor supply for pharmaceutical polyketide production in Streptomyces. Curr. Opin. Biotechnol. 69, 26–34. https://doi.org/10.1016/j.copbio.2020.11.006

Li, T.-L., Huang, F., Haydock, S.F., Mironenko, T., Leadlay, P.F., Spencer, J.B., 2004. Biosynthetic gene cluster of the glycopeptide antibiotic teicoplanin: characterization of two glycosyltransferases and the key acyltransferase. Chem. Biol. 11, 107–119. https://doi.org/10.1016/j.chembiol.2004.01.001

Li, X., Wang, M., Yin, L., Cao, J., Wang, R., Guo, W., Lu, J., Zhao, Z., Deng, Z., Hou, A., Xu, M., 2025. Phylogeny-informed discovery of new glycopeptide antibiotics produced by a minimal biosynthetic gene cluster. Org. Lett. 27, 2444–2449. https://doi.org/10.1021/acs.orglett.5c00378

Li, Z., Li, X., Xia, H., 2022. Roles of LuxR-family regulators in the biosynthesis of secondary metabolites in Actinobacteria. World J. Microbiol. Biotechnol. 38, 250. https://doi.org/10.1007/s11274-022-03414-1

Li, Z., Wang, H., Ding, D., Liu, Y., Fang, H., Chang, Z., Chen, T., Zhang, D., 2020. Metabolic engineering of *Escherichia coli* for production of chemicals derived from the shikimate pathway. J. Ind. Microbiol. Biotechnol. 47, 525–535. https://doi.org/10.1007/s10295-020-02288-2

Liao, H.-F., Lin, L.-L., Chien, H.R., Hsu, W.-H., 2001. Serine 187 is a crucial residue for allosteric regulation of *Corynebacterium glutamicum* 3-deoxy-D-arabino-heptulosonate-7-phosphate synthase. FEMS Microbiol. Lett. 194, 59–64. https://doi.org/10.1111/j.1574-6968.2001.tb09446.x

Light, S.H., Anderson, W.F., 2013. The diversity of allosteric controls at the gateway to aromatic amino acid biosynthesis. Protein Sci. Publ. Protein Soc. 22, 395–404. https://doi.org/10.1002/pro.2233

Light, S.H., Halavaty, A.S., Minasov, G., Shuvalova, L., Anderson, W.F., 2012. Structural analysis of a 3-deoxy-D-arabino-heptulosonate 7-phosphate synthase with an N-terminal chorismate mutase-like regulatory domain. Protein Sci. Publ. Protein Soc. 21, 887–895. https://doi.org/10.1002/pro.2075

Liu, K., Hu, H., Wang, W., Zhang, X., 2016. Genetic engineering of *Pseudomonas chlororaphis* GP72 for the enhanced production of 2-hydroxyphenazine. Microb. Cell Factories 15, 131. https://doi.org/10.1186/s12934-016-0529-0

Liu, K., Hu, X.-R., Zhao, L.-X., Wang, Y., Deng, Z., Tao, M., 2021. Enhancing ristomycin A production by overexpression of ParB-like StrR family regulators controlling the biosynthesis genes. Appl. Environ. Microbiol. 87, e01066-21. https://doi.org/10.1128/AEM.01066-21

Liu, Y.-J., Li, P.-P., Zhao, K.-X., Wang, B.-J., Jiang, C.-Y., Drake, H.L., Liu, S.-J., 2008. *Corynebacterium glutamicum* contains 3-deoxy-d-arabino-heptulosonate 7-phosphate synthases that display novel biochemical features. Appl. Environ. Microbiol. 74, 5497–5503. https://doi.org/10.1128/AEM.00262-08

Loll, P.J., Miller, R., Weeks, C.M., Axelsen, P.H., 1998. A ligand-mediated dimerization mode for vancomycin. Chem. Biol. 5, 293–298. https://doi.org/10.1016/s1074-5521(98)90622-6

Lütke-Eversloh, T., Stephanopoulos, G., 2007. L-tyrosine production by deregulated strains of *Escherichia coli*. Appl. Microbiol. Biotechnol. 75, 103–110. https://doi.org/10.1007/s00253-006-0792-9

Makitrynskyy, R., Ostash, B., Tsypik, O., Rebets, Y., Doud, E., Meredith, T., Luzhetskyy, A., Bechthold, A., Walker, S., Fedorenko, V., 2013. Pleiotropic regulatory genes *bldA*, *adpA* and *absB* are implicated in production of phosphoglycolipid antibiotic moenomycin. Open Biol. 3, 130121. https://doi.org/10.1098/rsob.130121

Menges, R., Muth, G., Wohlleben, W., Stegmann, E., 2007. The ABC transporter Tba of *Amycolatopsis balhimycina* is required for efficient export of the glycopeptide antibiotic balhimycin. Appl. Microbiol. Biotechnol. 77, 125–134. https://doi.org/10.1007/s00253-007-1139-x

Miller, B.R., Gulick, A.M., 2016. Structural biology of nonribosomal peptide synthetases, in: Evans, B.S. (Ed.), Nonribosomal Peptide and Polyketide Biosynthesis: Methods and Protocols. Springer New York, New York, NY, pp. 3–29. https://doi.org/10.1007/978-1-4939-3375-4_1

Mir, R., Jallu, S., Singh, T.P., 2015. The shikimate pathway: Review of amino acid sequence, function and three-dimensional structures of the enzymes. Crit. Rev. Microbiol. 41, 172–189. https://doi.org/10.3109/1040841X.2013.813901

Mulyani, S., Egel, E., Kittel, C., Turkanovic, S., Wohlleben, W., Süssmuth, R.D., van Pée, K.-H., 2010. The thioesterase Bhp is involved in the formation of β-hydroxytyrosine during balhimycin biosynthesis in *Amycolatopsis balhimycina*. ChemBioChem 11, 266–271. https://doi.org/10.1002/cbic.200900600

Narva, K.E., Feitelson, J.S., 1990. Nucleotide sequence and transcriptional analysis of the redD locus of *Streptomyces coelicolor* A3(2). J. Bacteriol. 172, 326–333. https://doi.org/10.1128/jb.172.1.326-333.1990

Nicolaou, K.C., Boddy, C.N., Bräse, S., Winssinger, N., 1999. Chemistry, biology, and medicine of the glycopeptide antibiotics. Angew. Chem. Int. Ed Engl. 38, 2096–2152. https://doi.org/10.1002/(sici)1521-3773(19990802)38:15%3C2096::aid-anie2096%3E3.0.co;2-f

O'Connor, S.E., 2015. Engineering of Secondary Metabolism. Annu. Rev. Genet. 49, 71–94. https://doi.org/10.1146/annurev-genet-120213-092053

Pelzer, S., Süssmuth, R., Heckmann, D., Recktenwald, J., Huber, P., Jung, G., Wohlleben, W., 1999. Identification and analysis of the balhimycin biosynthetic gene cluster and its use for manipulating glycopeptide biosynthesis in *Amycolatopsis mediterranei* DSM5908. Antimicrob. Agents Chemother. 43, 1565–1573. https://doi.org/10.1128/AAC.43.7.1565

Perkins, H.R., 1969. Specificity of combination between mucopeptide precursors and vancomycin or ristocetin. Biochem. J. 111, 195–205. https://doi.org/10.1042/bj1110195

Peschke, M., Brieke, C., Heimes, M., Cryle, M.J., 2018. The thioesterase domain in glycopeptide antibiotic biosynthesis is selective for cross-linked aglycones. ACS Chem. Biol. 13, 110–120. https://doi.org/10.1021/acschembio.7b00943

Pfeifer, V., Nicholson, G.J., Ries, J., Recktenwald, J., Schefer, A.B., Shawky, R.M., Schröder, J., Wohlleben, W., Pelzer, S., 2001. A polyketide synthase in glycopeptide biosynthesis: the biosynthesis of the non-proteinogenic amino acid (S)-3,5-dihydroxyphenylglycine. J. Biol. Chem. 276, 38370–38377. https://doi.org/10.1074/jbc.M106580200

Pickens, L.B., Tang, Y., Chooi, Y.-H., 2011. Metabolic engineering for the production of natural products. Annu. Rev. Chem. Biomol. Eng. 2, 211–236. https://doi.org/10.1146/annurev-chembioeng-061010-114209

Pootoolal, J., Thomas, M.G., Marshall, C.G., Neu, J.M., Hubbard, B.K., Walsh, C.T., Wright, G.D., 2002. Assembling the glycopeptide antibiotic scaffold: The biosynthesis of from *Streptomyces toyocaensis* NRRL15009. Proc. Natl. Acad. Sci. 99, 8962–8967. https://doi.org/10.1073/pnas.102285099

Puk, O., Bischoff, D., Kittel, C., Pelzer, S., Weist, S., Stegmann, E., Süssmuth, R.D., Wohlleben, W., 2004. Biosynthesis of chloro-β-hydroxytyrosine, a nonproteinogenic amino acid of the peptidic backbone of glycopeptide antibiotics. J. Bacteriol. 186, 6093–6100. https://doi.org/10.1128/jb.186.18.6093-6100.2004

Recktenwald, J., Shawky, R., Puk, O., Pfennig, F., Keller, U., Wohlleben, W., Pelzer, S., 2002. Nonribosomal biosynthesis of vancomycin-type antibiotics: a heptapeptide backbone and eight peptide synthetase modules. Microbiology 148, 1105–1118. https://doi.org/10.1099/00221287-148-4-1105

Ren, J., Cui, Y., Zhang, F., Cui, H., Ni, X., Chen, F., Li, L., Xia, H., 2014. Enhancement of nystatin production by redirecting precursor fluxes after disruption of the tetramycin gene from *Streptomyces ahygroscopicus*. Microbiol. Res. 169, 602–608. https://doi.org/10.1016/j.micres.2013.09.017

Reynolds, P.E., 1989. Structure, biochemistry and mechanism of action of glycopeptide antibiotics. Eur. J. Clin. Microbiol. Infect. Dis. Off. Publ. Eur. Soc. Clin. Microbiol. 8, 943–950. https://doi.org/10.1007/BF01967563

Rodriguez, A., Martnez, J.A., Flores, N., Escalante, A., Gosset, G., Bolivar, F., 2014. Engineering *Escherichia coli* to overproduce aromatic amino acids and derived compounds. Microb. Cell Factories 13, 126. https://doi.org/10.1186/s12934-014-0126-z

Ryu, Y.-G., Butler, M.J., Chater, K.F., Lee, K.J., 2006. Engineering of primary carbohydrate metabolism for increased production of actinorhodin in *Streptomyces coelicolor*. Appl. Environ. Microbiol. 72, 7132–7139. https://doi.org/10.1128/AEM.01308-06

Seong Choi, Y., W. Johannes, T., Simurdiak, M., Shao, Z., Lu, H., Zhao, H., 2010. Cloning and heterologous expression of the spectinabilin biosynthetic gene cluster from *Streptomyces spectabilis*. Mol. Biosyst. 6, 336–338. https://doi.org/10.1039/B923177C

Shabalin, I.G., Gritsunov, A., Hou, J., Sławek, J., Miks, C.D., Cooper, D.R., Minor, W., Christendat, D., 2020. Structural and biochemical analysis of *Bacillus anthracis* prephenate dehydrogenase reveals an unusual mode of inhibition by tyrosine via the ACT domain. FEBS J. 287, 2235–2255. https://doi.org/10.1111/febs.15150

Shawky, R.M., Puk, O., Wietzorrek, A., Pelzer, S., Takano, E., Wohlleben, W., Stegmann, E., 2007. The border sequence of the balhimycin biosynthesis gene cluster from Amycolatopsis balhimycina contains *bbr*, encoding a StrR-like pathway-specific regulator. J. Mol. Microbiol. Biotechnol. 13, 76–88. https://doi.org/10.1159/000103599

Shiio, I., Sugimoto, S., Miyajima, R., 1974. Regulation of 3-Deoxy-D-arabino-heptulosonate-7-phosphate Synthetase in *Brevibacterium flavum*. J. Biochem. (Tokyo) 75, 987–997. https://doi.org/10.1093/oxfordjournals.jbchem.a130501

Silakowski, B., Kunze, B., Müller, R., 2000. *Stigmatella aurantiaca Sg a15* carries genes encoding type I and type II 3-deoxy-d-arabino-heptulosonate-7-phosphate synthases: involvement of a type II synthase in aurachin biosynthesis. Arch. Microbiol. 173, 403–411. https://doi.org/10.1007/s002030000162

Song, J., Bonner, C.A., Wolinsky, M., Jensen, R.A., 2005. The TyrA family of aromatic-pathway dehydrogenases in phylogenetic context. BMC Biol. 3, 13. https://doi.org/10.1186/1741-7007-3-13

Sosio, M., Kloosterman, H., Bianchi, A., de Vreugd, P., Dijkhuizen, L., Donadio, S., 2004. Organization of the teicoplanin gene cluster in *Actinoplanes teichomyceticus*. Microbiology 150, 95–102. https://doi.org/10.1099/mic.0.26507-0

Speedie, M.K., Park, M.O., 1980. Regulation of tyrosine biosynthesis by phenylalanine in anthramycin-producing *Streptomyces refuineus*. J. Antibiot. (Tokyo) 33, 579–584. https://doi.org/10.7164/antibiotics.33.579

Spohn, M., Kirchner, N., Kulik, A., Jochim, A., Wolf, F., Muenzer, P., Borst, O., Gross, H., Wohlleben, W., Stegmann, E., 2014. Overproduction of ristomycin a by activation of a silent gene cluster in *Amycolatopsis japonicum* MG417-CF17. Antimicrob. Agents Chemother. 58, 6185–6196. https://doi.org/10.1128/aac.03512-14

Stegmann, E., Frasch, H.-J., Wohlleben, W., 2010. Glycopeptide biosynthesis in the context of basic cellular functions. Curr. Opin. Microbiol. 13, 595–602. https://doi.org/10.1016/j.mib.2010.08.011

Stegmann, E., Pelzer, S., Bischoff, D., Puk, O., Stockert, S., Butz, D., Zerbe, K., Robinson, J., Süssmuth, R.D., Wohlleben, W., 2006a. Genetic analysis of the balhimycin (vancomycin-type) oxygenase genes. J. Biotechnol. 124, 640–653. https://doi.org/10.1016/j.jbiotec.2006.04.009

Stegmann, E., Pelzer, S., Bischoff, D., Puk, O., Stockert, S., Butz, D., Zerbe, K., Robinson, J., Süssmuth, R.D., Wohlleben, W., 2006b. Genetic analysis of the balhimycin (vancomycin-type) oxygenase genes. J. Biotechnol., Highlights from ECB12 124, 640–653. https://doi.org/10.1016/j.jbiotec.2006.04.009

Sterritt, O.W., Lang, E.J.M., Kessans, S.A., Ryan, T.M., Demeler, B., Jameson, G.B., Parker, E.J., 2018. Structural and functional characterisation of the entry point to pyocyanin biosynthesis in *Pseudomonas aeruginosa* defines a new 3-deoxy-d-arabino-heptulosonate 7-phosphate synthase subclass. Biosci. Rep. 38, BSR20181605. https://doi.org/10.1042/BSR20181605

Stinchi, S., Carrano, L., Lazzarini, A., Feroggio, M., Grigoletto, A., Sosio, M., Donadio, S., 2006. A derivative of the glycopeptide A40926 produced by inactivation of the beta-hydroxylase gene in *Nonomuraea sp.* ATCC39727. FEMS Microbiol. Lett. 256, 229–235. https://doi.org/10.1111/j.1574-6968.2006.00120.x

Thykaer, J., Nielsen, J., Wohlleben, W., Weber, T., Gutknecht, M., Lantz, A.E., Stegmann, E., 2010. Increased glycopeptide production after overexpression of shikimate pathway genes being part of the balhimycin biosynthetic gene cluster. Metab. Eng. 12, 455–461. https://doi.org/10.1016/j.ymben.2010.05.001

Tianhui, X., Chiao, J.S., 1989. Regulation of the biosynthetic pathway of aromatic amino acids in *Nocardia mediterranei*. Biochim. Biophys. Acta BBA - Gen. Subj. 991, 6–11. https://doi.org/10.1016/0304-4165(89)90020-2

Toma, R.S.A., Brieke, C., J. Cryle, M., D. Süssmuth, R., 2015. Structural aspects of phenylglycines, their biosynthesis and occurrence in peptide natural products. Nat. Prod. Rep. 32, 1207–1235. https://doi.org/10.1039/C5NP00025D

Waglechner, N., McArthur, A.G., Wright, G.D., 2019. Phylogenetic reconciliation reveals the natural history of glycopeptide antibiotic biosynthesis and resistance. Nat. Microbiol. 4, 1862–1871. https://doi.org/10.1038/s41564-019-0531-5

Wang, S., Liu, D., Bilal, M., Wang, W., Zhang, X., 2022. Uncovering the role of PhzC as DAHP Synthase in shikimate pathway of *Pseudomonas chlororaphis HT66*. Biology 11, 86. https://doi.org/10.3390/biology11010086

Wohlleben, W., Mast, Y., Muth, G., Röttgen, M., Stegmann, E., Weber, T., 2012. Synthetic biology of secondary metabolite biosynthesis in actinomycetes: Engineering precursor supply as a way to optimize antibiotic production. FEBS Lett. 586, 2171–2176. https://doi.org/10.1016/j.febslet.2012.04.025

Xu, M., Wang, W., Waglechner, N., Culp, E.J., Guitor, A.K., Wright, G.D., 2022. Phylogeny-informed synthetic biology reveals unprecedented structural novelty in type V glycopeptide antibiotics. ACS Cent. Sci. 8, 615–626. https://doi.org/10.1021/acscentsci.1c01389

Xu, M., Wang, W., Waglechner, N., Culp, E.J., Guitor, A.K., Wright, G.D., 2020. GPAHex-A synthetic biology platform for Type IV–V glycopeptide antibiotic production and discovery. Nat. Commun. 11, 5232. https://doi.org/10.1038/s41467-020-19138-5

Xu, Y., Li, Y., Wu, Z., Lu, Y., Tao, G., Zhang, L., Ding, Z., Shi, G., 2022. Combining precursor-directed engineering with modular designing: an effective strategy for de novo biosynthesis of l-DOPA in *Bacillus licheniformis*. ACS Synth. Biol. 11, 700–712. https://doi.org/10.1021/acssynbio.1c00411

Yim, G., Thaker, M.N., Koteva, K., Wright, G., 2014. Glycopeptide antibiotic biosynthesis. J. Antibiot. (Tokyo) 67, 31–41. https://doi.org/10.1038/ja.2013.117

Yushchuk, O., Horbal, L., Ostash, B., Marinelli, F., Wohlleben, W., Stegmann, E., Fedorenko, V., 2019. Regulation of teicoplanin biosynthesis: refining the roles of *tei* cluster-situated regulatory genes. Appl. Microbiol. Biotechnol. 103, 4089–4102. https://doi.org/10.1007/s00253-019-09789-w

Zabala, D., Braña, A.F., Flórez, A.B., Salas, J.A., Méndez, C., 2013. Engineering precursor metabolite pools for increasing production of antitumor mithramycins in *Streptomyces argillaceus*. Metab. Eng. 20, 187–197. https://doi.org/10.1016/j.ymben.2013.10.002

Ziemert, N., Alanjary, M., Weber, T., 2016. The evolution of genome mining in microbes - a review. Nat. Prod. Rep. 33, 988–1005. https://doi.org/10.1039/c6np00025h

7. Appendix

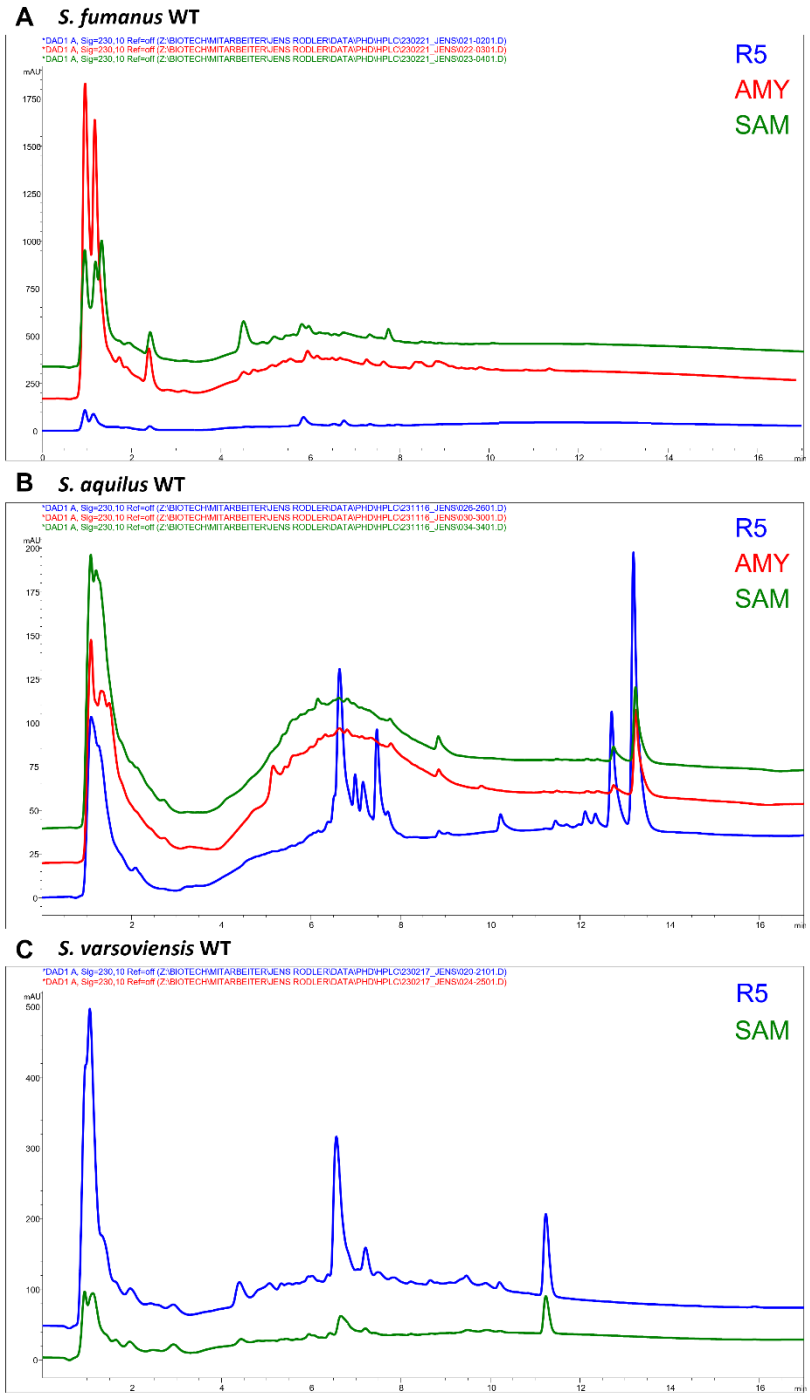

Figure A1: HPLC-UV/DAD chromatogram of *S. fumanus*, *S. aquilus* and *S. varsoviensis*. The chromatogram shows the UV signal at 230 nm. [A] *S. fumanus* and [B] *S. aquilus* were cultivated in R5, SAM and AMY medium. [C] *S. varsoviensis* DSM 40677 was cultivated in R5 and SAM medium.

A ***S. fumanus*** **cultivated in R5 medium**

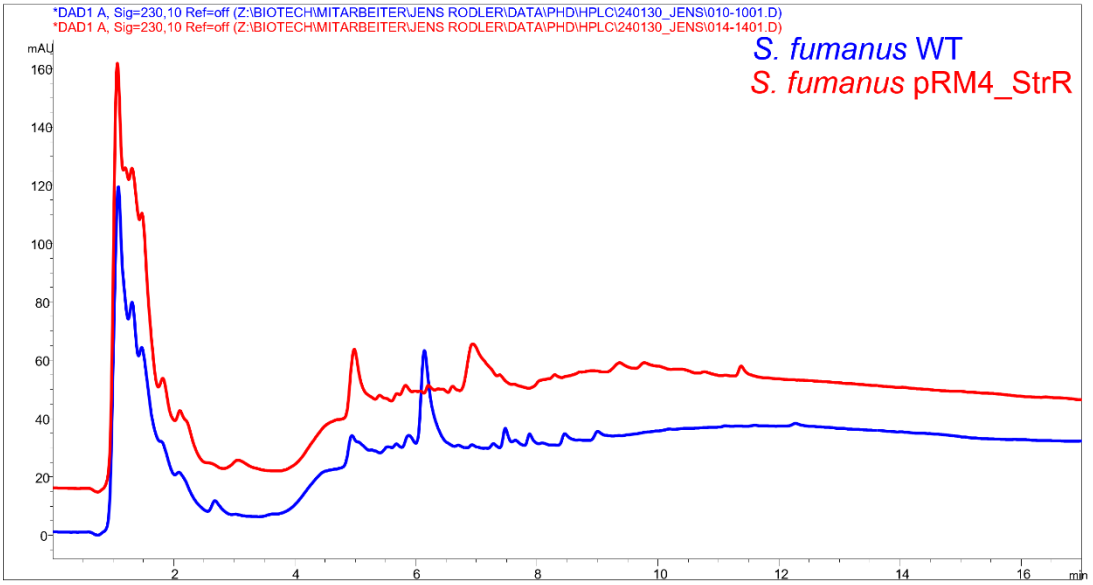

B ***S. aquilus*** **cultivated in R5 medium**

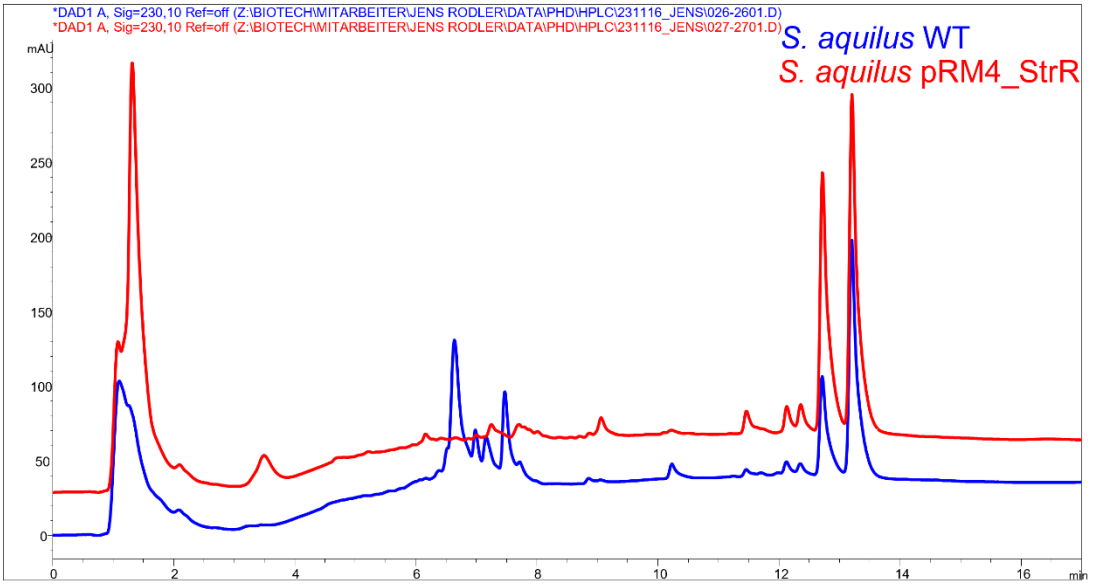

Figure A2: HPLC-UV/DAD chromatogram of *S. fumanus* and *S. aquilus* recombinant stains.. The chromatogram shows the UV signal at 230 nm. [A] *S. fumanus* WT, *S. fumanus* pRM4_StrR and [B] *S. aquilus* and *S. aquilus* pRM4_StrR were cultivated in R5 medium.

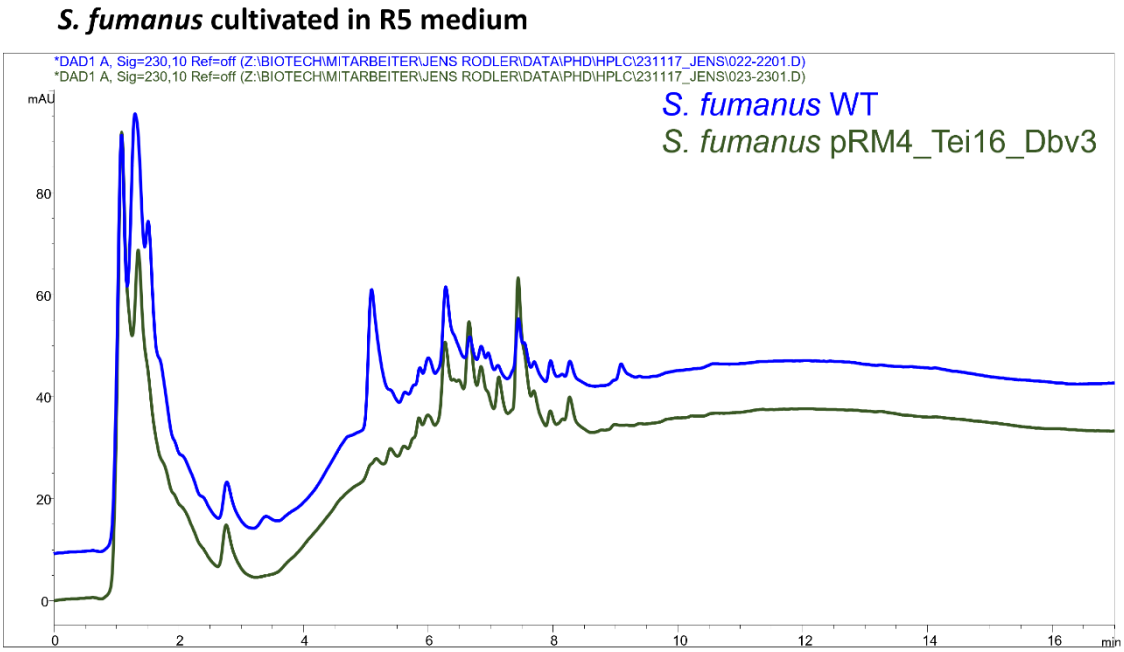

Figure A3: HPLC-UV/DAD chromatogram of *S. fumanus* WT and *S. fumanus* pRM4_Tei16_Dbv3. The chromatogram shows the UV signal at 230 nm. *S. fumanus* WT and *S. fumanus* pRM4_Tei16_Dbv3 were cultivated in R5 medium.

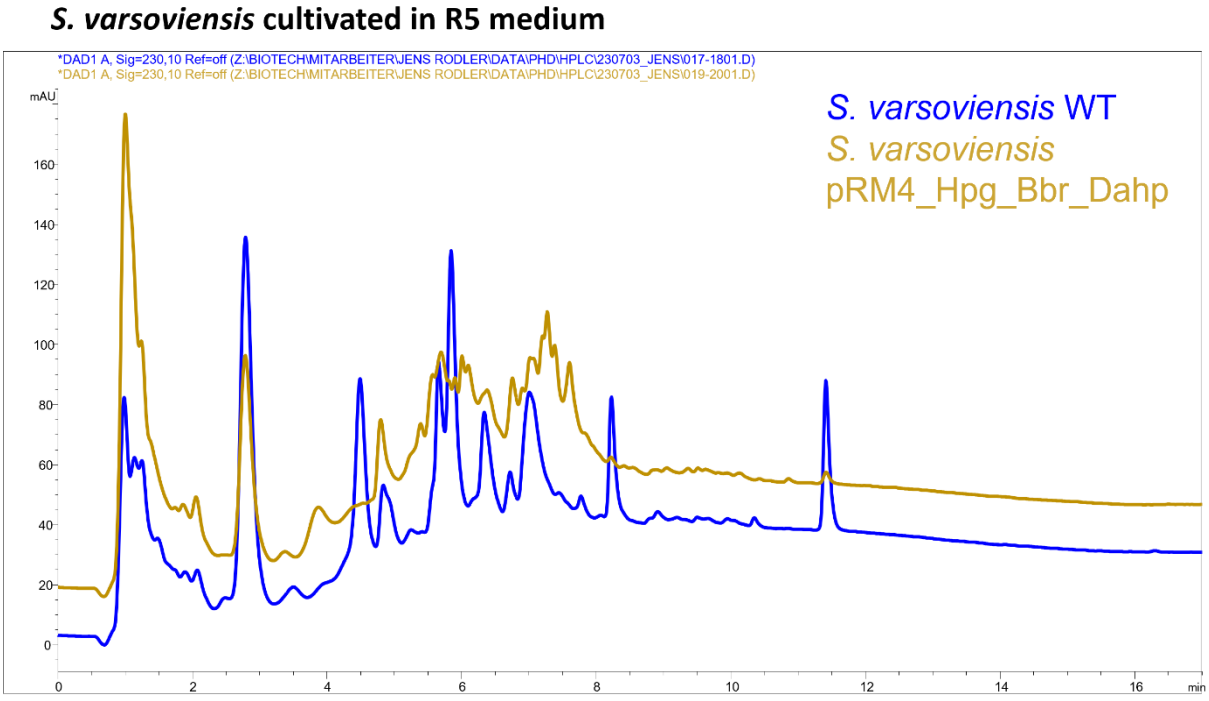

Figure A4: HPLC-UV/DAD chromatogram of *S. varsoviensis* WT and *S. varsoviensis* pRM4_Hpg_Bbr_Dahp. The chromatogram shows the UV signal at 230 nm. *S. varsoviensis* WT and *S. varsoviensis* pRM4_Hpg_Bbr_Dahp were cultivated in R5 medium.

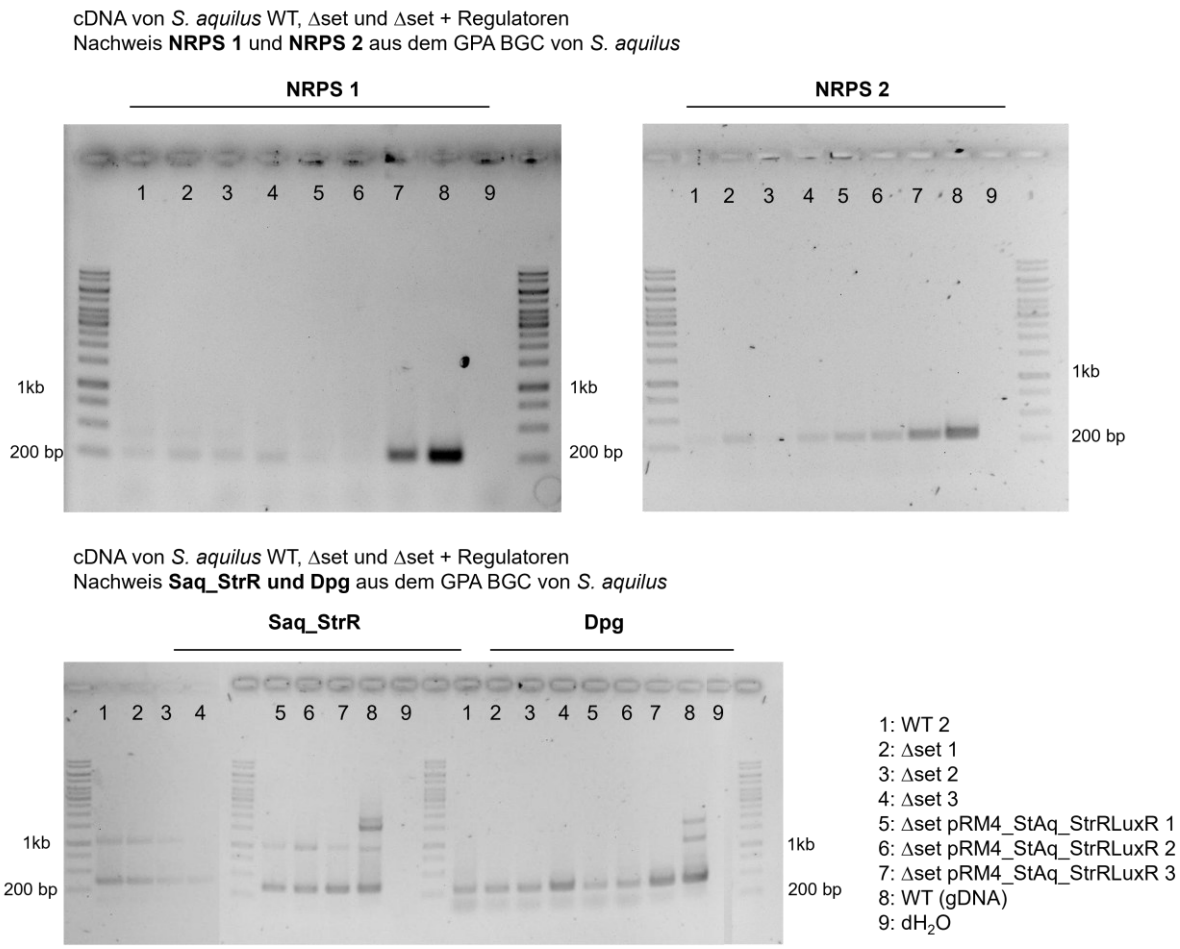

Figure A5: Detection of specific genes from the GPA BGC of *S. aquilus* using cDNA. cDNA from *S. aquilus* WT, *S. aquilus* ∆*set* pRM4_StAq_strRluxR (clones 1-3) was used to examine expression of the genes *nrps1*, *nrps2*, *saq_strR*, and *dpg*. Genomic DNA (gDNA) from the WT strain and dH_2O were included as controls. The expected bands of 271 bp for *nrps1*, 310 bp for *nrps2*, 351 bp for *saq_strR*, and 301 bp for *dpg* were detected in all samples tested. Figure adapted from Anna-Katharina Siegert (Master thesis, 2025).

7.1 Publication 3: Animating insights into the biosynthesis of glycopeptide antibiotics

Athina Gavriilidou, Martina Adamek, **Jens-Peter Rodler**, Noel Kubach, Anna Voigtländer, Leon Kokkoliadis, Chambers C Hughes, Max J. Cryle, Evi Stegmann, Nadine Ziemert

Current Opinion in Microbiology, 2024
https://doi.org/10.1016/j.mib.2024.102561

7.1.1 Publication 3

Animating insights into the biosynthesis of glycopeptide antibiotics

Author list:
*Athina Gavriilidou[1], Martina Adamek[1,2,3], **Jens-Peter Rodler**[2,4], Noel Kubach[1,2], Anna Voigtländer[5], Leon Kokkoliadis[2], Chambers C Hughes[2,3,4], Max J. Cryle[6,7,8], Evi Stegmann[2,3,4], Nadine Ziemert[1,2,3]*

Author affiliation and footnotes:
[1]Translational Genome Mining for Natural Products, Interfaculty Institute of Microbiology and Infection Medicine Tübingen (IMIT), Interfaculty Institute for Biomedical Informatics (IBMI), University of Tübingen, Tübingen, Germany
[2]Cluster of Excellence EXC 2124: Controlling Microbes to Fight Infections (CMFI), University of Tübingen, Tübingen, Germany
[3]German Centre for Infection Research (DZIF), Partner Site Tübingen, Tübingen, Germany
[4]Microbial Bioactive Compounds, Interfaculty Institute of Microbiology and Infection Medicine Tübingen, University of Tübingen, Auf der Morgenstelle 28, 72076 Tübingen, Germany
[5]Center for Media Competence (ZFM), University of Tübingen, Tübingen, Germany
[6]Department of Biochemistry and Molecular Biology, The Monash Biomedicine Discovery Institute, Monash University, Clayton, Victoria 3800, Australia
[7]EMBL Australia, Monash University, Clayton, Victoria 3800, Australia
[8]ARC Centre of Excellence for Innovations in Peptide and Protein Science, Clayton, Victoria 3800, Australia
Corresponding authors:

Abstract

The realm of natural product (NP) research is constantly expanding, with diverse applications in both medicine and industry. In this interdisciplinary field, scientists collaborate to investigate various aspects of NPs, including understanding the mode of action of these compounds, unraveling their biosynthetic pathways, studying evolutionary aspects, and biochemically characterizing the enzymes involved. However, this collaboration can be challenging as all parties involved come from very different backgrounds (such as microbiology, synthetic chemistry, biochemistry, or bioinformatics) and may not use the same terminology. Fortunately, contemporary technologies, such as videos, provide novel avenues for effective engagement. Recognizing the potency of visual stimuli in explaining complex processes, we envision a future where animations become more and more common in interdisciplinary communication, accompanying perspectives, and reviews. To demonstrate how such approaches can enhance the understanding of complex processes, we have animated the biosynthesis of the glycopeptide antibiotic vancomycin (https://youtu.be/TGAgC4c8hvo).

Introduction

Recent advances in microbiological research have shed light on the multifaceted role of natural products (NPs) derived from diverse organisms, including bacteria, fungi, and plants. They have many applications, such as in medicine and in industry, and therefore are the object of multiple scientific investigations. More specifically, researchers from different fields (e.g. microbiology, chemistry, bioengineering, and bioinformatics) attempt to elucidate different points related to NPs, be it their ecological role in their environment, their biosynthetic pathways, or their evolution, to name a few. Each of these subjects is usually covered by independent research groups, resulting in the field naturally becoming interdisciplinary. However, as our understanding of NPs deepens and becomes more intricate, effectively conveying this knowledge among scientists from various backgrounds, who may use different terminology, presents a challenge. One illustrative example is the study of glycopeptide antibiotic (GPA) biosynthesis.

GPAs are an important group of antibiotics, the first member of which - vancomycin - was discovered in 1953. Since then, 27 natural GPAs have been identified, complemented by the synthesis of numerous semisynthetic derivatives, some of which are currently used in the clinic for the treatment of infections caused by multiresistant Gram-positive bacterial pathogens [1–3]. Over the years, extensive studies (*in vivo* and *in vitro*) have been carried out to determine the biosynthesis and mechanism of action of GPAs [1,4–11]. The nomenclature ‘glycopeptide antibiotic’ succinctly summarizes their structural characteristics, which comprise a peptide backbone, typically consisting of seven amino acids and decorated with one or more sugar moieties. In addition, GPAs are crosslinked through the side chains of their aromatic amino acid residues, a feature that confers rigidity to the core structure, is essential for bioactivity, and represents a distinctive hallmark of this class of NPs. The peptide backbone is further modified by the addition of halogen atoms, sulfate moieties, sugar residues, and methyl groups during biosynthesis [1,12,13].

The biosynthesis of GPAs has been extensively studied due to their clinical importance [1,4–11] and the need to produce these complex molecules by fermentation of the producer strains, given the limitations of current chemical syntheses [11,14,15]. To provide an overview of the complex biosynthesis of GPAs and ameliorate the communication between scientists of different backgrounds with an interest in GPAs, the authors have produced a video explaining each step in the biosynthesis of the well-known GPA vancomycin (Supplementary Data 1).

Glycopeptide antibiotic classification

To date, the known GPA structures have been classified into five types (I–V) that are primarily distinguished by their exact structural compositions (Figure 1). Type I GPAs are characterized by a backbone comprising two aliphatic amino acids at positions 1 and 3 of the peptide and five aromatic amino acids, including the highly unusual nonproteinogenic amino acids β-hydroxytyrosine (Bht), 4-hydroxyphenylglycine (Hpg), and 3,5-dihydroxyphenylglycine (Dpg). The aromatic amino acids are crosslinked through three phenolic/biaryl (Figure 1) crosslinks [12]. Type II GPAs are similar to type I GPAs but differ by the substitution of the aliphatic residues at positions 1 and 3 with the aromatic amino acids Hpg and phenylalanine (Phe). However, these aromatic amino acids are not crosslinked [12]. In contrast to type II GPAs, the aromatic amino acids of type III GPAs are all crosslinked, and, consequently, type III GPAs possess an additional crosslink compared to type I/II GPAs [12]. Type IV GPAs maintain an identical core peptide sequence to type III GPAs but feature an acyl group attached to one of the pendant sugar residues. Notwithstanding these structural disparities, type I-IV GPAs share a common mechanism of antibiotic action involving the sequestration of the bacterial peptidoglycan precursor lipid II, thereby impeding the correct formation of the peptidoglycan. In contrast, type V GPAs constitute an outlier class concerning both structure and mode of action [13]. Structurally, they exhibit substantial variations, particularly the absence of glycosylation [13], and far more diverse peptide sequences. Importantly, type V GPAs have a unique mode of action, which has been shown to involve binding to autolysin molecules and inhibition of their hydrolytic activity on peptidoglycan during cell division [13].

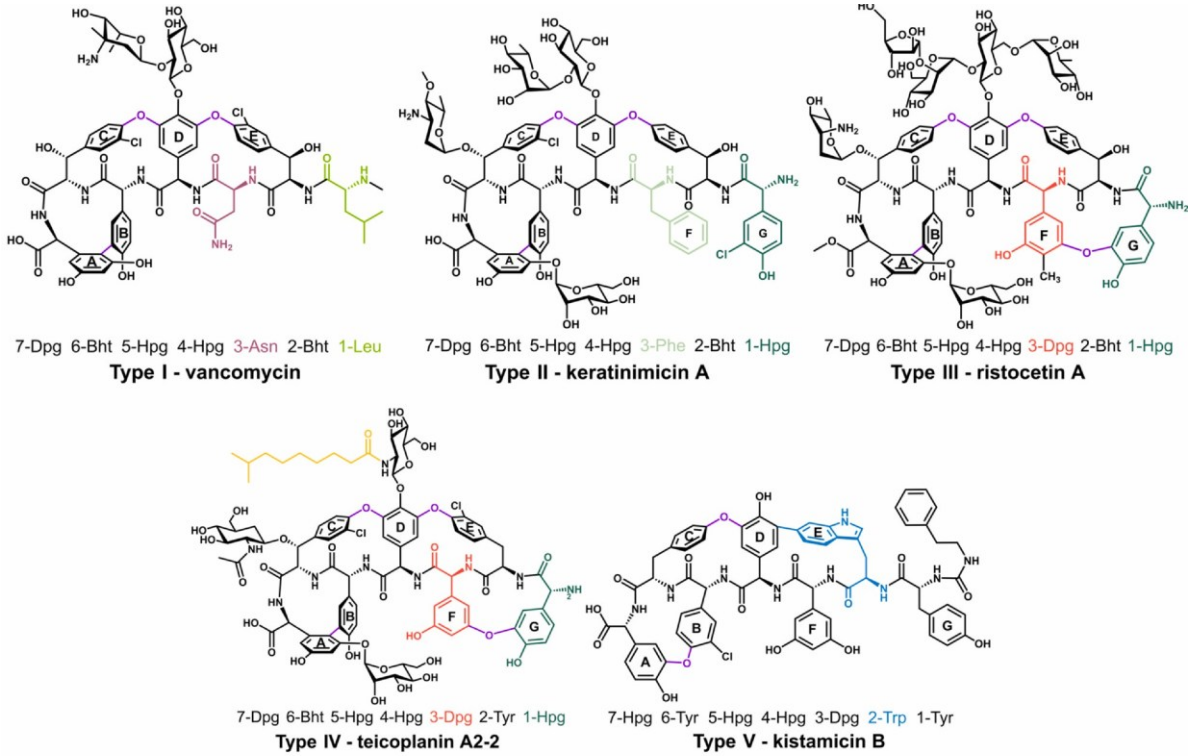

Type	Side chains of AAs in position 1 and 3 of the backbone	Number of crosslinks	Crosslinks	Additional unique characteristics
I	aliphatic (Leu/Ala & Asn/Glu)	3	A-B, C-O-D, D-O-E	-
II	aromatic (Hpg & Phe/Hpg)	3	A-B, C-O-D, D-O-E	-
III	aromatic (Hpg & Dpg)	4	A-B, C-O-D, D-O-E, F-O-G	-
IV	aromatic (Hpg & Dpg)	4	A-B, C-O-D, D-O-E, F-O-G	Acylated sugar moiety
V	variable	variable	variable	Trp in the backbone

Figure 1: Structural characteristics of the GPA types. The most important features for the classification of GPAs are listed and accompanied by examples of structures. The most significant characteristics for each type are color-coded. The aromatic rings of the amino acids (AAs) are sequentially labeled from A to G based on prior nomenclature [16]. Abbreviations: Tyr, tyrosine; Leu, leucine; Asn, asparagine; Bht, β-hydroxytyrosine; Hpg, 4- hydroxyphenylglycine; Dpg, 3,5-dihydroxyphenylglycine; Phe, phenylalanine, Trp, tryptophane. The SMILES of the structures can be found in Supplementary Table 1.

Glycopeptide antibiotic biosynthesis

The main processes shown in the animation are also described in the following sections.

Most of the biosynthetic genes required for the production of each GPA are localized in the bacterial genome within a so-called biosynthetic gene cluster (BGC), which can also include genes for export, regulation, and self-resistance. In principle, the biosynthesis of GPAs can be divided into three main steps: the first is the synthesis of nonproteinogenic amino acids. The next step is the formation of the peptide backbone

by the action of non-ribosomal peptide synthetases (NRPSs), which are large multimodular enzymes that assemble peptides, without the involvement of the ribosome, by the stepwise incorporation of individual amino acids. The final step is the modification of the peptide backbone.

Biosynthesis of nonproteinogenic amino acids

All established examples of type I-IV GPAs contain the nonproteinogenic amino acids Bht, Hpg, and Dpg [16] (Figure 2), which are not normally found within the cell. These amino acids are primarily generated by dedicated biosynthetic pathways that are typically encoded as subclusters within the GPA BGC. The precursors essential for the synthesis of Bht and Hpg biosynthesis, notably tyrosine (Tyr) and hydroxyphenylpyruvate (4- HPP), are derived from the shikimate pathway. In addition to Tyr as the amine donor, the synthesis of Dpg requires malonyl CoA as a precursor. Given the tightly regulated nature of the shikimate metabolism, bacteria have evolved mechanisms to circumvent this regulatory control and ensure the supply of precursors for secondary metabolite production. The producers of GPAs, for example, have acquired a second copy of the key enzymes of the shikimate pathway, which are also located within each GPA BGC [14,15].

The synthesis of Bht follows two different mechanisms depending on the type of GPA. In the first mechanism, Tyr gets incorporated into the peptide backbone during assembly and is then hydroxylated by a specific enzyme, a nonheme iron oxygenase [17,18]. Conversely, the second mechanism entails the biosynthesis of Bht before its incorporation by the main assembly line [19,20]. In the latter scenario, which occurs in the vancomycin biosynthetic pathway (Figure 2), a minimal NRPS activates Tyr [21], which is then hydroxylated by a cytochrome P450 monooxygenase [22]. Bht is cleaved from the minimal NRPS module by a specific thioesterase [23], resulting in free Bht for direct incorporation into the main assembly line.

Hpg is synthesized from 4-HPP by the action of two major enzymes encoded in the BGC (Figure 2), a 4- hydroxymandelate oxidase and a 4-hydroxymandelate synthase. Additionally, the amino group necessary for Hpg is derived from tyrosine in a reaction that is facilitated by the same aminotransferase also involved in Dpg biosynthesis (HptT/Pgat) [17,19].

Dpg is synthesized through a multistep biosynthetic process from malonyl-CoA. This pathway involves the orchestrated activities of four enzymes, DpgA-D (Figure 2), representing a type III polyketide synthase and modifying enzymes that iteratively condense the malonyl-CoA into 3,5-dihydroxyphenylglyoxylate. The final reaction involves a transamination, again using Tyr as substrate, which is catalyzed by HptT/Pgat [17,20–22].

The formation of the peptide backbone The synthesis of the peptide backbone of GPAs is catalyzed by an NRPS [22,24] (Figure 3), which is a large multimodular enzyme that assembles peptides without the involvement of the ribosome by the stepwise incorporation of individual amino acids. Each NRPS module contains distinct catalytic domains that perform specific functions. The adenylation (A) domains recognize and activate specific amino acids priming them for subsequent incorporation into the growing peptide chain [22,24]. Upon activation, the amino acid is covalently its D form [26]. In this way, the peptide chain is progressively extended until the finale module.

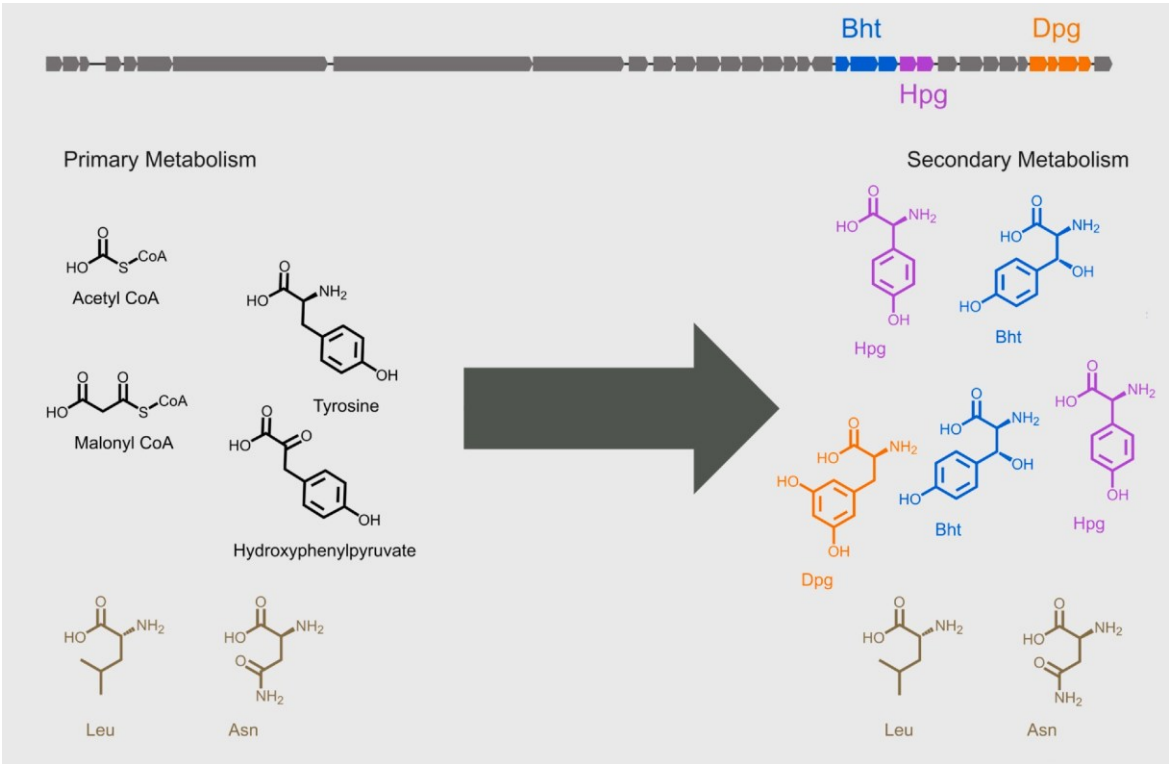

Figure 2: Precursor supply of nonproteinogenic amino acids. On the left are molecules involved in primary metabolism. Leucine (Leu) and asparagine (Asn) (in brown) are incorporated unmodified into the vancomycin backbone. The molecules in black (hydroxyphenylpyruvate, tyrosine, and malonyl CoA) are needed for the synthesis (symbolized by the big arrow) of the nonproteinogenic amino acids hydroxyphenylglycine (Hpg), β-hydroxytyrosine (Bht), and dihydroxyphenylglycine (Dpg) components of the vancomycin backbone. At the top, the BGC encoding the biosynthesis of vancomycin is shown, with the genes involved in the synthesis of each nonproteinogenic amino acid colored and labeled accordingly. This figure has been adapted from the animation (Supplementary Data 1).

In the case of type I-IV GPAs, there are typically three or four large genes encoding NRPSs, which include seven modules in total, one for each amino acid incorporated in the peptide backbone [24] (Figure 1). Each module includes an A-domain and a PCP-domain, while all but the first include a C-domain. In vancomycin biosynthesis, there are three NRPS enzymes, which include seven modules in linked as a thioester to the thiol group of a phosphopantetheine arm within an adjacent peptidyl carrier protein (PCP) domain. This enables *trans-acting* enzymes (not encoded within the NRPS genes but act on substrates while these remain bound to a PCP domain during NRPS-mediated peptide synthesis) to further modify the PCP-bound amino acid, for example, by halogenation [9] and hydroxylation [18]. The PCP domain then facilitates the translocation of the amino acid to the acceptor pocket of the condensation © domain [25]. C-domains, usually located at the N-terminus of a module, catalyze the formation of amide bonds between two PCP-bound substrates [25] by merging the amine group of the downstream acceptor amino acid onto the thioester linkage of the upstream donor substrate [22,24]. In addition, certain modules contain an epimerization domain (E domain), which converts the L- configured amino acid at the C-terminus of the peptide into a 3-3-1 pattern (Figure 3). Furthermore, modules 2, 4, and 5 include an E-domain, converting L-Bht, L-Hpg, and L-Hpg to their D configuration, respectively. After the completion of the peptide backbone assembly, the linear heptapeptide is bound to the PCP domain of the seventh and final module, which, in GPA biosynthesis, includes additional domains.

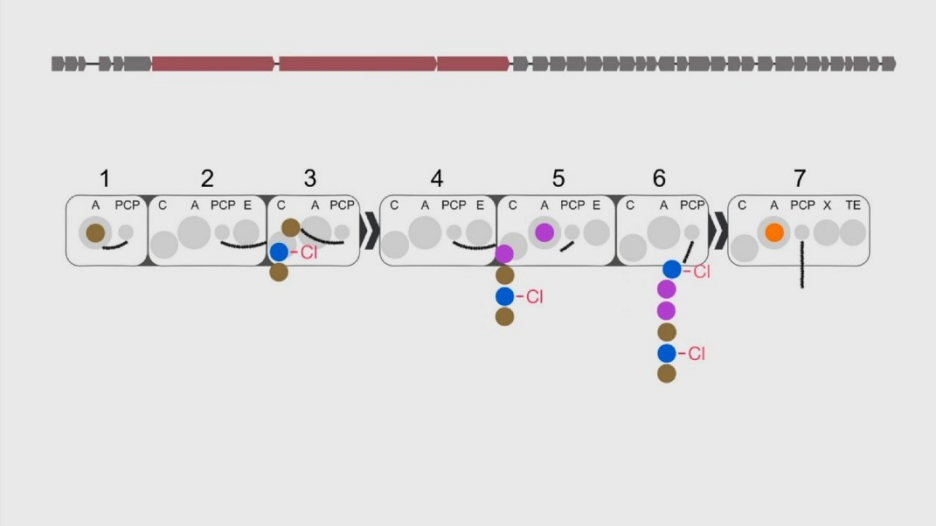

Figure 3: Backbone assembly of vancomycin via an NRPS. The BGC of vancomycin is shown at the top, with the genes encoding the NRPS enzymes colored in red. Below this is a schematic representation of the three NRPS proteins connected by their docking domains (black arrows). Each module is framed and numbered, and each functional domain is labeled accordingly. The colored circles each represent an amino acid (Figure 2) either waiting to be incorporated or already part of the growing peptide. The structure of the heptapeptide as it is released from the final module is shown below, with the amino acids colored the same as in Figure 2.
This figure was adapted from the animation (Supplementary Data 1).

Oxidative crosslinks and aglycone release

A key step in the assembly of GPAs by NRPSs is the recruitment of crosslinking enzymes to the last NRPS module (Figure 4). These enzymes, known as Oxy enzymes, belong to the cytochrome P450 superfamily [27] and are responsible for the crosslinking of the aromatic side chains within the peptide structure. The recruitment of the Oxy enzymes to the peptide is facilitated by a domain that is unique to GPA biosynthesis, known as the X-domain [23,28–31]. Structurally similar to C-domains, this domain uses a conserved interface to sequentially recruit P450 enzymes to the NRPS-bound peptide via a shuffling mechanism [32].
After crosslinking is completed, the terminal thioesterase domain catalyzes the release of the fully cyclized peptide product from the enzyme complex [33].

Modification of the peptide backbone

In addition to the crosslinked peptide backbone, type I- IV GPAs are characterized by the incorporation of sugar moieties (Figure 5). The synthesis of these sugar components requires various enzymes, such as epimerases, transaminases, dehydratases, and methyltransferases [34]. Once synthesized, the sugar moieties are linked to the cyclic peptide (aglycone) by specific glycosyltransferases, which are also typically encoded in the GPA BGC [24]. The abundance and diversity of these sugar moieties significantly contribute to the structural heterogeneity found in GPAs [32].
Moreover, many GPAs exhibit additional modifications, including methylation [24,35] — as in the case of vancomycin (Figure 5) — sulfation of amino acid side chains [24,36], and the acylation of sugar moieties [24].

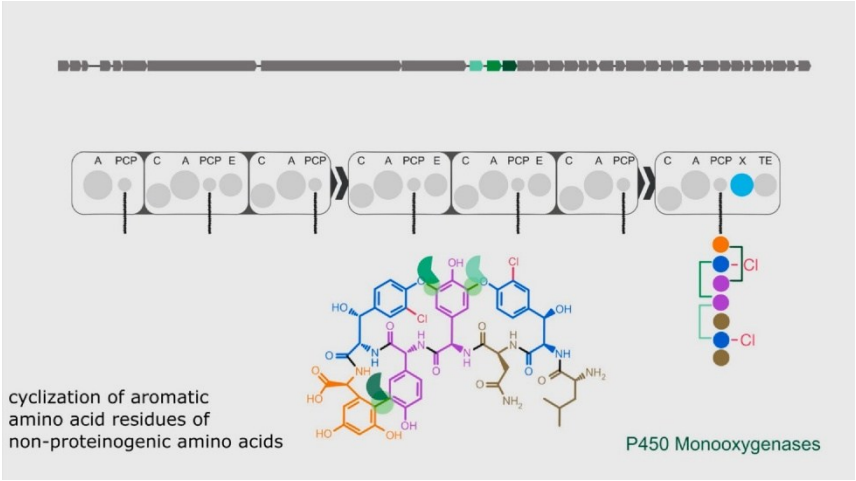

Figure 4: Cyclization reactions during vancomycin biosynthesis. The BGC of vancomycin is shown at the top, with the genes encoding the P450 monooxygenase enzymes colored in green. Below this is a schematic representation of the three NRPSs connected by their docking domains (black arrows). Each module is framed and each functional domain within is labeled accordingly. In the final module, the X-domain colored in blue recruits the cytochrome P450 monooxygenases, catalyzing the crosslinks at the PCP-bound heptapeptide. The crosslinked amino acids are connected by brackets. The structure of the heptapeptide as it is released from the final module is shown below, with the amino acids colored the same as their representative circles and the crosslinks highlighted in green. The green shapes represent the P450 enzymes. This figure has been adapted from the animation (Supplementary Data 1)

Export and mode of action

After GPA biosynthesis of vancomycin is complete (Figure 6a), the active compound is exported from the intracellular environment by a specific ATP-binding cassette (ABC) transporter [37]. Type I-IV GPAs inhibit the growth of Gram-positive bacteria by selectively binding to the D-alanyl-D-alanine (D-Ala-D-Ala) terminus of the cell wall precursor lipid II [38]. Upon binding to lipid II, vancomycin blocks essential enzymatic reactions involved in cell wall biosynthesis (Figure 6b), leading to bacterial cell death.

Future directions

GPAs are the products of a complex biosynthetic process involving multiple steps within a biochemical assembly line. The non-ribosomal peptide synthesis, numerous enzymes, and simultaneous chemical reactions involved make the explanation of NP biosynthetic pathways challenging. In this review, we offer an unconventional format for effective communication of such complex processes: the use of an animated video depicting the biosynthesis of vancomycin (Supplementary Data 1) (https://youtu.be/TGAgC4c8hvo). The effectiveness of educational cartoon movies as a means of transferring scientific knowledge, in general, has been established [39]. We believe that our example will inspire the use of animations and improved visualizations in microbiology, fostering interdisciplinary links with fields such as NP research. This dynamic approach serves as an effective means of communicating current information on biosynthesis to scientists from various backgrounds.

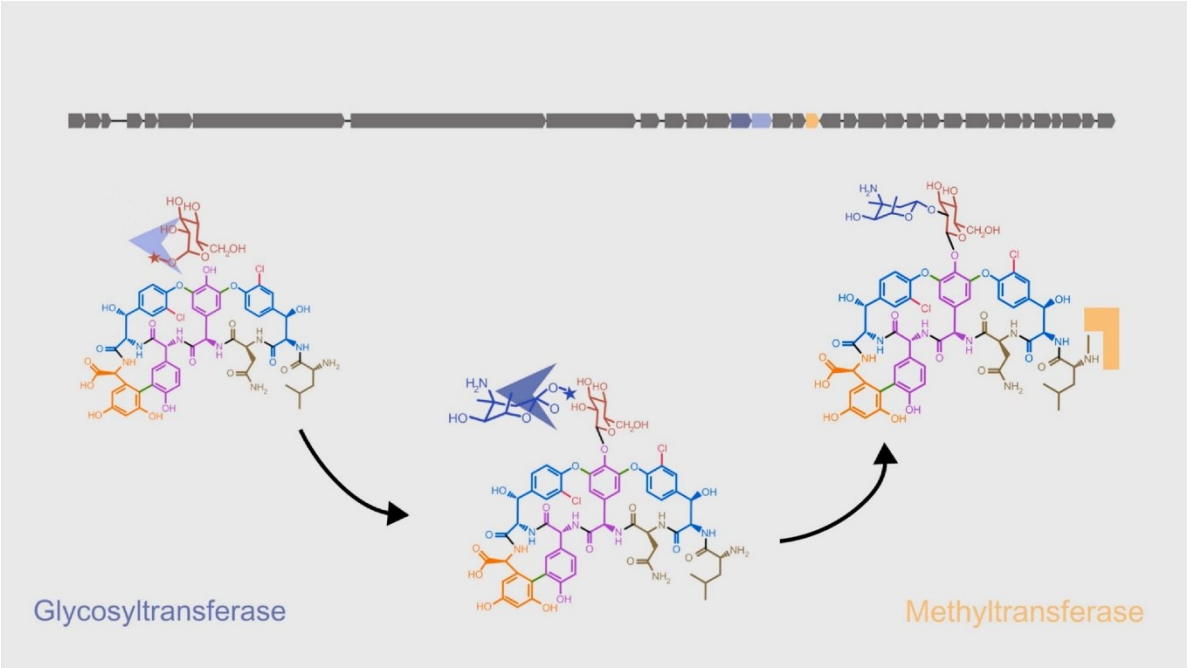

Figure 5: Post-assembly modifications of vancomycin. Shown on the top is the vancomycin BGC, with the genes encoding the glycosyltransferases and the methyltransferase in blue and yellow, respectively. Below, the three tailoring reactions are shown in order. The first glycosyltransferase (light blue shape) attaches the first sugar moiety to the fourth amino acid in the backbone. Then, the second glycosyltransferase (dark blue shape) attaches the second sugar moiety to the first sugar. Additionally, a methyltransferase (yellow shape) adds a methyl group to the first amino acid in the backbone.

The coloring scheme of the backbone amino acids follows that of Figure 2. 'Arrow' symbol is by 4B Icons from thenounproject.com. This figure has been adapted from the animation (Supplementary Data 1).

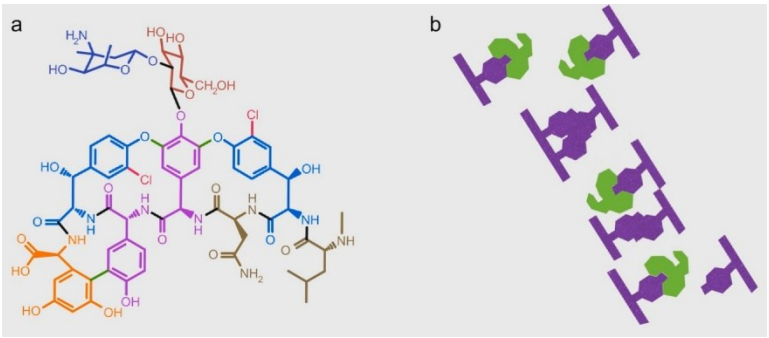

Figure 6: Final structure and mode of action of vancomycin. The final structure of vancomycin. The coloring scheme follows that of Figures 2–5. (b) Schematic representation of the mode of action of vancomycin. The green shapes represent vancomycin molecules, while the purple shapes represent the lipid II component of the bacterial cell wall. Once bound to lipid II, vancomycin blocks other vital enzymes from catalyzing cell wall reactions, leading to cell death.

Data Availability

All data come from publications cited and were used only for the provided visualizations.

Declaration of Competing Interest

The authors declare that they have no known competing financial interests or personal relationships that could have appeared to influence the work reported in this paper.

Acknowledgements

A. Gavriilidou and J. Rodler are grateful for the support of the Deutsche Forschungsgemeinschaft (DFG; Project ID No. 398967434-TRR 261). N. Ziemert, C. Hughes, and M. Adamek were supported by the German Center for Infection Research (DZIF) (TTU 09.716). N. Ziemert, M. Adamek, C. Hughes, L. Kokkoliadis, and E. Stegmann thank CMFI (Germany's Excellence Strategy–EXC 2124–390838134) for funding and structural support. This work was supported by Monash University and EMBL Australia. This research was conducted by the Australian Research Council Centre of Excellence for Innovations in Peptide and Protein Science (CE200100012) and funded by the Australian Government. We also thank L. lo Presti for invaluable comments on the manuscript.

Appendix A. Supporting Information

Supplementary data associated with this article can be found in the online version at doi:10.1016/j.mib.2024. 102561.

References and recommended reading

Papers of particular interest, published within the period of review, have been highlighted as:

• of special interest

•• of outstanding interest

1. Stegmann E, Frasch HJ, Wohlleben W: Glycopeptide biosynthesis in the context of basic cellular functions. Curr Opin Microbiol 2010, 13:595-602.
2. van Groesen E, Innocenti P, Martin NI: Recent advances in the development of semisynthetic glycopeptide antibiotics: 2014–2022. ACS Infect Dis 2022, 8:1381-1407.
3. Hansen MH, et al.: Resurrecting ancestral antibiotics: unveiling the origins of modern lipid II targeting glycopeptides. Nat Commun 2023, 14:7842.
4.Butler MS, Hansford KA, Blaskovich MAT, Halai R, Cooper MA: Glycopeptide antibiotics: back to the future. J Antibiot 2014, 67:631-644.
5. Mccormick MH, Mcguire JM, Pittenger GE, Pittenger RC, Stark WM: Vancomycin, a new antibiotic. I. Chemical and biologic properties. Antibiot Annu 1955, 3:606-611.
6. Hansen MH, Stegmann E, Cryle MJ: Beyond vancomycin: recent advances in the modification, reengineering, production and discovery of improved glycopeptide antibiotics to tackle multidrug-resistant bacteria. Curr Opin Biotechnol 2022, 77:102767.
• This review presents the latest advances in the study of glycopeptide antibiotics (GPAs), with an emphasis on the elucidation of the biosynthetic pathway.
7. Greule A, et al.: Kistamicin biosynthesis reveals the biosynthetic requirements for production of highly crosslinked glycopeptide antibiotics. Nat Commun 2019, 10:1-15.
8. Schoppet M, et al.: The biosynthetic implications of late-stage condensation domain selectivity during glycopeptide antibiotic biosynthesis. Chem Sci 2019, 10:118 133.
9. Kittilä T, et al.: Halogenation of glycopeptide antibiotics occurs at the amino acid level during non-ribosomal peptide synthesis. Chem Sci 2017, 8:5992-6004.
10. Wohlleben W, Stegmann E, Süssmuth RD: Chapter 18. Molecular genetic approaches to analyze glycopeptide biosynthesis. Methods Enzymol 2009, 458:459-486.
11. Truman AW, et al.: The role of Cep15 in the biosynthesis of chloroeremomycin: reactivation of an ancestral catalytic function. Chem Biol 2008, 15:476-484.
12. Chen S, Wu Q, Shen Q, Wang H: Progress in understanding the genetic information and biosynthetic pathways behind Amycolatopsis antibiotics, with implications for the continued discovery of novel drugs. Chembiochem 2016, 17:119-128.
13. Xu M, et al.: GPAHex — a synthetic biology platform for Type IV–V glycopeptide antibiotic production and discovery. Nat Commun 2020, 11:1-12.
14. Thykaer J, et al.: Increased glycopeptide production after overexpression of shikimate pathway genes being part of the balhimycin biosynthetic gene cluster. Metab Eng 2010, 12:455-461.
15. Goldfinger V, et al.: Metabolic engineering of the shikimate pathway in Amycolatopsis strains for optimized glycopeptide antibiotic production. Metab Eng 2023, 78:84-92.
• The authors applied a metabolic engineering approach to manipulate the key enzymes of the shikimate pathway and managed to optimise the production of balhimycin and ristomycin. This study underlines the dependency of the GPA biosynthesis on the shikimate pathway enzymes for the biosynthesis of the non-proteinogenic amino acids comprising the GPA peptide backbone.
16. Toma RSA, Brieke C, Cryle MJ, Süssmuth RD: Structural aspects of phenylglycines, their biosynthesis and occurrence in peptide natural products. Nat Prod Rep 2015, 32:1207-1235.
17. Stinchi S, et al.: A derivative of the glycopeptide A40926 produced by inactivation of the β-hydroxylase gene in Nonomuraea sp. ATCC39727. FEMS Microbiol Lett 2006, 256:229-235.
18. Kaniusaite M, et al.: A proof-reading mechanism for non- proteinogenic amino acid incorporation into glycopeptide antibiotics. Chem Sci 2019, 10:9466-9482.
19. Chen H, Walsh CT: Coumarin formation in novobiocin biosynthesis: beta hydroxylation of the aminoacyl enzyme tyrosyl-S-NovH by a cytochrome P450 NovI. Chem Biol 2001, 8:301-312.
20. Chen H, Hubbard BK, O'Connor SE, Walsh CT: Formation of beta- hydroxy histidine in the biosynthesis of nikkomycin antibiotics. Chem Biol 2002, 9:103 112.
21. Mulyani S, et al.: The thioesterase Bhp is involved in the formation of beta hydroxytyrosine during balhimycin biosynthesis in *Amycolatopsis balhimycina*. Chembiochem 2010, 11:266-271.
22. Miller BR, Gulick AM: Structural biology of non-ribosomal peptide synthetases.
Methods Mol Biol 2016, 1401:3-29.

• This chapter illustrates the protein structures of the non-ribosomal peptide synthetases (NRPSs), the core biosynthetic enzymes involved in GPA biosynthesis.
23. Haslinger K, Peschke M, Brieke C, Maximowitsch E, Cryle MJ: X- domain of peptide synthetases recruits oxygenases crucial for glycopeptide biosynthesis.
Nature 2015, 521:105-109.
24. Yim G, Thaker MN, Koteva K, Wright G: Glycopeptide antibiotic biosynthesis. J Antibiot 2014, 67:31-41.
• This review focuses on the advances on the elucidation of GPA mode of action and resistance mechanisms.
25. Izoré T, et al.: Structures of a non-ribosomal peptide synthetase condensation domain suggest the basis of substrate selectivity. Nat Commun 2021, 12:2511.
26. Luo L, et al.: Timing of epimerization and condensation reactions in nonribosomal peptide assembly lines: kinetic analysis of phenylalanine activating elongation modules of tyrocidine synthetase B. Biochemistry 2002, 41:9184-9196.
27. Greule A, Stok JE, Voss JJD, Cryle MJ: Unrivalled diversity: the many roles and reactions of bacterial cytochromes P450 in secondary metabolism. Nat Prod Rep 2018, 35:757-791.
28. Brieke C, Peschke M, Haslinger K, Cryle MJ: Sequential in vitro cyclization by Cytochrome P450 enzymes of glycopeptide antibiotic precursors bearing the X-domain from nonribosomal peptide biosynthesis. Angew Chem Int Ed Engl 2015, 54:15715-15719.
29. Peschke M, Gonsior M, Süssmuth RD, Cryle MJ: Understanding the crucial interactions between Cytochrome P450s and non- ribosomal peptide synthetases during glycopeptide antibiotic biosynthesis. Curr Opin Struct Biol 2016, 41:46-53.
30. Ulrich V, Peschke M, Brieke C, Cryle MJ: More than just recruitment: the X-domain influences catalysis of the first phenolic coupling reaction in A47934 biosynthesis by Cytochrome P450 StaH. Mol Biosyst 2016, 12:2992-3004.
31. Peschke M, Brieke C, Cryle MJ: F-O-G Ring formation in glycopeptide antibiotic biosynthesis is catalysed by OxyE. Sci Rep 2016, 6:35584.
32. Nicolaou KC, Boddy CNC, Bräse S, Winssinger N: Chemistry, biology, and medicine of the glycopeptide antibiotics. Angew Chem Int Ed Engl 1999, 38:2096-2152.
33. Peschke M, Brieke C, Heimes M, Cryle MJ: The thioesterase domain in glycopeptide antibiotic biosynthesis is selective for cross-linked aglycones. ACS Chem Biol 2018, 13:110-120.
34. Donadio S, Sosio M, Stegmann E, Weber T, Wohlleben W: Comparative analysis and insights into the evolution of gene clusters for glycopeptide antibiotic biosynthesis. Mol Genet Genom 2005, 274:40-50.
35. Brieke C, Yim G, Peschke M, Wright GD, Cryle MJ: Catalytic promiscuity of glycopeptide N-methyltransferases enables bio- orthogonal labelling of biosynthetic intermediates. Chem Commun 2016, 52:13679.
36. Kalan L, Perry J, Koteva K, Thaker M, Wright G: Glycopeptide sulfation evades resistance. J Bacteriol 2013, 195:167-171.
37. Menges R, Muth G, Wohlleben W, Stegmann E: The ABC transporter Tba of *Amycolatopsis balhimycina* is required for efficient export of the glycopeptide antibiotic balhimycin. Appl Microbiol Biotechnol 2007, 77:125-134.
38. Müller A, Klöckner A, Schneider T: Targeting a cell wall biosynthesis hot spot. Nat Prod Rep 2017, 34:909-932.
39. Tas Alicenap C: The use of animation and storytelling in science communication. Improving Scientific Communication for Lifelong